Neuroradiology (2022) 64 (Suppl 1):S1–S165
https://doi.org/10.1007/s00234-022-03012-w

ABSTRACTS

ESNR 2022

Published online: 8 August 2022

EUROPEAN SOCIETY OF NEURORADIOLOGY
Diagnostic and Interventional
45th ANNUAL MEETING
28th Advanced Course in Diagnostic Neuroradiology
13th Advanced Course in Interventional Neuroradiology
14th – 18th September 2022
Lisbon, Portugal

SCIENTIFIC COMMITTEE

Pedro Vilela
Meike Vernooij
Naci Koçer
Katarina Surlan Popovic
Chen Hoffmann
Luigi Manfrè
K. O. Lövblad
Majda Thurnher

LOCAL COMMITTEE

Pedro Vilela
Ana Braz
Ana Mafalda Reis
Catarina Brito
Cristina Moura
Duarte Vieira
Joana Mendes Graça
Luis Pedro Melo Freitas
Sandra Matias
Teresa Nunes

ESNR PRESIDENTIAL ADDRESS

It is with great pleasure that ESNR this year will have our Annual Meeting in Lisbon, Portugal organized by the Congress President Professor Pedro Vilela. This year's 45th Annual Meeting of the European Society of Neuroradiology (ESNR) will be a very special event as a truly on-site meeting in the beautiful city of Lisbon from 14th to 18th of September 2022.

At this 2022 Annual Meeting we will bring you a scientifically and educational meeting as in the old times with 130 national and international faculty presenting their lectures, interactive case sessions, and keynote lectures in person and with the possibility for all participants to interact and network face to face. The ESNR Annual Meeting will start with the Advanced Courses in Diagnostic and Interventional Neuroradiology on Thursday 15th September focusing on Individualized and Precise Neuroradiology. It will continue with State-of-the-Art, keynote lectures, educational and scientific lectures and presentations until Sunday18th of September. Several scientific sessions dedicated to different interesting topics including more than 200 scientific presentation will presented as oral and poster presentations. The presentations of the Honorary Members and Awards Ceremony will occur on Friday 16th of September, and the General Assembly on Saturday September 17th. This year a special session will be "ESNR meets Greece". The EBNR Diploma ceremony will be held late afternoon on Friday 16th of September where we will have an opportunity to congratulate those that have achieved their different Diplomas.

During this year Annual Meeting we will celebrate Prof. Raybaud, Prof. Hirsch, and Prof. Brooks as Honorary Members for their outstanding contributions to neuroradiology during their long and successful professional careers.

Prof. Vilela and the leadership of ESNR have put together a very interesting program brought to you for a very reasonable price and in a lovely location and we all hope that you will be there with us..

We cannot make up for the lack of social gathering, networking and meeting friends over the past 2 years but I do hope that this on-site ESNR Annual Meeting 2022 will give us the possibility to meet in person again, enjoy high educational and scientific presentations and have fun. I am looking forward to meeting you all.

Let us make this annual meeting great both scientifically, educational, and socially, and be a turning point that the world will resume to normal in near future.

Prof. Pia C Maly Sundgren
ESNR President

WELCOME ADDRESS

Dear Colleagues and Friends,

It is my great honour to welcome you to Lisbon for the next European Society of Neuroradiology (ESNR) Annual meeting. This meeting will provide an excellent learning experience and the opportunity to work together. The annual meeting and advanced course programmes are designed to address a wide range of topics from different neuroradiology diagnostic and interventional fields and for different levels of expertise.

Personalized neuroimaging will be the main topic of the advanced course. The pre-congress course will address value-based neuroimaging and imaging department management. The use of advanced individualized neuroimaging together with the artificial intelligence tools will allow for better clinical outcomes and higher levels of medicine-based value standards.

We have gathered a faculty of several distinguished speakers, from all around the world, to provide a comprehensive programme that covers the most important modern neuroimaging topics and latest innovations in diagnostic and interventional neuroradiology. It was also designed to accommodate a larger number of scientific presentations for better knowledge exchange and active participation of everyone. In this meeting we will have a task force for the young neuroradiologists. There will be a dedicated room with a program suggested by young Neuroradiologists.
This year we welcome Greece! The ESNR meets Greece with a special session devoted to Greek Neuroradiology. It is also our intention to take this opportunity to show to all participants of the congress, some of the Portuguese traditions, culture, art and history.
We have chosen a splendid venue to host the annual meeting. It is located at one of the most beautiful area in Lisbon, at the Tagus riverside, close to important world heritage monuments and with a spectacular landscape scenario. It is also a very wide space with large rooms having all the conditions to hold the meeting safely. Lisbon is recognized by the hospitality, safety, authenticity, multicultural atmosphere, intermixing old customs, ancient history, heritage monuments, new architecture, cultural and social entertainments.

We warmly welcome you to Lisbon; one of the most beautiful and historical European cities with an important heritage that you will enjoy discovering.

We hope that you will join us in this annual meeting.

Let's bring the Neuroradiology community back together in Lisbon!

Dr. Pedro Vilela
President of the 45th ESNR ANNUAL MEETING

The European Society of Neuroradiology – Diagnostic and Interventional Executive Committee

President	Pia Maly Sundgren
Vice-President	Tarek Yousry
Secretary General	Andrea Rossi
Treasurer	Cem Calli
Chairperson of the Subspecialty Committee Diagnostic Neuroradiology	Meike Vernooij
Chairperson of the Subspecialty Committee Head and Neck Neuroradiology	Katarina Surlan Popovic
Chairperson of the Subspecialty Committee Interventional Neuroradiology	Naci Koçer
Chairperson of the Subspecialty Committee Pediatric Neuroradiology	Chen Hoffmann
Chairperson of the Subspecialty Committee Spine Neuroradiology	Luigi Manfrè
Secretary of the Institutional Council	Paulina Due-Tønnessen

Institutional Council

Australia / NZ	C. Barras	Italy	L.Cirillo
Austria	E. Gizewski	Latvia	G. Krumina
Belgium	S. Van Cauter	Netherlands	M. Smits
Bosnia Herzegovina	Z. Merhemic	Norway	P. Due-Tønnessen
Brazil	R. Hoffmann Nunes	Poland	A. Zimny
Bulgaria	D. Zlatareva	Portugal	J. Graça
Croatia	M. Špero	Serbia	T. Stosic-Opincal
Denmark	M.E. Cortsen	Slovenia	K. Surlan Popovic
Finland	J. Pekkola	South Africa	C. Sperryn
France	F. Cotton	Spain	N. Bargalló
Germany	C. Zimmer	Sweden	R. Siemund
Greece	E. Kapsalaki	Switzerland	K. O. Lövblad
Gulf	L. Alsaraf	Turkey	I. Saatçi
Hungary	L. Kozák	Ukraine	O. Zemskova
Ireland	S. Looby	United Kingdom	K. Lobotesis

Institutional Members

Australian and New Zealand Society of Neuroradiology
Austrian Society of Neuroradiology
Belgian Society of Neuroradiology
Brazilian Society of Neuroradiology
British Society of Neuroradiologists
Bulgarian Society of Neuroradiology & Head and Neck Radiology
Danish Society of Neuroradiology
Dutch Society of Neuroradiology
Finnish Society of Neuroradiology
French Society of Neuroradiology
German Society of Neuroradiology
Greek Society of Neuroradiology
Gulf Neuroradiology Society

Hungarian Society of Neuroradiology
Irish Society of Neuroradiology
Italian Society of Neuroradiology
Latvian Society of Neuroradiology
Neuroradiology Section of the Association of Radiologists of Ukraine
Neuroradiology Section of the Association of Radiology of Bosnia & Herzegovina
Neuroradiology Section of the Croatian Society of Radiology
Neuroradiology Subgroup of the Radiological Society of South Africa
Norwegian Society of Neuroradiology
Polish Medical Society of Radiology - neuroradiology section
Portuguese Society of Neuroradiology
Serbian Society of Neuroradiology
Slovenian Section of Neuroradiology
Spanish Society of Neuroradiology
Swedish Society of Neuroradiology
Swiss Society of Neuroradiology
Turkish Society of Neuroradiology

Committees of the ESNR

Diagnostic Neuroradiology
Meike Vernooij **(Chair)**
Alexandre Krainik
Luc van den Hauwe
Ana Ramos
Antonella Castellano

Head and Neck Neuroradiology
Katarina Surlan Popovic **(Chair)**
Sotirios Bisdas
Bernhard Schuknecht
Sofie Van Cauter

Interventional Neuroradiology
Naci Koçer **(Chair)**
Omer Eker
Markus Möhlenbruch
Işıl Saatci
Kamil Zelenak

Pediatric Neuroradiology
Chen Hoffmann **(Chair)**
Maria Argyropoulou
Kshitij Mankad
Mariasavina Severino

Spine Neuroradiology
Luigi Manfrè **(Chair)**
Adrian Kastler
Chiara Zini
Inês Sofia Martins Gil de Almeida
Hosam Alqatami
Allan Brook
Bassem Georgy
Wende Gibbs
Joshua Hirsch

Rules
Philippe Demaerel **(Chair)**
Andrea Rossi
Marek Sasiadiek
Dojan Stojanov

Scientific Programme
Pedro Vilela **(Chair)**
Meike Vernooij
Naci Koçer
Katarina Surlan Popovic
Chen Hoffmann
Luigi Manfrè
K. O. Lövblad
Majda Thurnher

Membership
Cem Calli **(Chair)**
Martina Špero
Cenk Eraslan

Social Media
Gennaro D'Anna **(Chair)**
Efrosini Papadaki
Julia Fruehwald-Pallamar
Yelda Ozsunar Dayanir
Chiara Gaudino
Johan Van Goethem
Luc van den Hauwe
Nadya Pyatigorskaya
Rudiger Von Kummer

ESONR
Johan Van Goethem **(Chair)**
Luigi Manfrè
Naci Koçer
Chen Hoffmann
Katarina Surlan Popovic
Meike Vernooij
Majda M. Thurnher

Founding Members
P. Amundsen
P. Andersen
H. Backmund
K. Bergström
V. Bernasconi
A.S. Bligh
G. Bonte
J. Bories
G. Bradac
J.P. Braun
P. Buffard
J.W.D. Bull
E.H. Burrows
A. Calabrò
R. Chrzanowski
G. Cornélis
S. Cronqvist
K. Decker
P. Dettori
R. Djindjian

A. Donaldson
G. du Boulay
J. Duquesnel
Ph. Engel
L. Escudero
H. Fischgold
T. Greitz
G. Gryspeerdt
H. Hacker, Germany
D.T. Hawkins
R. Hoare
P. Huber
H.H. Jacobsen
J. Jeanmart
J. Jirout
E.M. Klausberger
J. Legré
B. Liliequist
E. Lindgren
G. Lombardi
J. Metzger
P. Moxon
D. Müller
R. Oberson
A. Passerini
L. Penning
J. Petrov
L. Picard
P. Potthoff
L. Psenner
R. Reid
J. Roulleau
M. Roth
G. Ruggiero
G. Salamon
W. Shepherd
J. Simon
F. Smaltino
J. Solé-Llenas
A. Tänzer
A. Thibaut
H. Vogelsang
A. Wackenheim
S. Wende
G. Westberg
I. Wickholm
O. Wiedermann
G.B. Ziedses des Plantes

THE ESNR AWARDS: THE EUROPEAN NEURORADIOLOGY AWARDS IN DIAGNOSTIC AND INTERVENTIONAL NEURORADIOLOGY

ESNR Awards
The European Society of Neuroradiology (ESNR) awards three Annual Scientific Prizes for the best works in Neuroradiology, each to the amount of €4000:

The **"ESNR Scientific Award (formerly known as the "Lucien Appel Prize of the ESNR")"**, to be awarded for the best Research submission.

The "**Pioneers and Past Presidents of European Neuroradiology Awards**", for the best submissions on Diagnostic Neuroradiology.

The "**Pioneers and Past Presidents of European Neuroradiology Awards**", for the best submissions on Interventional Neuroradiology.

The "ESNR-Springer Award" will be awarded by Springer to the first-named author (ESNR Member) of the most cited article of the latest impact factor together with the prize money of € 1000 and a free registration to the ESNR Annual Meeting of the current year. The Article will be highlighted on the journal webpage (Springer.com)

Rules of participation for ESNR Awards:

Article 1: The prizes reward the achievements of young scientists, under the age of 40 years on the day of application, working in the field of neuroradiology in a European centre and beeing Full, Associate or Junior Member of the ESNR (can be pending or active).

Article 2: The prizes, each to the amount of € 4000, are awarded every year at the Awards Ceremony during the annual congress of the ESNR, or during the Symposium Neuroradiologicum when the ESNR Annual Congress does not take place. The Awards Ceremony is a respected event during each congress; other simultaneous ESNR sessions are not allowed, and the ceremony may not be split in two or more parts. The Award Ceremony is conducted by the Chair of the Awards Committee, who also introduces the awardees and presents the prizes together with the ESNR President.

Article 3: The candidate must be the first author of an original work in the fields of research in neuroradiology: diagnostic or interventional neuroradiology. Applications can be placed for a scientific work that was:
a. published online or in print in a peer-reviewed scientific journal listed in SCI within the last 12 months before the date of submission, or
b. submitted, still unpublished, accepted or not yet accepted.
The candidate must not have received any other prize for the same work, and must not have received the ESNR award of the same category previously.

Article 4: All submissions must be **in English** and should include:

• application letter indicating the title of the scientific paper upon which the application is based, and reporting its status if not yet published;
• the scientific paper (unpublished or to be submitted);
• the full Curriculum Vitae and a photo of the candidate.

These documents must be exclusively submitted, as electronic attachments, via e-mail to the address indicated below. Please note that each submitted article and its relevant images should be included in a separate attachment.
By submitting the work the author agrees, if declared the winner, to present the work at the next ESNR Annual Congress or Symposium Neuroradiologicum. Should the winner be unable to participate because of proven urgent reasons, the presentation can be made by a co-author of the same paper. If no presentation is made, the prize money will not be awarded. Payment of the prize money is made after the relevant ESNR Annual Congress or Symposium Neuroradiologicum has taken place.

Article 5: A single author can apply for more than one prize with scientific papers on clearly different topics as confirmed by the Awards Committee.

Article 6: Authors are requested to indicate to which of the two awards categories each scientific paper is addressed. If the Awards Committee considers another category to be more appropriate, the submission may be re-classified.

Article 7: A Scientific Jury will assess and rate the submitted papers. The Jury is composed of the members of the Awards Committee, plus four internationally known specialists in neuroradiology, who will rate each application independently from each other. If the rating does not give clear results, the prize-winners will be identified by consensus of all jury members.
The members of the Scientific Jury should declare not to have a conflict of interests. In case of conflict of interests, the juror is excluded from the Scientific Jury for the current year and specific prize category, and is replaced by another juror of equal scientific standing.
The Chair of the Awards Committee shall be invited as a Faculty member to the ESNR Annual Meeting or Symposium Neuroradiologicum where the award ceremony takes place.

Article 9: The ESNR will advertise the prizes by a dedicated newsletter and in the society website, as of January 1st each year. The deadline for applications is set at March 1st each year. The Award Committee will designate the laureates after receiving the evaluations of the jurors, as a rule by May 1st. Should the Award Committee decide that, in any category, no submission meets sufficientquality requirements, no prize will be awarded in that category.

Article 10: All candidates will be notified in writing of the result of their application. The laureates will be invited to give a six-minute oral presentation at the Award Ceremony during the ESNR Annual Congress, or Symposium Neuroradiologicum when the ESNR Annual Congress does not take place. The congress registration fee of the laureates is waived; the travel expenses will be reimbursed.
The names of the laureates, as well as the titles and abstracts of their scientific works, will be placed on the ESNR website and published in the society pages of Neuroradiology. In case the winning paper is still unpublished, the authors agree that "Neuroradiology", the official ESNR journal, shall have the right of publication after peer-review.

Article 11: All possible questions and issues regarding the awarding of the Prizes shall be dealt with at the discretion of the Awards Committee and the ESNR Executive Committee. The decision of the ESNR Executive Committee is final**.**

Article 12: Candidacy implies full acceptance of the rules.
Please send your submissions to the attention of the
ESNR Secretary General
Email: info@esnr.org
The object of the email should read: ESNR award submission.

THE DEADLINE FOR RECEIPT OF SUBMISSIONS IS MARCH 1ST

ESNR Annual Congress, Advanced Course in Diagnostic Neuroradiology and Advanced Course in Interventional Neuroradiology of the ESNR.

The European Society of Neuroradiology holds each year a scientific congress at a place and date designated by the Executive Committee. On the day before the congress, Advanced Courses in Diagnostic Neuroradiology and Interventional Neuroradiology are organized in parallel sessions. The business meeting (General Assembly) of the Society is held in conjunction with this annual scientific congress.
Since its creation in 1969, the ESNR has organized 42 annual congresses. In recognition of the importance of the Symposium Neuroradiologicum, which is held every four years, no scientific congress of the ESNR is held when the Symposium takes place in Europe.

Future Annual Meetings

46th Annual Meeting

September 2023
Vienna, Austria
President: Majda Thurnher

47th Annual Meeting

September 2024
Paris, France
President: Fabrice Bonneville

The European Course in Neuroradiology

The European Course in Neuroradiology has been a story of success ever since the first course in Toulouse in 1984. More than 1000 young neuroradiologists have completed the cycle of three courses over the past 21 years. The ECNR was conceived as a means to create a common and shared culture, common meeting points and a common standard of knowledge. The form that was adopted and used for the coming 6 cycles, each consisting of three courses, included the major bodies of knowledge as described by the headlines; intracranial nervous system, the spine and spinal cord and the base of the skull, maxillofacial and head and neck neuroradiology.

European School of Neuroradiology (ESONR) - the new concept

The ESONR - European School of Neuroradiology - is the most important and complete training programme organized by the ESNR - European Society of Neuroradiology within the main frame, and in partnership with, the ESOR - European School of Radiology. The purpose of this training and education program is based on the vision of what the ESNR considers the range of competences and skills that are the basis of a high qualified neuroradiological activity. The program is designed to offer a pathway to reach such professional and cultural levels. The final points will be the examinations to be certificated at the different levels and in the different branches of this discipline.

Courses are organized at 3 different levels: 1st Level: **ESOR - Galen Foundation Courses in Neuroradiology**, 2nd level: ECNR - **Course in Neuroradiology, Diagnostic and Interventional** and finally 3rd level: **ESNR Advanced Courses of Higher Qualification in Interventional Endovascular Neuroradiology, Interventional Spine Neuroradiology, Advanced Diagnostic Neuroradiology and Paediatric Neuroradiology**.

ECNR - European Course in Diagnostic and Interventional Neuroradiology

The ECNR is the fundamental Neuroradiology course aimed at neuroradiologists, established or in training. It is based on cycles of four courses (modules), each lasting five days, dedicated to diagnostic and interventional neuroradiology. The full cycle is considered complete after the attendee has participated in all four modules, which can be done in a single cycle or in different cycles.
The scientific content of the course is determined by the ESONR Committee of the European Society of Neuroradiology, taking into account international standards and guidelines for training in diagnostic and interventional neuroradiology. The participating educators will be internationally renowned European experts, to be selected on the basis of their scientific background and educational skills to ensure high- quality lectures and interactive case discussions.

The following topics have been chosen, each to be covered in five full days of lectures and workshops:
- Anatomy, congenital malformations and genetics.
- Trauma, Infection, Inflammation and Degenerative Disease
- Tumours of the Brain and Spinal Canal
- Vascular Disease of the Brain and Spinal Canal

Seventh Cycle - Scientific Director: Guido Wilms (Leuven)
First Module: Embryology, Anatomy, Malformations - Crieff, October 4 –11, 2002 –Local Director:Wendy J. Taylor
Second Module: Tumours of the CNS - Riga, April 11 - 18, 2003 – Local Director: Cosma Andreula
Third Module: Vascular Disease of the CNS - Malta, October, 24 - 30, 2003 - Local Director: Athanassios Gouliamos
Fourth Module: Trauma and Degenerative Disease of the CNS - Riga, April 23-27, 2004 -Local Director: Johan Van Goethem

Eighth Cycle -Scientific Director: Ernst-Wilhelm Radü (Basel)
First Module: Embryology/Anatomy/Malformations/Genetics - Basel, October 22-26, 2004
Second Module: Tumors of the CNS - Basel, March 18-22, 2005
Third Module: Vascular Diseases of the CNS - Basel, October 21-25, 2005
Fourth Module: Trauma/Degenerative Diseases of the CNS - Basel, March 10-14, 2006

Ninth Cycle - Scientific Director: Ernst-Wilhelm Radü (Basel)
First Module: Embryology/Anatomy/Malformations/Genetics - Basel, October 20 - 24, 2006
Second Module: Tumours of the CNS - Basel, March 23 - 27, 2007
Third Module: Vascular Diseases of the CNS - Basel, November 2 - 6, 2007

Fourth Module: Trauma/Degenerative Diseases of the CNS - Basel, April 11 - 15, 2008

Tenth Cycle - Scientific Directors: Massimo Gallucci (L'Aquila), AlexRovira (Barcelona)
First Module: Embryology/Anatomy/Malformations/Genetics - Tarragona, October 10 – 14, 2008
Second Module: Tumors and Tumor-like Vascular Lesions-Rome, March 20 – 24, 2009
Third Module: Vascular Diseases - Tarragona, October 9-13, 2009
Fourth Module: Trauma/Degenerative/Metabolic/Inflammatory Diseases - Rome, March 19-23, 2010

Eleventh Cycle - Scientific Directors: Massimo Gallucci (L'Aquila), Alex Rovira (Barcelona)
First Module: Embryology/Anatomy/Malformations/Genetics - Tarragona, November 5-9, 2010
Second Module: Tumors and Tumor-like Vascular Lesions-Rome, March 25-29, 2011
Third Module: Vascular Diseases - Tarragona, October 28 - November 1, 2011
Fourth Module: Trauma/Degenerative/Metabolic/Inflammatory Diseases - Milano, April 12-16, 2012

Twelfth Cycle - Scientific Directors: Athanasios Gouliamos (Athens), E. Turgut Tali (Ankara)
First Module: Embryology/Anatomy/Development and Malformations of the CNS - Antalya, November 1-6, 2012
Second Module: CNS Tumors - Athens, April 8 – 13, 2013
Third Module: Vascular Diseases - Antalya, November 3-7, 2013
Fourth Module: Trauma/Degenerative/Metabolic/Inflammatory Diseases - Athens, April6-10, 2014

Thirteenth Cycle - Scientific Directors: Athanasios Gouliamos (Athens), E. Turgut Tali (Ankara)
First Module: Embryology/Anatomy/Development and Malformations of the CNS - Antalya, November 9-13, 2014
Second Module: CNS Tumors - Rhodes, April 14-18, 2015
Third Module: Vascular Diseases - Izmir, November, 2015
Fourth Module: Trauma/Degenerative/Metabolic/Inflammatory Diseases - Rhodes, April, 2016

Fourteenth Cycle - Scientific Directors: Majda M. Thurnher (Vienna), Johan Van Goethem (Antwerp)
First Module: Embryology/Anatomy/Development and Malformations of the CNS - Dubrovnik, October 16-20, 2016
Second Module: CNS Tumors - Antwerp, May 7-11, 2017
Third Module: Vascular Diseases - Dubrovnik, October 22-26, 2017
Fourth Module: Trauma, Infection and Degenerative Disease - Antwerp, May 6-10, 2018

Fifteenth Cycle - Scientific Directors: Majda M. Thurnher (Vienna), Johan Van Goethem (Antwerp)
First Module: Anatomy and Embryology - Dubrovnik, October 21-25, 2018
Second Module: CNS Tumors - Antwerp, April 29-May 3, 2019
Third Module: Vascular and Traumatic Diseases – Rovinj, 13 – 17 October 2019
Fourth Module: Degenerative, Metabolic and Inflammatory Diseases, Live Online Edition, 8-12 November 2020

Sixteenth Cycle - Scientific Directors: Majda M. Thurnher (Vienna), Johan Van Goethem (Antwerp)
First Module: Anatomy and Embryology – Live online course, 8-12 February 2021
Second Module: CNS Tumors – Live online course, 2- 6 May 2021
Third Module: Vascular and Traumatic Diseases – Live online course, 7-11 november 2021
Fourth Module: Degenerative, Metabolic and Inflammatory Diseases, Berlin, 1-5 May 2022

Neuroradiology
Neuroradiology, published by Springer Verlag, was founded as the official organ of the European Society of Neuroradiology in 1970. Since 2010 on, the Austrian Society of Neuroradiology, the Belgian Society of Neuroradiology, the British Society of Neuroradiologists, the Bulgarian Association of Radiology, the Czech Neuroradiological Society, the Dutch Society of Neuroradiology, the Finnish Society of Neuroradiology, the German Society of Neuroradiology, the Latvian Society of Neuroradiology, the Norwegian Society of Neuroradiology, the Neuroradiological Section of the Hellenic Radiological Society, the Neuroradiological Section of the Polish Radiological Society, the Portugese Society of Neuroradiology, the Romanian Society of Magnetic Resonance in Medicine, the Spanish Society of Neuroradiology, the Swedish Society of Neuroradiology and the Swiss Society of Neuroradiology decided to choose neuroradiology as their (in some cases second) official Journal. Submissions of articles can be done via the website: http://www.editorialmanager.com/nrad

NEURORADIOLOGY EDITORIAL BOARD 2022

SCIENTIFIC PROGRAM

WEDNESDAY 14th September 2022- Pre-meeting course:

Moderators:	**Paul Parizel / Pedro Vilela**
14:00-14:10	Introduction *Pedro Vilela, PT*
14:10-14:30	Leadership in imaging: a SWOT analysis *Paul Parizel, AU*
14:30-14:50	Leading in global health care: Value based medicine and patient integrated care *Isabel Vaz, PT*
14:50 – 15:10	European Union public health policies trends *Paulo Boto, PT*
15:10 – 15:30	Digital transformation: biomedical imaging advances *Javier Alvarez-Valle, UK*
15:30-16:00	**Coffee Break**
16:00-16:20	The role of universities and scientific societies in health care organization *Fausto Pinto, PT*
16:20-16:40	Value based methodology *Claudia Vaz, CH*
16:40-17:00	Value-base medicine in imaging *Karl Olof Lovblad, CH*
17:00 – 17:20	Innovation, cost-benefit analysis, and reimbursement strategies *Joshua Hirsch, US*
17:20 – 17:40	Innovation and ethics *Seon Kyu Lee, US*
17:40 -18:00	Final Remarks

THURSDAY 15th September 2022 – Meeting room 1

ADVANCED COURSE IN DIAGNOSTIC AND INTERVENTIONAL NEURORADIOLOGY

08:30-09:45:	**Introduction to Individualized and Precision Medicine**
Moderators:	**Pia Maly Sundgren SE, Paul Parizel AU**
08:30 - 08:45	Introduction to the advanced diagnostic course *Pedro Vilela, PT*
08:45-09:15	Imaging biomarkers in neurosciences *Tarek Yousry, UK*
09:15- 09:45	Artificial Intelligence in neuroimaging *Greg Zaharchuk, US*
09:45-10:15	**Coffee Break**

ADVANCED DIAGNOSTIC COURSE

10:15-12:15	**Individualized and Precision Medicine in inflammatory and chronic vascular diseases**
Moderators:	**Majda Thurnher AT, Meike Vernooij, NL**
10:15-10:35	Radiomics: new source of biomarkers *Marion Smits, NL*
10:35-10:55	Imaging biomarkers for movement disorders *Stephane Lehericy, FR*
10:55-11:15	Imaging biomarkers for Multiple Sclerosis, AntiMOG and AntiAQP4 disease *Alex Rovira, ES*
11:15 -11:35	Imaging biomarkers for vascular disease *Rolf Jager, UK*
11:35 – 11:55	Imaging biomarkers for dementia *Meike Vernooij, NL*
11:55 – 12:15	Imaging biomarkers in mental disorders *Jean Pierre Pruvo, FR*
12:15 – 14:00	**Lunch Break**
14:00-16:00	**Individualized and Precision Medicine in tumors**
Moderators:	**Cem Calli, Alex Rovira**
14:00-14:20	Imaging biomarkers in epilepsy *Nuria Bargallo, ES*
14:20-14:40	Imaging biomarkers for gliomas *Alberto Bizzi, IT*
14:40-15:00	Imaging biomarkers for pediatric brain tumors *Andrea Rossi, IT*
15:00 – 15:20	Individual patient treatment decision in gliomas *Hugues Duffau, FR*
15:20 -15:40	Imaging biomarker in autoimmune diseases *Pia Maly Sundgren, SE*
15:40 – 16:00	Quantitative imaging in Head and Neck *Sotirios Bisdas, UK*
16:00 – 16:30	**Coffee Break**
16:30-18:00	**Individualized and Precision Medicine in stroke**

THURSDAY 15th September 2022 - Meeting room 2

ADVANCED COURSE IN INTERVENTIONAL NEURORADIOLOGY: Individualized and Precise Neuroradiology

10:15-12:15	**Session title: Individualized and Precision Medicine in hemorrhagic stroke**
Moderators:	**Tommy Andersson, Charbel Mounayer**
10:15-10:35	Subarachnoid hemorrhage: outcome factors *Vitor Pereira, CA*
10:35-10:55	Treatment of unruptured intracranial aneurysms: a patient-based decision *Michihiro Tanaka, JP*
10:55-11:15	Treatment of ruptured intracranial aneurysms: a patient-based decision *Rene van der Berg, NL*
11:15-11:35	Flow diversion: individualized based decision *Saruhan Cekirge, TR*
11:35 – 11:55	Dural AVF controversies: individualized treatment decision *Tommy Andersson, SE*
11:55 – 12:15	AVM Controversies: individualized treatment decision *Charbel Mounayer, FR*
14:00- 16:00	**Individualized and Precision Medicine in acute arterial and venous stroke**
Moderators:	**Mario Muto, Georges Rodesch**
14:00-14:20	Individualized treatment in pediatric intracranial vascular diseases *George Rodesch, FR*
14:20-14:40	Venous thrombosis: who may benifit from EV treatment *Seon Kyu Lee, US*
14:40-15.00	Personalized and precise thrombectomy: what is better for my patient? *Tommy Andersson, SE*
15:00-15:20	Arterial dissection (and AIS): who, when and how to treat? *Arnd Doerfler, DE*
15:20 –15:40	Extracranial and intracranial stenosis: individualized patient decision *J Guilherme Pereira Caldas, BR*
15:40 – 16:00	Personalized and precise medicine in Percutaneous Spine treatment decision *Mario Muto, IT*
16:00-16:30	**Coffee Break**
Moderators:	**Tarek Yousry UK, Pedro Vilela PT**
16:30-17:00	Precision Medicine in Stroke *Catarina Fonseca, PT*
17:00-17:30	Individualized treatment decision in hemorrhagic stroke *Naci Koçer, TK*
17:30-18:00	Individualized treatment decision in acute ischemic stroke *Jens Fiehler, DE*

FRIDAY 16th September 2022 – Meeting room 1

08:00 – 08:30	Interactive cases *Clive Sperryn, Tracy Kilborn, Rui Duarte Armindo*
08:30 – 10:00	**ESNR - ASPNR SESSION: Pediatric neuro imaging session**

Moderators:	**David Mirsky, US, Chen Hoffmann**
08:30 – 08:50	Pediatric ischemic stroke *Manohar Shroff, US*
08:50 – 09:10	Pediatric Spinal Cord Stroke *V. Michelle Silvera, US*
09:10 – 09:30	Neonatal ischemic and hemorrhagic stroke: pitfalls and peculiarities *Nadine Girard, FR*
09:30 -09:50	Stroke mimics in children- exercise caution! *Kish Mankad, UK*
10:00 – 10:30	**Coffee Break**
10:30 – 12:00	**Opening Ceremony**
12:00 – 13:30	**Lunch**
13:30 - 14:00	**Keynote Lecture: The connectomal anatomy of the human brain** *Hugues Duffau /Fr*
14:00 -15:50	**Session*:* Glioma imaging**
Moderators:	**Marion Smits, NL, Paulina Due-Tonnessen**
14:00 – 14:10	Introduction: Glioma imaging challenges *Marion Smits, NL*
14:10 -14:30	The WHO classification and morphological evaluation of gliomas *Victor Suarez, ES*
14:30- 14:50	The neurosurgical perspective of glioma imaging *Domingos Coiteiro, PT*
14:50-15:10	Imaging pitfalls of cortical and low grade primary tumours *Nicoletta Anzalone, IT*
15:10-15:30	Advanced imaging techniques for pretreatment glioma evaluation *Paulina Due-Tønnessen, NO*
15:30-15:50	Advanced imaging techniques for posttreatment glioma evaluation *Renato Hoffmann, BR*
15:50 -16:20	**Coffee Break**
16:20 -18:00	**Session: Imaging in Neuroinflamation**
Moderators:	**Majda Thurnher, Philippe Demaerel**
16:20 -16:45	Advanced imaging in inflammation *Majda Thurnher, AT*
16:45 – 17:10	Pediatric encephalitis *Maria Argyropoulou, GR*
17:10 – 17:35	Viral and autoimmune encephalitis *Philippe Demaerel, BE*
17:35 – 18:00	Chronic inflammation in multiple sclerosis *Alex Rovira, ES*
18:00 – 18:30	**Covid Update**
18:00 – 18:15	Acute and Long Covid update *Stephane Kremer, FR*
18:15 – 18:30 SS	Oral papers on Covid
18:30 – 19:30	**EBNR DIPLOMA Ceremony**

FRIDAY 16th September 2022 – Meeting room 2

08:30 -10:00	**Session: Typical imaging findings of uncommon adult diseases**
Moderators:	**Turgut Tali, Fabrice Bonneville**
08:30 – 08:48	Pineal gland tumors *Fabrice Bonneville, FR*
08:48 – 09:06	Uncommon Intracranial infections *Carolina Tramontini, CO*
09:06 – 09:24	Uncommon adult brain tumors *Charles Romanowski, UK*
09:24 – 09:42	Adult onset of leukodystrophies *Leandro Lucato, BR*
09:42 – 10:00	Toxic and acquired metabolic brain lesions *Luc van de Hauwe, BE*
10:00 -10:30	**Coffee Break**
12:00 – 13:30	**Lunch**
14:00 – 16:00	**Session: Advanced MRI Techniques**
Moderator:	**Greg Zaharchuk /US**
14:00 – 14:20	Brain perfusion: ASL primetime? *Greg Zaharchuck, US*
14:20 – 14:40	ASL imaging beyond perfusion *Henk Musaerts, NL*
14:40 – 15:00	ASL in clinical practice *Rolf Jager, UK*
15:00 – 15:20	ASL - BOLD combined imaging *Yang Wang, US*
15:20 – 15:40	Resting State fMRI and brain connectivity: from research methods to clinical practice *Andrei Holodny, US*
15:40 – 16:00	CEST (Chemical Exchange Saturation Transfer) *Linda Knutsson, SE*
16:00 – 16:20	**Coffee Break**
16:20 – 18:00	**Session: Typical imaging findings of uncommon pediatric diseases**
Moderators:	**Nadine Girard, Chen Hoffmann**
16:20 -16:40	Pediatric relapsing demyelinating syndromes *Chen Hoffmann, IL*
16:40 -17:00	Infections on pediatric population *Leandro Lucato, BR*
17:00 -17:20	Congenital syndromic malformations *Leonardo Macedo, BR*
17:20 -17:40	Basal ganglia disorders in children *Zoran Rumboldt, HR*
17:40 - 18:00	In Memoriam Zoltan Patay
18:00 – 18:30	**Session: Glymphatic system update**
Moderators:	**Tatjana Stosic - Opincal, Geir Ringstad**
18:00 – 18:15	Human brain extra-vascular pathways and molecular clearance function assessed with CSF tracer (gMRI) *Geir Ringstad, NO*

18:15 – 18:30	Glymphatic MR imaging – a new clinical application of GBCAs *Alexander Radbruch, DE*

FRIDAY 16th September 2022 – Meeting room 3

08:30 -10:00	**Session: Acute Arterial Stroke**
Moderators:	**Wim van Zwam, Arnd Doerfler**
08:30 – 09:00	Trials: What have we learned and what must we do better *Wim van Zwam, NL*
09:00 – 09:30	Imaging-based patient selection for mechanical thrombectomy *Arnd Doerfler, DE*
09:30 – 10:00	The technical essentials of mechanical thrombectomy: overview and update *Luisa Biscoito, PT*
10:00 -10:30	**Coffee Break**
12:00 – 13:30	**Lunch**
14:00 – 16:00	**Session: Arteriovenous malformations, dural fistulae**
Moderators:	**Naci Kocer, TR, Vitor Pereira**
14:00 – 14:20	Dural AVF venous drainage: patterns of risk and embryological considerations *Misihiro Tanaka, JP*
14:20 – 14:40	Tinnitus behond dural AVF: new treatment options *Vitor Pereira, CA*
14:40 – 15:00	Dural AVF classification and effective treatment strategy *Salvatore Mangiafico, IT*
15:00 – 15:20	Transarterial bAVM treatment: the solution for better outcomes? *Isil Saatci, TR*
15:20 – 15:40	Transvenous bAVM treatment: the solution for better outcomes? *Charbel Mounayer, FR*
15:50 – 16:20	**Coffee Break**
16:20 – 18:00	**Session: Interventional Spine**
Moderators:	**Luigi Manfre, Joshua Hirsch**
16:20 -16:30	Introduction *Luigi Manfre, Joshua Hirsch*
16:30 -16:50	Once upon the time there was the T1 Spin-Echo: the metamorphosis of CT and MRI in Spine diagnosis *Johan Van Goethem, BE*
16:50 -17:10	Spinal imaging: What is there and what is missing can be the key to the latest interventional treatments *Allan Brook, US*
17:10 -17:30	How Diagnostic can change Interventional: Weight Bearing MR Imaging and Spine Interventions *Luigi Manfre, IT*
17:30-17:50	What we inject and what we will in the Future: how the evolution of biomaterials will change vertebral Augmentation *Alexis Kelekis, GR*
18:00 – 18:30	**Session: New horizons in the angio room**

Moderators:	**Zulejha Merhemic, SK Lee**
18:00 – 18:15	Subdural hematomas *SK Lee, US*
18:15 – 18:30	Digital subtraction myelography *Pasquale Mordasini, CH*

FRIDAY 16th September 2022 – Meeting room 4

08:30 – 10:00	**Scientific Session I - oral presentations Head&Neck**
Moderators:	**J Carlos Bustelo, Catarina Brito**
08:30 – 08:45	Best imaging prognostic features for head and neck tumors *J Carlos Bustelo, ES*
08:45 – 10:00	Oral papers
10:00 -10:30	**Coffee Break**
12:00 – 13:30	**Lunch**
14:00 – 15:50	**Scientific Session II - oral presentations Spine**
Moderators:	**Mario Muto, Ana Mafalda Reis**
14:00 – 14:15	Radiofrequency on spine metastasis *Mario Muto, IT*
14:15 -15:50	Oral papers
15:50 -16:20	**Coffee Break**
16:20-18:00	**Scientific Session III - oral presentations Tumors**
Moderators:	**Anouk van der Hoorn, Chiara Gaudino**
16:20- 16:45	Radiotherapy brain efffects: imaging overview *Anouk van der Hoorn, NL*
16:45 – 18:00	Oral papers

SATURDAY 17th September 2022 – Meeting Room 1

08:00 – 08:30	Interactive cases *Pedro Vilela / Antônio José da Rocha / Jasmina Boban*
08:30 – 10:00	**Session: Non acute Brain Ischemia**
Moderators:	**Rolf Jager, Pedro Vilela**
08:30 – 08:40	Introduction *Rolf Jager, UK*
08:40 – 09:00	SV White Matter disease: the neurologist perspective *Miguel Viana Baptista, PT*
09:00 – 09:20	Imaging findings in Small Vessel Disease *Alexander Krainik, FR*
09:20 – 09:40	Imaging findings in inflamatory vascular diseases *Rolf Jager, UK*
09:40 – 10:00	CVR (cerebral vasoreactivity) assessment *Jeroen Hendrikse, NL*
10:00 – 10:30	**Coffee Break**
10:30 – 12:00	**Session: ESNR meets Greece** **Eftixia Kapsalaki / Maria Argyropoulou**
12:00 – 13:30	**Lunch Break**

13:30 – 14:00	**Keynote Lecture: Mentorship in science** *Pia Maly Sundgren, SE*
14:00 – 15:50	**ESNR / ASNR Joint Session**
Moderator:	**Pia Maly Sundgren, SE**
14:00 – 14:25	Features to distinguish abusive from accidental head trauma *Michele Johnson, US*
14:25 – 14:50	Anterior corner hyperextension injuries of the neck *Jason Talbott, US*
14:50 – 15:15	Artificial Intelligence in trauma imaging *Larry Tanenbaum, US*
15:15 – 15:40	How to report brain trauma. International consensus recommendations regarding the practical implementation of common data elements for traumatic brain injury *Paul Parizel, AU*
15:40 -15: 50	Discussion
15:50 – 16:20	**Coffee Break**
16:20 – 17:20	**Session: Head and Neck imaging session**
Moderator:	**Eftychia Kapsalaki**
16:20 – 16:40	MRI protocols for pediatric Head and Neck diseases: do it right *Felice D'Arco, UK*
16:40 – 17:00	MR Neurography in the Head and Neck *Felix Kuhn, CH*
17:00 – 17:20	Endolymphatic hydrops - more than Meniere disease *Bernhard Schuknecht, CH*
17:30 – 19:00	**ESNR General Assembly**

SATURDAY 17th September 2022 – Meeting room 2

08:30 – 10:00	**Head and Neck imaging session**
Moderators:	**Jan Casselman, Leon van Rensburg**
08:30 – 08:40	Introduction *Leon van Rensburg, ZA*
08:40 – 09:00	Otalgia and hearing impairment *Jan Casselman, BE*
09:00 – 09:20	Pulsatile tinnitus *Katarina Surlan Popovic, SL*
09:20 – 09:40	Facial pain *Sofie Van Cauter, BE*
09:40 – 10:00	Vision impairment *Teresa Nunes, PT*
10:00 – 10:30	**Coffee Break**
12:00 – 13:30	**Lunch Break**
14:00 – 15:50	**Session: Imaging of the mind**
Moderators:	**Jean Pierre Pruvo, Nuno Sousa**
14:00 – 14:20	Introduction *Jean Pierre Pruvo, FR*
14:20 - 14:40	Stress and brain *Nuno Sousa, PT*

14:40 - 15:00	Current applications of MRI in psychotic events *Riyad Hanafi, FR*
15:00 - 15:20	Functionnal connectivity in bipolar disorders *Sidney Krystal, FR*
15:20 - 15:40	Applications of artificial intelligence in normal brain aging and psychiatry: ready for useful biomarker, *Renaud Lopes, FR*
15:40 - 15:50	Discussion
15:50 – 16:20	**Coffee Break**
16:20 – 17:20	**Session: MR meets PET in neuroimaging**
Moderators:	**Frederic Barkhof, Karl Lovblad**
16:20 – 16:40	Introduction to PET MR in neuroimaging *Karl Lovblad, CH*
16:40 – 17:00	Neuroimaging in dementia from MRI, PET to AI *Frederik Barkhof, NL*
17:00 – 17:20	PET MR in neurooncology *Heather Martin, SE*

SATURDAY 17th September 2022 – Meeting Room 3

08:30 – 10:00	**INR: Intracranial Aneurysms**
Moderators:	**Vitor Pereira, Laurent Spelle**
08:30 – 08:45	Is simple coilling old fashioned? *Laurent Spelle, FR*
08:45 – 09:00	Is stenting in the acute SAH phase unsafe? *Markus Moehlenbruch, DE*
09:00 – 09:15	Dissecting aneurysms: diagnosis and treatment challenges *Civan Islak, TR*
09:15 – 09:30	Blister aneurysms: diagnosis and treatment *Vitor Pereira, CA*
09:30 -09:45	Bifurcation aneurysms: which is the best EV approach? *Isil Saatci, TR*
09:45 – 10:00	Giant aneurysms: the ultimte challenge *Hubert Desal, FR*
10:00 – 10:30	**Coffee Break**
12:00 – 13:30	**Lunch Break**
14:00 – 15:50	**Session: INR: AIS**
Moderators:	**Hubert Desal, Juan Macho**
14:00 – 14:15	Balloon, Aspiration, Stent Retriever: what really matters *Antonin Krajina, CZ*
14:15 – 14:30	Distal Arterial Occlusions treatment *Alejandro Tomasello, ES*
14:30 -14:45	Vertebrobasilar AIS: what is the best stategy *Birgitta Ramgren, SE*
14:45 – 15:00	MT failure: causes and solutions *Juan Macho, ES*
15:00 – 15:15	Stenting in the acute setting of stroke (tandem/intracranial) *Pasquale Mordasini, CH*

15:15 – 15:30	How to deal with MT complications *Omer Eker, FR*
15:30 – 15:45	Pedriatric AIS treatment *Peter Sporns, NL*
15:50 – 16:20	**Coffee Break**
16:20 -17:20	State of the art Session: Vessel Wall Imaging
Moderator:	**Rolf Jager, Myriam Edjlali**
16:20 - 16:35	Technical considerations, use and pitfalls of VW MRI and applications in intracranial Aneuryms *Myriam Edjlali-Goujon, FR*
16:35 - 16:50	VW MRI and stroke applications *Jennifer Linn, DE*
16:50 - 17:05	VW MRI in intracranial vasculitis: is it the prime time? *Renato Hoffmann, BR*
17:05 - 17:20	VW MRI cases of the year *Majda Thurnher, AT*

SATURDAY 17th September 2022 – Meeting room 4

08:30 – 10:00	**Scientific Session IV- oral presentations Degenerative, demyelinating, infectious**
Moderators:	**Roberto Gasparotti, Teresa Nunes**
08:30 – 08:45	Susceptibility imaging in clinical practice *Roberto Gasparotti*
08:45 – 10:00	Oral papers
10:00 – 10:30	**Coffee Break**
12:00 – 13:30	**Lunch Break**
14:00 – 15:50	**Scientific Session V- oral presentations Cerebrovascular diseases**
Moderators:	**Jerome Hodel, FR, Pedro Melo Freitas**
14:00 – 14:15	Transient ischemic attack imaging *Jerome Hodel, FR*
14:15 – 15:50	Oral papers
15:50 – 16:20	**Coffee Break**
16:20 – 17:20	**Scientific Session VI- oral presentations Pediatric imaging**
Moderators:	**Gennaro D'Anna, IT, Sandra Matias**
16:20 – 16:45	Education, branding and networking with the media: A guide for Neuroradiologists *Gennaro D'Anna, IT*
16:45 – 17:20	Oral papers

SUNDAY 18th September 2022, Meeting Room 1

08:30 – 09:00	Interactive Cases *Majda Thurnher / Luc van den Hauwe / Domenico Tortora*
09:00 – 10:30	**Session: Artificial intelligence in Neuroimaging**

Moderators:	**Lajos Rudolf Kozák, Sven Haller**
09:00 – 09:20	The R-AI-DIOLOGY checklist: a practical checklist for evaluation of Artificial Intelligence tools in clinical neuroradiology *Sven Haller, CH*
09:20 – 09:40	AI in clinical neuroradiology: essential medicolegal basis and regulations *Alexander Radbruch, DE*
09:40 – 10:00	AI and automatic tools for acute ischemic stroke diagnosis: why 6 seconds ? *Dennis Hedderich, DE*
10:00 – 10:20	Automatic volumetry and lesion segmentation in neurodegeneration and MS: truly an added value? *Christian Federau, CH*
10:20 – 10:30	Discussion
10:30 – 11:00	**Coffee Break**
11:00 – 12:00	**Juniorsconnected@ESNR: get together**
11:00 - 11:15	How to start your own fMRI and DTI program *Andrej Holodny, US*
11:15 - 11:30	Tumor preoperative fMRI *Sofie van Cauter, BE*
11:30 - 11:45	On the role of intrinsic connectivity networks in clinical fMRI evaluation *Lajos Rudolf Kozák, HU*
	Open discussion
12:00 – 13:00	**Closing Ceremony**

SUNDAY 18th September 2022, Meeting room 2

Moderators:	**Turgut Tali, Eftychia Kapsalaki**
09:00 - 10:30	**My best pitfalls in neuroimaging**
09:00 - 09:15	Perfusion MR imaging *Cem Calli, TR*
09:15 - 09:30	Ictal / periictal MR imaging *Eftychia Kapsalaki, GR*
09:30 - 09:45	Lymphoma *Martina Špero, HR*
09:45 - 10:00	Head and neck emergency imaging *Chiara Gaudino, IT*
10:00 - 10:15	Spinal cord lesions *Seamus Looby, IE*
10:15 - 10:30	Spine infections *Turgut Tali, TR*
10.30-11.00	**Coffee break**
11:00 - 12:00	**Scientific Session VIII- oral presentations**

SUNDAY 18th September 2022, Meeting room 3

09:00 - 10:30	**Scientific Session VII- oral presentations Interventional**
09:00 – 09:15	My best pitfalls in Mechanical thrombectomy *Kamil Zelenak, SK*
09:15 – 10:30	Oral papers

ORAL PRESENTATIONS

1. DIAGNOSTIC – BRAIN

1-O1
USING SIMULTANEOUS PET AND ARTERIAL SPIN LABELING MRI TO MEASURE CEREBROVASCULAR REACTIVITY IN MOYAMOYA DISEASE

Moss Zhao[1], Michael Moseley[1], Gary Steinberg[1], Greg Zaharchuk[1]
[1]Stanford University, Stanford, USA

Background: Cerebrovascular reactivity (CVR) reflects the change in CBF in response to vasodilation. Studies have demonstrated that impaired CVR was associated with a higher risk of stroke. 15O-water PET has been the gold standard for CBF and CVR measurements. But it is impractical in most hospitals due to the requirement of an on-site cyclotron. ASL is a quantitative MRI technique that enables non-invasive CBF and CVR mapping.

Aim: Compare CVR measured by single- and multi-delay ASL using PET as the reference.

Methods: Data were collected from 26 Moyamoya patients (18-64 years, 16 females) using a simultaneous 3T PET/MRI system. Imaging data were acquired using single- and multi-delay ASL and 15O-water PET simultaneously at baseline and 15 minutes after the injection of acetazolamide. Gd-based PWI was acquired at the end of each imaging session. CBF of PET was computed using the single-compartment pharmacokinetic model; CBF of ASL was computed using the general kinetic model. CVR was computed as the percentage of CBF change compared with baseline CBF. Paired t-tests were performed to compare the mean CVR between the affected and unaffected territories.

Results/Conclusions: Our quantitative analysis showed that the CVR of the affected regions was significantly lower than the normal regions (by 68%, 52%, and 56% for PET, single-PLD PCASL, and multi-PLD PCASL respectively). Both single and multi-delay ASL were effective in detecting impaired CVR in Moyamoya patients. Multi-delay can potentially replace Gd-based PWI in stroke imaging.

1-O2
LANGUAGE REORGANIZATION IN PATIENTS WITH LEFT-HEMISPHERIC GLIOMAS IS ASSOCIATED WITH INCREASED CORTICAL VOLUME IN LANGUAGE-RELATED AREAS AND IN THE DEFAULT MODE NETWORK

Luca Pasquini[1,2], Mehrnaz Jenabi[1], Kyung Peck[1], Andrei Holodny[1,3]
[1]Memorial Sloan Kettering Cancer Center, New York, USA.
[2]Sant'andrea Hospital, La Sapienza University, Rome, Italy.
[3]Weill Medical College of Cornell University, New York, USA

Background: Language function may reorganize to overcome tumor invasion. However, it is unclear if functional reorganization is associated with structural modifications of the cortex. We investigated the cortical volume of atypical language dominant (AD) patients with left-hemispheric high-grade (HGG) and low-grade glioma (LGG).

Materials and Methods: We recruited left frontal-insular gliomas with fMRI and 3DT1-weighted images. We calculated hemispheric laterality (LI), defined as: AD if LI<0.2; left-dominant (LD) if LI>=0.2. We measured cortical volume in three voxel-based morphometry (VBM) analyses: total AD vs. LD patients; AD vs. LD patients with HGG; AD vs. LD patients with LGG. Minimum threshold of t-score=2 ($p<0.05$) was applied to identify significant voxel clusters >5mm3.

Results: We recruited 119 patients (44 LGG, 75 HGG; 64/119 AD, 55/119 LD). VBM demonstrated significantly increased cortical volume in AD vs. LD patients in the right inferior frontal gyrus (IFG), right superior temporal gyrus (STG), right insula, right fusiform gyrus (FG), right precentral gyrus, right temporal-parietal junction, right posterior cingulate cortex (PCC), right hippocampus, bilateral cerebellum. AD patients with HGG showed the same areas of increased cortical volume. AD patients with LGG displayed increased cortical volume in right IFG, right STG, right insula, right FG, right anterior cingulate cortex, right PCC, right dorsal-lateral prefrontal cortex.

Conclusion: Right-sided (atypical) language activations in patients with left-hemispheric gliomas are associated with increased cortical volume. Default-mode network nodes showed greater cortical volume in AD patients regardless of the tumor grade, supporting the idea of these cortices participating in the development of language plasticity.

1-O3
LONG-TERM BRAIN EFFECTS AFTER MILD TO MODERATE COVID. AN AUSTRIAN PERSPECTIVE

Emanuele Tommasino[1], Lukas Haider[2], Majda Thurner[2]
[1]University of l'aquila, L'Aquila, Italy. [2]Medical University of Wien, Vienna, Austria

While severe forms of COVID are associated with neurological symptoms, infarcts, vasculitis, (micro) hemorrhages, PRES, cytotoxic lesions of the corpus callosum, laminar cortical lesions, leptomeningeal enhancement, encephalitis, ocular involvement, and others, it is unclear if structural abnormalities are present after mild to moderate COVID-19. In 107 consecutive individuals mean age 44 years,mean days after SARS CoV-2 infection: 160 [sd: 102], hospitalized:non-hospitalized = 30:77) and 50 sex- and age-matched matched controls, a 3 T MRI of the brain was performed. The study protocol included standard and advanced MRI sequences to analyze the presence of structural brain abnormalities.
The frequency of white-matter hyperintensities consistent with small-vessel disease did not differ between subjects after mild-to-moderate COIVD-19 and matched controls. In a sub- analysis within the COVID-19 cohort, comparing hospitalized vs. non-hospitalized subjects, similarly, no difference was found (p= 0.500). Enlarged perivascular spaces were noted in both groups, and the total number of perivascular spaces was not significantly different between COVID-19 and controls. White-matter hyperintensities were correlated with perivascular spaces, R= 0.35 (95% confidence interval: 0.07 – 0.58, p-value= 0.0171) and age in subjects post COVID-19, R= 0.49 (95% confidence interval: 0.24 – 0.68, p-value= 0.0004).Patient-reported subjective
Our findings indicate that, in mild-to-moderate COVID-19, after around 160 days (sd: 102), there is no morphological evidence to suggest CNS involvement with a sample size of 107.

1-O4
LOWER CLAUSTRUM VOLUMES MEDIATE COGNITIVE DEFICITS IN SCHIZOPHRENIA

David Schinz[1,2], Neubauer Antonia[1,2], Schulz Julia[1,2], Hongwei Li[1], Benita Schmitz-Koep[1,2], Aurore Menegaux[1,2], Omar Darawsha[1], Brandl Felix[1], Priller Josef[1], Jil Wendt[1], Claus Zimmer[1], Dennis Hedderich[1,2], Christian Sorg[1,2]
[1]Technical University Munich, Munich, Germany. [2]TUM-NIC Neuroimaging Center, Munich, Germany

Background: Schizophrenia is a heterogeneous psychiatric disorder characterized by so-called positive and negative symptoms with altered perceptions, behaviors and impaired basal cognitive function like attention. The modulation of cognitive processes such as consciousness and attention is a function of the claustrum, which is developmentally linked to transient Subplate Neurons (SPN) similar to schizophrenia. Therefore, we hypothesized altered claustrum structure in patients with schizophrenia, which is associated with cognitive deficits of the patients.

Methods: Claustrum volumes were automatedly segmented by convolutional neural network approach in T1-weighted anatomical MRI of 90 patients with schizophrenia and 96 healthy controls from both the COBRE database and an independent MUNICH dataset. Claustrum volumes were analyzed for both, group differences and association with symbol-coding task performance by two-sample t-test, correlation, and mediation analysis.

Results: Patients' claustrum volumes were significantly reduced for about 13.3% ($p<0.001$) and correlated with reduced symbol-coding task scores ($r = 0.347$, $p = 0.001$). Additionally, these cognitive deficits were partially mediated by lower claustrum volumes (CI, -2.37l-0.35; Figure 1).

Figure 1. Schizophrenia, claustrum, and symbol-coding task.
(A) Lower claustrum volumes in schizophrenia (SCZ) measured by voxel-based morphometry, (B) are significantly associated with lower symbol-coding task (SCT) performance, and (C) mediate the effect on altered symbol-coding tanks performance.

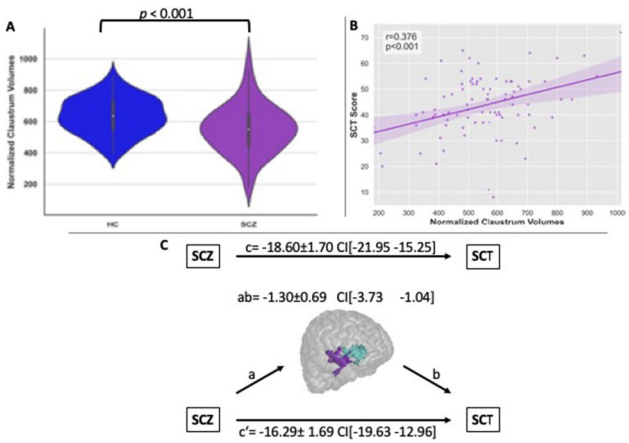

Discussion: Patients with schizophrenia have greatly reduced claustrum volumes, which are comparable with the greatest volume reductions, e.g. hippocampus, in schizophrenia and are significantly correlated with cognitive deficits. These findings fall in line with previous evidence of altered claustrum structure in neurodevelopmental disorders linked to SPN pathology. Furthermore, it corroborates the prominent role of the claustrum in basal cognitive function.

Conclusion: Significantly reduced claustrum volumes might contribute to cognitive deficits in patients with schizophrenia via SPN-pathology.

1-O5

CORRELATING MRI FEATURES WITH ADDITIONAL GENETIC MARKERS AND PATIENT SURVIVAL IN GRADE 2-3 IDH-MUTANT, 1P/19Q-INTACT INTRACRANIAL GLIOMAS

Arian Lasocki[1,2], Michael Buckland[3,4], Tahlia Molinaro[1], Jing Xie[1], James Whittle[1,2], Heng Wei[3], Frank Gaillard[5,2]
[1]Peter MacCallum Cancer Centre, Melbourne, Australia. [2]The University of Melbourne, Melbourne, Australia. [3]Royal Prince Alfred Hospital, Sydney, Australia. [4]University of Sydney, Sydney, Australia. [5]The Royal Melbourne Hospital, Melbourne, Australia

Introduction: The importance of molecular biomarkers in intracranial gliomas has led to research into correlating imaging features with tumour genotype. For example, in grade 2-3 gliomas, the T2-FLAIR mismatch sign is highly specific for an IDH-mutant, 1p/19q-intact tumour (having an isocitrate dehydrogenase mutation, but without combined loss of the short arm of chromosome 1 and long arm of chromosome 19). However, there has been less research into correlating such features with patient survival beyond just genotype. Additional molecular assessment has also recently been added to the diagnosis of IDH-mutant, 1p/19q-intact tumours, with homozygous CDKN2A/B deletion now designating a grade 4 tumor. Given the recency of this change, the literature on correlating imaging features with CDKN2A/B status in gliomas is sparse. This study correlates MRI features with CDKN2A/B status and overall survival in a cohort of IDH-mutant, 1p/19q-intact grade 2-3 gliomas.

Methods: 58 grade 2-3 adult-type diffuse gliomas with an IDH mutation and 1p/19q-codeletion were identified. CDKN2A/B results were available through next generation sequencing in 50/58 patients. Background patient data and survival data were obtained from hospital records. Preoperative MRIs were assessed independently by two neuroradiologists, with discrepancies resolved by consensus, noting the following conventional MRI features: tumour location, T2-FLAIR mismatch, well-defined tumour margins, contrast-enhancement and central necrosis. MRI features were correlated with CDKN2A/B status, type of IDH mutation (R132H-IDH1 or non-canonical) and patient survival. Survival data are presented as hazard ratios (HR) with 95% confidence intervals (CI).

Results: T2-FLAIR mismatch was present in similar proportions of tumours both with and without homozygous CDKN2A/B deletion (4/8 and 26/42, respectively). Similarly, it was present both with R132H-IDH1 mutations and non-canonical IDH mutations (30/50 and 7/8, respectively). 4/8 tumours with homozygous CDKN2A/B deletion were well-defined, only one demonstrated discrete nodular enhancement and none demonstrated central necrosis. T2-FLAIR mismatch did not influence survival (HR=0.92; p=0.977). However, well-defined tumour margins predicted longer survival (HR=0.36; 95% CI 0.16-0.79; p=0.008), while enhancement was associated with shorter survival (HR=3.86; 95% CI 1.52-9.82; p=0.004).

Conclusions: Conventional MRI features were not helpful in predicting homozygous CDKN2A/B deletion in our cohort. Despite being known to have a worse prognosis, these tumours did not exhibit more aggressive MRI appearances at initial diagnosis, thus formal molecular testing remains an important component of patient management. However, some MRI features were able to predict longer or shorter patient survival.

1-O6

DEEP-LEARNING BRAINAGE DEMONSTRATES ACCELERATED BRAIN AGING IN SYSTEMIC LUPUS ERYTHEMATOSUS PATIENTS

Grégory KUCHCINSKI[1,2,3], Theodor RUMETSHOFER[1,4], Kristoffer ZERVIDES[5], Renaud LOPES[3,6], Morgan GAUTHEROT[6], Jean-Pierre PRUVO[3,6], Anders BENGTSSON[5], Oskar HANSSON[7,8], Andreas JÖNSEN[5], Pia SUNDGREN[1,2]
[1]Department of Diagnostic Radiology, Clinical Sciences, Lund University, Lund, Sweden. [2]Lund University Bio-Imaging Center, Lund University,, Lund, Sweden. [3]Univ. Lille, Inserm, CHU Lille, U1172 - LilNCog - Lille Neuroscience & Cognition, Lille, France. [4]Department of Clinical Sciences, Division of Logopedics, Phoniatrics and Audiology, Lund University, Lund, Sweden. [5]Department of Clinical Sciences Lund, Rheumatology, Lund University, Skåne University Hospital, Lund, Sweden. [6]Univ. Lille, CNRS, Inserm, CHU Lille, Institut Pasteur de Lille, US 41 - UMS 2014 - PLBS, Lille, France. [7]Clinical Memory Research Unit, Lund University, Lund, Sweden. [8]Memory Clinic, Skåne University Hospital, Malmö, Sweden

Introduction: Systemic lupus erythematosus (SLE) is an autoimmune connective tissue disease affecting multiple organs in the human body, including the central nervous system. Among neuropsychiatric symptom, cognitive impairment is one of the most frequently reported with an estimated prevalence of at least 20%, even in patients with

normal-appearing MRI. Recently, an artificial intelligence method, called BrainAGE (Brain Age Gap Estimation), has been developed to measure the deviation of brain aging from a healthy population without cognitive or psychiatric disorders. Our aim was to provide evidence of accelerated brain aging in SLE patients using a Deep-Learning BrainAGE algorithm.

Methods: Seventy female patients with a clinical diagnosis of SLE and fulfilling 4 or more of the American College of Rheumatology classification criteria for SLE and 24 age-matched control females, free of autoimmune, neurological or psychiatric disorders, were prospectively included. All subjects underwent a 3T MRI acquisition, including a 3D-T1 sequence, a comprehensive neuropsychological evaluation and a measurement of neurofilament light protein (NfL) in plasma, a biomarker of neuronal damage. We used a BrainAGE algorithm with a 3D convolutional neural network architecture, previously trained on the 3D-T1 images of 1295 healthy female subjects from 18 to 70 years old to predict their chronological age. The trained algorithm was then applied to the 3D-T1 images of SLE patients and controls in order to compute the BrainAGE (= predicted age - chronological age). BrainAGE was compared between controls and SLE patients using a student-t test. SLE patients were divided into 2 groups according to the 2nd tertile of the BrainAGE distribution (high vs low BrainAGE). The association between high BrainAGE and (a) standardized cognitive tests scores and (b) age-adjusted plasma NfL was evaluated using logistic regression models.

Results: Mean chronological age of SLE patients and controls was 36 (+/-9) and 37 (+/-9) years, respectively (p=0.57). BrainAGE was significantly higher in SLE patients than in controls (+3.7 years, p=0.02). In SLE patients, high BrainAGE was associated with poorer cognitive performance: longer reaction times (p=0.008), lower psychomotor speed (p=0.02), processing speed (p=0.01), cognitive flexibility (p=0.049) and executive function (p=0.046). High BrainAGE was also significantly associated with higher plasma NfL, after adjusting for age (p=0.03).

Conclusion: Using a deep-learning BrainAGE algorithm, we provide evidence of accelerated brain aging in SLE patients, which reflected neuronal damage and cognitive impairment. BrainAGE could be evaluated as an additional diagnostic tool of brain involvement in SLE.

Keywords: Systemic Lupus Erythematosus, Brain Aging, Deep-learning

Figure: Illustrative cases with high versus low BrainAGE

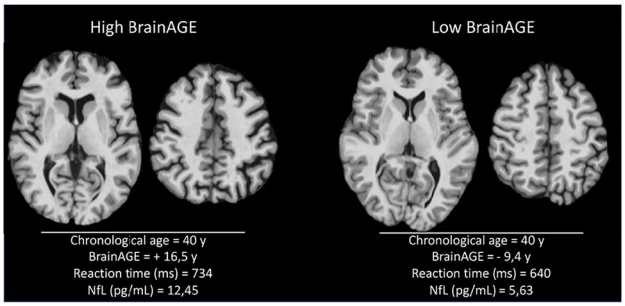

Skull-striped 3D-T1 images from 40-year patients with high (left) and low BrainAGE (right). Visual inspection demonstrates a higher level of atrophy in the high BrainAGE patient, with enlarged ventricles and sulci. The patient with high BrainAGE had also longer reaction time and higher level of neurofilament light chain (NfL) in plasma.

1-O7

ASL FOR BRAIN TUMOUR SURVEILLANCE: DO WE REALLY NEED TO CALCULATE CBF MAPS?

Wouter Teunissen[1], Anna Lavrova[2], Martin van den Bent[1], Esther Warnert[1], Marion Smits[1]
[1]Erasmus MC, Rotterdam, Netherlands. [2]University of Michigan Hospital, Ann Arbor, USA

Introduction: Perfusion MRI (pMRI) is one of the advanced MRI techniques used to distinguish between tumour progression (PD) and pseudoprogression (PsP) in patients with treated brain tumours. Arterial spin labelling (ASL) is one of the existing pMRI techniques and has been available for more than 20 years, but its clinical usage remains limited, in part due to the need for post-processing to obtain quantitative cerebral blood flow (CBF) maps from the non-quantitative perfusion weighted images (PWI). ASL has several advantages over other pMRI techniques, including the lack of need for exogenous contrast agent. Although it is expected that CBF maps and PWI maps provide similar information, our aim is to investigate that in a clinical setting. The second aim was to determine diagnostic accuracy to distinguish PD from PsP with CBF, PWI and visual assessment.

Methods: A consecutive cohort of 115 patients who underwent MRI surveillance containing ASL (all at 3T) for treated brain tumours was used. We determined the final diagnosis (PD, PsP) after ±6 months.Regions of interest were drawn in representative parts of tumours in the CBF maps and copied to the PWI. Ratios of the tumour ROI versus the normal appearing white matter were correlated and areas under the curve (AUC) were calculated to assess diagnostic accuracy. Additionally, lesions were visually classified as hypointense, isointense or hyperintense (compared to cortex intensity) and compared using a Kruskal-Wallis test. We calculated sensitivity and specificity both at a low (between hypointense and isointense) and a high (between isointense and hyperintense) threshold.

Results: A total of 173 lesions, both enhancing and non-enhancing, measured in 115 patients (93 glioma, 16 metastases and 6 lymphoma) showed a very high correlation of 0.96 (95% CI:0.88-0.99) between CBF ratios and PWI ratios. AUC was 0.76 (95%CI: 0.65-0.88) for CBF ratios and 0.72 (95%CI: 0.58-0.85) for PWI ratios. Visual assessment showed significant differences between the three categories (p<0.001; **figure**). Diagnostic accuracy of visual assessment showed a sensitivity of 57% and a specificity of 93% with a high threshold, and a sensitivity of 90% and a specificity of 67% with a low threshold.

Conclusion: PWI ratios and CBF ratios show an almost perfect correlation and comparable AUCs, therefore we suggest that quantification of CBF could be omitted. Visual classification shows that a hyperintense lesion indeed has a high CBF ratio. The high threshold, which is clinically most relevant, shows a high specificity of 93%.

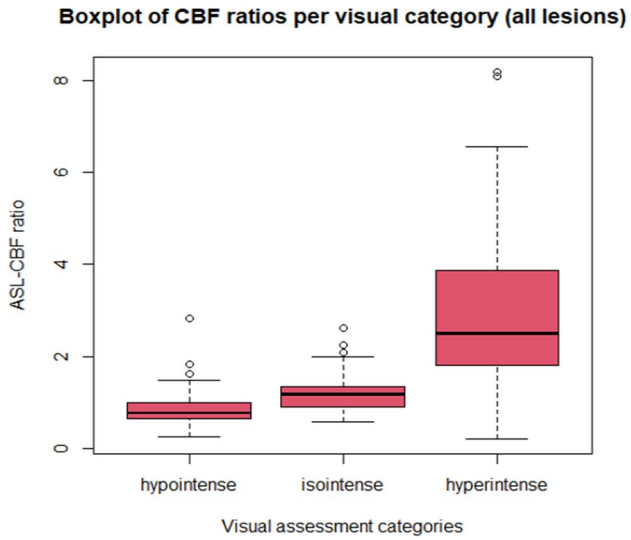

1-O8

VASARI SCORE SYSTEM IN DISCERNING BETWEEN DIFFERENT DEGREES OF GLIOMA: POSSIBLE APPLICATION IN MACHINE LEARNING

Mario Tortora[1], Laura Gemini[1], Ottavia Vargas[2], Carmine Sicignano[2], Valeria Piscitelli[2], Mariarosaria Giardiello[2], Gianvito Pace[2], Fabrizio Fasano[2], Giulia Marchello[3], Francesco Somma[2], Vincenzo D'Agostino[2], Alberto Negro[2]
[1]Dipartimento di Scienze Biomediche Avanzate - Università degli Studi di Napoli Federico II, Napoli, Italy. [2]UOC Neuroradiologia - Ospedale del Mare, Napoli, Italy. [3]Universitè Côte d'Azur, Inria, CNRS, Laboratoire J.A.Dieudonné, Nice, France

Introduction: The aim of our study is to evaluate the capacity of Vasari Score System in discerning between the different degrees of glioma with possible application in machine learning.

Methods: A retrospective study was conducted on 125 patients with glioma (M/F = 74/51; mean age: 55.30) of which we obtained the histological grade: G1 (1.6%), G2 (16.8 %), G3 (14.4%), G4 (67.2%). Each patient was analyzed blinded by two "resident" and a neuroradiologist with 10 years of experience with the evaluation of the 25 features of VASARI. Interobserver agreement was assessed by estimating ICCs (mild: <0.2; fair: 0.2-0.4; moderate: 0.4-0.6; substantially good: 0.6-0.8; excellent:> 0.8). The statistical analysis was conducted by looking for statistically significant differences for each VASARI characteristic between two groups (low grade: G1 and G2; high grade: G3 and G4). In particular, for each covariate we evaluated the distribution of the observations with box-plot and bar-plot. We then performed a univariate logistic regression to see the influence of the "VASARI" variable in the prediction of the "degree" response variable. Additionally, we performed a Wald test. We then calculated the Odd ratios and confidence intervals for each variable and the evaluation matrices with ROC curves in order to identify cut-off values, predictive of grade diagnosis.

Results: An excellent ICCs estimate (0.91) was obtained. There were statistically significant differences (p < .05) between the two study groups for: degree of post-contrast impregnation (F4); percentage of impregnating (F5), not impregnated (F6) and necrotic (F7) tissue. There are no statistically significant differences (p> .05) for the remaining VASARI features. From F4, a value of 3 has a 91% probability of being in the "high grade" group while the other two values' probability is much lower (56%). This model presents: accuracy 0.776; sensitivity 0.804; specificity 0.652; AUC 0.73. At the same time, from F5, a value of 5 as cut-off

to identify the "high grade" shows: accuracy 0.792; sensitivity 0.873; specificity 0.435; AUC 0.677. From F6, a value of 6 has a 100% probability of being in the "high grade" level with: accuracy 0.736; sensitivity 0.745; specificity 0.696; AUC 0.757. From F7, a value of 4 as a cut-off shows: accuracy 0.712; sensitivity 0.706; specificity 0.739; AUC 0.738.

Discussion & Conclusion: Specific resonance characteristics can be used to predict glioma grade with important prognostic implications. Standardization of these data, correlated with molecular profiles, can be used for the programming of Machine Learning software.

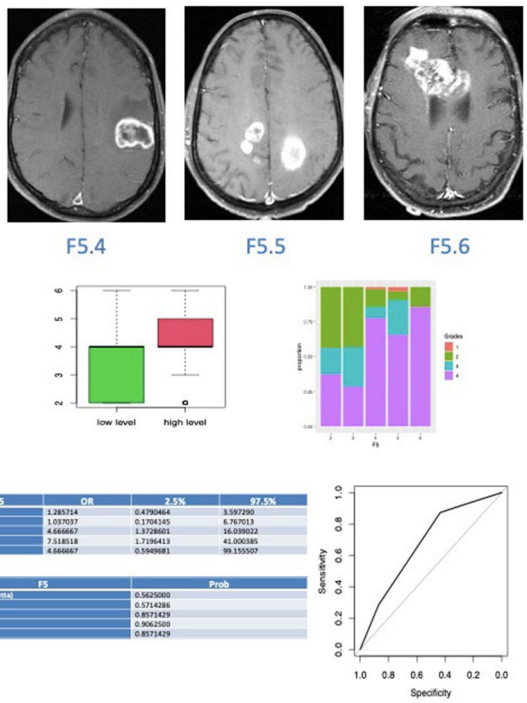

F5	OR	2.5%	97.5%
F5.2	1.285714	0.4790464	3.597290
F5.3	1.037037	0.1704145	6.767013
F5.4	4.666667	1.3728601	16.039022
F5.5	7.518518	1.7196413	41.000385
F5.6	4.666667	0.5949681	99.155507

F5	Prob
F5.2 (intercetta)	0.5625000
F5.3	0.5714286
F5.4	0.8571429
F5.5	0.9062500
F5.6	0.8571429

An example of the statistical evaluations carried out for each VASARI characteristic. In particular, the evaluation of the F5 (percentage of impregnating neoplastic tissue) is illustrated.

1-O9

PREOPERATIVE MRI CHARACTERIZATION OF MOLECULARLY DEFINED GLIOBLASTOMAS.

Anna Latysheva
Oslo University Hospital- Rikshospitalet, Oslo, Norway

Introduction: Diffuse astrocytic glioma, IDH-wildtype, with molecular features of glioblastoma are described as diffuse glioma, IDH-wildtype, without vascular proliferation or necrosis but bearing a molecular signature of glioblastoma according to the 2021 WHO classification of tumors of the central nervous system, 5th edition. The absence of classic MRI findings (irregularly shaped lesion with peripheral contrast-enhancement and central necrosis) in such tumors makes it challenging to differentiate those neoplasms from low-grade gliomas. The aim of this study was to search for specific radiological characteristics that would allow identification of these glioblastomas, defined solely on the basis of molecular features that might be helpful for individualized treatment and prognosis prediction.

Materials and Methods: Twenty-five features from the Visually Accessible Rembrandt Image (VASARI) and three internally derived MRI features were assessed in 63 adult patients with untreated diffuse glioma, included 22 diffuse astrocytic gliomas, IDH-wildtype, with molecular features of glioblastoma (CNS WHO grade 4) and 41 diffuse gliomas WHO grade 2 and 3. The Mann-Whitney U-test and logistic regression were used to assess the ability of MRI features to identify glioblastomas, defined based on molecular features only.

Results: Multifocal or multisentric presentation, affection of central structures such as basal ganglia, thalamus, ependymal and gyriform infiltration were most frequently observed features in molecular glioblastomas, but none of the MRI features showed significant correlation.

Conclusion: This study showed the limitations of conventional radiogenomics to identify molecularly defined glioblastomas. Further studies using quantitative imaging features might be helpful to predict these tumors.

1-O10

DSC MRI DETECTS ABNORMAL CEREBRAL PERFUSION IN PATIENTS WITH SYSTEMIC LUPUS ERYTHEMATOSUS WITH AND WITHOUT NEUROPSYCHIATRIC MANIFESTATIONS

Tim Salomonsson[1], Theodor Rumetshofer[1,2], Anders Bengtsson[3], Kristoffer Zervides[3], Malte Knutsson[1], Ronnie Wirestam[4], Jimmy Lätt[5], Andreas Jönsen[3], Linda Knutsson[4,6,7], Pia C. Sundgren[1,5,8]
[1]Department of Clinical Sciences/Radiology, Lund University, Lund, Sweden. [2]Department of Clinical Sciences/Division of Logopedics, Phoniatrics and Audiology, Lund University, Lund, Sweden. [3]Department of Clinical Sciences/Rheumatology, Lund University, Skåne University Hospital, Lund, Sweden. [4]Department of Medical Radiation Physics, Lund University, Lund, Sweden. [5]Department of Medical Imaging and Physiology, Skåne University Hospital, Lund, Sweden. [6]Russell H. Morgan Department of Radiology and Radiological Science, Johns Hopkins University School of Medicine, Baltimore, MD, USA. [7]F.M. Kirby Research Center for Functional Brain Imaging, Kennedy Krieger Institute, Baltimore, MD, USA. [8]Lund University Bioimaging Center, Lund University, Lund, Sweden

Keywords: SLE, Cerebral perfusion, DSC MRI, White matter hyperintensities.

Introduction: Dynamic susceptibility contrast MRI (DSC MRI) has previously shown cerebral perfusion alterations in patients with systemic lupus erythematosus (SLE) compared to healthy controls (HC), however the results have been inconclusive. Additionally, white matter hyperintensities (WMHs) are common MRI findings in SLE patients, however they are non-specific with a pathophysiology that is not fully understood. Considering these scattered findings, this study investigated perfusion based measures in different regions of interest (ROIs) and WMHs in SLE patients and compared the findings with HC. The SLE cohort was also divided into subgroups based on neuropsychiatric manifestations (NPSLE and non-NPSLE).

Methods: Conventional and DSC MRI were performed on a 3T scanner (Skyra, Siemens, Erlangen, Germany) in a cohort of 64 SLE patients (38 NPSLE, 26 non-NPSLE) and compared to 19 HC. Perfusion based parameters such as cerebral blood flow (CBF), cerebral blood volume (CBV), mean transit time (MTT) and blood brain barrier (BBB) permeability estimates (K2) were calculated using tracer-kinetic modeling with leakage correction (only for SLE patients). CBF, CBV and MTT were normalized with the left middle cerebellar peduncle and measured in 26 ROIs, and alongside K2 in manually segmented WMHs and normal appearing white matter (NAWM) in the bilateral centrum semiovale. Statistical analyses were done using SciPy 1.2.1 (RRID:SCR_008058), and Bonferroni correction was applied to account for multiple comparisons.

Results: The differences in SLE compared to HC are summarized in Table 1. The most prevalent finding was a significantly decreased MTT, primarily obtained in gray matter (GM) regions including the insula, posterior thalamus, hypothalamus, cingulate gyrus, basal ganglia; frontal and parietal GM, with corresponding trends of increased CBF and decreased CBV. Similar patterns were found in both NPSLE and non-NPSLE patients compared to HC, however no significant differences were seen between NPSLE and non-NPSLE. Additionally, significantly increased CBF, CBV, MTT, and K2 were detected in WMHs compared to NAWM in the SLE patients (Figure 1).

Conclusion: In this study, we found that SLE patients regardless of neuropsychiatric manifestations exhibit alterations in cerebral perfusion related metrics compared to HC, and certain GM areas could be of particular importance when conducting future research. We are the first to our knowledge to investigate K2 in SLE, and our findings in WMHs, where especially K2 was significantly elevated, support that there is a BBB dysfunction in SLE patients that possibly
originates from inflammation and could be related to WMH formation.

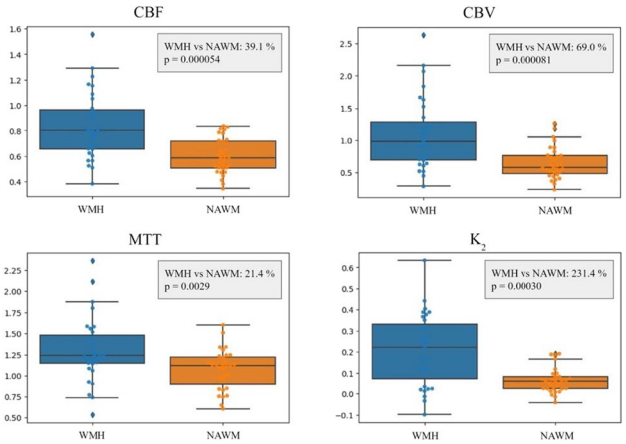

Figure 1. White matter hyperintensities (WMH) compared to normal appearing white matter (NAWM) in the systemic lupus erythematosus (SLE) cohort. K_2 and normalized cerebral blood flow (CBF), cerebral blood volume (CBV) and mean transit time (MTT) are shown with the increase in percent relative to NAWM.

Table 1. Results compared to HC in the SLE cohort. The discrepancies in normalized perfusion based measures are presented as percentages showing the increase or decrease in SLE relative to the values obtained in HC.

Region of interest	CBF		CBV		MTT	
	SLE vs HC (%)	P value	SLE vs HC (%)	P value	SLE vs HC (%)	P value
Pons	-18.5 %	0.0061	-34.6 %	0.0013	-18.9 %	0.0012
R Insula (ant.)	21.2 %	0.021	**-41.6 %**	**< 0.0001**	**-50.4 %**	**< 0.0001**
L Insula (ant.)	34.3 %	0.0011	-17.1 %	0.23	**-32.7 %**	**< 0.0001**
R insula (post.)	8.4 %	0.32	**-39.5 %**	**0.00025**	**-42.7 %**	**< 0.0001**
L Insula (post.)	18.7 %	0.049	-25.0 %	0.035	**-32.2 %**	**< 0.0001**
R Hypothalamus	15.2 %	0.036	-18.0 %	0.029	**-26.4 %**	**< 0.0001**
L Hypothalamus	18.9 %	0.025	-28.7 %	0.0019	**-37.7 %**	**< 0.0001**
R Nc. caudatus	21.7 %	0.0077	-15.3 %	0.11	**-30.5 %**	**< 0.0001**
L Nc. caudatus	**45.8 %**	**< 0.0001**	-18.3 %	0.045	**-40.3 %**	**< 0.0001**
R Putamen	16.7 %	0.055	**-45.2 %**	**< 0.0001**	**-50.6 %**	**< 0.0001**
L Putamen	**37.9 %**	**0.00038**	-25.4 %	0.0030	**-41.6 %**	**< 0.0001**
R Post. thalamus	4.9 %	0.39	-26.9 %	0.0011	**-29.3 %**	**< 0.0001**
L Post. thalamus	2.8 %	0.41	**-29.6 %**	**0.00050**	**-31.7 %**	**< 0.0001**
Cingulate gyrus	3.2 %	0.26	-38.9 %	0.0044	**-37.8 %**	**< 0.0001**
Frontal GM	14.1 %	0.13	-28.6 %	0.043	**-36.1 %**	**< 0.0001**
Parietal GM	8.6 %	0.34	-20.6 %	0.17	**-23.0 %**	**0.00033**
Corpus callosum (ant.)	**40.8 %**	**< 0.0001**	8.6 %	0.12	-17.9 %	0.045
Corpus callosum (post.)	10.4 %	0.094	4.5 %	0.48	-11.7 %	0.076
R Frontal WM	-17.3 %	0.0019	**-32.2 %**	**0.00031**	-20.0 %	0.00072
L Frontal WM	1.2 %	0.38	-14.0 %	0.16	-16.4 %	0.018
R Temporal WM	9.3 %	0.19	4.8 %	0.49	-6.0 %	0.36
L Temporal WM	-6.6 %	0.27	-9.4 %	0.29	-1.7 %	0.81
R Occipital WM	-8.6 %	0.14	-29.9 %	0.0059	**-27.1 %**	**0.00048**
L Occipital WM	-19.7 %	0.0016	-24.1 %	0.010	-9.1 %	0.085
R Parietal WM	-1.9 %	0.35	-14.5 %	0.087	-18.5 %	0.0027
L Parietal WM	-0.2 %	0.40	-15.3 %	0.087	-19.5 %	0.0010

Values shown in bold were significant after correction for multiple comparisons (Bonferroni).
CBF = Cerebral blood flow, CBV = Cerebral blood volume, MTT = Mean transit time, SLE = Systemic lupus erythematosus, HC = Healthy controls, R/L = Right/Left, Ant./Post. = Anterior/Posterior, WM = White matter, GM = Gray matter, Nc. = Nucleus.

1-O11
METASTATIC GBM: RARE BUT REAL!

Valèria Richart[1], Antonio Morales-Rosa[1], Teresa Pujol[1], Laura Oleaga[1], Estela Pineda[1], Izaskun Valduvieco[1], Josep González[1], Marta García de Herreros[1], Sofía González-Ortiz[1]
[1]Hospital Clinic de Barcelona, Barcelona, Spain

Introduction: Glioblastoma (GBM) is a highly aggressive tumor with a poor prognosis that constitutes the most

frequent primary human brain tumor. Extracranial metastasis is a rare occurrence with unknown pathogenesis, but evidence has shown an increase in cases over the last decades.

Methods: The main objective of this review is to present three recent cases of metastatic glioblastoma treated at our tertiary center. In addition, we will discuss the radiological findings of extracranial metastases, their differential diagnosis, and underlying pathological mechanisms.

Results:
Case 1: 48-year-old male diagnosed with a left frontal-temporal glioblastoma. US biopsy, CT neck, and PET/CT described multiple cervical lymph nodes, lung, and bone metastases.
Case 2: 68-year-old male diagnosed with a right frontal lobe glioblastoma. Bone marrow aspiration confirmed medullar infiltration and spinal cord MR described multiple bone metastases.
Case 3: 51-year-old male diagnosed with a right temporal glioblastoma and leptomeningeal dissemination. Spinal cord MR described multiple bone metastases and enlarged cervical lymph nodes.

Discussion: Extracranial GBM metastases primarily affect the lungs, lymph nodes, and bones. The actual pathogenesis of metastatic spread remains unknown. There is currently no established standard treatment, but symptomatic treatment of these metastases can be carried out. So, radiologists have to be vigilant for the appearance of extracranial lesions and recommend appropriate imaging tests in the presence of symptoms not explained by the brain alteration.

Conclusion: Radiologists should be aware of the possibility of extracranial GMB metastases, in order to provide an early diagnosis that can change the therapeutic management and improve the quality of life of these patients.

1-O12
THE ROLE OF ARTERIAL SPIN LABELING AND DYNAMIC CONTRAST ENHANCED TECHNIQUES IN THE FOLLOW-UP OF PATIENTS WITH CENTRAL NERVOUS SYSTEM NEOPLASIA. A COMPARISON WITH THE F-DOPA PET EXAMINATION

Allegra Romano[1], Andrea Romano[1], Giulia Moltoni[1], Serena Palizzi[1], Francesco Dellepiane[1], Valentina Frezza[1], Olga Gagliardo[1], Alessandro Bozzao[1]
[1]Sapienza Università di Roma, Facoltà di Medicina e Psicologia, Dipartimento NESMOS U.O.C. Neuroradiologia Azienda Ospedaliero-Universitaria "Sant'Andrea", Rome, Italy

Introduction: To evaluate the role of magnetic resonance perfusion techniques: Arterial Spin Labeling and Dynamic Contrast Enhanced in the differential diagnosis between disease recurrence and radiation necrosis in patients with central nervous system neoplasia treated surgically and with adjuvant radio-chemotherapy.

Methods: From January and December 2021, fourteen patients with primary CNS neoplasia treated surgically and with adjuvant radio-chemotherapy and subsequent courses of chemotherapy were recruited. Patients included in the study presented an area of altered enhancement either for radiation necrosis or disease recurrence; all of them underwent an MRI examination including ASL and DCE perfusion and F-DOPA PET examination.
CBF (ASL), Ktrans, vp, ve, kep (DCE) and SUVmax, relative SUV (PET F-DOPA) values were calculated for each lesion. The lesions were classified as radiation necrosis or disease recurrence based on the clinical-radiological evolution at minimum two follow-ups. The ROC curve was calculated.

Results: Statistically significant ($p < 0.05$) higher values of CBF (ASL), Ktrans, Vp (DCE), SUVmax and SUVrel (PET) were obtained in disease recurrence compared to radiation necrosis. Among the three techniques, ASL showed the highest sensitivity and specificity (respectively 90% and 100% cut-off CBF: 31) in the differential diagnosis between the two conditions.

Discussion and Conclusion: ASL and DCE MRI perfusion can be helpful in the differential diagnosis between disease recurrence and radiation necrosis in patients with primary CNS neoplasia treated with radiotherapy. In addition to being the technique with the highest diagnostic accuracy, ASL is also the easiest to be used in clinical practice as it does not require the administration of contrast medium.

Figure 1. Patient with GBM and left anterior thalamic disease recurrence (arrows), clearly visible on the CBF perfusion map of ASL, false negative on F-DOPA PET

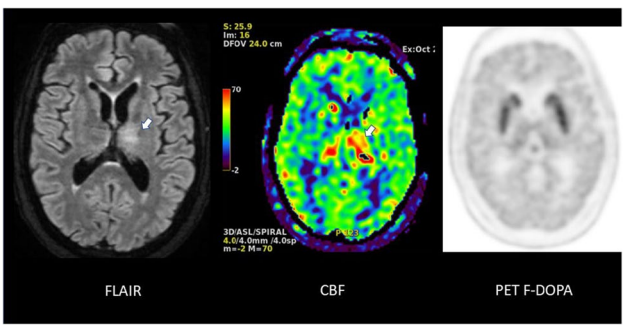

1-O13
VERTIGO – A CHALLENGE IN ACUTE STROKE PATIENTS

Liv Jorunn Høllesli[1,2], Maud Beate Børresen Halvorsen[3], Martin W. Kurz[3,4], Soffien Chadli Ajmi[3,5], Kathinka D. Kurz[1,2]
[1]Stavanger Medical Imaging Laboratory (SMIL), Department of Radiology, Stavanger University Hospital, Stavanger, Norway. [2]Department of Electrical Engineering and Computer Science, University of Stavanger, Stavanger, Norway. [3]Neurology Research Group, Department of Neurology, Stavanger University Hospital, Stavanger, Norway. [4]Department of Clinical Medicine, University of Bergen, Bergen, Norway. [5]Department of Quality and Health Technology, University of Stavanger, Stavanger, Norway
Vertigo – a challenge in acute stroke patients

Introduction: In acute ischemic stroke (AIS) rapid treatment with intravenous thrombolysis (IVT) is crucial for a good outcome. We implemented in situ simulation-based team-training, leading to a considerable reduction of median door-to-needle time (27 to 13 minutes p<0.001). In this study, we assessed the influence of faster treatment times on the number of IVT treated stroke mimics (SM), and especially the effect on those presenting with vertigo. Additionally, we assessed occurrence of intracerebral hemorrhage (ICH) after IVT.

Methods: All suspected AIS patients treated with IVT between January 1st, 2015 and December 31st, 2020 were prospectively registered. On February 1st, 2017 weekly in situ simulation-based team-training involving the complete stroke treatment chain was introduced. Patients with SM and ICH were identified after diagnostic work-up. SM patients with vertigo at onset were reassessed.

Results: From 2015 to 2020, 959 patients were treated with IVT under suspicion of acute ischemic stroke. After introduction of simulation training the number of SM treated with IVT increased significantly (15.9% vs 24.4%, p=0.003). There were no ICH complications in the SM patients before introduction of simulation-based team-training, while two SM patients suffered from asymptomatic ICH after introduction of simulation training (p=0.57). When sub-grouping SM into pre-specified categories, only the SM patients presenting with vertigo increased significantly (17.6 vs 35.3%, p<0.001).
Of the 64 patients with vertigo treated with IVT, only 25 (39.1%) were clinically sufficiently evaluated in the emergency room (ER) (including HINTS test), and 51 (79.7%) were discharged with an unspecific dizziness diagnosis. ENT doctors examined two patients acutely in the ER, and five patients during the hospital stay while having persistent clinical symptoms. The rest of the patients either had diminished symptoms when seen by the ENT doctor (n=12) or were not examined at all (n = 45, 70.3%). Except two patients (one with clinical contraindications), all patients were assessed with MRI during their hospital stay (96.9%).

Discussion & Conclusion: Simulation training seems to be safe. The benefit of faster treatment and quality improvement achieved through simulation training seems to outweigh the associated risks of treating more SM patients with IVT. However, a quality improvement (QI) program on the initial diagnostic work up of patients with vertigo would be beneficial. Such a QI program could have a distinct potential to save radiological and clinical resources and could reduce treatment associated patient risks.

1-O14
THREE-DIMENSIONAL FRACTAL DIMENSION AND LACUNARITY FEATURES MAY NONINVASIVELY PREDICT TERT PROMOTER MUTATION STATUS IN GRADE 2 MENINGIOMAS

So Yeon Won[1], Yae Won Park[2], Sung Soo Ahn[2], Jinna Kim[2], Seung-Koo Lee[2]
[1]Kangbuk Samsung Hospital, Sungkyunkwan University School of Medicine, Seoul, Korea, Republic of. [2]Yonsei University College of Medicine, Seoul, Korea, Republic of

Introduction: The 2021 World Health Organization classification includes telomerase reverse transcriptase promoter (TERTp) mutation status as a factor for differentiating meningioma grades. Therefore, preoperative prediction of TERTp mutation may assist in clinical decision making. However, no previous study has applied fractal analysis for TERTp mutation status prediction in meningiomas. The purpose of this study was to assess the utility of three-dimensional (3D) fractal analysis for predicting the TERTp mutation status in grade 2 meningiomas.

Methods: Forty-eight patients with surgically confirmed grade 2 meningiomas (41 TERTp-wildtype and 7 TERTp-mutant) were included. 3D fractal dimension (FD) and lacunarity values were extracted from the fractal analysis. A predictive model combining clinical, conventional, and fractal parameters was built using logistic regression analysis. Receiver operating characteristic curve analysis was used to assess the ability of the model to predict TERTp mutation status.

Results: Patients with TERTp-mutant grade 2 meningiomas were older (P = 0.029) and had higher 3D FD (P = 0.026)

and lacunarity (P = 0.004) values than patients with TERTp-wildtype grade 2 meningiomas. On multivariable logistic analysis, higher 3D FD values (odds ratio = 32.50, P = 0.039) and higher 3D lacunarity values (odds ratio = 20.54, P = 0.014) were significant predictors of TERTp mutation status. The area under the curve, accuracy, sensitivity, and specificity of the multivariable model were 0.84 (95% confidence interval 0.71-0.93), 83.3%, 71.4%, and 85.4%, respectively (Figure 1).

Discussion and Conclusion: 3D FD and lacunarity may be useful imaging biomarkers for predicting TERTp mutation status in grade 2 meningiomas. Our model may be used for preoperative, noninvasive prediction of TERTp mutation status in meningiomas and may allow clinicians to choose a more aggressive treatment for TERTp-mutant meningiomas.

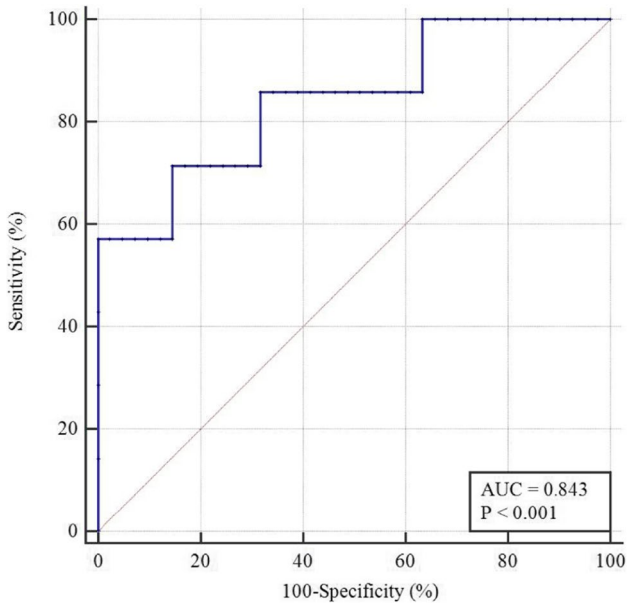

1-O15
AUTOMATED ASPECTS SOFTWARE TO ASSIST IN CLINICAL DECISIONING FOR MECHANICAL THROMBECTOMY

Julie Lambert[1], Bram Dewachter[1], Jelle Demeestere[1], Philippe Demaerel[1], Robin Lemmens[1]
[1]University Hospital Leuven, Leuven, Belgium

Keywords: stroke – artificial intelligence – multidetector computed tomography

Introduction: The Alberta Stroke Program Early CT Score (ASPECTS) quantifies early ischemic changes in middle cerebral artery (MCA) stroke on non-contrast CT (NCCT) but suffers from interrater variability. We examined agreement between clinically assessed ASPECTS and software-based automated ASPECTS (RAPID, Ischemaview).

Methods: We retrospectively included patients presenting with a MCA occlusion who underwent mechanical thrombectomy between 2015 and 2018 at the Leuven University Hospital (Belgium). Two readers rated ASPECTS on 175 NCCTs, which were subsequently processed by RAPID ASPECTS. Conventional and automated ASPECTS were compared to two gold standards: expert neuroradiologist ASPECTS based on NCCT only (E-GS), and consensus reading of two experienced readers based on all available baseline information, including CT perfusion (C-GS). Finally, raters re-examined their scores using RAPID ASPECTS as a computer assisted detection (CAD) tool. Agreement to determine thrombectomy eligibility based on ASPECTS was studied with ASPECTS >5 as a cutoff, according to the American Heart Association guidelines. This dichotomized analysis was compared without and with CAD. We used weighted kappa (wκ) to assess agreement between individual raters and also to assess agreement between gold standard ratings and conventional and RAPID ASPECTS respectively. We used Cohen's kappa (κ) to assess agreement for the ASPECTS >5 cutoff.

Results: Agreement between E-GS and conventional ASPECTS readings was fair to moderate (reader 1: wκ= 0.32 and reader 2: wκ= 0.43), and moderate for RAPID ASPECTS (wκ= 0.40). Agreement with C-GS was fair for all ratings (reader 1: wκ= 0.34; reader 2: wκ= 0.35; RAPID ASPECTS: wκ= 0.31). Agreement on ASPECTS >5 cutoff was fair to moderate between conventional raters and E-GS (reader 1: κ= 0.42; reader 2: κ= 0.37) and fair between conventional raters and C-GS (reader 1: κ=0.27 and reader 2: κ= 0.33). Interrater agreement for conventional ASPECTS was fair (wκ= 0.23) and improved to moderate (wκ= 0.51) using RAPID ASPECTS as CAD. Agreement on ASPECTS >5 cutoff improved with CAD to substantial (reader 1: κ= 0.68; reader 2: κ= 0.66) compared to E-GS and to moderate (reader 1: κ= 0.41; reader 2: κ= 0.57) compared to C-GS.

Conclusion: In conclusion, although automated ASPECTS individually performs similar to conventional ASPECTS, its use as a CAD tool improves interrater agreement and selection of patients for endovascular treatment.

1-O16

MEAN DIFFUSIVITY AND FRACTIONAL ANISOTROPY AT THE MESOSCOPIC LEVEL IN MENINGIOMA TUMORS: RELATION WITH CELL DENSITY AND TISSUE ANISOTROPY

Jan Brabec[1], Magda Friedjungová[2], Daniel Vašata[2], Elisabet Englund[3], Linda Knutsson[1,4,5], Filip Szczepankiewicz[1], Pia C Sundgren[6,7,8], Markus Nilsson[6]
[1]Medical Radiation Physics, Lund University, Lund, Sweden. [2]Department of Applied Mathematics, Faculty of Information Technology, Czech Technical University, Prague, Czech Republic. [3]Division of Pathology, Department of Clinical Sciences, Lund University, Lund, Sweden. [4]Russell H. Morgan Department of Radiology and Radiological Science, Johns Hopkins University School of Medicine, Baltimore, USA. [5]F.M. Kirby Research Center for Functional Brain Imaging, Kennedy Krieger Institute, Baltimore, USA. [6]Diagnostic Radiology, Lund University, Lund, Sweden. [7]Lund University Bioimaging Center, Lund University, Lund, Sweden. [8]Department of Imaging and Physiology, Skåne University Hospital, Lund University, Lund, Sweden

Introduction: Mean diffusivity (MD) and fractional anisotropy (FA) from diffusion tensor imaging (DTI) correlates negatively with cell density (CD)[1,2] and positively with tissue anisotropy[3,4], respectively. It is, however, not clear whether additional features may be relevant[5]. This is of importance for the interpretation of local changes MD or FA in terms biological features. Here, we quantified whether CD and tissue anisotropy computed from histology images explain variability in MD and FA and compare that to the performance of an artificial neural network (ANN).

Methods: 16 tumor samples were obtained and sliced into blocks of approximately 35x20x2mm^3 and scanned at Bruker 9.4T scanner. DTI[6] was performed (TR=2.5s, TE=30ms, resolution=200×200×200μm^3, b-values 100, 1000 and 3000s/mm^2). Specimens were cut into 4–5μm thick slices, stained with Hematoxylin&Eosin and coregistered to MR by a non-linear approach. CD and image anisotropy (IA) were obtained using QuPath software[7] and structure tensor analysis, respectively, and used to predict MD and in-plane FA (FA_{IP}). These features were also predicted from histology patched by an ANN[8] (fine-tuned EfficientNetV2) and results evaluated based on residual maps and using R^2.

Results: Panel I shows a meningioma where MD correlated with CD (part A in Panel I) and one where it did not (part C). Part B and D exemplifies two histology corresponding to voxels MR voxels without residuals but with different CD and similar MD. Panel II shows R^2 for all samples for prediction by CD or IA (blue bars) and ANN (red bars) in MD (part A) and FA_{IP} (part B) on the mesoscopic level (part 1) and on the whole-sample level (part 2). Panel III shows 4 features qualitatively associated with errors in MD prediction: tumor vasculature (part A), microcysts (B), psammoma bodies (C) or tissue cohesivity (D).

Discussion: Across tumors, we reproduced associations between CD and MD (R^2=0.58), and IA and FA_{IP} (R^2=0.82). However, within individual samples there were cases where the association between CD and MD was weak or even absent but ANN approach performed better (Panel II). That may be partially due to poor MRI-to-histology coregistration in the through-plane direction. However, we could identify specific features that contributes to a variation in MD beyond CD (Panel III). Egnell et al. found that collagen content is associated with MD[9].

Conclusion: It is likely that other features apart from CD and IA are of importance for the local interpretability of MD and FA.

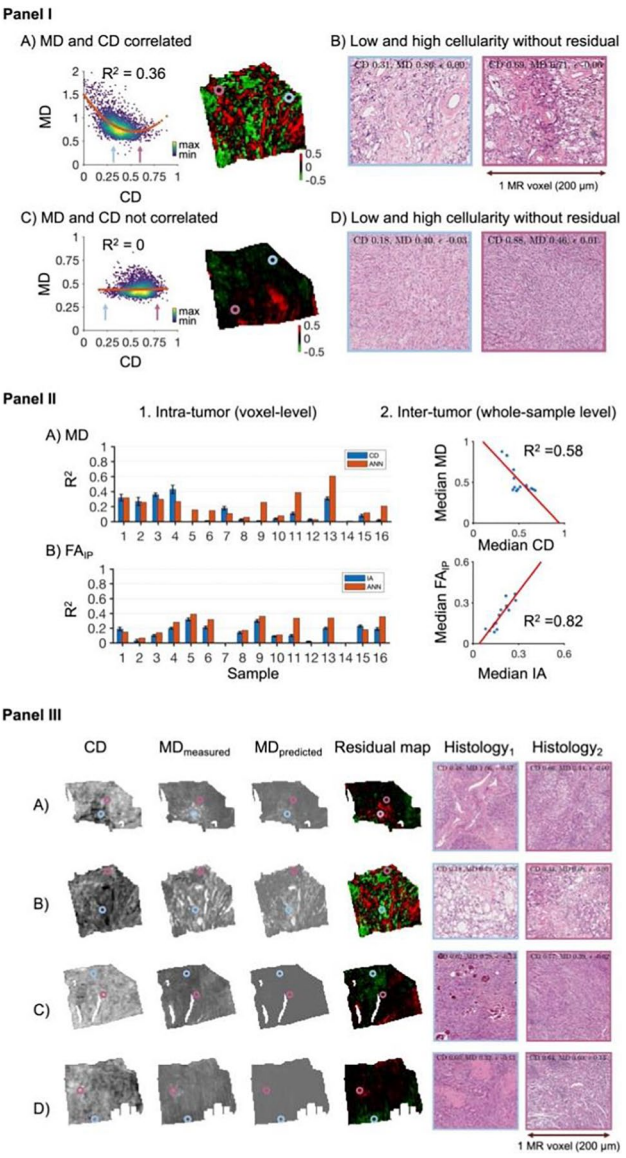

1-O17

ASSESSING CENTRAL NERVOUS SYSTEM INVOLVEMENT IN FABRY DISEASE WITH DEEP LEARNING AND THE BRAIN-AGE PARADIGM

Giuseppe Pontillo[1], Alfredo Montella[1], Mario Tranfa[1], Eleonora Riccio[1], Maria Petracca[1], Antonio Pisani[1], Sirio Cocozza[1], Arturo Brunetti[1]
[1]University of Naples "Federico II", Naples, Italy

Introduction: CNS involvement in Fabry disease (FD), a rare X-inherited lysosomal storage disorder, is mainly characterized by vascular pathology, whose severity may greatly vary according to several factors. However, while recommended follow-up of patients with FD includes brain MRIs, an accurate evaluation of FD-related brain damage is hampered by the lack of quantitative imaging biomarkers. In this regard, the brain-age paradigm has emerged as a promising approach, quantifying the extent to which a subject deviates from healthy brain-aging trajectories. Here, we aimed to assess CNS involvement in FD using deep learning and the brain-age paradigm.

Methods: All images used in the study were minimally preprocessed (i.e., rigidly registered to MNI space and N4 bias field corrected) 3D T1-weighted brain MRI scans.
A 3D Inception-ResNet-V2 network was trained to predict chronological age and evaluated on an external cohort of healthy subjects (HS) from 8 open-source datasets (2160 subjects, male/female: 1293/867, mean age [range]: 33 [4-86]), split in training (64%=1382), validation (16%=346) and test (20%=432) sets. For hyperparameter optimization, models with different values were trained for 200 epochs using the ADAM optimizer, and accuracy was measured with mean absolute error (MAE).
Lastly, age bias (i.e., underestimation of age in older subjects and vice versa) was statistically corrected and the final model was applied to an internal cohort of 30 genetically confirmed FD patients with no prior cerebrovascular accidents (mean age [range]: 43 [20-68]) and 78 age- and sex-comparable HS (mean age [range]: 46 [14-77]).
The difference between predicted and chronological age (brain-predicted age difference, brain-PAD), considered as an index of structural brain health, was compared between the two groups using bootstrapped t-test.

Results: Following age bias correction, the final brain-age model had validation and testing MAEs of 3.527 (R2=0.917) and 3.640 (R2=0.917), respectively (Figure 1).
FD patients and HS of the internal cohort were not significantly different in terms of age (t=0.85, p=0.40) or sex ratio (Chi-Square=1.66, p=0.28).
When applying the brain-age model, FD patients showed significantly higher mean brain-PAD compared to HS (2.97 vs 0.49 years, Cohen's d=0.412, p=0.043) (Figure 2).

Discussion & Conclusion: On average, FD patients show significantly higher than normal brain-predicted age, reflecting "accelerated" brain aging and possibly capturing FD-related brain damage.
Brain-PAD encodes relevant information about brain pathology in FD, bearing potential as a clinical biomarker to monitor disease progression and treatment efficacy.

Figure 1. Scatter plots showing the relationship between chronological and brain-predicted age in the validation (*left panel*) and test (*right panel*) sets.

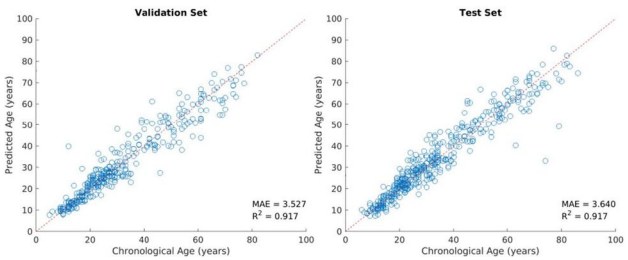

Figure 2. Violin plots showing the distribution of brain-PAD values in FD patients and healthy subjects.

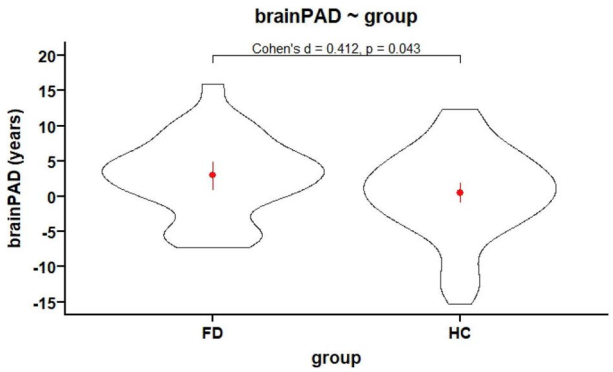

1-O18

POST-REVASCULARIZATION HEMODYNAMICS IN MOYAMOYA PATIENTS EVALUATED WITH ASL

Rui Duarte Armindo[1,2], Moss Zhao[2], Benjamin Yim[2], Andrew Gauden[2], Michael Moseley[2], Gary Steinberg[2], Greg Zaharchuk[2]
[1]Hospital Beatriz Ângelo, Lisbon, Portugal. [2]Stanford University, Stanford, USA

Purpose: Cerebrovascular reactivity (CVR) reflects the change in cerebral blood flow (CBF) in response to a vasoactive stimulus. Previous studies have demonstrated that impaired CVR in Moyamoya disease (MMD) patients was associated with a higher risk of stroke[1]. Arterial spin labeling

is a quantitative MRI technique that enables non-invasive CBF and CVR measurement[2], with demonstrated effectiveness in identifying CVR impairment in MMD patients before surgery[3]. Here, we compare the CBF and CVR of Moyamoya patients using ASL before and after bypass surgery.

Materials and Methods: Imaging data were acquired from 24 MMD patients (16-54 years, 21 females) using a 3T MRI system. All patients had unilateral or bilateral vessel occlusions at the MCA, ACA and/or PCA. Single and multi-PLD (5 PLDs) PCASL 2 data were acquired at baseline and 15 minutes after the injection of the vasodilator acetazolamide (15 mg/kg with a maximum of 1 g). CBF was computed using the general kinetic model[4]. CVR was calculated as the percentage of CBF change compared with baseline. Flow territories (right and left MCA, ACA and PCA) were defined based on the Harvard-Oxford structural atlases[5]. Mean CVR within the regions affected by occlusions and normal territories was computed for each subject. Paired t-tests were performed to compare the mean CVR between the affected and unaffected territories.

Results: CVR of the affected regions was significantly higher after revascularization (increased on average by 5.3% and 9.5%, measured respectively by single and multiple-PLD PCASL, $p<0.02$), implying improved perfusion and lower stroke risk. Figure 1 shows the distribution of CVR values before and after surgery and Figure 2 presents one illustrative case.

Conclusion: Bypass surgery significantly improved CBF and CVR in the affected territories of MMD patients. Single and multiple-PLD PCASL can effectively measure these changes when access to the gold standard O15 PET is difficult.

Acknowledgments: This work is supported by the American Heart Association (Grant: 826254), the National Institutes of Health (Grant: R01EB025220-02 and 4R00NS102884-03) and the Luso-American Development Foundation (Grant: 2020/A-210498).

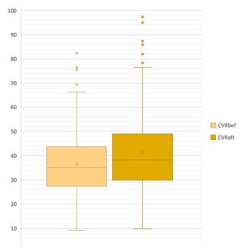

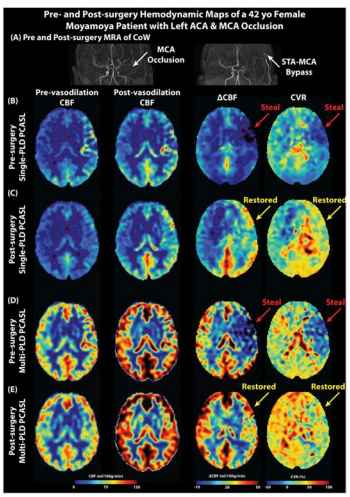

1-O19

EARLY MRI BIOMARKERS IN AMYOTROPHIC LATERAL SCLEROSIS (ALS): MORPHOMETRY, DTI AND FUNCTIONAL CONNECTIVITY

José Manuel Hidalgo Gómez de Travecedo[1], María Teresa Cabada Giadás[1], Juan Carlos Quizhpilema Cedeño[2], Tamara Laxe Vidal[1], Mikel San Miguel Oroz[1], Francisco Javier Díaz Leiva[1], Pablo Lecumberri Villamediana[2], Marisol Gómez Fernández[2], Ivonne Jericó Pascual[1]
[1]Hospital Universitario de Navarra, Pamplona, Spain. [2]Universidad Pública de Navarra, Pamplona, Spain

Introduction: Amyotrophic lateral sclerosis (ALS) is a chronic and progressive neurodegenerative disease characterized by damage to the upper and lower motor neurons, whose diagnosis is currently based on clinical criteria.
The aim of this study is to analyse structural and functional MRI parameters in newly diagnosed ALS patients in order to define early imaging biomarkers.

Methods: 29 ALS patients diagnosed according to El Escorial criteria and 26 age-matched healthy controls were included (mean age ± SD = 64.51 ± 10.28 years, range = 45-85). All participants underwent a basal MRI scan (3T MAGNETOM Vida, Siemens Healthineers, Erlangen, Germany), including a sagittal 3D T1 MPRAGE scan, 64-dir Diffusion Tensor Imaging (DTI), perfusion study (arterial spin labeling –ASL-) and resting-state Blood-Oxygen Level Dependent fMRI. Patients underwent an additional follow-up MRI scan 6 months later.
Structural MRI analysis was performed with FreeSurfer v7.2.0. DTI data was processed using the TRActsConstrained by UnderLying Anatomy (TRACULA) tool. BASIL tool of the FSL library was used to analyze the ASL sequence. Resting-state connectivity networks were derived in Matlab using the CONN toolbox v20.b and SPM12.

Results: Comparing patients and controls, several significant differences were found. In the morphometric study, a decrease in cortical thickness was observed in different areas, highlighting the left rolandic region, both amygdala and cerebellum ($p<0,001$). In the DTI study, the most relevant differences in the anisotropy fraction (AF) were found in both anterior temporal regions and in the left frontal lobe. Also noteworthy is the asymmetrical involvement of the pyramidal pathways with left predominance, left superior longitudinal fasciculus and left frontal aslant tract. In the functional connectivity study, significant differences were found in the motor network in superior and middle frontal and left fusiform gyri.
At 6 months there was a decrease in the cortical thickness of the bilateral cingulate gyrus and a decrease in AF in different

areas (both frontals and right temporal and corpus callosum) with involvement of the bilateral pyramidal pathway. No differences in connectivity were found throughout this period.

Discussion & Conclusion: ALS demonstrates involvement of motor and non-motor areas as shown by morphometry, DTI and cortical activity in the initial stage of the disease with a left-predominant asymmetric pattern, with progression over time.
Damage found in the association fascicles supports the relationship of this disease with the group of frontotemporal dementias and allows a better understanding of the non-motor symptoms in these patients.

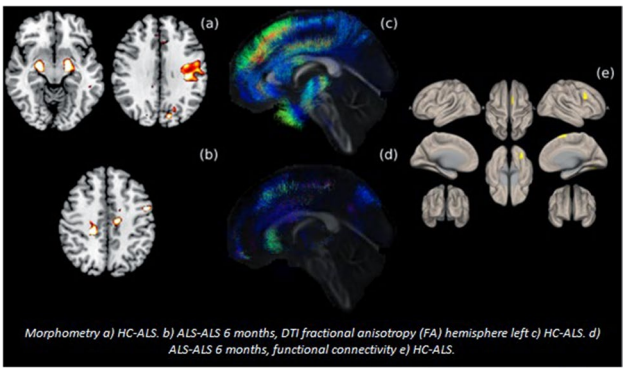

Morphometry a) HC-ALS. b) ALS-ALS 6 months, DTI fractional anisotropy (FA) hemisphere left c) HC-ALS. d) ALS-ALS 6 months, functional connectivity e) HC-ALS.

1-O20
DISTINCT RESTING-STATE FMRI FEATURES OF FATIGUE IN CLINICALLY ISOLATED SYNDROME AND MULTIPLE SCLEROSIS: ACCOUNTING FOR THE CONFOUNDING EFFECT OF CONCURRENT DEPRESSION SYMPTOMS

Efrosini Papadaki[1,2], Despina Antypa[1], Theodora Panou[1], Emmanouella Kosteletou[2], Nicholas John Simos[2], Antonios Kagialis[1], Vasileios Mastorodemos[1], Panagiotis Simos[1,2]
[1]University of Crete, Heraklion, Greece. [2]Foundation for Research and Technology, Heraklion, Greece

Background: Fatigue and depression are common, often overlapping, symptoms in patients with clinically isolated syndrome (CIS) and multiple sclerosis (MS). Resting-state functional MRI (rs-fMRI) provides measures of neural activity and function, through various indices of regional functional connectivity (FC). Additionally, time-shift analysis (TSA) of rs-fMRI timeseries can provide complementary information regarding regional cerebral perfusion alterations. This method quantifies hemodynamic transfer speed through the temporal shift of low-frequency BOLD signal fluctuations relative to the blood flow in major cerebral veins.

Purpose: The aim of the present cross-sectional study was to identify common and distinct pathophysiological substrates between self-rated fatigue and depression symptoms in patients with CIS and relapsing-remitting MS (RR-MS), by using rs-fMRI.

Methods and Materials: 24 CIS and 29 RR-MS patients were examined using rs-fMRI to assess hemodynamic response patterns (through TSA), functional brain connectivity (FC; via Intrinsic Connectivity Contrast maps), and hemodynamic-connectivity coupling. These regional maps were correlated with self-reported fatigue scores, controlling for depression, and with depression symptom scores, controlling for fatigue. 39 healthy volunteers were, also, studied.

Results: In CIS, fatigue was associated with accelerated hemodynamic response in the insula, hyperconnectivity of the dorsolateral prefrontal cortex, and evidence of increased functional and hemodynamic engagement of the left amygdala. In RR-MS patients, fatigue was associated with accelerated hemodynamic response in the insula and medial superior frontal cortex, increased functional role of the left amygdala, and hypoconnectivity of dorsal orbitofrontal cortex. Conversely, depression severity among CIS patients was linked to indications of reduced functional and hemodynamic engagement of the left amygdala, and hypoconnectivity of the anterior cingulate gyrus. Depression symptom severity among RR-MS patients was associated with delayed hemodynamic response in the medial superior frontal gyrus, hypoconnectivity of the insula, ventromedial thalamus, dorsolateral prefrontal cortex and posterior cingulate, and indications of increased functional status of the medial orbitofrontal cortex.

Conclusion: The present study shows distinct functional connectivity and hemodynamic responses, as well as different magnitude and topography of hemodynamics-connectivity coupling, associated with fatigue and depression in early and later stages of MS.

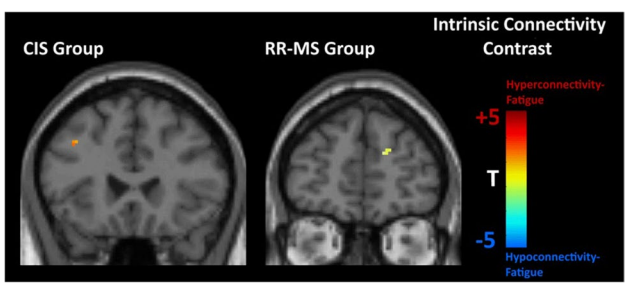

1-O21

MRI BASED PREDICTION OF SURGICAL OUTCOME IN TRIGEMINAL NEURALGIA

Tomas Sakinis[1], Geir Ringstad[1], Per K. Eide[1], Pål A. Rønning[1], Haldor Slettebø[1]
[1]Oslo University Hospital - Rikshospitalet, Oslo, Norway

Introduction: Neurovascular contact (NVC) is the most frequent cause of trigeminal neuralgia (TN). The role of MRI in TN has traditionally been to exclude other causes. Since 2018, MRI has become essential to separate between "classical TN" and "idiopathic TN" based on NVC-grade. In 2020, a new clinical syndrome - "TN associated with solitary pontine lesion"- was also described, with pontine lesions similar to, yet distinct from, multiple sclerosis lesions. Microvascular decompression surgery is the favored treatment for most cases that do not respond to medication, but not everyone responds to surgery, and some experience symptom recurrence. Today, the TN diagnosis and treatment are mainly based on clinical findings. We aimed to assess whether MRI can be used to predict surgical outcome.

Methods: We retrospectively collected preoperative MRIs from patients with TN who were treated with microvascular decompression surgery in 2005-2016. Studies without thin, heavily T2-weighted images were excluded. We obtained ethical committee approval and gathered informed consent and questionnaires from 100 patients. Blinded scoring of NVC-grade, nerve atrophy and the presence of solitary pontine lesion along the trigeminal nerve pathways was performed (Fig. 1). Morphological trigeminal nerve change was defined as the presence of high-grade NVC (impression or dislocation) and/or nerve atrophy. Optimal surgical outcome was defined as Barrow Neurological Institute pain intensity score 1 ("no pain, no medications") with no recurrence during the follow-up period (average 8 years). Differences in MRI findings between groups were measured using Two Proportion Z-test.

Results: Optimal surgical outcome was achieved in 66/100 patients. In these, morphological changes of the symptomatic trigeminal nerves were present in 82% (54/66, positive predictive value 88%, $p<0.001$). Solitary pontine lesion was diagnosed in 10 patients, none of whom had an optimal outcome (sensitivity 29%, specificity 100%, $p<0.001$). On the initial MRI report 9/10 pontine lesions were not mentioned. The remaining 24 patients with a non-optimal outcome had morphological nerve changes in 29% (7/24, negative predictive value 59%, $p<0.001$).

Discussion & Conclusion: MRI can predict surgical outcome in trigeminal neuralgia with good accuracy. Almost 90% of patients with morphological nerve changes and no pontine lesion had optimal surgical outcome. In contrast, when morphological nerve changes and pontine lesions were absent, only 41% had optimal outcome. The study indicates that solitary pontine lesions are especially predictive of a non-optimal outcome and are underdiagnosed in TN.

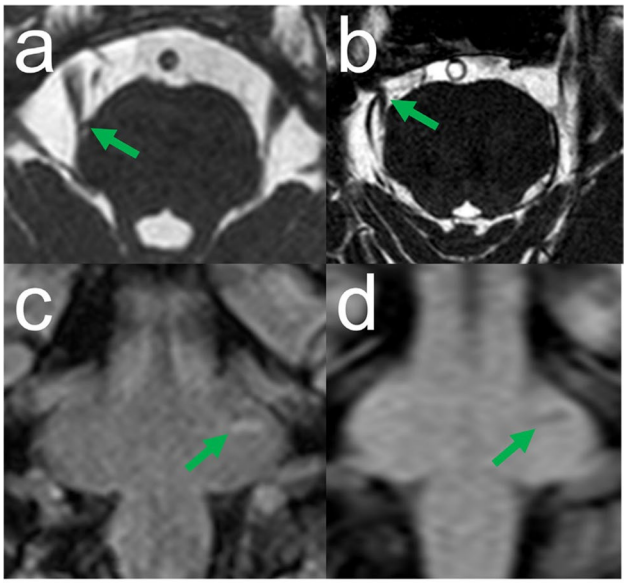

Figure 1. Examples of NVC and solitary pontine lesion. a - Simple NVC with no morphological changes of the right nerve. b – Right morphological nerve changes c,d – Left solitary pontine lesion on coronal T2 flair and T1, respectively.

1-O22

CLINICAL OUTCOME ASSESSMENT IN PATIENTS WITH CROSSED CEREBELLAR DIASCHISIS IN ACUTE ISCHEMIC STROKE

João Oliveira[1], Denil Tribovane[1], Catarina Brito[1], Pedro Vilela[1]
[1]Hospital Beatriz Ângelo, Loures, Portugal

Introduction: Crossed cerebellar diaschisis (CCD) is defined as a decreased cerebellar perfusion and glucose metabolism caused by supratentorial dysfunction of the contralateral hemisphere. This phenomenon is most likely caused by a reduction of the cortico-pontine-cerebellar pathways excitatory impulses. CCD can be observed both in the acute and chronic phases of cerebral injury, in about one-third of patients. Nuclear medicine studies have shown that CCD severity may be a prognostic factor for recovery time and treatment outcome in stroke patients.

Methods: Ninety-three patients with supratentorial middle cerebral artery ischemic stroke were evaluated by CT perfusion (CTP) image-processing, reviewed from January 2021 to December 2021. We performed an analysis on ROI

placed on the most significant slice in the CCD positive cases assessed by visual inspections. Clinical evaluation and outcome assessment was performed using modified Rankin scale (mRS) at the time of entry and discharge. Patients with hemorrhagic lesions, stroke mimics, posterior or bilateral strokes and high-grade carotid stenosis were excluded from the study. Patients with inadequate CTP maps due to technical reasons such as excessive motion artifacts, or incomplete coverage of the cerebellum were also excluded.

Results: CCD was found in 27 of 93 ischemic stroke patients (29%) by CTP, who met inclusion criteria. Quantitative perfusion analysis was performed on 55 patients divided into two groups: CCD-positive (n=27) and a random selection of CCD-negative patients (n=28). The mean age was 76.9 (SD=13.7) for CCD-positive and 73.2 (SD=15.9) for the CCD-negative group. The mean time from symptoms onset was 5h vs 6h in CCD-positive and negative, respectively. Admission NIHSS and cerebral collateral circulation were not statistically different (p=0.874, two-sample t-test and p=0.436, two-tailed Mann-Whitney U, respectively). The CCD-positive group had lower CBF and CBV in the contralateral cerebellar hemisphere ($p<0.01$ in both, two-tailed Mann-Whitney U) and higher circulation times (MTT: p=0.01; TTD: p=0.03; and TMax: p=0.02, two-tailed Mann-Whitney U). Furthermore, CCD-positive patients had worse discharge mRS score (p=0.042, two-sample t-test). Other clinical factors (age, sex, NIHSS, time from symptom onset and cerebral collateral pattern) did not correlate significantly with the presence of CCD ($p>0.05$).

Conclusions: CTP is a fast, widely available method to study CCD, which can be easily detected by assessing the perfusion maps. During the acute phase of stroke, the presence of CCD may serve as a predictor for worse clinical outcome in these patients.

1-O23

ROLE OF PERFUSION-WEIGHTED IMAGING (PWI) IN MONITORING RESPONSE TO REGORAFENIB IN PATIENTS WITH RECURRENT GBM.

Elena Trincia[1], Anna Dallorto[1], Matteo Bendini[1], Ingrid Inches[1], Giovanna Favaro[1], Valentina Polo[2], Mario Moro[3], Roberta Ruda'[4], Francesco Di Paola[1]
[1]UOC Neuroradiology, Ospedale Ca' Foncello, Treviso, Italy. [2]Oncology Unit, Ospedale Ca' Foncello, Treviso, Italy. [3]UOC Neurosurgery, Ospedale Ca' Foncello, Treviso, Italy. [4]UOC Neurology, Castelfranco Veneto, Italy

Perfusion-weighted imaging (PWI) is increasingly used in patients with brain tumors since it facilitates the differential diagnosis between progressive disease and pseudoprogression.

Regorafenib is a multitarget drug which has recently been approved as a second line therapy in GBM tumor recurrent after standard treatment.

Few studies have investigated how PWI is able to detect the antiangiogenetic effect of the drug in such patients.

Aim of the study was to define the role of MR PWI in a population of patients treated with Regorafenib at the time of recurrence.

We prospectively analyzed the MR scans of all the patients who were treated with Regorafenib from May 2020 to May 2022, each scan being performed every two cycles. Acquisitions were performed using a 3-Tesla scanner (Magnetom Vida, Siemens Healthineers, Erlangen), and a standard protocol including diffusion-weighted imaging (DWI), 2D T2-weighted TSE and FLAIR, 3D-FLAIR, T1-weighted gradient echo with fat saturation, before and after injection of gadolinium, and dynamic susceptibility contrast (DSC) PWI. Patients whose examinations were inadequate, or incomplete were excluded.

PWI was evaluated through Syngo.Via software by using several region-of-interest (ROIs), each of 25-30 mm2, to sample tumor tissue; the highest cerebral blood volume (CBV) values were compared to those of a ROI of the same size sampling the healthy contralateral white matter.

Response to treatment was reported according to RANO criteria.

We enrolled 12 patients from May 2020 to May 2022; 7 patients are evaluable. Three patients were excluded because of rapid clinical progression; two patients have their first follow-up examinations scheduled in June 2022.

At the first MRI 5 out of 7 patients displayed a decrease of the CBV values in the tumor tissue, corresponding to stable disease in 2 cases and partial response in 1 case (fig. 1A and 1B) according to RANO criteria; in 2 patients progressive disease was reported. Two patients exhibited an increase in the CBV values, in the setting of progressive disease (fig. 2A and 2B).

These initial findings suggest that MR-PWI could represent a surrogate imaging parameter for an earlier assessment of response (and possibly of non- response). These data should be validate in a larger series of patients. The study in ongoing.

Fig. 1: baseline (fig. 1A) and follow-up MRI (fig. 1B) in a 50-year-old patient. Partial response (RANO criteria) and decrease in CBV values.

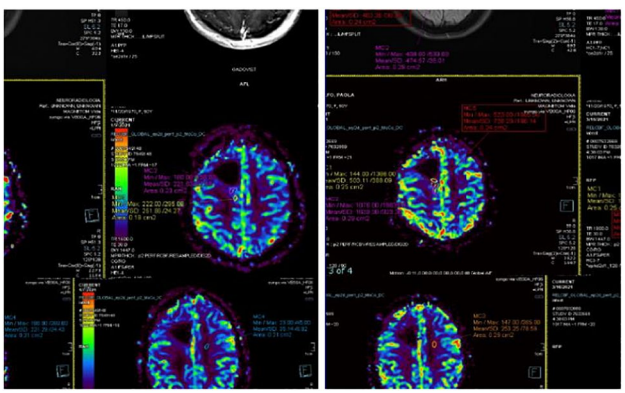

Fig. 2: baseline (fig. 2A) and follow-up MRI (fig. 2B) in a 29-year-old patient. Progressive disease.

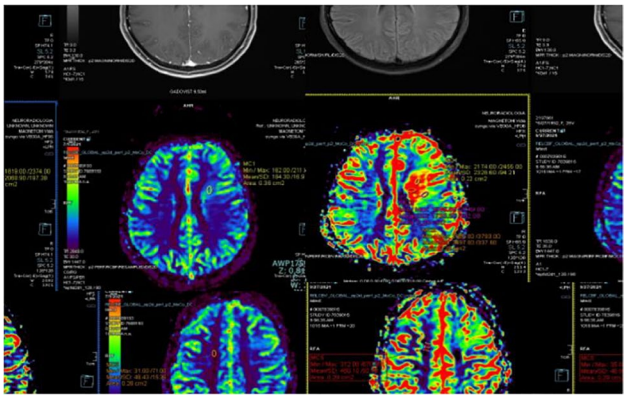

1-O24

FEATURES OF MRI IMAGING OF BRAIN DEMYELINATION FOCI IN PATIENTS WITH CHRONIC HERPESVIRUS ENCHEPHALITIS TYPES 4 AND 6

Viktoriia Ponomarenko[1]
[1]State Institution "Zaporozhye Medical Academy of Postgraduate Education of the Ministry of Health of Ukraine", Kyiv, Ukraine, Zaporizhzhia, Ukraine

Purpose: We aim to research the features of the shape, number and location of foci in brain structures during MRI examination in three groups of patients: patients with a clinically confirmed diagnosis of multiple sclerosis, with a PCR-negative result of the presence of herpes viremia types 4 and 6; patients with clinically confirmed multiple sclerosis, PCR-positive result of viremia type 4 of the herpes virus; patients with clinically confirmed multiple sclerosis, PCR-positive result of viremia type 6 herpes virus.

Patients and Methods: Retrospective cohort study. 52 patients were examined. Age group from 20 to 40 years, with no signs of hypercholesterolemia, with no plaques in the carotid and vertebral arteries during duplex scanning, with a clinically confirmed diagnosis of multiple sclerosis. Clinical diagnosis of multiple sclerosis at our institution between November 19, 2018 – December 19, 2020.

Results: Total number of patients N=52. Control group of patients (control N=25) with a clinically confirmed diagnosis of multiple sclerosis, with a PCR-negative result of the presence of herpes viremia types 4 and 6. First group of patients (N=15) with clinically confirmed multiple sclerosis, PCR-positive result of viremia type 4 of the herpes virus. Second group of patients (N=12) with clinically confirmed multiple sclerosis, PCR-positive result of viremia type 6 herpes virus. In accordance with statistical calculations, the data on the distribution of lesions in the brain have a normal distribution and the curves plotted according to the graph are bell-shaped symmetrical curves. The indicators of asymmetry (skewness) and kurtosis were used. The obtained values approach zero or slightly deviate from zero, which corresponds to the minimum error when applying the statistical analysis coefficients.

Conclusions: The differences between the number and location of foci were statistically significant. In first group of patients with clinically confirmed multiple sclerosis, caused by HHV 4, the number of foci is less than in second group of patients with a positive HHV6 PCR test, and there is also a specific location of foci in HHV4 exclusively in the subcortical regions of the frontal and temporal lobes, whereas patients with HHV6, the location of foci was noted mainly in the periventricular white substance near the walls of the bodies of the lateral ventricles, and the corpus callosum, in the smallest number in the subcortical white matter of the cerebral hemispheres.

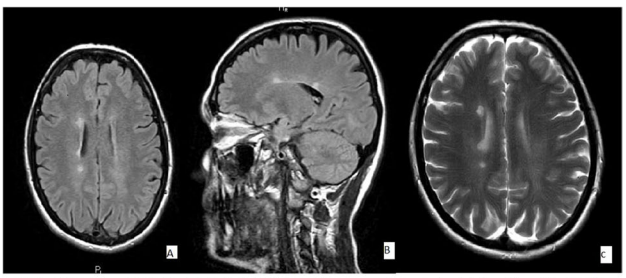

FLAIR ax (A), FLAIR sag (B), T2-WI ax (C). Patient with lesions of the corpus callosum, periventricular white matter. Viremia of herpes virus type 6 was confirmed by PCR.

1-O25

EVALUATION OF MICROSTRUCTURAL CHANGES IN CENTRAL OLFACTORY PATHWAY IN POST SARS-COV-2 INFECTED RECOVERED PATIENTS

Neeraj Sharma[1], Chirag Ahuja[1], Sameer Vyas[1], Paramjeet Singh[1], Sudhir Pathak[2], Ashish Bhalla[1], Naresh Panda[1], Aastha Takkar[1], GD Puri[1]
[1]PGIMER, Chandigarh, India. [2]University of Pittsburgh, Pittsburgh, USA

Introduction: Olfactory dysfunction (OD) in the form of anosmia and ageusia is commonly encountered with COVID-19 infection lasting variably from few weeks to months. Its pathogenesis has been under rigorous review with olfactory epithelial cells believed to be viral entry portal. The nature of involvement of olfactory pathway in the brain is not completely known which forms the basis of the current study which aimed at evaluating changes in microstructural integrity in central olfactory pathway in post SARS-CoV-2-infected recovered patients using MR based diffusion tensor imaging (DTI).

Methods: In this prospective comparative study, 40 post covid-19 recovered patients (20 having OD during active Covid-19 infection- group A; and 20 not having OD during active Covid-19 infection- group B) along with 20 healthy controls were enrolled. DTI (30 direction) was perfomed in the enrolled subjects on a 3T MR scanner using standard parameters. MR signal abnormalities on conventional MRI sequences along with diffusivity parameters (FA, MD, AD, RD values) were evaluated in 54 out of 181 segmented gray-white matter regions in all these groups. Morphometric parameters (regional cortical thickness, gray and white matter volumes) were also assessed in 18 selected cortical subcortical regions of the brain constituting the olfactory pathway by automated VBM and atlas based analysis.

Results: There was significant reduction in mean FA value in bilateral parahippocampal cortex, with significantly increased mean AD, RD, MD values in left rostral anterior cingulate cortex, regional white matter of left isthmocingulate, insular region and in bilateral anterior thalamic radiation (ATR) in group A vs group B. Morphometric evaluation revealed significantly increased mean gray matter voume (GMV) in medial and lateral orbito frontal cortex (OFCs), rostral and caudal anterior cingulate cortex with increased mean regional white matter volume (WMV) in entorhinal cortex in group A as compared to controls.

Discussion and Conclusion: The DTI and morphometric abnormalities selectively in the olfactory pathway indicate possible disruption of microstructural integrity in these areas in recovery phase of SARS CoV-2 infection possibly either as direct response due virus invasion of the neurons or more likely as a sympathetic response to olfactory epithelial dysfunction secodary to viral injury. DTI thus provides an objective measure of OD in patients of Covid-19 infection.

Table 1:-Brain areas showing significant difference for FA values in group A and group B

Location	Group-A Mean	Group B Mean	P Value
Ctx-rh-parahippocampal	0.122±0.0117	0.139±0.0324	.044
Ctx-lh-parahippocampal	0.125±0.0139	0.133±0.0230	0.008

Table 2: Brain areas showing significant difference for MD values in group A and group B

Location	Group A Mean	Group B Mean	P Value
ATR Right	.0001±0.0002	.0000±0.0001	.007
ATR left	.0010±0.0001	.0010±0.0001	.000
ctx-lh- rostralanteriorcingulate	.0001±0.0001	.0000±0.0001	.037

Table 3: Brain areas showing significant difference for RD values in group A and group B

Location	Group A	Group B	P Value
wm-lh-insula	0.001±0.0001	0.001±0.0000	.0|0
ctx-lh- rostralanteriorcingulate	0.001±0.0001	0.001±0.0001	.0|6

Table 4: Brain areas showing significant difference for AD values in group A and group B

Location	Group A	Group B	P Value
lh-wm-isthumascingulate	0.001±0.0000	0.001±0.0001	.000
ctx-lh-rostralanteriorcingulate	0.001±0.0001	0.001±0.0001	0.019

Table 5:-Brain areas showing significant difference for cortical volume in group A and controls

Location	Group A regional cortical volume mean±std	Control Group regional cortical volume mean±std	Mean difference	P Value
lh_caudalanteriorcingulate volume	3224.08±592.792	2774.35±337.612	449.703	.037
lh_lateralorbitofrontal_ volume	8908.89±997.962	8163.80±840.917	745.091	.035
rh_lateralorbitofrontal_ volume	8712.00±614.321	7910.95±658.043	801.050	.003
rh_medialorbitofwntal_ volume	4546.53±432.912	4156.80±510.653	389.726	.040

Table 6: Brain areas showing significant difference for WM volume between group A and Controls

Location	Group A WM volume mean±std	Control group WM volume mean±std	Mean difference	P value
wm-rh-entorhinal	1211.63±112.20	1070.86±741.44	274.964	.015

1-O26

MRI RADIOMICS FOR PREDICTION OF SURVIVAL IN GLIOBLASTOMA

Effrosyni Styliara[1], Loukas G Astrakas[2], George Alexiou[3], Maria I Argyropoulou[1]

[1]Department of Radiology, Medical School, University of Ioannina, Ioannina, Greece. [2]Department of Medical Physics, Medical School, University of Ioannina, Ioannina, Greece. [3]Department of Neurosurgery, Medical School, University of Ioannina, Ioannina, Greece

Introduction: Glioblastoma is the most frequent and most aggressive primary malignant brain tumor in adults. Although patients with glioblastoma have very dismal prognosis, little progress has been made towards non-invasive prediction of their survival. Radiomics can provide imaging biomarkers of survival by extracting many quantitative features from MRI images using data characterization algorithms. This study aims to identify robust radiomic features for survival prediction of glioblastoma patients.

Methods: Thirty-eight GBM-patients, with IDH- wild type were selected. All patients were imaged on the same 1.5T MRI scanner with the same exam protocol (T1W, T2W, FLAIR, DTI, DSC, MRS) and underwent the same treatment protocol. Data analysis included segmentation of four subregions (enhancing portion, solid non enhancing portion, necrosis, edema) of the tumor (itk-snap), radiomics features extraction (pyradiomics) and selection (LASSO) and then survival analysis (Cox regression model). Statistical significance was set at $p<0.05$.

Results: Among the 1883 radiomic features studied, the Large Dependence High Gray Level Emphasis (LDHGLE) of the enhancing subregion of the rCBV map was the only independent predictor, negatively associated with the survival (P=0.026). LDHGLE is a texture feature and measures the joint distribution of large dependence with higher gray-level values or the homogeneity in high rCBV values.

Conclusion: Radiomics is a very promising tool allowing non-invasive prediction of survival in glioblastoma patients. The homogeneity of the high rCBV areas in the enhancing subregion of the CBV maps indicate adequate angiogenesis enabling the disease to spread and could be used as a biomarker of survival.

Keywords: MRI Radiomics, Glioblastoma, Neuro-oncology

1-O27
TOWARD A VENDOR AGNOSTIC AI ASSISTANT SYSTEM FOR BRAIN METASTASIS DETECTION ON MRI

Wan-Yuo Guo[1,2,3,4], Ethan Tu[2]
[1]Taipei Veterans General Hospital, Taipei, Taiwan. [2]Taiwan AI Labs, Taipei, Taiwan. [3]China Medical University, Taichung, Taiwan. [4]National Yang Ming Chiao Tung University, Taipei, Taiwan

Introduction: The majority of deep learning artificial intelligence (AI) models for imaging diagnosis demonstrate diminished model performance on external dataset. We employ multiple steps in model development, refinement, validation and test on MRI from wide-ranging vendors and hospitals to avoid performance diminishing. The works present our development of a clinically applicable vendor agnostic AI assisted system for brain metastasis detection on MRI.

Methods: AI model training based on MRI of 1029 patients with brain metastases from a single institute and single MRI brand was conducted. A benchmark algorithm of 2D Mask R-CNN was used and resulted in an initial model (DeepMets®). Model generalization of DeepMets® was then carried out over a nationwide population-based dataset via deep active learning on 559 patients (randomized from 3125) from National Health Insurance Administration (NHIA) medi-cloud, Taiwan. Iterative refining process using the ResNext50 U-Net architecture with attention mechanisms were undertaken and resulted in a newer version model (DeepMets-Plus®). Final testing of the model was conducted on a dataset of brain metastasis consisted of 152 patients (489 metastases) from 19 hospitals and three MRI vendors. Sizes of the metastases were median 7 (4-40) mm in maximum diameters. The ground truth of the final test was obtained from a consensus of three experienced neuroradiologists, with 30 (25-36) years professional experience in neuroradiology.

Results: The performance of DeepMets® were: sensitivity 96%, precision 86%, and f1 91%. It dropped to sensitivity 76%, precision 45% and f1 48%, initially, on the NHIA dataset. After three active learning rounds with Ensemble & Post, DeepMets-Plus® yielded the final performance of sensitivity 0.86%, precision 0.90%, and f1 0.87%. For DeepMets-Plus®, the intersection over union between ground truth and model inference were 0.718, 0.210-0.904 (median, range). The centroid and Hausdorff distances were, respectively, 0.617, 0.124-2.154 mm and 2.512, 0.469-7.469 mm.

Discussion: The initial model (DeepMets®) has high performance in detecting brain metastases on MRI. However, being stemmed from its high imaging homogeneity training dataset, the high performance of DeepMets® is applicable only on in-house dataset with single vendor and uniform imaging parameters. DeepMets-Plus® gains model generalization while keeps similar model performance with training conducted on MRI of wide-ranging vendors from multiple hospitals.

Conclusion: With the access to a national-scale dataset, we demonstrate significant improvements in performance and model generalization across vendors and imaging parameters for brain metastasis detection. The improved model is developing into a useful clinical tool for assisting diagnosis.

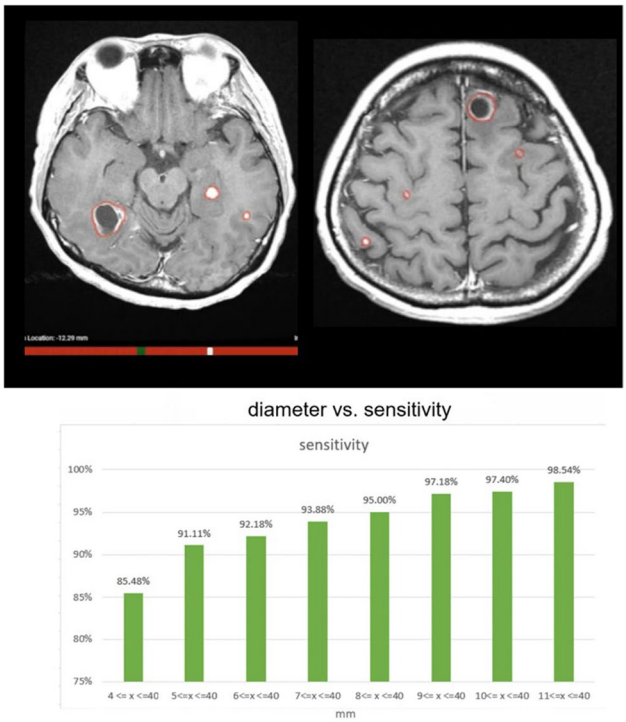

1-O28
NEUROVASCULAR COMPLICATIONS OF TRAUMA

Laura Saitta[1], Luca Roccatagliata[1,2], Martina Resaz[1], Giacomo Rebella[1], Claudia Rolla Bigliani[1], Giancarlo Salsano[1], Bruno Del Sette[1], Nicola Mavilio[1], Lucio Castellan[1]
[1]Department of Diagnostic and Interventional Neuroradiology, IRCCS Ospedale Policlinico San Martino, Genoa, Italy. [2]Dipartimento di scienze della salute (DISSAL), Università di Genova, Genoa, Italy

Introduction: The objective of this work is to describe the spectrum of cerebrovascular complications of trauma and to report the most common underlying mechanisms and radiological features. The following pathological entities will be addressed: post-traumatic aneurysms, post-traumatic carotid-cavernous fistula (CCF), post-traumatic arterial dissection/

occlusion, arterial rupture/avulsion and post-traumatic venous thrombosis. The associated risk of brain ischemia makes early diagnosis of cerebrovascular complications a pivotal point of radiological evaluation of trauma patients.

Background: Traumatic head injuries typically cause intracranial bleeding including intraparenchymal hemorrhage, subarachnoid hemorrhage, subdural hematomas and epidural hematomas. Uncommonly, trauma can cause cerebrovascular complications, which involve either the arterial or the venous side. The type and severity of brain injury depend on the traumatic mechanism, on the site of impact and on the osseous structures possibly involved. The more common underlying traumatic mechanism is blunt trauma, while penetrating trauma is by far less frequent. With regard to the arterial side, the underlying histopathological damage characterizes the resulting traumatic complication. Dissection, occlusion, pseudo-aneurysms or artero-venous fistulas present with different types of involvement of the three arterial layers (i.e. intima, media and adventitia). With respect to the venous side, a dural tear adjacent to a venous sinus or less frequently a compressive effect may be the pathomechanisms underlying post-traumatic venous thrombosis.

Discussion: Non-contrast computed tomography (CT) and CT-Angiography (CTA) are the most important techniques for diagnosis. Angiography is useful to confirm CTA findings and plays a key role in treatment. Magnetic resonance imaging (MRI) is useful in selected cases, for example to evaluate the presence of acute ischemia. Early diagnosis, especially in vascular lesions related to potential brain ischemic consequences, is key for a better outcome, and the radiologists should be trained to recognize the instances requiring to proceed with CTA in a traumatized patient. The modified Denver criteria, especially in their expanded version are the most used criteria for screening blunt cerebrovascular injuries. Also, the Boston criteria have been proposed. Moreover, the Denver scale classifies the features of vascular injury according to the CTA findings in 5 grades (I-V), with increasing risk of brain ischemia in relation to higher grades of arterial injury (carotid arteries or vertebral arteries).

Conclusions: Neurovascular complications are not common after head trauma, but they must not be overlooked because they might lead to severe consequences and be life threatening. Early diagnosis and endovascular treatment can be lifesaving.

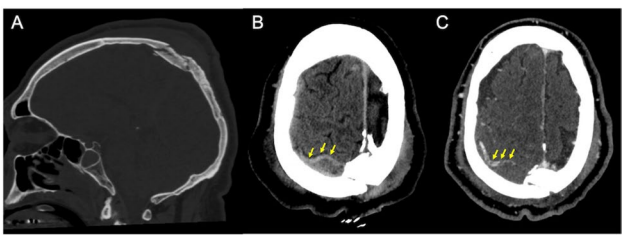

1-O29
FUNCTIONAL DIVERSIFICATION OF THE CONTRALESIONAL PRIMARY MOTOR CORTEX IS RELATED TO MOTOR FUNCTION IN STROKE PATIENTS

Zsigmond Tamás Kincses[1], Péter Klivényi[2], Nikoletta Szabó[2], Dániel Veréb[1]
[1]University of Szeged, Department of Radiology, Szeged, Hungary. [2]University of Szeged, Department of Neurology, Szeged, Hungary

Background: The contralesional primary motor cortex undergoes plastic connectivity changes during post-stroke motor recovery. However, the nature of these changes were mostly investigated in interhemispheric connections. Here we investigate changes of intrahemispheric functional connectivity in the contralesional primary motor cortex and how it relates to motor function using a gradient-based approach.

Methods: We recruited 17 patients with left medial cerebral artery stroke and 17 age- and sex-matched healthy participants. Data from the Human Connectome Project were used as reference to validate functional gradients based on intrahemispheric functional connectivity. Muscle strength of patients was assessed using the Medical Research Council grading. Participants underwent T1-weighted and 10-minute resting state functional MRI scans. Connectopic mapping was used to define functional gradients in the right primary motor cortex (Haak et al., 2018). Using a spatial regression model to describe the gradients, we compared model coefficients between groups using a Kruskal-Wallis test and assessed the relationship between model parameters and clinical characteristics with partial Spearman's rank correlation.

Results: The functional gradient of the right primary motor cortex was similar using whole-brain and intrahemispheric functional connectivity in the reference group. Spatial model coefficients were not different from healthy participants in stroke patients (corrected $p>0.05$). However, the coefficients in patients correlated with the muscle strength of the affected upper (Figure 1.) and lower limbs and NIHSS scores, corrected for age, sex and time since stroke ($R=-0.569$, $p<0.033$; $R=-0.573$, $p<0.032$; $R=0.535$, $p<0.049$ respectively). The alterations mainly manifested in a steeper-than-normal change of connectivity profiles along a mediolateral axis, and better motor function was associated with increasingly steep diversity curves.

Conclusion: Plastic changes of intrahemispheric functional connectivity in the contralesional primary motor cortex of stroke patients might manifest as altered functional

gradients, which correspond to motor function and clinical condition.

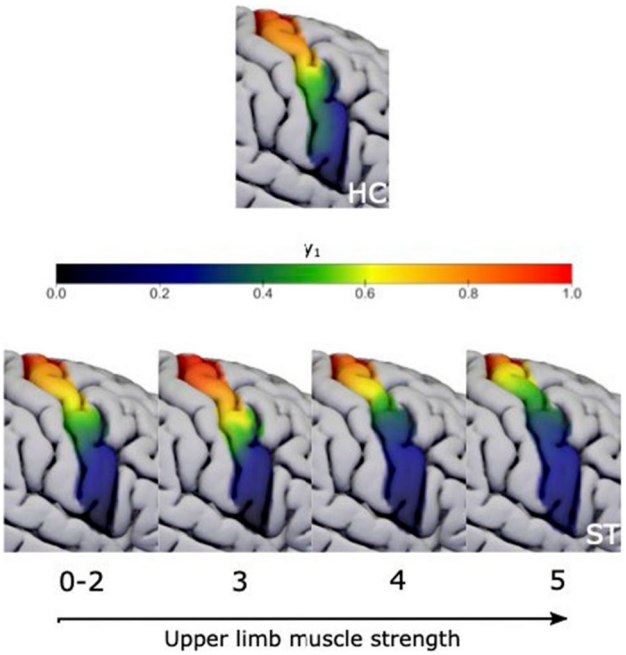

1-O30

SEMI-AUTOMATED TEXTURE ANALYSIS TO DIFFERENTIATE TREATMENT-RELATED CHANGES FROM RECURRENT TUMOR

Gokcen Coban[1], Ahmet Yasir Altınbulak[1], Kader KarliOguz[1]
Hacettepe University, Medical School, Department of Radiology, Ankara, Turkey

Purpose: To differentiate treatment-related changes from recurrent tumors is a challenge in monitoring grade 4 gliomas receiving chemoradiotherapy. Our aim is to differentiate these entities using semi-automated texture analysis.

Materials and Methods: This IRB-approved prospective analysis was performed on patients with grade-4 gliomas (54 IDH-mutant and 66 IDH-wild types). On a 3.0 T system, a total of 120 patients were scanned (Signa Architect, GE Healthcare). Three hundred thirty-six radiomic features were produced from contrast-enhanced T1-weighted, fluid-attenuated inversion recovery (FLAIR) imaging and apparent diffusion coefficient (ADC)maps. Texture analysis was carried out with postprocessing tools (Olea Sphere, version 3.0, Olea Medical, La Ciotat, France). Using a semiautomated region-growing segmentation method, two raters separately segmented the tumors.

Result: Our preliminary texture analysis of the 120 resection cavities demonstrated that the gray-level co-occurance matrix features based on the FLAIR and contrast-enhanced T1-weighted images; neighboring gray-level dependence matrix; and gray-level run-length matrix based on ADC maps are promising to distinguish resection cavity changes (AUC > 0.840; accuracy > 85%).

Conclusion: Texture analysis can be used to differentiate pericavitary treatment-related changes from recurrent tumors, and could help to reduce the need for reoperation in follow-up MRI studies.

2. INTERVENTIONAL

2-O1

CLINICAL AND PROCEDURAL COMPARATIVE EVALUATION OF MRGFUS VIM ABLATION IN ESSENTIAL TREMOR AND PARKINSON'S DISEASE

Emanuele Tommasino[1], Federico Bruno[1], Alessandra Splendiani[1]
[1]University of L'Aquila, L'Aquila, Italy

Objectives: To evaluate the procedural and clinical outcome differences in patients with ET and PD treated by unilateral MRgFUS Vim ablation.

Methods: We evaluated 101 patients (46 ET, 55 PD). Clinical scores (CRST for tremor, QUEST for quality of life, MOCA for cognitive assessment) were recorded before treatment and with follow-up at 1 day and 1, 6, and 12 months. Technical parameters were recorded in all procedures. A comparison of all variables was made between the two groups.

Results: In ET patients, CRST scores improved by 63.1% immediately after treatment. The improvement remained substantially stable at the following 1-month, 6-months, and 1-year follow-up, with mild recurrence of tremor in 4 patients. In PD patients, CRST scores improved by 64% at 1 day, 56% at 1 month, and 59.2% at 1 year, with mild recurrence of tremor in 4 patients. Tremor reappearance occurred in 7 patients between the 3- and 6-months follow-up. QUEST and MOCA score changes were not statistically significant between the two groups. Thalamotomy-related complications occurred in 6 ET patients and 6 PD patients. No statistically significant differences were found between the two groups regarding technical procedural parameters, except for a higher number of sonications in the PD group.

Conclusions: MRgFUS is an effective treatment for both ET and PD patients, with milder deterioration of tremor and QoL scores improvement in the PD group during the follow-up.

2-O2
MECHANICAL THROMBECTOMY FOR ACUTE ISCHEMIC STROKE IN COVID-19 PATIENTS: MULTICENTER EXPERIENCE IN 111 CASES

Hanna Styczen[1], Volker Maus[2], Lukas Goertz[3], Martin Köhrmann[4], Christoph Kleinschnitz[4], Sebastian Fischer[2], Markus Möhlenbruch[5], Iris Mühlen[6], Bernd Kallmünzer[7], Franziska Dorn[8], Asadeh Lakghomi[8], Matthias Gawlitza[9], Daniel Kaiser[9], Joachim Klisch[10], Donald Lobsien[11], Stefan Rohde[12], Gisa Ellrichmann[13], Daniel Behme[14], Maximilian Thormann[15], Fabian Flottmann[16], Laurens Winkelmeier[16], Elke R Gizewski[17], Lukas Mayer-Suess[18], Tobias Boeckh-Behrens[19], Isabelle Riederer[19], Randolf Klingebiel[20], Björn Berger[20], Martin Schlunz-Hendann[21], Dominik Grieb[21], Ali Khanafer[22], Richard du Mesnil de Rochemont[23], Christophe Arendt[23], Jens Altenbernd[24], Jan-Ulrich Schlump[25], Adrian Ringelstein[26], Vivian Jean Marcel Sanio[26], Christian Loehr[27], Agnes Maria Dahlke[27], Carolin Brockmann[28], Sebastian Reder[28], Ulrich Sure[29], Yan Li[1], Ruben Mühl-Benninghaus[30], Thomas Rodt[30], Kai Kallenberg[31], Alexandru Durutya[31], Mohamed Elsharkawy[32], Paul Stracke[32], Mathias Gerhard Schumann[33], Alexander Bock[33], Omid Nikoubashman[34], Martin Wiesmann[34], Hans Henkes[22], Pascal J Mosimann[35], René Chapot[35], Michael Forsting[1], Cornelius Deuschl[1]

[1]Institute for Diagnostic and Interventional Radiology and Neuroradiology, University Hospital Essen, Essen, Germany. [2]Department of Radiology, Neuroradiology and Nuclear Medicine, University Medical Center Langendreer, Bochum, Germany. [3]Department of Diagnostic and Interventional Radiology, University Hospital Cologne, Cologne, Germany. [4]Department of Neurology and Center for Translational Neurosciences and Behavioral Sciences (CTNBS), University Hospital Essen, Essen, Germany. [5]Department of Neuroradiology, University of Heidelberg, Heidelberg, Germany. [6]Department of Neuroradiology, University of Erlangen-Nuremberg, Erlangen, Germany. [7]Department of Neurology, University of Erlangen-Nuremberg, Erlangen, Germany. [8]Department of Neuroradiology, University Hospital Bonn, Bonn, Germany. [9]Institute and Policlinic of Neuroradiology, Universitatsklinikum Carl Gustav Carus, Dresden, Germany. [10]Department of Diagnostic and Interventional Radiology and Neuroradiology, Helios General Hospital Erfurt,, Erfurt, Germany. [11]Department of Diagnostic and Interventional Radiology and Neuroradiology, Helios General Hospital Erfurt, Erfurt, Germany. [12]Department of Radiology and Neuroradiology, Klinikum Dortmund gGmbH, Dortmund, Germany. [13]Department of Neurology, Klinikum Dortmund gGmbH, Dortmund, Germany. [14]Department of Neuroradiology, University Hospital Magdeburg, Magdeburg, Germany. [15]Department of Radiology, University Hospital Magdeburg, Magdeburg, Germany. [16]Department of Diagnostic and Interventional Neuroradiology, University Hospital Hamburg-Eppendorf, Hamburg, Germany. [17]Department of Neuroradiology, Medical University of Innsbruck, Innsbruck, Austria. [18]Department of Neurology, Medical University of Innsbruck, Innsbruck, Austria. [19]Department of Diagnostic and Interventional Neuroradiology, Klinikum rechts der Isar, Technical University of Munich, Munich, Germany. [20]Department of Diagnostic and Interventional Neuroradiology, University Hospital OWL (Campus Bethel), Bielefeld, Germany. [21]Department of Radiology and Neuroradiology, Klinikum Duisburg - Sana Kliniken, Duisburg, Germany. [22]Clinic for Neuroradiology, Klinikum Stuttgart, Stuttgart, Germany. [23]Institute of Neuroradiology, University Hospital Frankfurt and Goethe University, Frankfurt am Main, Germany. [24]Department of Radiology and Neuroradiology, Gemeinschaftskrankenhaus Herdecke, Herdecke, Germany. [25]Department of Neuropediatrics, Gemeinschaftskrankenhaus Herdecke, Herdecke, Germany. [26]Department of Radiology and Neuroradiology, Kliniken Maria Hilf, Moenchengladbach, Germany. [27]Department of Radiology and Neuroradiology, Klinikum Vest, Recklinghausen, Germany. [28]Department of Neuroradiology, University Medical Center Mainz, Mainz, Germany. [29]Department of Neurosurgery and Spine Surgery, University Hospital Essen, Essen, Germany. [30]Department of Radiology, Klinikum Lueneburg, Lueneburg, Germany. [31]Department of Neuroradiology, Klinikum Fulda, Fulda, Germany. [32]Clinic for Radiology, University Hospital Muenster, Muenster, Germany. [33]Department of Neuroradiology, Vivantes Klinikum Neukoelln, Berlin, Germany. [34]Department of Diagnostic and Interventional Neuroradiology, University Hospital Aachen, Aachen, Germany. [35]Department of Neuroradiology, Alfried Krupp Hospital Ruttenscheid, Essen, Germany

Background: Data on the frequency and outcome of mechanical thrombectomy (MT) for large vessel occlusion (LVO) in patients with COVID-19 is limited. Addressing this subject, we report our multicenter experience.

Methods: A retrospective cohort study was performed of consecutive acute stroke patients with COVID-19 infection treated with MT at 26 tertiary care centers between January 2020 and November 2021.

Results: We identified 111 out of 11 365 (1%) patients with acute or subsided COVID-19 infection who underwent MT due to LVO. Cardioembolic events were the most common etiology for LVO (38.7%). Median baseline National Institutes of Health Stroke Scale score and Alberta Stroke Program Early CT Score were 16 (IQR 11.5–20) and 9 (IQR 7–10), respectively. Successful reperfusion (mTICI ≥2b) was achieved in 97/111 (87.4%) patients and 46/111 (41.4%)

patients were reperfused completely. The procedure-related complication rate was 12.6% (14/111). Functional independence was achieved in 20/108 (18.5%) patients at discharge and 14/66 (21.2%) at 90 days follow-up. The in-hospital mortality rate was 30.6% (33/108). In the subgroup analysis, patients with severe acute COVID-19 infection requiring intubation had a mortality rate twice as high as patients with mild or moderate acute COVID-19 infection. Acute respiratory failure requiring ventilation and time interval from symptom onset to groin puncture were independent predictors for an unfavorable outcome in a logistic regression analysis.

Conclusion: Our study showed a poor clinical outcome and high mortality, especially in patients with severe acute COVID-19 infection undergoing MT due to LVO

2-O3

SAFETY OF BOTULINUM TOXIN STELLATE GANGLION BLOCK IN THE TREATMENT OF ELECTRICAL STORM OR REFRACTORY VENTRICULAR ARRHYTHMIAS: CASE SERIES

Irene Dixe de Oliveira Santo[1], Douglas Silin[1], Riddhi Borse[1], Mark Blitzer[2], Juan Carlos Perez Lozada[1]
[1]Yale Radiology and Biomedical Imaging, New Haven, USA. [2]Yale School of Medicine - Cardiology, New Haven, USA

Introduction: Electrical storm (ES) is a life-threatening syndrome defined as 3 or more sustained episodes of ventricular arrhythmia (VA) or appropriate shocks from an implantable cardioverter-defibrillator (ICD) within 24 hours. Several studies have now shown that minimally invasive stellate ganglion block (SGB) with local anesthetics is safe and provides a reduction in VA burden in a significant fraction of patients. However, the duration of the effect is short and dependent on the type of anesthetic agent used. One potential solution would be to use longer-lasting agents like botulinum toxin (BT). Our goal was to evaluate the safety of performing an SGB with BT.

Methods: We describe a case series in which SGB with BT was performed in an attempt to manage ES or refractory VAs. Patient selection was conducted by a multidisciplinary team involving cardiology, anesthesiology, interventional radiology (IR), and surgery. Data was captured prospectively in all patients who were admitted or transferred to Yale-New Haven Hospital and treated with SGB with BT for refractory VA between July 2021 and May 2022. Additional retrospective data was gathered by the IR team from the EMR. Regarding the dose, a solution containing 100 IU BT reconstituted with 2 cc of sterile saline and mixed with 8 cc of 1% lidocaine was used, with 5 cc injected per side. All the possible adverse effects (AEs) described in the literature were discussed at length with the patients involved in this case series.

Results: From the patients included in our study, the only AEs noted were minimal left upper extremity weakness and numbness in one of the patients which resolved within less than 24 hours. No other immediate or long-term AEs were documented in the remaining patients.

Discussion: According to the literature, BT has been rarely associated with swelling, pain at the injection site, itching, muscle weakness, ipsilateral Horner's syndrome, flushing, and an increase in temperature of the ipsilateral upper extremity. Anaphylaxis, dysphagia, and difficulty breathing can also occur on extremely rare occasions.

Conclusion: SGB with BT was found to be safe in our small case series. Nevertheless, larger RCTs are needed to determine safety on a larger scale as well as determine the efficacy and duration of the effect. Furthermore, the dose of BT used in our study was based on the literature available for other indications. Further research may be required to determine the optimal dosage for ES and refractory VA.

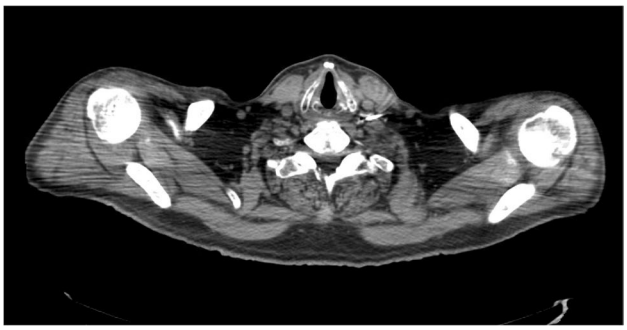

2-O4

INCIDENCE, CLINICAL SIGNIFICANCE AND LONGITUDINAL SIGNAL CHARACTERISTICS OF ISCHEMIC LESIONS RELATED TO DIAGNOSTIC CEREBRAL CATHETER ANGIOGRAPHY

David Schinz[1], Thomas Zimmermann[1], Kornelia Kreiser[2], Claus Zimmer[1], Jan Kirschke[1], Tobias Boeckh-Behrens[1], Hans Liebl[1]
[1]Department of Diagnostic and Interventional Neuroradiology, Klinikum rechts der Isar, Technical University Munich, Munich, Germany. [2]Department of Radiology/Neuroradiology, Universitäts- und Rehabilitationskliniken Ulm gGmbH, Ulm, Germany

Background: Digital subtraction angiography (DSA) of the brain is a routine procedure with a low incidence of

complications. Nevertheless, it is known to be associated with presumably clinically inapparent lesions detectable on diffusion-weighted imaging (DWI). However, there is a lack of data regarding the incidence, causative factors, clinical relevance of DWI-lesions as well as the longitudinal signal development of these lesions. We prospectively evaluated the incidence of DWI-lesions after elective DSA in healthy subjects and evaluated the lesions longitudinally using state-of-the-art MRI.

Methods: Eighty-two subjects undergoing elective diagnostic DSA were examined by MRI within 24 hours after DSA. DWI-lesions were systematically evaluated and measured. Neurological status of the subjects was assessed by clinical neurological examination and additional evaluation of subjective well-being using a modified health questionnaire before and after DSA. Subjects showing DWI-lesions received a follow-up MRI after a median of 5.1 months and were again questioned for neurological symptoms.

Results: After DSA 28% of 82 examined subjects showed a total number of 54 DWI-lesions on MRI. At follow-up, 20% of the lesions converted into persisting hyperintense FLAIR-lesions (Fig. 1). After DSA, none of the subjects showed a newly developed clinically apparent neurological deficit. Risk factors associated with the occurrence of DWI-lesions were long intervention time ($p < 0.001$), history of arterial hypertension, visible calcified plaques, and less experience of the examiner. While clinical examination did not show newly developed neurological deficits, self-perceived neurological changes as documented by the questionnaire used were at-trend significantly higher at follow-up.

Figure 1. Persistent high-signal lesion at follow-up.

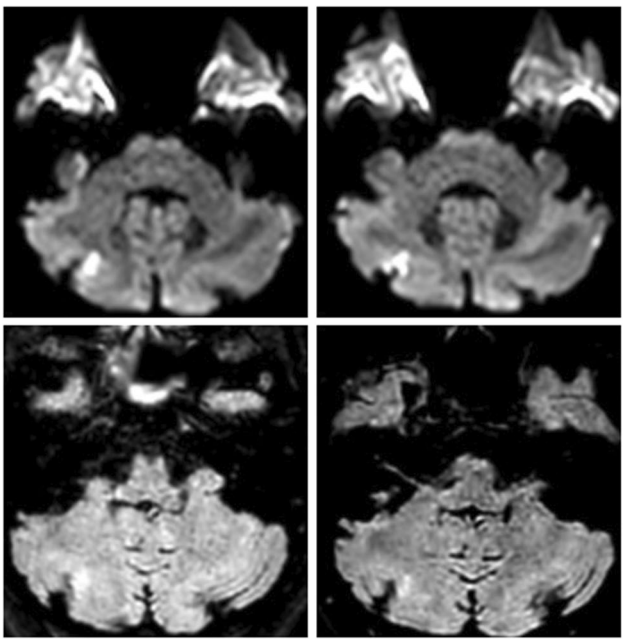

Upper row shows DWI at different heights after DSA with a high-signal ischemic lesion of the right cerebellar lobe. Bottom row shows FLAIR after DSA (left) and at follow-up (right) 3 months later with persistent hyperintensity.

Discussion: DSA is associated with a considerable number of microischemic lesions which in part are not fully reversible and remain as scar lesions in brain tissue. Likely due to small size and inconsistent location of the lesions, no apparent neurological deficits were observed related to lesion occurrence. However, subtle self-perceived changes may be associated with these lesions. Therefore, special attention is needed to reduce microischemic events to a minimum.

Conclusion: Presumably inapparent DWI-lesions are not fully reversible and subtle changes occur in some patients even in the absence of clear neurological deficits. Special attention should be given to cautious catheterization if plaques are present and optimal preparation with shorter intervention time.

2-O5
ENDOVASCULAR TREATMENT OF DISTAL MEDIUM VESSEL OCCLUSIONS USING MICROCATHETER ASPIRATION THROMBECTOMY

Dominik Grieb[1,2], Björn Greling[3], Katharina Schulz[1], Frederik Boxberg[1], Katharina Melber[1], Omar Abu-Fares[2], Heinrich Lanfermann[2], Martin Schlunz-Hendann[1], Dan Meila[3,4]
[1]Department of Radiology and Neuroradiology, Sana Kliniken Duisburg, Duisburg, Germany. [2]Department of Diagnostic and Interventional Neuroradiology, Medical School Hannover, Hannover, Germany. [3]Department of Interventional Neuroradiology, Johanna-Étienne-Hospital, Neuss, Germany. [4]Department of Diagnostic and Interventional Radiology, Helios Klinikum Krefeld, Krefeld, Germany

Introduction: Endovascular treatment (EVT) seems to be beneficial in distal medium vessel occlusion (DMVO) stroke even beyond middle cerebral artery (MCA) - M2 segment. However, data about aspiration thrombectomy of DMVOs is scarce since common aspiration catheters are usually too large for small distal intracranial arteries. We report our initial experiences using the microcatheter aspiration thrombectomy (MAT) technique for DMVOs in the MCA territory.

Methods: We retrospectively analyzed all acute ischemic stroke (AIS) patients that underwent MAT of a primary or secondary DMVO in the M3 or M4 segment between 01/2019 and 10/2021. Recanalization rates, procedural safety and outcome data were recorded.

Results: MAT of acute M3 and M4 occlusions was performed in 19 patients with AIS (primary DMVOs: 6; secondary DMVOs:

13). Successful revascularization to DMVO TICI ³ 2b was achieved in 58 % (11/19) with a single pass in all of them. NIHSS score at admission was 12 and 3 at discharge, respectively. 68 % (13/19) had a good clinical outcome at discharge (mRS 0-2). No symptomatic complications related to MAT occurred.

Discussion: Different recanalization devices for DMVOs including the 3MAX and low profile self-expandable stent retrievers (SRs) have already been used with promising results. However, the comparability is limited since the minority of occlusions in the appropriate studies are beyond the level of M2. Even in the so far only study on MAT for DMVOs, more than one third of cases were M2 occlusions. We excluded M2 occlusions because these are generally treated with thrombectomy techniques similar to large vessel occlusions. Initial results of M3 occlusions treated with Tigertriever 13 showed slightly higher recanalization rates (73.9% with DMVO TICI ≥ 2b) than with the MAT in our study (58% with DMVO TICI ≥ 2b. However, hemorrhagic complication rates following SR based thrombectomy in DMVOs seems to be considerably higher (up to 41%) than with MAT.

Conclusion: MAT of DMVOs in the MCA territory is a technically feasible and effective treatment with a notably low complication rate.

Keywords: stroke, thrombectomy, distal medium vessel, aspiration

Literature:

Crockett MT et al. J Neurointerv Surg 2019;11:714-8.
Fischer S et al. Neuroradiology 2021; https://doi.org/10.1007/s00234-021-02792-x.
Guenego A et al. Interv Neuroradiol 2021; https://doi.org/10.1177/15910199211039926.

Figure: NIHSS 9. Isolated right M3 occlusion (A-C) and full recanalization (DMVO-TICI 3) after MAT (E, F). Note position of microcatheter tip in the proximal part of the clot (dotted arrow in D) and Sofia 5F in Truncus inferior (black arrow in D).

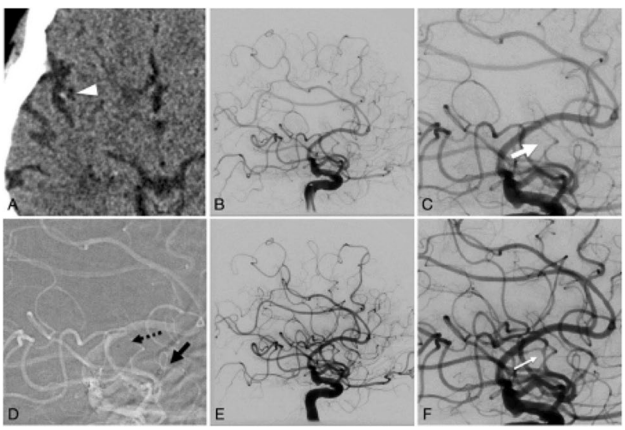

2-O6

ANGIOGRAPHIC CLOT SIGNS IN ENDOVASCULAR THROMBECTOMY DO NOT PREDICT OUTCOME IN PATIENTS WITH ACUTE LARGE VESSEL OCCLUSION OF ANTERIOR CIRCULATION

André Miranda[1], André Araújo[1], Ramy Abdelnaby[2], Marta Rodrigues[1], Jörg B. Schulz[2], Martin Wiesmann[3], Omid Nikoubashman[4], Arno Reich[2], Sergio Castro[1], Manuel Ribeiro[1], João Pinho[2]
[1]Interventional Neuroradiology Unit, Centro Hospitalar Vila Nova de Gaia/Espinho, Vila Nova de Gaia, Portugal. [2]Department of Neurology, University Hospital, RWTH Aachen University, Aachen, Germany. [3]Department of Diagnostic and Interventional Neuroradiology, University Hospital, RWTH Aachen University, Aachen, Portugal. [4]Department of Diagnostic and Interventional Neuroradiology, University Hospital, RWTH Aachen University, Aachen, Germany

Introduction: The angiographic appearance of the occlusion site has been suggested to influence outcomes of stroke patients with large vessel occlusion (LVO) who undergo endovascular treatment (EVT). Our aim was to study the association of angiographic clot signs with stroke aetiology and determine its prognostic role on angiographic and clinical outcomes in stroke patients with anterior circulation LVO.

Methods: We conducted a multicentric retrospective study based on prospective registries of acute ischemic stroke patients. We included consecutive patients with carotid-T, M1 or M2 occlusion who underwent EVT during a period of 3 years. Intraprocedural angiographic configuration of occlusion site before mechanical thrombectomy was reviewed by two independent observers, blinded to outcomes. Angiographic and clinical outcomes were compared between clot sign groups.

Results: We included 903 patients, with median age of 78 [interquartile range (IQR) 67-85] years, 59.8% were male, median baseline NIHSS 14 [IQR 9-18], of which 344 (39.5%) received intravenous thrombolysis. The meniscus sign was present in 170 (18.8%) cases, tram-track sign in 120 (13.3%), cut-off sign in 389 (43.1%) and tapered sign in 198 (21.9%) patients (Figure 1). Interobserver agreement was moderate (κ=0.60). LVO was observed in carotid-T in 129 (14.7%), M1 in 463 (52.8%) and M2 in 285 (32.5%) cases. Specifically, LVO was less frequently detected in carotid-T in tapered sign (8.1%; p=0.002). The presence of meniscus sign was more often observed in cardioembolic stroke (75.9%; p=0.009) while intra-cranial stenosis was more common in tapered occlusions (9.3%; p=0.005). Successful (mTICI 2b-3) and complete recanalization (mTICI 3) were observed in 811 (92.5%) and 555 (63.3%) cases,

respectively, and did not differ significantly between clot sign groups. Stent-retriever alone was more successful in recanalization (mTICI 2b-3) in tapered sign (55.2% vs 43.2%; p=0.000) whereas combined stent-retriever and contact aspiration was more successful in cut-off sign (66.2% vs 31.05%; p=0.000). Number of passes, in-hospital mortality and favourable outcome (mRS 0-2) at 90 days were similar between clot sign groups. In multivariable binary logistic regression, angiographic clot signs were not significantly associated with successful reperfusion, first pass effect or favourable outcome.

Conclusion: The angiographic configuration of occlusion site in acute ischemic stroke of anterior circulation who undergo EVT does not influence successful recanalization or clinical outcomes, but may associate with stroke aetiology (cardioembolic vs arterial stenosis). Further research is needed to determine the importance of clot sign in choice of endovascular technique (stent-retriever vs combined technique).

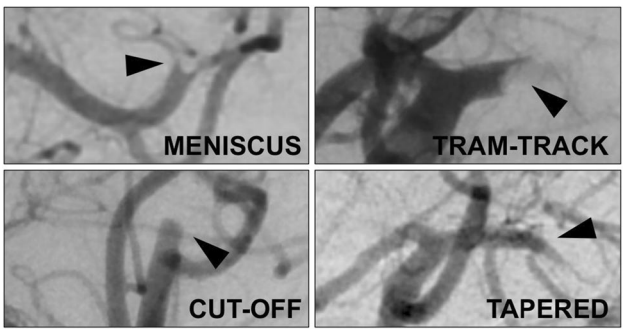

Figure 1. Angiographic configuration of occlusion sites before endovascular treatment (mechanical thrombectomy).

2-O7

DEEP LEARNING-BASED AUTOMATED DEVICE DETECTION FOR ASSESSMENT STANDARDISATION IN MECHANICAL THROMBECTOMY

Helena Guerreiro[1], Maximilian Nielsen[2], Thilo Sentker[2], Evelin Schmidt[3], Helge Kniep[1], Jens Fiehler[2], Rene Werner[2]
[1]Diagnostic and Interventional Neuroradiology, University Medical Center Hamburg-Eppendorf, Hamburg, Germany. [2]University Medical Center Hamburg-Eppendorf, Department of Computational Neuroscience, Hamburg, Germany, Hamburg, Germany. [3]Eppdata GmbH, Hamburg, Germany, Hamburg, Germany

Introduction: The clinical benefits of mechanical thrombectomy with stent retriever has shown in the last years irrefutable evidence. A post-operative reconstruction of procedural steps is due to the lack of conformity in image documentation often challenging. In order to simplify the complexity of image evaluation, an automated image interpretation could be applied. In this way, a relation between procedural stage, used device and thrombolysis in cerebral infarction scoring (TICI) as previously described1 could be assessed.

Aim of this Study: To prove the feasibility of a deep learning algorithm for the recognition of clot extraction devices in digital subtraction angiography (DSA) image data, obtained during mechanical thrombectomy. We aim to identify the presence of a stent retriever (SR) on a given DSA-Series and whether the device corresponds to a Solitaire (Medtronic, Minnesota, USA).

Methods: A total of 1784 Series were analyzed. The images were divided in three classes: no device (n=1614), solitaire (n=80) or other devices (n=170), covering several different manufactureres. A combination of deep neural network and multihead-attention block2 was used. Dimensionality reduction from 2d+t to 2D was achieved by applying a maximum intensity projection on each view. Each view is then encoded using an XCiT based encoder Network3.Finaly both image representations are fused using a multihead attention module and classified through a linear layer. The whole network was trained in an end-to-end fashion with standard cross entropy as a loss function

Results: Regarding presence of SR, 94% of the no device series and 89% including a device were identified correctly. The device Solitaire could be identified in most instances (82%), other devices are still classified accurate above chance, 21% were confused with Solitaire. Overall the balanced accuracy is 81%.

Conclusion: Automated assessment of DSA images on the presence and differentiation of devices is feasible. Its application on evaluation of wider data sets should be further evaluated.

2-O8

NOVEL SYNTHETIC CLOT ANALOGS FOR IN-VITRO STROKE MODELLING

Helena Guerreiro[1], Nadine Wortmann[2], Thomas Andersek[2], Tuan N. Ngo[1], Andreas Frölich[1], Dieter Krause[2], Jens Fiehler[1], Anna A. Kyselyova[1], Fabian Flottmann[2]
[1]Diagnostic and Interventional Neuroradiology, University Medical Center Hamburg-Eppendorf, Hamburg, Germany. [2]Hamburg University of Technology, Institute of Product Development and Mechanical Engineering Design, Hamburg, Germany, Hamburg, Germany

Introduction: The increased demand for training of mechanical thrombectomy in ischemic stroke urges the creation of

new simulation models for training and device assessment. Clot characterization has shown to play a role in procedural planning and thrombectomy device effectiveness.

Aim of the study: In this study, we aim to analyze the characteristics and applicability of completely synthetic, animal-free clots developed by the authors, in the setting of an in-vitro model of mechanical thrombectomy.

Methods: Synthetic clots based on agarose (n=12) and silicone (n=11) were evaluated in a previously described in-vitro neurointervention simulation of mechanical thrombectomy with clot extraction devices. 9 clots were excluded due to insufficient vessel occlusion and failure to integrate with clot extraction device. Synthetic thrombi were characterized and compared using a categorical score-system on vessel occlusion, elasticity, fragmentation, adherence and device integration.

Results: Both agarose-based and silicone-based clots demonstrated relevant flow arrest and a good integration with the clot extraction device. Silicone-based clots scored higher on adherence to the vessel wall and elasticity. Calcified clots of mixed nature were simulated with addition of 3D printed structures.

Conclusion: Selected synthetic clots can successfully be implemented in an in-vitro training environment of mechanical thrombectomy. The clots' different properties might serve to mimic fibrin-rich and red blood cell human thrombi.

2-O9

DISTAL EMBOLIZATION IN RELATION TO RADIOLOGICAL THROMBUS CHARACTERISTICS, TREATMENT DETAILS, AND FUNCTIONAL OUTCOME: RESULTS OF THE ESCAPE-NA1 TRIAL

Fouzi Bala[1,2], Manon Kappelhof[3], Johanna Ospel[2], Petra Cimflova[2], Wu Qiu[2], Nishita Singh[2], Mohammed Almekhlafi[2], Bijoy Menon[2], Michael Hill[2], Mayank Goyal[2]
[1]CHU Lille, Lille, France. [2]University of Calgary, Calgary, Canada. [3]Department of Radiology and Nuclear Medicine, Amesterdam, Netherlands

Introduction: Distal embolization (DE) is a common complication of endovascular treatment (EVT). We aimed to investigate the association of radiological thrombus characteristics and treatment details with distal embolization (DE).

Methods: Patients with thin-slice (≤2.5 mm) baseline non-contrast CT and CT-angiography from the ESCAPE-NA1 trial (Efficacy and safety of nerinetide for the treatment of acute ischemic stroke) were included. Thrombus annotation was performed manually on co-registered scans by readers blinded to clinical data. We assessed thrombus location, distance from ICA terminus, length, perviousness, absolute attenuation, and hyperdense artery sign (HAS). In addition, we evaluated balloon guide catheter (BGC) use during EVT, first-line EVT approach, the number of thrombectomy passes, and prior intravenous thrombolysis (IVT) administration. DE was defined as the occurrence of emboli distal to the target artery or in new territories during EVT. The association between thrombus characteristics, treatment details and DE was evaluated using descriptive statistics and multivariable mixed-effects logistic regression, resulting in adjusted odds ratios (aOR) with 95% confidence intervals (95%CI). Interaction between IVT and radiological thrombus characteristics was assessed by adding interaction terms to separate models.

Results: In total, 496/1105 (44.9%) ESCAPE-NA1 patients were included. DE was detected in 251/496 patients (50.6%). Patients with DE had longer thrombi (median 28.5 mm [IQR 20.8-42.3] versus 24.4 mm [IQR 17.1-32.4], p<0.01). There were no statistically significant differences in the other thrombus characteristics. Independent predictors of DE were thrombus length (aOR 1.02, 95%CI 1.01-1.04), BGC use (aOR 0.49, 95%CI 0.29-0.85) and number of passes (aOR 0.82, 95%CI 0.67-0.96). In patients with HAS, IVT reduced the odds of DE (aOR 0.47, 95%CI 0.28-0.79), pinteraction=0.03.

Conclusion: DE was associated with longer thrombi, no BGC use, and more EVT passes. IVT was associated with a reduced risk of DE in patients with HAS. These findings may support treatment decisions on IVT and EVT approaches

2-O10

PERIVASCULAR MACROPHAGES - MEDIATORS OF MICROVASOSPASMS AFTER *SUBARACHNOID HEMORRHAGE*?

Julian Schwarting[1,2,3], Xiangjiang Lin[2,3], Nicole A. Terpolilli[2,4,3], Nikolaus Plesnila[2,3]
[1]Department of Diagnostic and Interventional Neuroradiology, Klinikum rechts der Isar, Technische University Munich, Munich, Germany. [2]Institute for Stroke and Dementia Research (ISD), Munich University Hospital, Munich, Germany. [3]Munich Cluster for System Neurology (SyNergy), Munich, Germany. [4]Department of Neurosurgery, Munich University Hospital, Munich, Germany

Background: The first 72 hours after Subarachnoid hemorrhage (SAH) are characterized by perfusion deficits in the cerebral microcirculation. Spasms of arterial microvessels

occur in patients and after experimental SAH. Recently, inactivation of perivascular macrophages (PVM) has been demonstrated to improve neurological outcome after experimental SAH; the mechanisms of this phenomenon are not clear yet.

Aim of this study: To Investigate the role of perivascular macrophages (PVM) for the formation of microvasospasms after experimental SAH.

Methods: C57Bl6 mice received liposomes w/o Clodronate (n=8/each) ivc seven days before SAH. SAH was induced by filament perforation under continuous monitoring of CBF and ICP. Six hours after SAH induction, the cerebral microcirculation was investigated by in-vivo 2-photon microscopy. Caliber variations of the cerebral microvasculature were analyzed in nine standardized regions of interest. Histological quantification of PVMs with CD206 and Laminin staining was performed after transcardial perfusion.

Results: PVM were located around 0 and 1st order penetrating arterioles and depleted by Clodronate ($p<0.01$). After SAH, MVS predominantly occurred in pial arteries (17 IQR 6/animal), 0 and 1st order penetrating arterioles (9 IQR 3 and 2 IQR 2/animal). Macrophage depletion reduced the number of MVS/animal (to 4 IQR 9 in pial vessels, $p=.005$, 1 IQR 1 in 0, $p<.001$, and 0 IQR 1 in 1st order penetrating arterioles, $p=.11$).

Conclusion: Our results suggest that PVM are involved in microvasospasm formation after experimental SAH.

2-O11

EVALUATION OF CAROTID BIFURCATION PLAQUE VULNERABILITY: COMPARING MRI AND ULTRASOUND-BASED MODALITIES

Federica Rea De Falco[1,2], Zsolt Kulcsar[2], Tilman Schubert[2], Miklos Krepuska[2]
[1]Department of Neurology, University Hospital Zürich, Zürich, Switzerland. [2]Department of Neuroradiology, University Hospital Zürich, Zürich, Switzerland

Introduction: Vulnerable plaques are important risk factors for the development of TIA and ischemic stroke. The vulnerability of carotid artery plaques can be evaluated using MRI. The value of plaque evaluation using ultrasound remains understudied. We aimed to evaluate the congruency of ultrasound compared to MRI for the prediction of plaque vulnerability.

Methods: In a retrospective analysis a cohort of stroke/TIA admitted to the University Hospital Zürich fulfilled the criteria of a combined special protocol of plaque visualization utilizing MRI/ ultrasound and CTA of the carotid bifurcation due to suspected unstable plaques within the 24 hours after admission. The hallmark of carotid plaque characteristics, such as haemorrhage, ulceration, lipid-rich necrotic core, thin/ruptured fibrous cap degree of stenosis of 13 patients (8 male, 5 female, mean age 73 years) were categorized by two blinded investigators.

Results: 6 plaques were classified as vulnerable on MRI, and 6 plaques were suspected to be unstable on ultrasound. 1 patient was considered uncertain. 9 (75%) of patients' MRI and ultrasonographic techniques were in agreement and classified vulnerable.

Conclusions: Through a retrospective analysis using a multimodal approach in a regular stroke workup setting, we demonstrate that ultrasound of the carotid bifurcation may be a suitable tool in predicting plaque vulnerability (true negatives).

3. PEDIATRIC

3-O1

GUIDELINES FOR MAGNETIC RESONANCE IMAGING IN PEDIATRIC HEAD AND NECK PATHOLOGIES: A MULTICENTRE INTERNATIONAL CONSENSUS PAPER

Felice D'Arco[1,2], Livja Mertiri[1,3], Pim de Graaf[4], Bert De Foer[5], Katarina S. Popovič[6], Maria I. Argyropoulou[7], Kshitij Mankad[1], Hervé J. Brisse[8,9], Amy Juliano[10], Mariasavina Severino[11], Sophie Van Cauter[12,13], Mai-Lan Ho[14,15], Caroline D. Robson[16], Ata Siddiqui[2,17], Steve Connor[2,17,18], Sotirios Bisdas[19,20]
[1]Radiology Department, Great Ormond Street Hospital for Children, London, United Kingdom. [2]Radiology Department, Guy's and St Thomas' NHS Foundation Trust, London, United Kingdom. [3]Faculty of Medicine and Dentistry, Sapienza University of Rome, Rome, Italy. [4]Department of Radiology and Nuclear Medicine, Cancer Center Amsterdam, Amsterdam UMC, Vrije Universiteit Amsterdam, Amsterdam, Netherlands. [5]Radiology Department, GZA Hospitals, Antwerp, Belgium. [6]Neuroradiology department, Clinical Institute of Radiology, University Medical Center Ljubljana, Zaloška 7, 1000 Ljubljana, Ljubljana, Slovenia. [7]Department of Clinical Radiology and Imaging, Medical School, University of Ioannina, Ioannina, Greece. [8]Imaging Department, Institut Curie, Paris, France. [9]Institut Curie, Paris Sciences et Lettres (PSL) Research University, Paris, France. [10]Department of Radiology,

Massachusetts Eye and Ear, Harvard Medical School, Boston, USA. [11]Neuroradiology Unit, IRCCS Istituto Giannina Gaslini, Genoa, Italy. [12]Department of Medical Imaging, Ziekenhuis Oost-Limburg, Genk, Belgium. [13]Faculty of Medicine and Life Sciences, Hasselt University, Hasselt, Belgium. [14]Nationwide Children's Hospital, Columbus, USA. [15]The Ohio State University, Columbus, USA. [16]Department of Radiology, Boston Children's Hospital, Harvard Medical School, Boston, USA. [17]Department of Neuroradiology, Kings College Hospital NHS Foundation Trust, London, United Kingdom. [18]School of Biomedical Engineering and Imaging Sciences, St Thomas' Hospital, King's College, London, United Kingdom. [19]Lysholm Department of Neuroradiology, The National Hospital for Neurology & Neurosurgery, University College London Hospitals NHS Foundation Trust, London, United Kingdom. [20]Department of Brain Repair and Rehabilitation, UCL Queen Square Institute of Neurology, London, United Kingdom

The use of standardized imaging protocols is paramount in order to facilitate comparable, reproducible images and to optimize patient care. Standardized MR protocols are lacking when studying head and neck pathologies in the pediatric population. We propose an international, multicentre consensus paper focused on providing the best combination of acquisition time/technical requirements and image quality. Distinct protocols for different regions of the head and neck and for specific pathologies or clinical indications are recommended.

Methods: We first assessed the variability of head and neck protocols across institutions in Europe and North America, and then provided a consensus based on the opinion of the members of different European radiology societies and specific committees.
A first paper version was drafted by the co-first authors and the last author. The draft was subsequently circulated among the co-authors and collaborators of the COMPS group and representatives of the endorsing scientific societies.

Results: We propose specific MR protocols for each head and neck region and, in some cases, for specific diseases, with a range of technical parameters. Optional sequences are also added.

Conclusions: MR imaging in pediatric head and neck pathology is very complex. We propose standardized MR protocols to help the readers in approaching pediatric head and neck pathologies and to help minimize the variability and maximize diagnostic efficiency. We discussed the added value of CT in specific areas or diseases, basics and optional/alternative MR sequences depending on the clinical problem/region of interest.

3-O2

CEREBRAL BLOOD FLOW PATTERNS IN PRETERM AND TERM NEONATES ASSESSED WITH PSEUDO-CONTINUOUS ARTERIAL SPIN LABELING PERFUSION MRI

Eleonora Piccirilli[1,2], Antonio M. Chiarelli[1,2], Carlo Sestieri[1,2], Daniele Mascali[1,2], Darien Calvo Garcia[1,2], Adele Primavera[3], Rita Salomone[3], Richard G. Wise[1,2], Antonio Ferretti[1,2], Massimo Caulo[1,4,2]
[1]University of Chieti, Department of Neuroscience, Imaging and Clinical Sciences, Chieti, Italy. [2]Institute for Advanced Biomedical Technologies (ITAB), University of Chieti, Chieti, Italy. [3]University Hospital of Chieti, Department of Paediatrics, Neonatology and Neonatal Intensive Care Unit, Chieti, Italy. [4]University of Chieti, Department of Radiology, Chieti, Italy

Abnormalities in CBF distribution may play a role in functional modifications of the brain in preterm infants. Our aim was to evaluate modifications of CBF patterns assessed with pCASL in preterm (PT) and full-term (FT) infants using a data-driven model. 72 PT and 51 FT with no major neonatal morbidity were scanned within 7 days of TEA on a 3T; the standardized MR protocol included a pCASL. GMH and PVL were also evaluated, stratifying PT into those without (PT_H) and those with prematurity-related brain injury (PT_{PVL} and PT_{GMH}). The grey matter CBF (CBF_{GM}) was extracted from 90 ROIs of the UNC Infant Atlas and normalized through z-scoring ($nCBF_{GM}$). The ROIs were combined using hierarchical clustering (HC) applied on $nCBF_{GM}$ of healthy neonates. Differences in $nCBF_{GM}$ within the clusters as a function of prematurity and prematurity-related brain injuries were evaluated by multiple one-way ANOVAs. The HC identified 4 main clusters of ROIs: Fronto-Temporal, Parieto-Occipital, Insular-Deep Grey Matter and SensoriMotor. In Fronto-Temporal, $nCBF_{GM}$ was higher in FT compared to all PT_H ($p<.05$), with a positive association between $nCBF_{GM}$ and GAB ($r=.37$; $p<.01$) and higher in PT_{PVL} compared to PT_H ($p<.05$).In SensoriMotor, $nCBF_{GM}$ was lower in FT compared to all PT_H ($p<10^{-3}$) with a negative association between $nCBF_{GM}$ and GAB ($r=.42$, $p<10^{-3}$). In Insular-DMG, $nCBF_{GM}$ was higher in

PT_H compared to PT_{PVL} ($p<.05$) and to PT_{GMH} ($p<0.1$). CBF_{GM} at TEA distributes heterogeneously within 4 clusters of ROIs both as a function of GAB between PT_H and PT with brain injuries.

3-O3
DEVELOPMENT OF FETAL VENTRICULAR VOLUME REFERENCE NORMS USING NNUNET

Minerva Zhou[1], Pierre Nedelec[1], Hannah Kang[1], Kimberly Wagas[1], David Weiss[2], Andreas Rauschecker[1]
[1]University of California - San Francisco, San Francisco, USA. [2]Georgia Institute of Technology, Atlanta, USA

Introduction: Using deep learning methods to segment and measure ventricular volume of fetal brain MRIs.

Methods: We applied nnU-Net to segment the ventricular system of 91 nonpathologic and 9 pathologic fetal brain MRIs across a variety of gestational ages (19-36 weeks). Twenty fetal brain MRIs from our institution were reconstructed to high-resolution 3D volumes using slice-to-volume reconstruction and then manually segmented and combined with the MICCAI Fetal Tissue Annotation Challenge data to generate a dataset of 100 fetal brain MRI volumes, which were randomly split into 80 training studies and 20 test studies in a 5-fold cross-validation. Performance was assessed using Dice coefficients and volume comparison to manual reference segmentation. A normative reference of ventricular volume across gestational ages was generated using the 91 nonpathologic training studies.

Results: The nnU-Net predicted segmentation of fetal ventricles with median Dice score of 0.90 (IQR 0.88-0.93; Fig 1A). The automatically computed ventricular volume measurements were highly correlated with manual measurements (Pearson's r=0.99, P<0.001, Fig 1B). A normative range of ventricular volumes across gestational ages was developed using the automated segmentation volumes. All 9 patients with hydrocephalus were predicted to be greater than two standard deviations higher than the age-specific reference mean (Fig 1C). Intracranial volumes, calculated from manual segmentation, increase with gestational age while ventricular volumes remain relatively constant (Fig 1D).

Discussion & Conclusion: Deep learning techniques can quickly and accurately quantify ventricular volume on fetal brain MRI and subsequently identify hydrocephalus based on a normative reference standard.

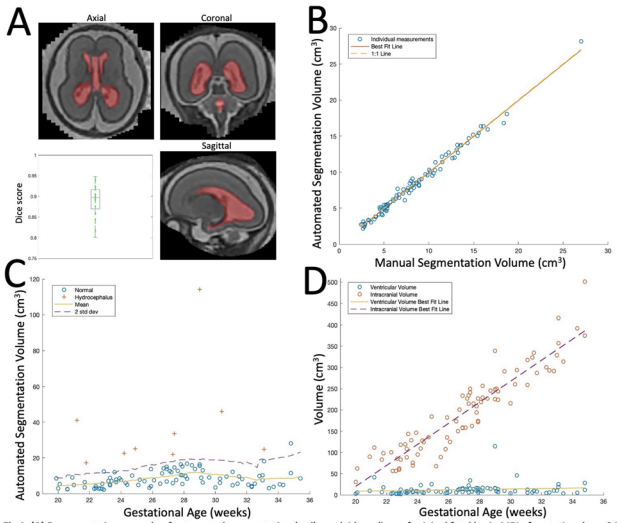

Fig 1. (A) Representative example of automated segmentation (red) overlaid on slices of original fetal brain MRI of gestational age 24 weeks and 5 days in various planes. (Lower left) Model performance with individual Dice scores and box plot comparing automated to manual segmentation. **(B)** Scatterplot with strong agreement between manual and automated segmentation with best fit line and 1:1 identity line shown, nearly overlapping. **(C)** Ventricular volumes as a function of gestational age across 91 normal fetal brain MRIs (o) with 9 fetal brains with hydrocephalus (+) which fall outside of the range of normative values. **(D)** Intracranial and ventricular volume as a function of gestational age demonstrating intracranial volumes increasing with gestational age while ventricular volumes remain relatively constant.

3-O4
IN OUR CHILDREN'S EYES - ORBITAL IMAGING FINDINGS FROM A PEDIATRIC HOSPITAL COHORT

Fátima Hierro[1], André Miranda[2], Pedro Bem[1], Joana Nunes[2], Ana Geraldo[2]
[1]Hospital Pedro Hispano, Matosinhos, Portugal. [2]Centro Hospitalar de Vila Nova de Gaia, Vila Nova de Gaia, Portugal

Introduction: The pediatric orbit, as well as the pathologies that can affect it, differ from typical adult findings, and not just because of its smaller size - children are not small adults. In pediatric neuroradiology, it is essential to know the most frequent malformative pathology, as well as conditions that may require urgent intervention.

Methods: The objective of this pictorial essay is to systematize the main pathological groups that can affect this anatomical region in children and to correlate the imaging presentation with the clinical presentation and histological and genetic diagnosis, whenever available.

Pediatric studies from Centro Hospitalar de Vila Nova de Gaia, a tertiary hospital in Portugal, performed between January 2013 and March 2022 were reviewed, identifying those in which there were abnormal orbital findings.

Results: We have identified illustrative cases from all pathological subgroups: malformative, infectious, inflammatory,

neoplastic, traumatic and idiopathic pathology affecting the orbit. Thirty-one children with orbital imaging manifestations were identified. MRI was used in majority of the studies in this population, however in six of the cases characterization of the orbits was performed by CT due to the nature of the pathology, with expected predominant bone involvement, or because it was an urgent clinical context.

Conclusion: Indications for imaging the pediatric orbit are numerous, including malformative, tumoral (e.g. retinoblastoma), inflammatory (e.g. demyelinating), infectious, and even traumatic pathology.
Recognition of the most common orbital finding, as well as rare pathologies that require urgent intervention, makes it possible to avoid submitting the child to unnecessary tests and therapies, as well as implementing appropriate treatment in a timely manner.

Keywords: pediatric; orbit; marformation

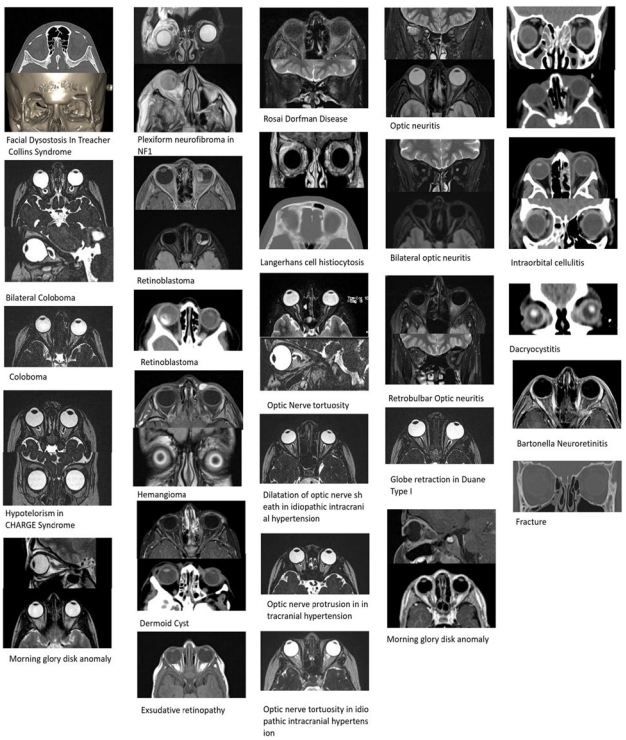

3-O5
CONGENITAL OPTIC NERVE ANOMALIES – WHAT THE NEURORADIOLOGIST NEEDS TO KNOW

Bruno Cunha[1], Carla Conceição[1]
[1]Neuroradiology Department, Centro Hospitalar Universitário de Lisboa Central, Lisboa, Portugal

Introduction: Although rare, congenital optic nerve anomalies are not uncommonly encountered in pediatric neuroradiology practice. While they may occur in isolation, they are frequently associated with other CNS developmental anomalies or systemic polymalformative syndromes. Isolated unilateral or asymmetrical anomalies with no significant functional vision changes can be an incidental finding on brain MRI. On the other hand, bilateral anomalies with significant visual impairment and syndromic cases with complex clinical pictures motivate an extensive diagnostic work-up, in which the neuroradiologist will play a crucial role.

Methods: We provide a pictorial review of congenital optic nerve anomalies, focusing on its characteristic imaging findings, including frequently associated CNS developmental anomalies, and its differential diagnosis.

Results: The main congenital optic nerve anomalies are optic nerve aplasia/hypoplasia and excavated optic disc anomalies, including optic disc coloboma and morning glory disc anomaly.
Imaging findings of optic nerve hypoplasia consist of unilateral or bilateral thickness reduction of the optic nerve and optic chiasm. It is frequently associated with other CNS developmental anomalies, most often septo-optic dysplasia.
Optic disc coloboma presents as a focal posterior defect in the globe with vitreous herniation. It may occur in isolation, with other globe abnormalities or in association with several syndromes, such as CHARGE (Coloboma, Heart defect, Atresia choanae, Retarded growth and development, Genital hypoplasia, and Ear anomalies/deafness) syndrome, Aicardi syndrome and renal-coloboma syndrome.
MRI findings of morning glory disc anomaly consist of funnel-shaped morphology of the optic disc with elevation of the adjacent retinal surface, presence of abnormal tissue within the distal optic nerve and focal discontinuity of the uveoscleral coat. It is most frequently an isolated sporadic condition, although it can also be associated with sphenoidal cephalocele, Moyamoya disease and PHACE (Posterior fossa malformations, Haemangioma, Arterial anomalies, Coarctation of the aorta and cardiac defects, and Eye abnormalities) syndrome.

Discussion & Conclusion: The neuroradiologist plays a crucial role in the management of children with congenital optic nerve anomalies. Familiarization with the different congenital optic nerve anomalies, its characteristic imaging findings and main associations are key for a confident diagnosis. Optic nerve hypoplasia should be differentiated from optic nerve atrophy, which can develop in diverse settings, such as in hereditary optic neuropathies. Importantly, optic disc coloboma and morning glory disc anomaly are distinct entities which can be differentiated on imaging. While colobomas are frequently associated with other developmental

anomalies, morning glory disc anomaly is most often an isolated sporadic condition.

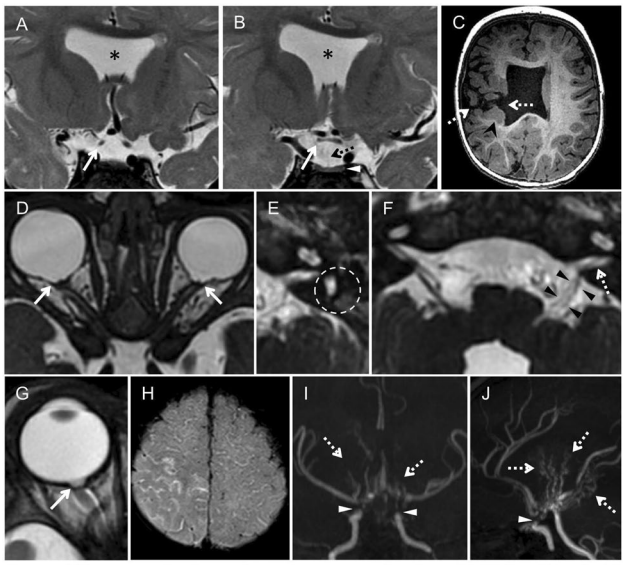

Figure 1. Different examples of congenital optic nerve anomalies. Coronal T2-WI (A and B) and axial T1-WI (C) show unilateral right-sided **optic nerve hypoplasia** (arrows in A and B) in a 10-months-old male infant. Additional findings include absence of the septum pellucidum (asterix in A and B), a small pituitary gland (arrowhead in B), with a barely visible hypoplastic pituitary stalk (dotted arrow in B), and unilateral schizencephaly (dotted arrows in C) with adjacent polymicrogyria (arrowhead in C). This may be referred to as septo-optic dysplasia plus. Axial 3D FIESTA reconstructions (D-F) show bilateral **optic nerve colobomas** (arrows in D) in a 5-months-old male infant, with associated bilateral semi-circular canal aplasia (left side shown; traced circle in E), left-sided facial-vestibulocochlear nerve complex hypoplasia (arrowheads in F) and slight stenosis of the internal auditory canal (dotted-arrow in F). This is a case of CHARGE syndrome. Axial T2-WI (G) showing a **morning glory disc anomaly** in a 6-months-old male infant. Axial T2-FLAIR (H) shows bilateral sulcal hyperintensities – ivy sign (most prominent on the right hemisphere). Coronal (I) and sagittal (J) MRA MIP reconstructions show marked stenosis of the terminal supraclinoid internal carotid arteries (arrowheads in I and J) and extensive lenticulostriate and thalamoperforating collaterals (dotted-arrows in I and J). This is Moyamoya disease.

3-O6

REFERENCE BIOMETRIC CENTILES OF THE BRAIN IN VERY PRETERM NEWBORNS WITH NORMAL LONG TERM NEURODEVELOPMENTAL OUTCOME: A MR IMAGING STUDY AT A TERTIARY NEONATAL INTENSIVE CARE UNIT

Stefania Criscuolo[1], Claudia Cinnante[2], Cristiano Michele Girlando[1], Monica Fumagalli[3], Fabio Maria Triulzi[4], Giorgio Conte[1]
[1]Università degli Studi di Milano Statale, Milano, Italy. [2]Istituto Auxologico Italiano, Milano, Italy. [3]Università degli studi di Milano Statale, Milano, Italy. [4]Università degli Studi di Milano Statale, Milano, Italy

Purpose: To assess the linear biometry of the brain structures in a cohort of very preterm newborns with normal brain MRI and long-term neuro-developmental outcome, using MR imaging (MRI) at term equivalent age (TEA).

Materials and methods: we retrospectively assessed 72 brain MR examinations of very preterm newborns (below 32 weeks of gestation), performed at TEA, without reported pathological MR findings and with normal 5-years neurodevelopmental outcome as defined by the Griffiths Mental Development Scales. To trace the reference centiles, two paediatric neuroradiologists assessed the following measurements: cerebral bi-frontal diameter (BFD), cerebral bi-temporal diameter (BTP), cerebral bi-parietal diameter (BPD), length of the corpus callosum (LCC), cerebral fronto-occipital diameter (FOD), vermian antero-posterior diameter (vAPD), vermian cranio-caudal diameter (vCCD), pontine antero-posterior diameter (pAPD), pontine cranio-caudal diameter (pCCD), cerebellar latero-laterale diameter (cLLD) lateral ventricles width right (LVr) and left (LVl).

Results: Gestational age-dependent reference centiles (5th,10th, 25th,50th, 75th,90th, 95th centile) were calculated. Lin's concordance correlation coefficient (CCC) showed a good inter-operator agreement for BFD, BTD, BPD, CLLD and FOD. We observed a gender effect on BFD and vCCD, which were significantly larger in male compared to female infants . Infants born small for gestational age (SGA) or who developed extra-uterine growth retardation (EUGR, defined as weight < 10th percentile at hospital discharge) had smaller supratentorial and infratentorial diameters, compared with infants with appropriate weight for gestational age (AGA) and those with normal postnatal growth. Prematurity-related comorbidities did not seem to affect the dimensions of the measured brain structures.

Conclusion: we reported reference biometric centiles of the brain structures in very pre-term newborn at TEA, which may be a reliable tool to assess the brain development in severe prematurity.

4. HEAD & NECK

4-O1

MAGNETIC RESONANCE IMAGING-BASED RADIOMICS FOR THE PREDICTION OF PROGRESSION-FREE SURVIVAL IN PATIENTS WITH NASOPHARYNGEAL CARCINOMA: A SYSTEMATIC REVIEW AND META-ANALYSIS

Yangsean Choi[1]
[1]Seoul St. Mary's Hospital, Seoul, Republic of Korea

Advanced non-metastatic nasopharyngeal carcinoma (NPC) has variable treatment outcomes. However, there are no prognostic biomarkers for identifying high-risk patients with NPC. The aim of this systematic review and meta-analysis was to comprehensively assess the prognostic value of magnetic resonance imaging (MRI)-based radiomics for untreated NPC. The PubMed-Medline and EMBASE

databases were searched for relevant articles published up to August 12, 2021. The Transparent Reporting of a Multivariable Prediction Model for Individual Prognosis or Diagnosis (TRIPOD) checklist was used to determine the qualities of the selected studies. Random-effects modeling was used to calculate the pooled estimates of Harrell's concordance index (C-index) for progression-free survival (PFS). Between-study heterogeneity was evaluated using Higgins' inconsistency index (I2). Among the studies reported in the 57 articles screened, 10 with 3458 patients were eligible for qualitative and quantitative data synthesis. The mean adherence rate to the TRIPOD checklist was 68.6±7.1%. The pooled estimate of the C-index was 0.762 (95% confidence interval, 0.687–0.837). Substantial between-study heterogeneity was observed (I2 = 89.2%). Overall, MRI-based radiomics shows good prognostic performance in predicting the PFS of patients with untreated NPC. However, more consistent and robust study protocols are necessary to validate the prognostic role of radiomics for NPC.

4-O2

INTRAPLAQUE HEMORRHAGE ON MRA: DO SIGNAL ABNORMALITIES PERSIST ON FOLLOW-UP IMAGING?

John Benson[1], Adnan Shahid[1], Laurence Eckel[1], Dong Kun Kim[1], Jason Little[1], Nobert Campeau[1], Greta Liebo[1], Julie Guerin[1], Luis Savastano[1]
[1]Mayo Clinic, Rochester, USA

Background and Purpose: Intraplaque hemorrhage (IPH) in carotid atherosclerosis demonstrates increased signal on MRA images. Little remains known about how this signal changes on subsequent examinations.

Materials and Methods: A retrospective review was completed of patients that had IPH on a neck MRA between 1/1/2016 and 3/25/2021, defined as ≥200% signal intensity of the sternocleidomastoid muscle on MPRAGE images. Examinations were excluded if the patients had undergone carotid endarterectomy between examinations or had poor quality imaging. IPH volumes were calculated by manually outlining IPH components. Up to 2 subsequent MRAs, if available, were assessed for both the presence and volume of IPH.

Results: 104 patients were included, of which 90 (86.5%) were male. IPH was on the right in 49 patients (average volume = 175.1 mm3), and on the left in 71 patients (average volume 197.4 mm3). 22 had at least one follow-up (average 444.7 days between exams), and 6 had two follow-up MRAs (average 489.5 days between exams). On the first follow-up, 19 (86.4%) plaques had persistent hyperintense signal in the region of IPH. The second follow-up showed persistent signal in 5/6 plaques (88.3%). Most IPH volumes (17/22; 77.3%) decreased on the first follow-up (average change: -50.1 mm3), whereas 4/6 (66.7%) increased between the first and second follow-up exams (average change: +22.7 mm3).

Conclusions: IPH usually retains hyperintense signal on follow-up MRAs, possibly representing recurrent hemorrhage or cellular debris. IPH volume changes are less predictable, and tend to decrease on the first follow-up, but increase on the second.

4-O3

HEAD AND NECK INFECTIONS. HOW, WHEN AND WHERE?

Eva Gómez Roselló[1], Gemma Laguillo[1], Quiles Ana[1], Nerses Nersesyan[1], Jaldo Francisco[1]
[1]hospital Josep Trueta, Girona, Spain

Head and neck infections are a frequent cause of consult in the emergency. Most of them won´t need any imaging, but imaging becomes necessary when the antibiotic treatment fails or a complication is suspected
Frequently the infection source is already known. The imaging is so addressed to detecting: the presence of abscess that can lead to surgical drainage, the extension of the infection, and their possible complications. The involvement of deep spaces is proof of their severity. Contrast-enhanced-CT is the main technique used in the emergency.
Neck infections are challenging for many radiologists because of the complex anatomy and potentially serious consequences of delayed or improper diagnosis. The purpose of this presentation is first to help radiologists to understand the intricate anatomy of the head and neck and to review the imaging appearances of a variety of head and neck infections that bring patients to the emergency department. In second place these conditions will be presented based on their primary location of involvement. The main complications will be reviewed.

4-O4

MÉNIÈRE'S DISEASE – WHAT THE NEURORADIOLOGIST NEEDS TO KNOW

Hugo Loureiro Cadilha[1], Guilherme Martins[1], Joana Freitas[1], Rita Sousa[1]
[1]Neuroradiology Department, Centro Hospitalar Universitário Lisboa Norte, Lisbon, Portugal

Introduction: Ménière's disease (MD) is a chronic inner ear condition, with a prevalence of 200-500 per 100000

individuals. Clinically, it is characterized by a recurrent syndrome of spontaneous vertigo, unilateral low-frequency sensorineural hearing loss, aural fullness, and tinnitus. Its pathophysiology involves the relative increase in endolymphatic space of the membranous labyrinth – endolymphatic hydrops (EH) – partially obliterating the perilymphatic space. The most used diagnostic criteria, proposed in 2015 by the Barany Society, are exclusively based on clinical and audiometric data. Variations in these symptoms can make it a challenging diagnosis, and full onset of the disease might take more than a decade. Currently, the disease's substract can be definitively demonstrated in vivo by MRI, different disease endotypes can be identified by imaging, key image findings can corroborate or be useful exclusion factors for MD when clinical diagnosis is uncertain, and image features can predict progression of unilateral to bilateral disease.

Methods: We briefly review MD's pathophysiology, current clinical diagnostic criteria, MRI protocol essentials, crucial features for appropriate EH grading, and highlight promising image findings in CT and MRI examinations, to summarize the state of the art relevant to the neuroradiologist's practice.

Discussion & Conclusion: The latest imaging criteria for MD were proposed in 2019, encompassing cochlear and vestibular hydrops grading, and assessment of the intensity of gadolinium signal in the perilymphatic space as a surrogate for disruption of the hemato-perilymphatic barrier. The combination of these findings may aid in the diagnosis of definite MD, in patients with suspected MD by clinical criteria. The angular trajectory of the vestibular aqueduct (ATVA) in CT and MRI correlates with different endolymphatic sac pathologies (degeneration and hypoplasia) in MD patients. ATVA is a radiological marker predicting unilateral to bilateral disease progression and may help understanding clinically meaningful disease subgroups. We further illustrate features believed to be associated with MD such as lower modiolar area, vestibular aqueduct stenosis, high riding jugular bulb, and dehiscence of the semicircular canals. Finally, we summarize a standardized methodology to analyze and report conventional and endolymphatic hydrops imaging, as thus the role of the neuroradiologist is ever more relevant in MD.

Keywords: *ménière's disease, endolymphatic hydrops, hemato-perilymphatic barrier, angular trajectory of the vestibular aqueduct, modiolar area, vestibular aqueduct stenosis*

4-O5

NASAL SINUS MALIGNANT TUMOR – MORE THAN MEETS THE EYE: A CASE REPORT AND LITERATURE REVIEW

Inês Prisco[1], Pedro Bem[1], Fátima Hierro[1], Duarte Rosa[1], Gustavo Lopes[1], Miguel Baptista[1], Ana Reis[1]
[1]Hospital Pedro Hispano, Matosinhos, Portugal

Introduction: Malignant tumors of sinonasal tract are extremely rare and comprise 3% of all head and neck malignant tumors. Among epithelial tumors, squamous cell carcinoma is the most common, followed by adenocarcinoma, overall presenting with a poor survival rate.

Methods: We present a case of a 46 years-old Caucasian male, with no relevant medical history, presenting to our hospital with three-month evolution of epistaxis and right nasal cavity obstruction as well as right-sided blurred vision complaints. He was submitted to a brain CT and MRI.

Results: Brain CT performed on another institution showed an extensive lesion occupying the right nasal cavity. The patient was evaluated on our institution by otolaryngology colleagues, with a visible lesion on the nasal endoscopy occupying the right nasal cavity. He had also right proptosis. He was submitted to a nasal sinus MRI, documenting an expansive lesion with heterogenous mixed signal on T2, and mostly hypointense on T1, with a cerebriform signal pattern, with presumable origin on the infundibulum; there were moderate contrast enhancement and right orbit and frontal process of the maxilla extension. Imaging characteristics were highly suggestive of inverted papilloma, although other types of sinonasal tumors like squamous cell carcinoma could not be excluded. A needle-biopsy was performed just before the MRI examination and it was positive for epithelioid melanoma with S-100 protein, HMB-45 and melan-A positive markers.

Discussion: Our main goal is to analyze the radiological characteristics of this case as well as to review Neuroradiologist's role on diagnostic imaging of these lesions. We report a case of a lesion with features that are described in the literature as typical for inverted papilloma, but, that, surprisingly turned out to be of a completely different origin. Although the neuroradiologist should always aim for a possible list of differential diagnosis in a radiological report, we must bear in mind that one of the most important roles of the reporting physician is to adequately stage a suspicious lesion, regardless of its etiology, in order to plan the

best therapeutic strategy within a multidisciplinary board of specialists.

Conclusion: Although malignant sinonasal tumors are rare, sinonasal melanomas are rarer, accounting for 0.5–2% of all melanomas and approximately 4% of melanomas of the head and neck. This case shows that typical T1 hypersignal of melanocytic tumor may be absent, acting as a confounding diagnosis factor, alerting the neuroradiologist for the possibilities of radiological presentations of these conditions.

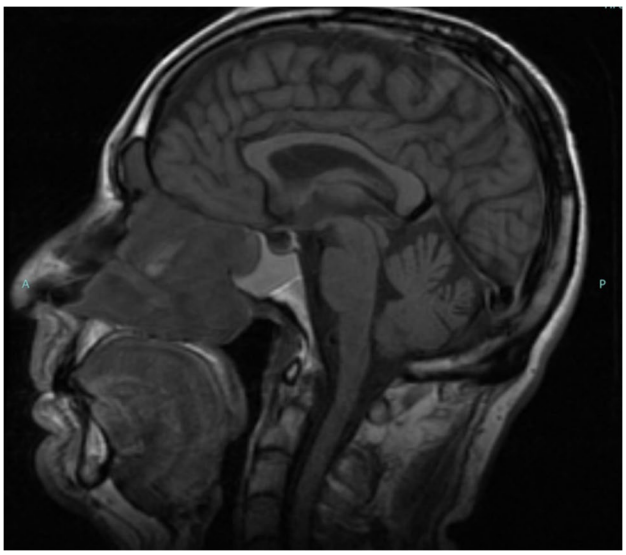

4-O6

IMAGING CHARACTERISTICS, DEMOGRAPHICS AND PROGNOSIS IN ACUTE INVASIVE FUNGAL SINUSITIS: A RETROSPECTIVE CASE SERIES

José Maria Sousa[1], Stefano Pinto[2], Ana Isabel Almeida[1], Carina Reis[1], António Sarmento[2,3], Luísa Sampaio[1,3]
[1]Department of Neuroradiology, Centro Hospitalar Universitário de São João, E.P.E., Porto, Portugal. [2]Department of Infectious Diseases, Centro Hospitalar Universitário de São João, E.P.E., Porto, Portugal. [3]Faculty of Medicine, Oporto University, Porto, Portugal

Introduction: Given growing immunocompromised population, opportunistic diseases are becoming more prevalent. In this setting, acute invasive fungal sinusitis (AIFS), although rare, is a life-threatening disease. It remains a challenge, frequently with diagnostic and therapeutic delays and significant morbidity/mortality, due to diverse clinical presentations and absence of distinguishing radiological features.

Aim: The present study aims to describe demographic, pathologic and imaging characteristics of patients with AIFS.

Methods: From a prospective database between January 2010 and March 2022, 13 patients with AIFS were identified. A retrospective analysis was conducted - demographic, pathological and clinical characteristics were reviewed by an infectiologist and imaging characteristics were independently reviewed by two neuroradiologists.

Results: This sample (n=13) had a mean age of 59 and male predominance (85%). Eleven patients (85%) were immunocompromised due to several underlying diseases, including diabetes (77%), hematologic malignancies (47%) and steroid use (23%). Two cases occurred in immunocompetent patients (one with mild disease).
The majority (85%) of patients presented acutely with unspecific symptomatology - fever, facial pain and nasal congestion.
Pathological analysis revealed Aspergillus and Mucoromycetes to be the most common pathogens (combined tally of 85%), with additional solitary cases of Scedosporium Boydii and Schizophyllum Commune. All patients underwent antifungal therapy with intravenous amphotericin B with stepdown therapy to voriconazol (after histopathologic exclusion of mucormycosis).
All patients underwent head CT and 11 had MRIs. Sinus involvement was most commonly bilateral (54%) and multiple (62%), most frequently in the ethmoid (85%) and sphenoid (77%) sinus. Intrasinusal focal hyperdensities were present in 54% of patients. Four patients had evidence of bone sclerosis. Bone erosion was present in 8 patients (62%) affecting all sinuses except for the frontal (n=0) and bone expansion was concurrently present in two cases.
MRI showed variable signal intensity (SI) and contrast enhancement: 3 showed focal areas of lack of contrast enhancement, and the remaining 8 patients distributed equally into heterogeneous and homogeneous enhancement; T2SI was predominantly low (n=8/11) with corresponding hyperintensity in T1WI.
Extra-sinonasal location included intracranial compartment (70%), orbit (62%), pterygopalatine fossa (38%) and the infratemporal fossa (23%). Concerning intracranial extension, cavernous sinus was the most frequent location (78%) with accompanying thrombosis in half.
Thirty-five percent of patients underwent surgical treatment and 43% died.

Conclusions: AIFS showed frequent bony erosion and extrasinonasal involvement, as well as variable signal intensities in MRI imaging, predominantly hypointense in T2WI. Absence of bone erosion/sclerosis should not exclude AIFS hypothesis.

Keywords: Fungus; sinusitis; infectious

4-O7

MACROCALCIFICATIONS DO NOT ALTER MALIGNANCY RISK WITHIN THE 2017 EUROPEAN THYROID IMAGING REPORTING AND DATA SYSTEM (EU-TIRADS) WHEN PRESENT IN NON-HIGH SUSPICION THYROID NODULES.

Ana Cecilia Sánchez González[1], Víctor Pérez[1], Olalla Vazquez[1], Khaled El Hamshari[1], Esther Granell[1]
[1]Corporación sanitaria Parc Tauli, Sabadell, Spain

Introduction: Current literature describes an increased risk of malignancy in nodules with macrocalcifications. The malignancy rate is highly variable, ranging between 16% and 52% depending on the series. However, these articles do not classify the nodules with macrocalcifications according to their US risk.

AIMS and objectives: To determine the malignancy risk of thyroid nodules with isolated macrocalcifications and / or rim calcifications when present in Non-High Suspicion Thyroid Nodules (NHSTN).

Methods and materials: Retrospective study reviewing all fine-needle aspiration biopsies (FNAB) of thyroid nodules done in our center from January 2014 to December 2020. We rejected the nodules with previous FNAB. We selected the nodules with macrocalcifications (defined as echogenic foci >1 mm in size with posterior shadowing and / or peripheral - rim dystrophic calcifications) and classify them in groups following the 2017 European Thyroid Imaging Reporting and Data System (EU-TIRADS). Finally, we calculated the rate of malignancy and compare them with the rest of the nodules for each subgroup. For this purpose, we used Chi-square comparison tests.

Results: Of 1536 biopsied thyroid nodules in our center from January 2014 to December 2020, 1224 met criteria for EU-TIRADS 3 (Low Risk) or EU-TIRADS 4 (Intermediate Risk). Five nodules were unclassifiable following EU-TIRADS due to their complete circumferential - rim calcifications restricting further sonographic assessment. The remaining 307 were classified in other EU-TIRADS category or had previous FNAB and therefore they were excluded of our study. From our 1224 nodules selected, we classified 943 as EU- TIRADS 3 and 281 as EU-TIRADS 4. Of the 943 EU-TR3 nodules, 59 of them had macrocalcifications and 884 did not have macrocalcifications. The malignancy rate in these two groups was 5.7% and 3.4% respectively. Of the 281 EU-TR4 nodules, 40 of them had macrocalcifications and 241 did not. The malignancy rate in these two groups was 20.7% and 21.8%. A p value < 0.05 indicated statistical significance. The results were not significantly different in both groups (TR3 p=0.358, TR4 p=0.894).

Conclusions: Macrocalcifications in thyroid nodules do not increase the malignancy risk in a statistically significant way when present in non-high suspicion thyroid nodules (EU-TIRADS 3 and EU-TIRADS 4).

4-O8

DENTAL MRI ENABLES TO MONITOR PERIODONTAL EDEMA IN *T2 STIR SEQUENCES* IN HIGH-GRADE *PERIODONTAL DISEASE*

Julian Schwarting[1], Florian A. Probst[2], Magdalena Griesbauer[1], Yoana Malenova[2], Matthias Folwaczny[3], Monika Probst[1]
[1]Department of Diagnostic and Interventional Neuroradiology, Klinikum rechts der Isar, Technische University Munich, Munich, Germany. [2]Department of Oral and Maxillofacial Surgery and Facial Plastic Surgery, University Hospital, Ludwig-Maximilians-University, Munich, Germany. [3]Department of Restorative Dentistry and Periodontology, University Hospital, Ludwig-Maximilians-University, Munich, Germany

Background: Periodontal disease can be visualized in 3T MRI with T2-weighted STIR and Fast Field Echo T1-weighted Black Bone sequences. Hyperintense edema and bone loss correlate to the typical clinical findings periodontal pocket depth and gum bleeds. Aim of this study was to investigate the reversibility of imaging findings through standard treatment in the timespan of 3 months in correlation to the clinical examination status, in order to determine whether MRI imaging can be used to monitor disease activity.

Methods: 36 patients with generalized periodontitis were prospectively analyzed and were imaged with 3D isotropic T2-weighted STIR and Fast Field Echo T1-weighted Black bone sequences before and 3 months after standard therapy. Bone edema depth was measured in 164 teeth in the STIR sequence before and after treatment. Results were compared with standardized clinical examinations according to the periodontal screening index (PSI).

Results: Periodontitis results in bone edema adjacent to affected teeth with an average depth of 1.8± 0.18mm. 3 months after therapy, mean edema depth shrunk to 1.5± 0.14 mm, p<.01. Edema reduction was observed only in patients with bleeding on probing (BOP) before treatment (2.0± 0.21 mm vs. 1.7± 0.16mm, p<.01), while there was no change in patients without BOP(0.71± 0.19mm vs. 0.75± 0.21mm). Changes were observed most prominently in patients with

clinically measured periodontal pockets >5mm depth (3.4± 0.36mm vs. 2.4± 0.26 mm, p ≤ .001).

Conclusion: Periodontal osseous edema in T2 STIR imaging can be used to monitor inflammation in patients with high-grade periodontal disease. This provides additional information for therapy monitoring and could potentially validate future therapy methods.

4-O9
ISOLATED CONJUNCTIVAL LYMPHOMA: A CAUTIONARY TALE.

Igor Nosek[1], Miloš Vuković[1], Jasmina Boban[1,2], Duško Kozić[1,2]
[1]Oncology Institute of Vojvodina, Sremska Kamenica, Serbia. [2]Faculty of Medicine of the University of Novi Sad, Novi Sad, Serbia

Introduction: Non-Hodgkin's lymphomas account for around 50% of all orbital malignancies (Ferreri et al., 2008), while extranodal marginal zone lymphoma (EMZL), previously mucosa-associated lymphoid tissue lymphoma (MALT), constitutes around 80% of conjunctival B-cell non-Hodgkin lymphomas (Tanenbaum et al., 2019).

Case report: A 45-year old female presented with a chronic, sessile, sub-epithelial mass confined to the conjunctiva of the right eye. Initial MRI revealed a mass in the right superolateral aspect of the right orbit, misinterpreted as an enlarged lacrimal gland, possibly due to infection. Ophthalmologic evaluation, performed following the initial MRI, revealed a discoid mass of the right conjunctiva, characterized as the appearance of the "salmon patch". Biopsy confirmed the diagnosis of conjunctival EMZL (Picture 1).

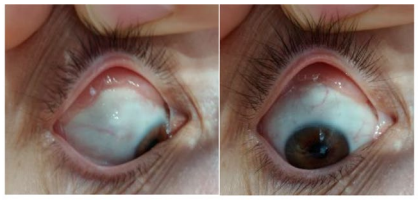

Picture 1: "Salmon patch" appearance of isolated conjunctival EMZ lymphoma.

A follow-up MRI was performed to evaluate the extent of the primary lesion, and to exclude regional metastasis. At this time MRI showed a nearly symmetrical mass of the conjunctiva, measuring up to 5mm thick. The mass was hyperintense on T2W/FLAIR/T2W FS sequences, and isointense on T1W sequences, relative to the lacrimal gland (Picture 2).

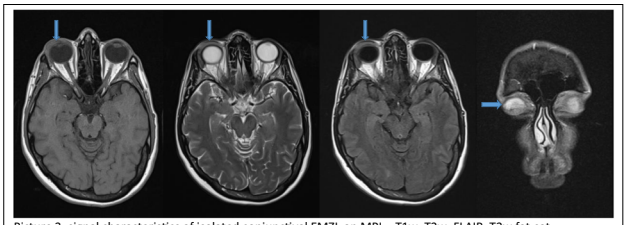

Picture 2: signal characteristics of isolated conjunctival EMZL on MRI – T1w, T2w, FLAIR, T2w fat-sat.

It showed homogenous contrast enhancement and restricted diffusion (Picture 3).

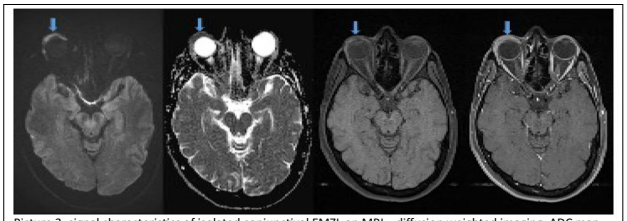

Picture 3: signal characteristics of isolated conjunctival EMZL on MRI – diffusion weighted imaging, ADC map and contrast enhancement on T1w FS sequences.

Whole body PET imaging utilizing FDG was performed, showing a SUV of 6,88 in the lesion, and confirming that the lesion is not part of systemic disease (Picture 4).

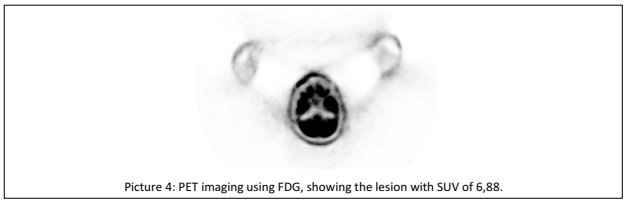

Picture 4: PET imaging using FDG, showing the lesion with SUV of 6,88.

Discussion: Conjunctival lymphoma is more prevalent among the elderly, especially women, and usually presents as a chronic sub-epithelial mass - a „salmon patch" (Sassone et al., 2016). Diagnosis should be based on ophthalmologic examination, including high resolution optical coherence tomography (HR-OCT) followed by biopsy in order to establish the correct diagnosis, due to the possibility of misdiagnosis when using CT and MRI as the first line diagnostic tool, without proper clinical workup, as highlighted in this case. However, further workup should include computed tomography (CT) or magnetic resonance imaging (MRI) of the orbit for local staging, as well as full-body positron emission tomography in order to evaluate the presence and extent of systemic disease, due to different therapeutic choices in each case. The gold standard treatment is radiation therapy, especially in cases of monocular involvement (Tanenbaum et al., 2019). Other treatment options include chemotherapy and antibiotics (Ferreri et al., 2005 and 2006).

Conclusion: Isolated conjunctival lymphoma should be diagnosed by an ophthalmologist, while staging should be performed via CT or MRI, followed by PET-CT to

exclude systemic disease - which dictates the therapeutic approach.

Keywords: MALT; EMZL; MRI; orbit; conjunctiva.

5. SPINE

5-O1

SPINAL INVOLVEMENT IN PEDIATRIC FAMILIAL CAVERNOUS MALFORMATION SYNDROME

Ana Geraldo[1,2], Aysha Luis[3,4], César Augusto P. F. Alves[5], Domenico Tortora[6], Joana Guimarães[7,8], Sofia Reimão[9,10], Marco Pavanello[11], Patrizia de Marco[12], Marcello Scalla[13,14], Valeria Capra[12], Andrea Rossi[6,15], Erin Simon Schwartz[5], Kshitij Mankad[3], Mariasavina Severino[6]
[1]Centro Hospitalar Vila Nova de Gaia/Espinho, Vila Nova de Gaia, Portugal. [2]Clinica Universitária de Radiologia, Lisboa, Portugal. [3]Department of Radiology, Great Ormond Street Hospital for Children NHS Foundation Trust, London, United Kingdom. [4]Department of Radiology, King´s College London, London, United Kingdom. [5]Department of Radiology, Children's Hospital of Philadelphia, Philadelphia, USA. [6]Neuroradiology Unit, IRCCS Istituto Giannina Gaslini, Genoa, Italy. [7]Department of Neurology, Centro Hospitalar Universitário de São João, Porto, Portugal. [8]Department of Clinical Neusosciences and Mental Health, Faculty of Medicine of the University of Porto, Porto, Portugal. [9]Neurological Imaging Department, Hospital de Santa Maria, Lisboa, Portugal. [10]Clínica Universitária de Imagiologia, Faculty of Medicine of the University of Lisbon, Lisboa, Portugal. [11]Neurosurgery Unit, IRCCS Istituto Giannina Gaslini, Genoa, Italy. [12]Medical Genetics Unit, IRCCS Istituto Giannina Gaslini, Genoa, Italy. [13]Department of Neurosciences, Rehabilitation, Ophthalmology, Genetics, Maternal and Child Health, Università Degli Studi di Genova,, Genoa, Italy. [14]Pediatric Neurology and Muscular Diseases Unit, IRCCS Istituto Giannina Gaslini,, Genoa, Italy. [15]Department of Health Sciences (DISSAL), University of Genoa, Genoa, Italy

Introduction: The aim of the study was to assess the prevalence and characteristics of spinal cord cavernous malformations (SCCM) and intraosseous spinal vascular malformations (ISVM) in a pediatric familial cerebral cavernous malformation (FCCM) cohort and evaluate clinico-radiological differences between children with (SCCM+) and without (SCCM-) SCCM.

Methods: All patients with a pediatric diagnosis of FCCM evaluated at three tertiary pediatric hospitals between January 2010 and August 2021 with 1 whole spine MR available were included. Brain and spine MR studies were retrospectively evaluated, and clinical and genetic data collected. Comparisons between SCCM+ and SCCM- groups were performed using student-t/Mann-Whitney or Fisher exact tests, as appropriate.

Results: Thirty-one children (55% boys) were included. Baseline spine MR was performed (mean age= 9.7 years) following clinical manifestations in one subject (3%) and as a screening strategy in the remainder. Six SCCM were detected in five patients (16%), in the cervico-medullary junction (n=1), cervical (n=3), and high thoracic (n=2) regions, with one appearing during follow-up. A tendency towards an older age at first spine MR (P=0.14) and 1 posterior fossa lesion (P=0.13) was observed in SCCM+ patients, lacking statistical significance. No subject demonstrated ISVM.

Conclusion: Although rarely symptomatic, SCCM can be detected in up to 16% of FCCM patients using diverse spine MR protocols and may appear de novo. ISVM were instead absent in our cohort. Given the relative commonality of asymptomatic SCCM, serial screening spine MR should be considered in FCCM starting in childhood.

5-O2

WHOLE-BODY FASCICULATION DETECTION IN AMYOTROPHIC LATERAL SCLEROSIS (ALS) USING MOTOR UNIT MRI (MUMRI)

Linda Heskamp[1], Matthew G Birkbeck[1,2], Julie M Hall[2,1], Ian S Schofield[1], Timothy L Williams[2], Hugo de Oliveira[2], Roger G Whittaker[1,2], Andrew M Blamire[1]
[1]Newcastle University, Newcastle upon Tyne, United Kingdom. [2]Newcastle upon Tyne Hospitals NHS Foundation Trust, Newcastle upon Tyne, United Kingdom

Introduction: Amyotrophic lateral sclerosis (ALS) is a neurological disorder characterised by motor neuron degeneration. Early identification is critical, because ~50% of the patients die within 30 months of disease onset. One of the earliest disease hallmarks is fasciculation, i.e. pathological spontaneous contraction of motor units. Fasciculation has therefore been recognised as an important diagnostic marker and must be studied in all anatomical regions (lower limb, upper limb, thoracic and bulbar region). In routine care, fasciculation is detected with needle EMG, but this technique is invasive and has limited coverage.
We have developed a novel non-invasive way to detect fasciculation using magnetic resonance imaging (MRI), called motor unit MRI (MUMRI). On these scans, fasciculation manifests as transient signal voids. Here, we aimed to detect the fasciculation rate using MUMRI in ALS patients compared to healthy controls in the four body regions relevant for diagnosing ALS.

Methods: We recruited 10 ALS patients (7 male, 64±7 years) and 10 healthy controls (7 male, 58±10 years). Lower

leg muscles, paraspinal muscles, arm (biceps) and tongue were scanned using a diffusion weighted MUMRI sequence. Per body region, we acquired 4 slices/second for 1 minutes (240 images/region).
For each image, transient signal voids were annotated using an automatic detection algorithm. The fasciculation rate was calculated as the number of detected signal voids normalised to sampled muscle area and acquisition time.

Results: The average fasciculation rate over all body regions was higher in ALS patients compared to healthy controls (median [IQR]: 1.28 cm-2min-1 [0.36-2.20] vs. 0.07 cm-2min-1 [0.04-13]; p<0.001). At body region level, the fasciculation rate was also higher in ALS patients compared to healthy controls for the arm (p=0.001), paraspinal muscles (p=0.002) and lower legs (p=0.003), but not the tongue (p=0.077).
Furthermore, the fasciculation rate was expressed into a z-score, using healthy control values as reference (z-score>3 defined abnormal). This showed that 9/10 ALS patients had an increased fasciculation rate (z-score>3) in at least one body region, and 4/10 ALS patients had an increased fasciculation rate in at least two body regions.

Conclusion: 'Whole-body' MUMRI detects fasciculation in muscle regions important in diagnosing ALS. All ALS patients, except one, deviated from healthy controls by showing an increased fasciculation rate in at least one body region, with often one of the other body regions unaffected. These findings are in line with the heterogeneous disease onset known in ALS and support our whole-body approach.

5-O3
SEX LIFE AND LOW BACK PAIN: THE IMPACT OF INTRADISCAL OZONE THERAPY IN PATIENTS WITH HERNIATED LUMBAR DISC.

Laura Gemini[1], Mario Tortora[1], Gianvito Pace[2], Mariarosaria Giardiello[2], Carmine Sicignano[2], Fabrizio Fasano[2], Gemma Taglialatela[2], Valeria Piscitelli[2], Francesco Somma[2], Vincenzo D'agostino[2], Alberto Negro[2]
[1]università Di Napoli"Federico Ii", Napoli, Italy. [2]ospedale Del Mare, Napoli, Italy

Purpose: To assess the improvement of sexual impairment after percutaneous intradiscal ozone therapy in patients complaining of low back pain due to lumbar disc herniation.

Methods and Materials: Between January 2018 and June 2021, 157 consecutive imaging-guided percutaneous intradiscal ozone therapies were performed on 122 patients with low back pain (LBP) and/or sciatic pain due to lumbar disc herniation. Oswestry Disability Index (ODI) was administered before the treatment and at 1- month and 3-month follow-up and the ODI Section 8 (ODI-8/sex life) values were retrospectively reviewed to evaluate the improvement of sexual impairment and disability.

Results: Mean age of patients was 54.63±12.40.Technical success was achieved in all cases (157/157). Clinical success was registered in 61.97% (88/142) of patients at 1-month follow-up and in 82.69% (116/142) at 3-month follow up. The mean ODI-8/sex life was 3.73 ± 1.29 before the procedure, 1.71 ± 1.37 at 1-month follow up and 0.44 ± 0.63 at 3-month follow up. Compared to older patients, subjects under 50 years showed a significantly slower recovery of sexual impairment (p-value 0.003). The treated levels were L3-L4, L4-L5 and L5-S1 in 4, 116 and 37 patients, respectively. Patients with L3-L4 disc herniation showed less of sexual disability at presentation, with a significantly faster improvement of sexual life (p-value 0.03).

Conclusions: Percutaneous intradiscal ozone therapy is highly effective in reducing sexual impairment due to lumbar disc herniation, and the improvement is faster in older patients and in case of L3-L4 disc involvement.

5-O4
REVIEW OF COCCYDYNIA AND GANGLION IMPAR BLOCKADE

Pedro Bem[1], Inês Prisco[1], Fátima Hierro[1], Miguel Baptista[1], Joana Martins[1], Ana Mafalda Reis[1]
[1]Pedro Hispano Hospital, Matosinhos, Portugal

Introduction: Our goal with this work is to present a brief review of coccydinia, in terms of history, clinical presentation, treatment and evolution. Additionally, we will expose a case of long standing coccydinia that we treat with minimal invasive surgery at our hospital center in Matosinhos, Portugal, under CT-guidance.

Methods: We made a review of recent papers published in PubMed since 2010, with specific keywords like Coccyx, pain–intractable, sacrococcygeal region, tailbone pain and ganglion impar blockade.
Classic symptoms include midline pain located below the sacrum and above the anus, most commonly occurs in adolescents and adults and has an estimated prevalence of around 1% of all back pain conditions. Symptoms are worse while sitting or during transitions from sitting to standing.
With this in mind, we reviewed our patients list and came across a case with long standing pain in the sacrococcygeal region, with almost no benefits with conservative treatment

and with marked impact in his daily life. This is the case of a 53-year-old male patient referenced to our department with low back pain since the beginning of the COVID-19 pandemic, when he was working from home, and the symptoms have been present for almost two years. He was evaluated by multiple doctors, and tried different cushions, oral medications, as well as pelvic floor physical therapy with close to no improvement. The patient was studied with CT and an MRi and we proposed a minimal invasive treatment with CT-guided injection for ganglion impar blockade.

Results: CT-guided guided injection for ganglion impar blockade was considered successfully achieved in this procedure. The patient was observed for one hour before discharge and there were no documented complications. In the first few days the patient referred a decrease of almost 50% of his pain (subjective scale), and after two months he was capable of returning to work and was able to stop taking most of the analgesic pills.

Conclusion: Coccyx (tailbone) pain substantially decreases the quality of life for patients who suffer with this condition and contributes to waste of resources, with economic impact. So it is necessary to draw attention and give greater relevance to this diagnosis and emphasize that neuroradiology, with minimally invasive treatments of the spine, can make an incredible contribution and have a positive impact on the quality of life of these patients and prevent the establishment of chronic back pain.

5-O5

ASSESSMENT OF THE INTERVERTEBRAL FORAMINA IN ISTHMIC SPONDYLOLISTHESIS IN THE CONTEXT OF RADICULOPATHY: A 3D ANALYSIS.

Denil Tribovane[1], Ana Maria Braz[1], Pedro Vilela[1]
[1]Hospital Beatriz Ângelo, Loures, Portugal

Introduction: Isthmic spondylolisthesis corresponds to the anterior translation of one vertebral segment relative to the next caudal segment as a result of a bone defect of the pars interarticularis. Most isthmic spondylolisthesis are asymptomatic, often discovered incidentally on radiographs, although up to 25% of affected individuals will report a variable clinical syndrome of low back and/or radiculopathy. The purpose of this study was to perform a three-dimensional CT study analysis of the intervertebral foramina shape and volume, to assess the possibility of isthmic spondylolisthesis being an isolated cause of radiculopathy.

Methods: The shape and volume of the intervertebral foramina in patients with and without spondylolisthesis at the L4-L5 level due to bilateral isthmic lysis were evaluated by two neuroradiologists, one with 22 years of experience (O-1) and the other with 3 years of experience (O-2), using a post-processing software. The foraminal volumes and cross-sectional measurements obtained by the neuroradiologists were compared using a two-sample t-test. The foraminal volumes and cross-sectional measurements between the control and isthmic spondylolisthesis groups were also compared using a two-sample t-test. Evaluation of the equality of variance between the neuroradiologists´ measurements for inter-observer reproducibility was performed using Levene´s test. The significance level was set at $p < 0.05$.

Results: The study sample comprised 36 patients (14 men and 22 women): a study group of 18 subjects with grade I or II spondylolisthesis at the L4-L5 level due to bilateral isthmic lysis and a control group of 18 age-matched subjects without spondylolisthesis. There were no statistically significant differences in volume measurements between the observers ($p > 0.05$) while maintaining equal variances ($p > 0.05$). There were also no significant differences in the volume of the left or right L4/L5 intervertebral foramen between subjects with and without isthmic spondylolisthesis ($p > 0.05$). A significant change was observed in the overall shape of the foramina ($p < 0.05$).

Conclusion: Our results showed that in a neutral supine position, mild spondylolisthesis (slippage consistent with grade I or II) resulting from bilateral spondylolysis was not associated with significant changes in intervertebral foraminal volume, but there was a significant and quantifiable foraminal shape change that reduced the fatty space surrounding the nerve root, which could better explain the radicular pain in this population.

5-O6

VERTEBRO-MEDULLARY TRAUMA AND KLIPPEL-FEIL SYNDROME: IMPORTANCE OF IMAGE – ABOUT A CLINICAL CASE

João Pedro Lucas[1], Inês Prisco[2], Ana Mafalda Reis[2], Fréderic Ramalho[1], Joana Novais[1], João Costa[1], Fernando Macedo[1], Miguel Rocha[1]
[1]Hospital Senhora da Oliveira, Guimarães, Portugal. [2]Hospital Pedro Hispano, Matosinhos, Portugal

Introduction: Klippel-Feil Syndrome is a rare condition known by multi-systemic alterations and congenital fusion of the cervical vertebrae, specially C2-C3 and C5-C6. May be associated with other musculoskeletal pathologies, like Sprengel deformity and congenital scoliosis. Hypermobility on the non-fused segments may lead to supra and infra-adjacent segments disease, namely

discal pathology and predispose to myelopathy, even in minor trauma cases. Image has a core role in characterization of these entities.

Methods: Woman of 43 years old, admitted on the Emergency Room after motorcycle accident, with dorso-cervicalgy and limbs paraesthesia, without other complaints. It was performed spine radiography, CT and MRI.

Results: Radiography of the spine showed fracture of D8 and cervical fusion block on C2-C3 and C6-C7. Cervical CT study didn't show recent fractures, images of articular dislocation or any other trauma-related injuries, besides the presence of the already mentioned fusion blocks, with diffuse disc-vertebrae degenerative alterations, spinal-cord molding on C3-C4 and C4-C5 with possible foraminal compromise of the left root of C6. On the dorsal segment the fracture of D8 was confirmed without backing of the posterior wall. The MRI study showed a posterior discal protrusion on C3-C4, conditioning the molding of the spinal-cord, presenting an area of hypersignal on T2 and STIR, that translates an oedema associated with small hypotensive foci on T2, suggesting post-traumatic medullar contusion, with no signs of myelopathy on the other medullar segments.

Discussion: The predisposition to develop discal pathology on the Klippel-Feil Syndrome translates the importance of searching this entity when the diagnosis is made. Equally, if there is trauma and the diagnosis is already established, these patients may have the indication to do an urgent MRI, due to susceptibility to develop myelopathy.
Two months after the accident, the patient remained with complaints of paraesthisia of the upper limbs; it as performed a C3-C4 discectomy and anterior cervical arthrodesis with cage C3-C4, 6 months after the initial admission.

Conclusion: On Klippel-Feil Syndrome, predisposition to discal pathology reflects in the beginning of the symptoms on younger ages. Despite surgery, the hypothesis of percutaneous nucleosis on C3-C4 must be considered due to the age of the patient and the objective of keeping the normal biomechanics of the spine. Cervical hypermobility and the higher susceptibility in cases of trauma reflect the importance of considering the realization of urgent MRI to increase diagnostical accuracy and the best clinical outcome, emphasizing the importance of a multidisciplinary approach.

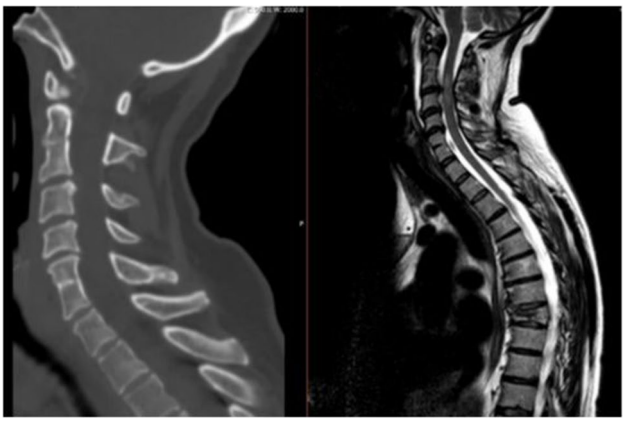

5-O7

PERCUTANEOUS ANTERIOR STABILIZATION OF A1 AND A2 THORACOLUMBAR BURST FRACTURES WITH STAND-ALONE SPINEJACK DEVICE. A SINGLE CENTER EXPERIENCE.

Altin Stafa[1], Enrico Giordan[2], Jacopo Del Verme[2], Roberto Zanata[2], Stefano Curtolo[1], Francesco Di Paola[1]
[1]Neuroradiology Dpt, Ca'Foncello Hospital, ULSS 2 Marca Trevigiana, Treviso, Italy. [2]Neurosurgery Dpt, Ca'Foncello Hospital, ULSS 2 Marca Trevigiana, Treviso, Italy

Thoracolumbar fractures often require anterior support in order to avoid or reduce the post-traumatic hyperkyphosis. The SpineJack device proved favorable in the treatment of vertebral compression fractures with satisfactory pain relief, vertebral height restoration, and low rates of above adjacent fractures, in neurologically intact fractures. Recently it is increasingly used also for the treatment of burst fractures.
We prospectively collected 64 A1 and A2 split fractures (T6-L3 levels) of 58 patients (19-63 yo) treated at our center between 2017 and 2021, with percutaneous implant of Spinejack as a stand-alone treatment.
The percutaneous intervention was performed in the angio suite using a biplanar angio DSA equipment by the interventional neuroradiology team, after common clinical discussion and decision with the spine neurosurgery team for every single case.
1 month, 3 moths and 1 year CT follow-up was performed. Safety and efficacy of the treatment is discussed. Age, sex, type and level, pain, operative and discharge time, vertebral body heights, posterior wall retropulsion, vertebral and local kyphosis angles and vertebral body volume is analyzed.
We conclude that stand-alone percutaneous anterior stabilization using SpineJack device is a safe and effective technique for the treatment of A1 and A2 thoraco-lumbar burst fractures.

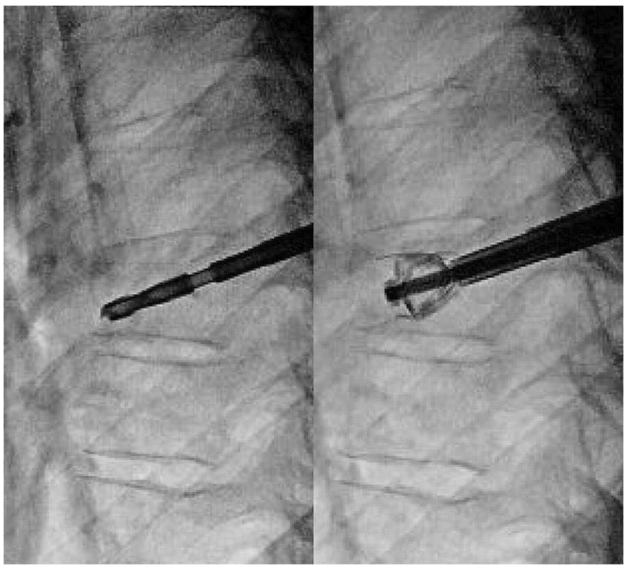

5-O8

NEUROSURGICAL PRACTICE PATTERNS IN NEURORADIOLOGY IMAGING REPORT UTILIZATION FOR MANAGEMENT OF SUSPECTED LUMBAR SPINAL STENOSIS

Oleksandr Strelko[1], Michael Mooney[2], Jacob Rachlin[3]
[1]Loyola University Chicago Stritch School of Medicine, Chicago, USA. [2]Brigham Women's Hospital, Harvard Medical School, Boston, USA. [3]Veterans Affairs Health System Boston, Boston, USA

Introduction: The interprofessional gap between neurosurgeons and neuroradiologists has been increasing steadily since the implementation of electronic health record systems and remote radiology readings. Our aim was to survey and report the current practices employed by neurosurgeons in utilizing neuroradiology reports for management of patients with lumbar spinal stenosis (LSS).

Methods: A voluntary, anonymized survey was distributed among a group of neurosurgeons affiliated with the Veteran's Affairs Health System. Survey questions were aimed at assessing the trends and the subsequent practice patterns in neurosurgical utilization of neuroradiology reports in patients with LSS.

Results: 20 respondents across all surveyed centers completed the survey. 95% (19/20) of respondents had an on-site radiologist, while 80% (16/20) had access to a neuroradiologist. 95% (19/20) of respondents report having imaging routinely read by a neuroradiologist. 40% (8/20) of the neurosurgeons read the ordered radiology reports less than 50% of the time. Only 20% of respondents always read the neuroradiology report. 60% (12/20) of the surveyed neurosurgeons frequently reported major discrepancies between imaging interpretation among neuroradiologists and the surveyed neurosurgeons, while only 45% (9/20) neurosurgeons subsequently contact the neuroradiologist to discuss and rectify discrepancies. Furthermore, a majority of neurosurgeons do not routinely participate in conferences where imaging is discussed.

Discussion & Conclusion: The survey results demonstrate that neurosurgeons give little value to neuroradiology reports, do not routinely consult with neuroradiologists and often proceed with treatment when major discrepancies in imaging interpretation exist. Overall, our findings suggest that the interprofessional gap between neuroradiologists and neurosurgeons continues to widen, leading to a low rate of both neuroradiology imaging report use and collaboration between neuroradiologists and neurosurgeons when treating patients with suspected LSS. Whether such practices lead to altered surgical outcomes and affect healthcare costs warrants further investigation.

5-O9

ANALYSIS OF MODIC DEGENERATIONS DETECTED IN MAGNETIC RESONANCE IMAGING WITH DEEP LEARNING TECHNIQUES

Mehmet Yüksek[1], Adem Yokuş[1], Harun Arslan[1], Murat Canayaz[2], Zülküf Akdemir[1]
[1]Yüzüncü Yıl University, Faculty of Medicine, Department of Radiology, Van, Turkey. [2]Yüzüncü Yıl University, Faculty of Engineering, Department of Computer Engineering, Van, Turkey

Keywords: Modic degeneration, artificial intelligence, deep learning, convolutional neural networks

Introduction: Modic degenerations are quite common in lumbar magnetic resonance imaging (MRI) taken with low back pain complaints. Modic degenerations are divided into three types according to T1 and T2 weighted images. In this study, we aimed to analyze the modic degeneration findings detected in MRI by using deep learning techniques.

Methods: Sagittal T1, sagittal and axial T2-weighted lumbar MRI images were analyzed in a total of 307 patients who underwent lumbar MRI between 2016 and 2021 (125 females, 182 males, age range 19-86 years). Modic degenerations were categorized and marked as 3 types according to T1 and T2 signal changes. The deep learning technical part of our study consists of two independent stages, namely classification and segmentation. During the first stage, the categorized data was classified with convolutional

neural network (CNN) architectures such as DenseNet-121, DenseNet-169 and VGG-19. At the next stage, segmentation was performed with U-Net architecture over the marked pictures. In the deep learning process, 80% of the data set was used for training and 20% for testing.

Results: At the classification stage, the success rates in Modic type 1, Modic type 2, Modic type 3 degenerations were 98%, 96%, 100% in DenseNet-121, 100%, 94%, 100% in DenseNet-169, in VGG-19 98%, 92%, 97% respectively found. In the segmentation phase, the success rate was 71% with the U-Net architecture.

Discussion and Conclusion: In recent years, developments in artificial intelligence affect our lives in many ways. Especially with the increase in the number of radiological examinations in our country, the workload of radiologists is increasing day by day. Evaluation of MRI findings of modic degenerations in the etiology of low back pain with deep learning architectures can significantly reduce the workload of the radiologist by providing ease of diagnosis. In addition, deep learning modalities can facilitate the diagnosis and follow-up of spinal diseases.

E-POSTERS (original and unedited texts as received by the authors)

1. DIAGNOSTIC

IMAGING ADVANCED TECHNIQUES

1-P1

ROLE OF VESSEL WALL IMAGING IN VARIOUS CNS INFECTIONS

Neha Choudhary[1], Sameer Vyas[1], Chirag Ahuja[1], Ajay Kumar[1], Manish Modi[1], Naveen Sankhyan[1], Renu Suthar[1], Paramjeet Singh[1]
[1]Post Graduate Institute of Medical Education and Research, Chandigarh, India

Purpose: CNS infections can cause infectious vasculitis which can be detected by vessel wall imaging (VWI). In this prospective study, we aim to study the role and usefulness of VWI in various CNS infections.

Materials and methods: A total of 101 cases of tubercular meningitis (TBM), 12 cases of non-tubercular bacterial infections, 12 cases of fungal, and 15 cases of viral infections underwent high-resolution pre-and post-contrast VWI and TOF-MRA in addition to routine sequences. Site of vascular enhancement, pattern of enhancement (smooth or nodular), and stenosis were assessed on VWI. Statistical analysis was performed to study the association between VWI findings and infarctions.

Results: Infarctions were found in 49 cases (48.5%) of TBM, 5 cases (41.7%) of bacterial infections, 7 cases (58.3%) of fungal infections, and 7 cases (46.6%) of viral infections. Vessel wall enhancement was seen in 67 cases (66.3%) of TBM, 5 cases (41.7%) of bacterial infections, 9 cases (75%) of fungal, and 7 cases (46.6%) of viral infections. There was significant association between arterial enhancement on VWI and infarctions in their territories in TBM, fungal, and viral groups. In TBM group, severity of vascular involvement increased with increasing severity of the disease. The pattern of enhancement or stenosis on VWI was not significantly associated with infarctions. VWI had better sensitivity for detection of vascular involvement than TOF-MRA.

Conclusion: VWI helps in the detection of vascular involvement in various CNS infections which can improve the prognosis of the disease by prompting early treatment to prevent catastrophic vascular complications.

1-P2

BIOMETRY AND PROBABILISTIC ANATOMICAL ATLAS OF THE NORMAL ANTERIOR VISUAL PATHWAYS USING DEDICATED HIGH-RESOLUTION 3D MRI.

Emanuele Pravatà[1,2], Andrea Diociasi[3], Luca Roccatagliata[3], Riccardo Navarra[4], Luca Carmisciano[3], Alessandro Cianfoni[1], Chiara Zecca[5,2], Claudio Gobbi[5,2]
[1]Neuroradiology, Neurocenter of Southern Switzerland, Lugano, Switzerland. [2]Università della Svizzera Italiana, Lugano, Switzerland. [3]Dipartimento di Scienze della Salute, Università di Genova,, Genova, Italy. [4]Institute for Advanced Biomedical Technologies, Chieti, Italy. [5]Neurology, Neurocenter of Southern Switzerland, Lugano, Switzerland

Introduction: There is currently a lack of a methodological framework to perform quantitative group-level studies assessing the structural characteristics of the anterior visual pathways, and of its intraorbital (iOrb), intracanalicular (iCan), intracranial (iCran), optic chiasm (OC) and tract (OT) subdivisions. Here, by employing dedicated 3D high-resolution MRI in a group of 24 healthy volunteers, we present the salient biometry characteristics of the entire aVP, and propose a probabilistic atlas based on a newly-developed processing pipeline.

Materials and Methods: Data included 0.6mm3 steady-state free-precession images acquired from 24 healthy participants using a 3T scanner with a 64ch head coil. Labels were obtained by manual segmentation of each aVP subdivision.

Standardization was conducted by straightening and normalization of the aVP labels, with cross sectional area (CSA) preservation, by means of in-house developed Matlab scripts. Four biometry measurements were extracted: volume, length, CSA, and ellipticity index (Ei). A probabilistic atlas (the aVP24) was generated by averaging all the subjects' normalized labels. Mixed linear models were used to investigate between-subject coefficient of variability (CV) and dependency on age and sex.

Results: We included 14 male and 10 female participants, aged 35.8 ± 9 (SD) years. Overall aVP volume, length, CSA and Ei were respectively 485.70 mm3 (75.15) 61.02 mm (3.97) 8.41 mm2 (1.06), 0.35 (0.04). CSA exhibited the lowest CV (1.9). CSA decreased from iOrb to iCan (P<0.001) and was highest in OC (14.37 mm2). Ei was lowest in iOrb (0.15, P<0.001) approaching an almost circular cross section, but increased progressively until OC (0.57). No effect of side, age and/or sex was found in any measurement. Figure presents the aVP24 probabilistic atlas, illustrating the spatial probability map and the general morphology of the entire aVP (A) and its subdivisions (B).

Conclusions: Optic nerve damage may be linked to a variety of inflammatory, degenerative and/or vascular conditions which would benefit from group-level quantitative MRI investigations. The proposed MRI biometry data extraction and standardization framework lays grounds for spatial-resolved, group-level analyses of the entire aVP structure.

Keywords: optic pathway, optic nerve, MRI, atlas, biometry

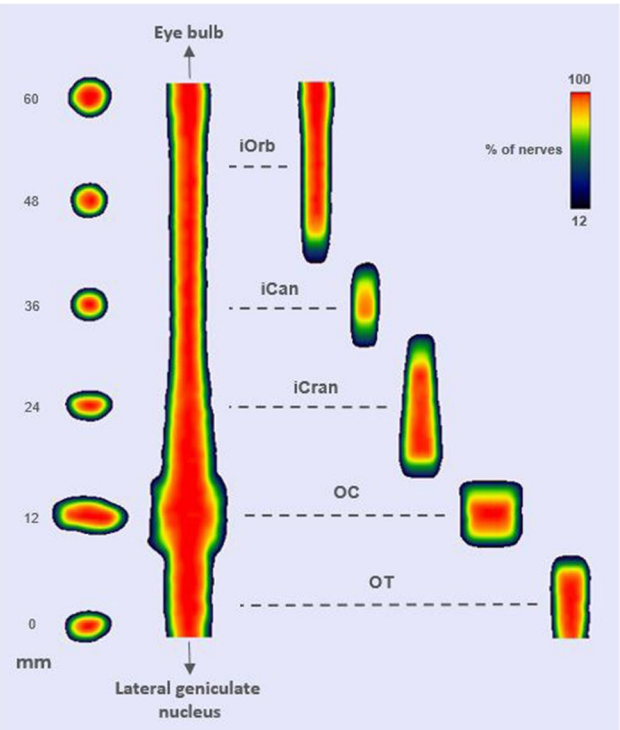

1-P3

MOLECULAR IMAGING WITH AMIDE PROTON TRANSFER WEIGHTED MRI FOR ROUTINE ASSESSMENT OF BRAIN TUMOURS AND TUMOUR MIMICS

Wai-Yung Yu[1], Hui Ping Oh[1], Septian Hartono[1], Yih Yian Sitoh[1]
[1]National Neuroscience Institute, Singapore, Singapore

Purpose: Molecular imaging with amide proton transfer-weighted (APTw) MRI on high field 3 tesla (3T) magnets is a recent development, not yet widely adopted in mainstream clinical imaging. APTw MRI allows an indirect measure of amide protons in intrinsic mobile proteins and peptides, which are abundant in tumour cells compared to normal brain tissue. We report our experience with APTw MRI in the routine assessment of brain tumours and tumour-like lesions.

Materials: Over a 2 year period, 100 patients with brain tumours and tumour-like conditions had routine clinical MRI at 3T with conventional morphologic scans as well as molecular imaging with APTw MRI. Color coded APTw maps were compared with the corresponding morphologic images, supplemented with perfusion weighted MRI in selected cases. APTw signal evaluation was performed at the contrast enhancing areas, peri-tumoural non-enhancing areas, cystic/necrotic or hemorrhagic areas. Confirmatory diagnosis was made via histology or surveillance follow-up imaging.

Results: APTw MRI can predict histologic grade in gliomas and assist in differentiating tumour progression from treatment effects. It is useful in distinguishing glioma from lymphoma and other non-mitotic conditions. In extra-axial meningiomas, APTw MRI differentiates benign and atypical meningiomas. Radiological caution is required in cystic/necrotic or hemorrhagic areas where APTw signal is increased, particularly in cases of intracerebral hemorrhage. There are practical challenges with regard to scan artefacts and magnetic field inhomogeneity; and in post-operative assessment with metallic implants.

Conclusion: APTw MRI is a practical molecular imaging technique that does not require intravenous contrast injection and is a valuable adjunct in the routine clinical imaging of patients with brain tumours and tumour mimics.

1-P4

THE MYELIN WATER FRACTION AS A MARKER OF AGE-RELATED MYELIN CONTENT CHANGES IN THE NORMAL-APPEARING CEREBRAL WHITE MATTER, CORRELATED WITH DIFFUSION TENSOR IMAGING

Jeeyoung Kim[1], Se Won Oh[1], Jimin Kim[1], Hyun Gi Kim[1], Dongyeob Han[2]
[1]Eunpyeong St. Mary's Hospital, Seoul, Korea, Republic of. [2]Siemens Healthineer Ltds, Seoul, Korea, Republic of

Conventional magnetic resonance imaging (MRI) provides an excellent spatial depiction of the cerebral white matter (WM), but lacks specificity for the evaluation of microstructural changes.
Myelin water image is highly specific for myelin and more sensitive for assessing the integrity of WM and myelin content. In contrast, diffusion tensor imaging (DTI) is sensitive to the neuronal effects of aging of the WM, but lacks the specificity for myelin content.
The purpose of this study was to evaluate the value of myelin water fraction (MWF) as a marker for age-related myelin change in normal-appearing major WM, using a recently proposed MWF-map reconstruction approach and correlated with DTI parameters (fractional anisotropy (FA), radial diffusivity (RD), or mean diffusivity (MD)).
We studied 72 cognitive normal, healthy subjects (23 males, 49 females; mean age 60.7 years, age range 49-73 years) who underwent multi-echo gradient echo (mGRE) and DTI in 3T MRI between November 2020 and February 2021. Region-of-interest-based (ROI) analysis was performed on MWF map extracted from 3D mGRE using complex model fitting (CF-MWF) and artificial neural networks (ANN-MWF) and DTI. In each subject, a total number of 10 ROIs (both centum semiovale, frontal, parietal and temporal WM, and the genu- (GCC) and splenium (SCC) of corpus callosum) were defined in distinct brain regions on each corresponding MWF and DTI images.
The ANN-MWF values showed good correlation with the CF-MWF values (Pearson correlation coefficient 0.556, p value < 0.001). ANN-MWF values significantly decreased with age in total ROI (Pearson's correlation t = - 0.28, p value = 0.016) and have shown to be more specific to age-related changes of the centrum semiovale (Pearson's correlation coefficient - 0.418, p value < 0.001) and genu of corpus callosum (Pearson's correlation coefficient - 0.269, p value = 0.021). Changes of ANN-MWF values were associated with negative correlation of RD (Pearson's correlation coefficient - 0.325, p value = 0.005) and MD (Pearson's correlation coefficient - 0.344, p value = 0.003). FA significantly decreased with age (Pearson's correlation coefficient - 0.261, p value = 0.026), but there was no significant correlation with ANN-MWF values.
We conclude that MWF is a useful marker for the assessment of age-related myelin alterations in the cerebral WM.

1-P5

PHOSPHOROUS MAGNETIC RESONANCE SPECTROSCOPY IN GLIOMAS WITH DIFFERENT SUBTYPES AND GRADES

Malik Galijasevic[1], Helena Viktoria Rieder[1], Ruth Steiger[1], Nadja Gruber[2,3], Tanja Janjic[1], Stephanie Mangesius[1], Julian Mangesius[1], Astrid Ellen Grams[1], Elke Ruth Gizewski[1]
[1]Medical University of Innsbruck, Innsbruck, Austria. [2]University of Innsbruck, Innsbruck, Austria. [3]VASCAge GmbH, Innsbruck, Austria

Purpose: To determine differences in the ratio of phosphorus metabolites, intracellular pH and magnesium (Mg) in different types and grades of gliomas dependent on isocitrate dehydrogenase 1 (IDH-1) and 1p19q mutation status by phosphorus magnetic resonance spectroscopy (31-P-MRS).

Methods and materials: 5 patients with grade 2, 5 patients with grade 3 glioma, and 41 patients with grade 4 glioma were studied by 31-P-MRS. Metabolite ratios, intracellular pH and Mg levels were compared between gliomas with different grades, IDH-status, and 1p19q-status.

Results: Grade 4 gliomas had a higher intracellular pH than lower grade gliomas (LGG). Grade 2 gliomas had the lowest pH compared to grade 3 and grade 4 tumors. Phosphocreatine/adenosine triphosphate (PCr/ATP) and inorganic phosphate/ATP (Pi/ATP) ratios were significantly higher in grade 2 and 3 tumors which significantly decreased with higher tumor grade. Astrocytomas had significantly lower Pi/ATP than oligodendrogliomas.

Conclusion: High grade gliomas showed markers of higher amount of ATP-turnover and higher apoptotic activity, as well as higher intracellular pH than LGG. Marker of higher apoptotic activity was increased in oligodendrogliomas compared to astrocytomas.

Limitations: This was a single-center study with a small patient number in the LGG group. We are currently conducting further analyses on a bigger cohort.

Ethics committee approval: The study was conducted in accordance with the Declaration of Helsinki, and approved by the local Ethics Committee of the Medical University of Innsbruck, Austria. Informed consent was obtained from all subjects involved in the study.

Funding for this study: This research received no external funding.

1-P6

CLINICAL APPLICATION OF ARTIFICIAL INTELLIGENCE IN MULTIPLE SCLEROSIS: DOES AUTOMATED LESION SEGMENTATION HELP?

David Berhanu[1,2], Inês Carneiro[1], Miguel Castelo-Branco[3], Sónia Batista[4], Daniela Jardim Pereira[5], João V. Duarte[3]
[1]Serviço de Imagiologia Neurológica, Centro Hospitalar Universitário Lisboa Norte, Lisbon, Portugal. [2]Faculdade de Medicina da Universidade de Lisboa (Lisbon School of Medicine), Lisbon, Portugal. [3]Instituto de Ciências Nucleares Aplicadas à Saúde, Coimbra, Portugal. [4]Serviço de Neurologia, Centro Hospitalar Universitário de Coimbra, Coimbra, Portugal. [5]Área Funcional de Neurorradiologia, Serviço de Imagem Médica, Centro Hospitalar Universitário de Coimbra, Coimbra, Portugal

Introduction: It is well established that lesion load in Multiple Sclerosis (MS) correlates with disease progression, disability and symptom severity, enhancing the value of lesion quantification and segmentation. However, automated lesion segmentation tools are scarcely used in clinical practice.
We intend to review the pearls and pitfalls of automated analysis, as well as the important caveats that are preventing its transfer to clinical setting.

Methods: We tested automated segmentation of T2-weighted lesions in 21 subjects, which included 12 patients with MS and 9 controls, at two time-points. We performed automated lesion segmentation and quantification of brain MRI using the LST toolbox for SPM. Lesion quantification was compared with manual analysis in order to assess sensitivity of automated software. Regions of imprecise segmentation were also noted. Additionally, longitudinal analysis was performed to assess reproducibility and to estimate new lesions, compared to manual segmentation.

Results: Automated segmentation of supratentorial T2 hyperintensities showed a high sensitivity (90%), however when infratentorial and cortical/juxtacortical lesions were considered sensitivity was significantly reduced (73%). Additionally, we identified false positive lesions in virtually every subject, which were mainly located in the periventricular white matter and represented a pitfall of the automated software. The reported number of lesions was less accurate than the estimated lesion volume, which should be complemented by visual analysis to increase specificity. Automated segmentation of MRI data took approximately 8 minutes and required reasonable expertise, which may be an important limiting factor to widespread implementation.

Conclusions: Our findings suggest that automated analysis is a fast and effective tool to complement clinical practice, improving the analysis of T2-weighted images in patients with MS. Also, it provides a useful quantitative analysis of lesion volume changes over time, which can potentially be incorporated in future clinical decisions. Additionally, concomitant visual analysis should be performed, which identifies periventricular areas overestimated as lesions and it helps to reduce the false positives in the analysis, increasing specificity.

1-P7

EVALUATION OF AUTOMATED HIPPOCAMPAL SEGMENTATION IN STROKE PATIENTS

Marianne Schell[1], Philipp Vollmuth[1], Martin Bendszus[1]
[1]Department of Neuroradiology, Heidelberg, Germany

Introduction: Deep learning methods can produce reproducible results in a matter of seconds. Although a variety of segmentation algorithms have already been proposed, their application to new more complicated datasets is uncertain and may fail in the presence of severe structural abnormalities – commonly seen in stroke patients.
Here we tested the cross-domain transferability of recent deep-learning based hippocampal segmentation methods.

Methods: Six recent, deep learning-based segmentation algorithms were tested on a multicentric, open-source dataset ATLAS of 655 stroke patients with T1-weighted sequences [1]: e2dhipseg, [2], HippMapp3r [3], hippodeep [4], FastSurfer [5], QuickNat [6], and AssemblyNet [7]. We estimated a virtual ground truth segmentation using the simultaneous truth and performance level estimation (Staple) algorithm [8], a weighted voting method to compute the probabilistic "true" segmentation.
With an agreement approach using multidimensional scaling the (dis)similarities of the segmentation algorithms were evaluated based on common metrices such as volume, volumetric similarity (VolS), Dice score and the 95th quantile of Hausdorff distance (HD). Finally, the metrices were used to rank the algorithms.

Results: Compared to the virtually generated Staple ground truth, only FastSurfer showed no significant difference between the volumes (paired t-test: p-value = 0.638) with the highest intraclass correlation of .863. But, when comparing the VolS of the ipsilateral and contralateral sides, 4 of 6 methods showed a significant decrease in similarity (see Table 1). All algorithms achieved good segmentation results with mean values between .885 and .985 in VolS, .856 and .940 in Dice and 2.24 and 3.61 in HD (see Figure 1 for a representative example). A comparison of different evaluation metrices shows a different similarity ranking of the algorithms within each patient (Figure 2). Figure 3 shows the results of the multidimensional scaling, where the proximity between each pair of segmentation algorithms represents the similarity between these two algorithms.

Discussion: The metrices showed the different requirements for the algorithms. Although current state-of-the-art methods achieved in general good results, four of six algorithms showed a significant decline when comparing the ipsilesional side with the contralateral side. Interestingly, higher volumetric similarity does not imply a better overlap (Dice), suggesting misalignment of the segmentation results. So far, there is no one-size-fits-all approach; the best segmentation method should be chosen depending on the research question.

Table 1: Volumetric similarities to Staple segmentation between ipsilesional and contralesional side for all segmentations. Higher values denote more similar volume to Staple ground truth.

	ipsilateral mean±sd	contralesional mean±sd	p-value	Confidence Interval
e2dhipseg	0.870±0.078	0.865±0.082	0.109	[-0.00078,0.0078]
hippmapp3r	0.806±0.170	0.815±0.170	<0.001	[-0.029,-0.012]
hippodeep	0.939±0.079	0.964±0.029	<0.001	[-0.032,-0.019]
fastsurfer	0.963±0.076	0.979±0.031	<0.001	[-0.021,-0.0094]
quicknat	0.938±0.094	0.939±0.078	0.613	[-0.0061,0.0036]
assemblynet	0.934±0.044	0.941±0.025	<0.001	[-0.011,-0.004]

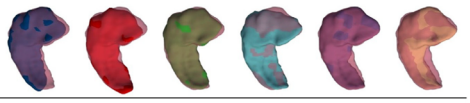

	e2dhipseg	hippmapp3r	hippodeep	fastsurfer	quicknat	assemblynet
Volume in mm³	3167	3422	3475	3836	3585	3305
VolS (Rank)	0.901 (6)	0.939 (4)	0.947 (3)	0.996 (1)	0.962 (2)	0.922 (5)
DICE (Rank)	0.881 (5)	0.878 (6)	0.935 (2)	0.926 (3)	0.955 (1)	0.884 (4)
HD (Rank)	3,74 (6)	3 (4)	1.73 (2)	2.24 (3)	1.41 (1)	3.32 (5)

Figure 1: Representative example of segmentation of the right hippocampus. All segmentations are superimposed on the Staple segmentation (transparent red). Below, table of metrices (volume, volumetric similarity, Dice score, and Hausdorff distance) for this example, ranks in parentheses.

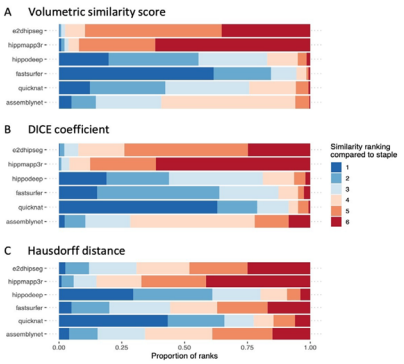

Figure 2: Proportion of ranks for each method and metric. Ranks were calculated for each hippocampus based on the different algorithms compared to Staple segmentation. Blue for more similar cases; i.e., higher volumetric similarity and DICE scores or lower Hausdorff distance.

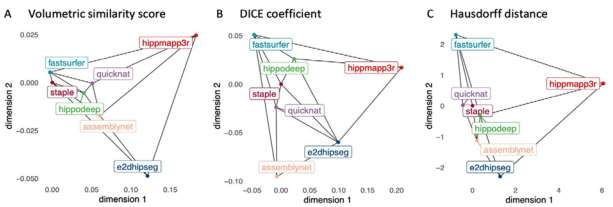

Figure 3: Classical metric multidimensional scaling maps for all segmentations based on the mean distance matrix for all paired comparisons. Proximity can be interpreted as similarity. Edges are based on Delaunay triangulation, where the most similar algorithms are connected by an edge in the graph.

Conclusion: The results of this study show that hippocampal segmentation methods still need improvement. Currently, there is no unified approach to this problem, and further research is needed.

1-P8
BIOMETRY OF THE FLAIR HYPERINTENSITY OF THE SPLENIUM OF THE CORPUS CALLOSUM

Ozkan Unal[1], Yasin Özdemir[1], Onur Simsek[1]
[1]SBU Dr. Abdurrahman Yurtaslan Onkoloji SUAM, Ankara, Turkey

Background and Purpose: Focal hyperintensity of the splenium of the corpus callosum was previously reported as an age-related change and a complication of radiotherapy (1). This study aims to present reference biometry of splenial FLAIR hyperintensity of the corpus callosum in different age groups.

Materials and Methods: In this Institutional-review board-approved retrospective cohort study, we analyzed the cerebral MR imaging of 975 participants and excluded patients with intracranial mass, selective radiotherapy history, known cerebrovascular disease, and white matter disease. A blinded radiologist measured the hyperintense thickness of the splenium on axial FLAIR MR imaging. The interobserver agreement was investigated by repeating the measurements by another blind radiologist in a randomly selected group. We investigated the effect of age and sex on the thickness.

Results: The participants were divided into different groups according to their age and gender. Minimum, maximum, and median values of the thickness of the splenium on FLAIR were provided for each group. On the Mann Whitney U test, no significant difference was found between the measurements of female and male participants. On the Kruskal Wallis Variant Analysis, the splenial thickness of the patients older than 66 years was significantly higher (p<0,01). Inter-observer agreement was excellent.

Conclusion: The thickness ranges of the splenium of the corpus callosum on FLAIR MR imaging vary according to age, and increased thicknesses are within normal limits in older age groups.

Keywords: Corpus callosum, splenium, FLAIR, hyperintense

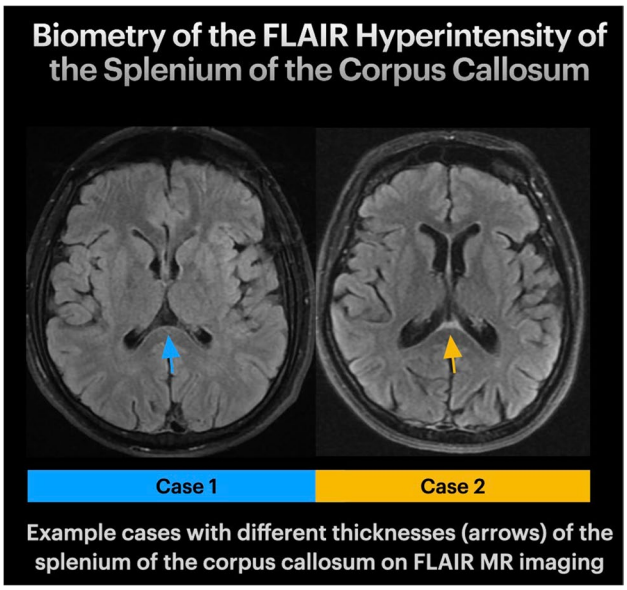

1-P9

CORRELATIONS BETWEEN ADC HISTOGRAM ANALYSES OF INTRACRANIAL PARENCHYMAL METASTASES AND PATHOLOGICAL PROPERTIES OF BREAST CANCER

Diba Saygılı Öz[1], Burcu Savran[1], Nazan Çiledağ[1], Özkan Ünal[1], Berna Karabulut[1]
[1]Ankara Oncology Health Application and Research Hospital, Ankara, Turkey

Introduction: The aim of this study was investigating the relationship between the ADC histogram parameters of brain metastases of breast cancer with conventional MRI findings of metastases, the histopathological and immunohistochemical features of the primary tumor.

Methods: ADC histogram analysis was performed for 55 lesions that were intracranial parenchymal metastases of breast cancer, with 1.5 Tesla MR device and a software.
ADC histogram parameters(voxel number, volume, ADCmin, ADC10%, ADC25%, ADC50%, ADC75%, ADC90%, ADCmax, skewness, kurtosis, entropy) of metastases were compaired with patient age(<40, ≥40), conventional MRI findings(localization, morphology, maximum diameter of metastases), histopathological(subtype, grade, lymphovascular invasion(LVI)) and immunohistochemical data(ER,PR,HER-2,ki- 67,molecular subtype)of the primary masses. Mann-Whitney U, Kruskal Wallis, independent samples t-test, and Spearman correlation analysis were used for statistical assessment.

Results: There were significant relationship with morphology. The voxel count(p=0,002), volume(p=0,003), all ADC percentiles(p<0,01) and ADCmax(p<0,01) were found to be significantly higher in cystic and semisolid lesions compared to solid lesions. Also, skewness(p=0,041) and kurtosis(p=0,022) values of semisolid lesions were found to be significantly higher than cystic lesions.
Also there were significant relationship with ER and PR status. All ADC percentiles and ADCmax values of ER/PR + cases were lower than ER/PR – cases(p<0,01). Studies have shown that ER/PR is associated with high cellularity and also reduces perfusion by inhibiting angiogenesis. Both factors cause a decrease in the amount of extracellular water. This may explain the lower ADC value in ER/PR positive cases than in negative cases.
Furthermore there were significant relationship with ki-67 status. ADC percentiles(p<0,05) and ADCmax(p<0,05) values of Ki-67 + cases were higher than ki-67 - cases.
Other significant relationships were found with molecular subtypes with ADC percentiles(p<0,05). Those results were compatible with immunohistochemical markers.
Statistically significant and positive correlations were found between the lesion diameter and the number of voxels, lesion volume, all ADC percentiles, ADCmax, entropy measurements(p=0,001).
No significant correlations were found between age, localization, grade, HER-2 status, LVI with ADC histogram parameters.

Conclusion: Breast cancer is highly heterogeneous disease both histopathologically, molecularly, genetically. Conventional imaging methods do not adequately reflect the internal heterogeneity of tumors.
As showned in this study, the parameters obtained from the ADC histogram analysis of brain metastases of breast cancer can reflect morphology and size of metastases, also immunohistochemical characteristics of the primary masses quantitatively.

Keywords: Breast Neoplasms, Magnetic Resonance Imaging, Metastasis

1-P10

DYNAMIC SUSCEPTIBILITY CONTRAST ENHANCED (DSC) MRI PERFUSION IN STATUS EPILEPTICUS

Silvana Sarria Estrada[1], Estevo Santamarina[1], Manuel Quintana[1], Manuel Toledo[1], María Sueiras[1], Cristina Auger[1], Alex Rovira[1]
[1]Vall d'Hebron University Hospital, Barcelona, Spain

Introduction: Physiological variations associated with status epilepticus (SE) include cerebral edema and perfusion abnormalities. MRI assessment using diffusion-weighted (DW), T2-weighted (W), T2w fluid-attenuated inversion

recovery (FLAIR) and perfusion (DSC) sequences can be associated with prolonged epileptic activity.

Methods: We retrospectively analyzed patients with focal onset SE during a period of 4 years, who underwent a MRI SE protocol during the hospitalization. All MRIs included the following sequences: DSC, T2W, FLAIR, DW and post-contrast T1W. All patients had a follow-up MRI within the 6 months following the baseline MRI.

Results: From 121 patients with SE and MRIs during the study period, 44 met the inclusion criteria. They were 28 (63.6%) men and 59, 5 years (SD 16.47). The main cause was tumors (n: 17; 38,6%).
We observed SE related lesions in T2-FLAIR (n=12; 27, 3%), DW (n=16;36.4%) and focal hiperperfusion DSC (n=21; 47.7%). One single patient showed leptomeningeal contrast enhancement.
The DSC hyperperfusion was associated with the presence of areas of high-signal in T2-FLAIR (57.1% vs. 0.0%; $p<0.001$) and restricted diffusivity in DW (61.9% vs. 13.0%; $p<0.001$).
In the follow-up MRI, changes in the acute phase recovered. The hippocampus showed abnormalities in 10 cases (22.7%). Diffuse brain atrophy was observed in 9 cases (20.5%) and mesial temporal sclerosis was developed in 3 patients (6.8%).

Conclusions: The inclusion of DSC perfusion combined with T2 enhanced sequences in the assessment of the MRI SE protocol may contribute to the diagnosis and it is likely associated with the prognosis of the patients.

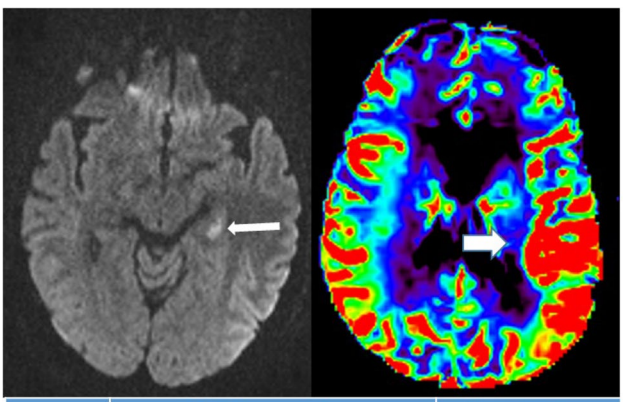

	MRI abnormalities		Related SE
PWI	Hiperperfusion	Hipoperfusion	
	28 (63,6%)	5 (11,4%)	21 (47,7%)

1-P11

TEMPORO-SPATIAL STRUCTURAL CHARACTERIZATION OF DEEP WHITE MATTER TRACTS ACROSS THE SPECTRUM OF HUNTINGTON'S DISEASE

Montserrat Domingo Ayllon[1,2], Estela Càmara Mancha[2]
[1]Radiology Department - University Hospital Joan XXIII, Tarragona, Spain. [2]Diffusion MRI and Brain Connectivity Group of Cognition and Brain Plasticity Unit (IDIBELL), Barcelona, Spain

Introduction: Although white matter (WM) abnormalities and subcortical iron accumulation are causal factors of neurodegeneration in Huntington's disease (HD), the relationship between WM changes and iron accumulation is not clear yet. A multimodal temporo-spatial characterization of WM tracts (microstructural integrity and iron content) could help to understand the dynamics of the physiopathology process underlying HD.

Methods: Thirty-one HD gene-expansion carriers and twenty-four healthy controls participated in this study. DTI and T2*-relaxometry were employed to characterize the structural connectivity and the iron distribution of eighteen WM tracts.
Three approaches have been used for the statistical analysis: average measure, segmental measures based on anatomic division of the tracts, and measures along the tract considering multiple points. One way-ANOVA and post-hoc Tukey were performed to detect statistically significant differences ($p<0.05$) among groups.

Results: Bilateral cortico-spinal tracts (CST), anterior thalamic radiations (ATR), cingulates and the corpus callosum are already affected in early presymptomatic stages, demonstrating incipient disintegration. However, increased iron levels were exclusively observed in right CST and ATR.
In symptomatic stages, there is a widespread disintegration of all the tracts assessed, with reduced iron levels for those tracts affected first with the exception of both CST which kept the iron content increased, and, with preserved iron levels for those tracts affected afterwards.
Methodologically, along-the-tract measures were more sensitive than mean measures to detect differences between controls and presymptomatic subjects. Segmental measures allowed to assess the spatial pattern of neurodegeneration.

Discussion: Striatal medium spiny neurons are the most susceptible to mutant Huntingtin entailing basal ganglia atrophy with disruption of cortico-basal ganglia-thalamo-cortical circuits. Consequently, different WM tracts included in these circuits are presumed to be affected in presymptomatic stages as demonstrated in our study: motor function

depending on putamino-pallidal connections (CST), limbic system depending on ventral striatum (cingulate), and executive function depending on caudate (ATR, forceps minor and forceps major).
Associative tracts (uncinate, inferior longitudinal, superior longitudinal fronto-parietal and fronto-temporal fasciculus) are also altered in symptomatic stages, most probably as a consequence of transaxonal degeneration when the brain breaks down globally.
In addition, the analysis based on segments and along-the-tract allows to visualize the spatial gradient and is more sensitive to detect anomalies in presymptomatic stages.

Conclusion: This study has allowed to depict the temporo-spatial dynamics of WM tracts disintegration in presymptomatic and symptomatic stages of HD. In particular, while all tracts showed widespread disintegration, motor-related tracts present higher iron levels than non-motor-related tracts.

1-P12
DIFFERENTIATION OF HIGH-GRADE GLIOMA AND BRAIN METASTASIS USING INTRAVOXEL INCOHERENT MOTION MRI

Miloš Keřkovský[1,2], Marek Dostál[1,3], Tereza Kopřivová[1,2], Tomáš Jůza[1,3], Václav Vybíhal[4], Eduard Neuman[4], Petr Matula[5], Michal Kozubek[5]
[1]University Hospital Brno, Department of Radiology and Nuclear Medicine, Brno, Czech Republic. [2]Masaryk University, Faculty of Medicine, Department of Radiology and Nuclear Medicine, Brno, Czech Republic. [3]Masaryk University, Faculty of Medicine, Department of Biophysics, Brno, Czech Republic. [4]University Hospital Brno, Department of Neurosurgery, Brno, Czech Republic. [5]Masaryk University, Faculty of Informatics, Department of Visual Computing, Brno, Czech Republic

Introduction: Magnetic resonance imaging (MRI) plays a key role in the diagnosis of brain tumors, however, their differential diagnosis using conventional visual evaluation may be difficult, because different types of tumors may share a number of common features. Several advanced quantitative MRI techniques based on diffusion imaging like intravoxel incoherent motion (IVIM) have been introduced in recent years, which have a potental to provide deeper insight into ultrastructural tissue pathology and possibly enable more precise differentiation of various histological entities. In this pilot study, we evaluate the potential of IVIM to differentiate between high-grade glioma (HGG) and brain metastasis.

Methods: The study group included 44 patients, 26 with histopathologically confirmed HGG and 18 with brain metastasis. All patients underwent MRI examination of the brain prior to surgery, the imaging protocol comprised sequences for morphological evaluation including contrast enhanced 3D T_1 acquisition and IVIM sequence using 10 different b values (0 – 2000 s/mm^2). The brain tumours were segmented on structural images semi-automatically using ITK-SNAP software differentiating particular tissue components (enhancing and non-enhancing parts of the tumour core and surrounding oedema). Maps of different parameters were calculated from IVIM data (f, D*, D and K) using MITK software and segmentation masks were registered to IVIM images. Subsequently, we performed histogram analysis to evaluate all voxels belonging to the segmentation masks of particular tissues, calculating mean, median, SD, 5th, 25th, 75th and 95th percentile values for all IVIM parameters. All these values were compared between HGG and metastasis subgroups using Kruskal-Wallis ANOVA and ROC statistical analysis.

Results: We found overall 18 parameters, which differed significantly between HGG and metastasis groups. They included some histogram values of all IVIM parameters measured both within the tumour core and surrounding oedema ($p \leq 0.04$). According to ROC analysis, the greatest power to discriminate between the groups revealed 25th and 5th quartiles together with median values of f parameter measured in oedema; sensitivity and specificity of f 25th quartile was 91.3% and 78.6% respectively, AUC 0.922 ($p<0.001$). The same parameter was also the strongest predictor measured in enhancing tumour core with sensitivity 64%, specificity 100% and AUC 0.893 ($p<0.001$).

Discussion & Conclusion: Our pilot data indicate that IVIM technique may be helpful in differentiation between HGG and metastasis through quantitative analysis of the diffusion properties within different components of the brain mass lesions.

1-P13
INTRACRANIAL VESSEL-WALL IMAGING: BEYOND LUMINAL ABNORMALITIES AND INTO THE VASCULAR WALL

Ana Isabel Almeida[1], José Maria Sousa[1], Sara Carvalho[1], Carina Reis[1]
Department of Neuroradiology, Centro Hospitalar Universitário de São João, E.P.E., Porto, Portugal

Introduction: Intracranial vessel-wall imaging (iVWI) provides evaluation of pathologic processes specific to the vessel wall, increasing the diagnostic accuracy for an array of vasculopathies, including in ischemic stroke (IS).

Objectives and Methods: We reviewed the current literature about iVWI technique and conducted a retrospective analysis

of all patients undergoing iVWI between 01/01/2017 and 25/05/2022 in our Institution in order to: summarize the typical imagiological patterns and select illustrative cases for each vasculopathy; evaluate the correlation between the final clinical diagnosis and imagiological findings in our sample; assess commonly encountered artifacts and pitfalls; and describe the evolution of our own institutional protocol based upon the published technical requirements for iVWI acquisition.

Results: After excluding patients with aneurysms (n=19), our sample size consisted of 60 patients, mean age of 53 ± 13 years-old, with 46 (77%) having IS. VWI findings were suggestive of atherosclerosis in 20 patients, vasculitis in 11 patients, reversible cerebral vasoconstriction syndrome in 3 patients, arterial dissection in 3 patients, and Moyamoya in 2 patients; a clot was detected in 2 cases. The study was unremarkable in 16 cases and inconclusive in 3. Although the clinical workup was not concluded in 10% of the cases, the remaining iVWI findings were clinically confirmed in all but one patient.
Accurate iVWI interpretation is critically dependent on adequate imaging technique and on the observer experience. Normal variations (including incomplete signal suppression of blood flow, the presence of vasa vasorum or adjacent veins) may be misinterpreted as pathological when either of these factors is lacking. The small size and tortuous orientations of intracranial arteries pose unique technical challenges, requiring high spatial resolution images with high signal-to-noise and contrast-to-noise ratios. In our Institution, the experience with iVWI has evolved from pre- and post-contrast 2D acquisitions to isotropic 3D sequences with intrinsic "black blood" properties (SPACE) and an additional specialized blood suppression technique, mostly acquired using a 3 T scanner.

Discussion and Conclusion: Vessel-wall imaging is a useful complement to conventional luminal imaging techniques in the differential diagnosis of vasculopathies, thus helping to unveil the aetiology of cryptogenic stroke and prevent further vascular events. However, technical limitations and the personnel experience required for interpretation may limit more generalized applicability.

Keywords: Intracranial vessel-wall; vasculopathies; ischemic stroke

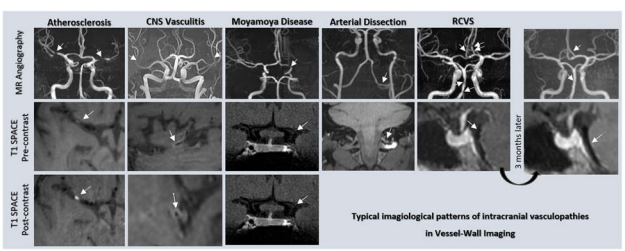

1-P14

ACTIVITY ALTERATIONS OF VARIOUS BRAIN REGIONS IN ALCOHOL INTOXICATED DRIVERS: A SYSTEMATIC REVIEW AND META ANALYSIS OF FUNCTIONAL MAGNETIC RESONANCE IMAGING STUDIES

Rasa Beheshti[1], Ali Norouzi[1], Sama Rahnemayan[2], Hossein Hosseinifard[3], Morteza Ghojazadeh[2], Alireza Lotfi[1]
[1]Student Research Committee, Tabriz University of Medical science, Tabriz, Iran, Islamic Republic of. [2]Neuroscience Research Center, Tabriz University of Medical Sciences, Tabriz, Iran, Islamic Republic of. [3]Research Center for Evidence-Based Medicine, Tabriz University of Medical Sciences, Tabriz, Iran, Islamic Republic of

Introduction: Drunk driving is one of the main causes of traffic accidents and causalities. Years of functional magnetic resonance imaging (fMRI) research have revealed various effects of alcohol intoxication on drivers' brains; however, there is no comprehensive list of the exact brain regions involved. Our goal was to conduct a systematic review and meta-analysis in order to develop more effective alcohol abuse prevention and intervention efforts.

Methods: Pubmed, Scopus, Embase, WoS, Proquest, Ovid, and Google Scholar were systematically searched to find fMRI studies comparing intoxicated drivers to non-intoxicated drivers. The eligibility criteria were used to screen the articles. Meta-analysis was performed on MNI and Talairach coordinates from included studies using the ALE method in GingerALE2.3.6. The threshold for ALE maps was set at P0.05. Mango software was used to view the ALE maps that were overlaid on the MNI 152 template.

Results: After removing duplicates, 593 articles were found. Only four articles were included in the meta-analysis after screening and eligibility. According to ALE analysis, alcohol intoxicated drivers have significantly lower activation of the medial region of the right superior frontal gyrus, left thalamus, and left anterior cingulate gyrus when compared to non-intoxicated drivers. They also reveal increased activation in the right parietal operculum, right planum polare, right precentral gyrus, medial segment of the right superior frontal gyrus, right superior frontal gyrus, left angular gyrus, left superior frontal gyrus, and left superior motor cortex.

Conclusion: This is the first meta-analysis to provide key hyper- and hypo-activation regions while driving while inebriated. The regional abnormalities revealed in this study could be used as biomarkers to better understand the underlying brain mechanisms of impaired driving performance while intoxicated, and to develop effective prevention

methods to reduce the risk of intoxication-related traffic accidents.

Keywords: alcohol intoxication; drunk driving; fMRI; Meta-Analysis; Systematic Review

1-P15

NEUROMELANIN IMAGING IN PROGRESSIVE SUPRANUCLEAR PALSY

Ângelo Dias[1,2], Rita Moiron Simões[3,4], Carla Guerreiro[1,2,5], Carlos Morgado[1,5], Joaquim J. Ferreira[2,4,6], Sofia Reimão[1,5,6]
[1]Department of Neurological Imaging, Hospital de Santa Maria, Centro Hospitalar Lisboa Norte, Lisbon, Portugal. [2]Instituto de Medicina Molecular João Lobo Antunes, Faculdade de Medicina, Universidade de Lisboa, Lisbon, Portugal. [3]Neurology Department, Hospital Beatriz Ângelo, Loures, Portugal. [4]CNS-Campus Neurológico Sénior, Torres Vedras, Portugal. [5]Imaging University Clinic, Faculdade de Medicina da Universidade de Lisboa, Lisbon, Portugal. [6]Laboratório de Farmacologia Clínica e Terapêutica, Faculdade de Medicina, Universidade de Lisboa, Lisbon, Portugal

Progressive supranuclear palsy (PSP) is a neurodegenerative disorder characterized by the accumulation of abnormal forms of tau protein within brain cells currently requiring neuropathological examination for a definite diagnosis.
The classical clinical presentation of PSP consists of vertical supranuclear gaze palsy, postural instability and falls within the first year of symptom onset. These symptoms although highly specific may be absent. Moreover, patients with PSP often show a wide range of clinical manifestations that frequently overlap with Parkinson's disease (PD), making the diagnosis of PSP a clinical challenge, especially in early disease stages.
Early and reliable diagnosis of PSP is of great importance as there are considerable differences in disease course, prognosis and management when compared to PD. Several brain MRI findings have been investigated as possible early imaging disease biomarkers, but still with limited success.
Substantia nigra pars compacta (SNpc) is a dopaminergic brain region known to be severely affected in both PD and PSP. Degenerative changes of the SNpc dopaminergic neurons can be accurately identified using *in vivo* T1-weighted neuromelanin-sensitive magnetic resonance imaging.
This study aims to analyse the SNpc neuromelanin (SNpc-NM) signal in PSP patients, compared to age- and sex-matched patients with PD and healthy controls.
Thirty PSP patients, ten PD patients with 2 to 5 years disease duration and fourteen healthy controls were included.
All patients were evaluated by a neurologist specialized in movement disorders with more than 10 years of experience. The diagnosis of PSP and PD followed the National Institute of Neurological Disorders and Stroke and Society for PSP and the UK Brain Bank criteria, respectively.
Both the area and intensity of SNpc-NM signal were analyzed. The area of SNpc-NM signal was measured using a semi-automatic segmentation algorithm. High signal intensity of the lateral and medial SNpc subregions was evaluated with contrast-to-noise ratio (CNR) between SN areas and cerebral peduncles. All imaging analysis was done blinded to the clinical data.
This study presents findings on SN NM area and signal intensity changes in patients with PSP compared to PD and healthy controls that may contribute to improve the accuracy of parkinsonian syndromes' diagnosis. The pattern of SN NM changes can become an important biomarker of PSP and aid to improve the accuracy of the differential diagnosis with PD.

1-P16

INCREASED SPECIFICITY OF DIFFUSION MRI BY TENSOR-VALUED DIFFUSION MRI AND IMAGING-HISTOLOGY CORRELATIONS

Jan Brabec[1]
[1]Medical Radiation Physics, Lund University, Lund, Sweden

Diffusion MRI (dMRI) reflects diffusion of water in tissue and is sensitive to the tissue microstructure (Nilsson et al., 2018;Alexander et al., 2019). Although it is sensitive, its main drawback is, that it lacks specificity to particular microstructural features which hinders further advancement of diffusion MRI.
The first reason why dMRI is lacking specificity is that that endless number of microstructural features map onto only relatively few dMRI measurement observables. Typically, the diffusion signal vs b-value yields just two observables—its initial slope and departure from exponential decay at higher b-values. If the measurements are extended in several directions, voxel-level anisotropy as another observable can be added (Basser et al., 1994). Therefore, the inference from the outcome of dMRI measurements to specific tissue features may not be possible, unless new ways of signal preparation that would lead to new dMRI observables are introduced. Another reason why dMRI is lacking specificity is that dMRI measurements are interpreted without knowing all relevant features that influence the diffusion of water (Novikov et al., 2018). To find features of relevance, microstructure modelling has been proposed as a means to convert unspecific observables into parameters with specific interpretations. However, the current interpretations tend to rely on singular features such as cellularity (in cancer) or simple models of axons as straight-cylinders (white matter). Features of the tissue on the mesoscopic level, such as the heterogeneity in cancer or long-range geometrical aspects of

axons, has so far been overlooked (Nilsson et al., 2012). By investigating how to enrich dMRI measurements and what features are of relevance and, we can arrive at improved diffusion MRI protocols that may be used in the clinical studies.

To address the first problem, a new observable to the diffusion MRI can be added by a new way of diffusion encoding—by so-called tensor-valued diffusion MRI (Szczepankiewicz et al., 2016;Westin et al., 2016). We have evaluated the feasibility of the new protocol for use in cancer imaging in a wide range of intracranial tumors and found that it is feasible in a clinically relevant scan times (Nilsson et al., 2020). We investigated whether diffusion-weighted imaging (DWI) obtained with spherical tensor-valued encoding (STE) can be used to suppress white matter and enhance the conspicuity of glioma hyperintensities unrelated to white matter (Brabec et al., 2022a). We found that the contrast mechanism of high b-value DWI equipped with spherical encoding results in a stronger suppression of white matter than conventional DWI, and may, therefore, be more sensitive and specific for assessment of glioma tumors and DWI-hyperintensities. We also investigated whether tensor-valued diffusion MRI can add to the preoperative prediction of meningioma consistency, grade and type and found it can facilitate their prediction (Brabec et al., 2022b).

To address the second problem that is concerned with how mesoscopic properties of microstructure influences dMRI we performed two studies in axons in white matter and in cancer. In cancer, we quantified the degree to which mean diffusivity (MD) and fractional anisotropy (FA) from diffusion tensor imaging (DTI) correlates negatively with cell density (CD) and positively with tissue anisotropy in meningioma tumors, respectively, and compared that to the performance of an artificial neural network (ANN; accepted abstract at the Annual meeting of ESNR 2022, submission ID: 120). Across tumors, we reproduced associations between CD and MD, and IA and in-plane FA. However, within individual samples there were cases where the association between CD and MD was weak or absent so that both high or low CD led to similar MD and ANN approach performed better. That may be partially due to poor MRI-to-histology coregistration in the through-plane direction but we could identify specific features, such as tumor vasculature, microcysts, psammoma bodies or tissue cohesivity that contributes to a variation in MD beyond CD. It is likely that other features apart from CD and IA are of importance for the local interpretability of MD and FA. In axons in white matter, we investigated whether a synthetic diffusion MRI signal can be attributed to straight-cylinders or non-straight propagation of axons, referred to as undulations (Brabec et al., 2020). We found that fiber undulations contribute to a diffusion time dependence similar to that of straight cylinders and, therefore, axonal undulations can bias diameter estimation strategies if straight cylinders are used to model the intra-axonal diffusion. We suggest that diffusion encoding with encoding power at shorter diffusion times might be required to resolve effects of undulations and sizes. In summary, we found that advanced diffusion MRI encoding can add value to cancer imaging (Nilsson et al., 2020;Brabec et al., 2022a;Brabec et al., 2022b) and that collective tissue behavior need to be considered when interpreting dMRI measurements in terms of biological underpinnings (Abstract ID: 120, ESNR 2022)(Brabec et al., 2020).

NEURODEGENERATIVE

1-P17

WHAT HAPPENS WITH AGING: WHAT IS NORMAL AND WHAT IS PATHOLOGICAL? – WHAT CAN THE NEURORADIOLOGIST REALLY TELL?

Joana Freitas[1,2], Inês Carneiro[1], Hugo Cadilha[1], Sofia Reimãi[1,2,3]

[1]Serviço de Imagiologia Neurológica, Centro Hospitalar Universitário Lisboa Norte, Lisboa, Portugal. [2]Clínica Universitária de Imagiologia da Faculdade de Medicina da Universidade de Lisboa, Lisboa, Portugal. [3]Laboratório de Farmacologia Clínica do Instituto de Medicina Molecular da Faculdade de Medicina da Universidade de Lisboa, Lisboa, Portugal

Background: Brain aging is a complex and dynamic process of structural, metabolic and functional changes, with high inter-subject variability. Post-mortem studies in brains of aged individuals without neurological disease consistently show the presence of amyloid plaques, neurofibrillary tangles, Lewy bodies, and neuronal loss. These findings, when increased, are also hallmarks of neurodegenerative diseases, leading to the hypothesis that neurodegenerative diseases and normal brain aging are linked. Age-related brain changes are often overlooked in clinical neuroradiology practice. Knowledge of normal changes in brain aging is crucial to distinguish and evaluate patterns of normal versus abnormal aging in imaging examinations. Magnetic resonance imaging (MRI) is widely used in the noninvasively assessment of structural and functional brain changes in aging.

Objectives: Summarize the main structural changes that occur in the brain with "normal" aging, illustrating the most relevant normal and abnormal findings that neuroradiologists need to be aware of, including the use of visual rating scales that may aid in daily practice to identify abnormal changes.

Methods and Results: We reviewed the most relevant structural imaging brain changes seen in normal aging and the

indicated scales to differentiate between normal brain aging and abnormal findings.

Discussion: Imaging of the brain in patients with suspected neurodegenerative diseases is common and challenging, since there is an overlap between normal brain aging and neurodegenerative diseases. Therefore, recognizing age-related brain changes, such as brain atrophy (global and regional), white matter T2 signal hyperintensities, silent brain infarcts, cerebral microbleeds, enlarged perivascular spaces, and iron accumulation, is crucial to assess normal changes and to exclude pathologic patterns of neurodegenerative diseases. MRI improves the ability to differentiate normal and abnormal findings. Qualitative rating scales enable visual assessment of these changes and standardized language between healthcare professionals. Also, we propose the use of a checklist for reading and reporting brain examinations in the elderly.

Keywords: brain aging, neurodegeneration, atrophy, microbleeds, iron deposition, perivascular spaces

1-P18

COMPARISONS OF ^{18}F-FLORAPRONOL PET, ^{18}F-FDG PET, AND MRI BETWEEN NORMAL SUBJECTS AND MILD COGNITIVE IMPAIRMENT PATIENTS

Byeong Hyeon Byeon[1], Su Yeon Park[2], Jeong Ho Ha[2], Dae Yoon Chi[3], Sang Moo Lim[1]
[1]Department of Nuclear Medicine, Korea Cancer Center Hospital, Korea Institute of Radiological & Medical Sciences, Seoul, Korea, Republic of. [2]Department of Neurology, Korea Cancer Center Hospital, Korea Institute of Radiological & Medical Sciences, Seoul, Korea, Republic of. [3]Research Institute of Labeling, FutureChem Co., Ltd, Seoul, Korea, Republic of

Introduction: In the course of neurodegenerative diseases, especially Alzheimer's disease, it is known that the accumulation of beta-amyloid in the brain precedes the decrease in metabolic function or the decrease in cerebral cortical volume. The purpose of this study was to compare the beta-amyloid accumulation, glucose metabolism, and cerebral cortical volume between normal control (NC) subjects and mild cognitive impairment (MCI) patients using ^{18}F-Florapronol amyloid PET, ^{18}F-FDG PET, and MRI, respectively.

Methods: Twenty-nine NC subjects (mean age = 73.4 y) and 28 MCI patients (mean age = 66.9 y) were enrolled from a prospective single center clinical trial. ^{18}F-Florapronol PET, ^{18}F-FDG PET, and structural MRI were performed within a week interval. Standardized uptake value ratio (SUVR)-the SUV ratio of cerebral cortex to the cerebellar cortex (^{18}F-Florapronol PET) or pons (^{18}F-FDG PET)- and the cerebral cortical volume from the MR images (MRV) were extracted by using the automated software of Veuron-Brain-pAb2 (Heuron Inc., Republic of Korea, iheuron.com).

Results: The mean SUVR for ^{18}F-Florapronol PET were significantly higher in MCI patients than NC subjects (1.36 vs 1.24, $P < 0.001$). On the other hand, there were no statistically significant differences between the mean SUVR for 18F-FDG PET (1.51 vs 1.51, $P = 0.054$) or the mean MRV (342 mL vs 361 mL, $P = 0.094$) between MCI patients and NC subjects.

Discussion & Conclusion: The cortical uptake of amyloid PET was higher in MCI patients than NC subjects, while there was no difference in either glucose metabolism or cortical between two groups. These findings suggest that brain amyloid accumulation precedes the decrease in metabolic function or cerebral cortical atrophy in the early stage of neurodegenerative disease.

1-P19

EUROPEAN INTER-SOCIETAL DELPHI CONSENSUS FOR THE BIOMARKER-BASED ETIOLOGICAL DIAGNOSIS OF NEUROCOGNITIVE DISORDERS

Meike Vernooij[1], Tarek Yousry[2], Cristina Festari[3], Federico Massa[4], Matteo Cotta Ramusino[5], Flavio Nobili[6], Giovanni Frisoni[7]
[1]Department of Radiology & Nuclear Medicine; Erasmus MC, Rotterdam, Netherlands, [2]Lysholm Department of Neuroradiology and the Neuroradiological Academic Unit, Department of Brain Repair and Rehabilitation, University College London Hospitals NHS Foundation Trust National Hospital for Neurology and Neurosurgery, London, United Kingdom, [3]Laboratory of Alzheimer's Neuroimaging and Epidemiology, IRCCS Istituto Centro San Giovanni di Dio Fatebenefratelli, Brescia, Italy, [4]Department of Neuroscience, Rehabilitation, Ophthalmology, Genetics, Maternal and Child Health (DINOGMI), University of Genoa, Genoa, Italy, [5]IRCCS Mondino Foundation, Pavia, Italy, [6]IRCCS Ospedale Policlinico San Martino, Genoa, Italy, [7]Laboratory of Neuroimaging of Aging (LANVIE), University of Geneva, Geneva, Switzerland

Background: Cerebrospinal fluid (CSF) and imaging biomarkers are necessary for the aetiological diagnosis of neurocognitive disorders, but evidence on their rational use in the clinic is incomplete. Since November 2020, a European multidisciplinary task force of 22 experts from eleven relevant scientific societies has defined a diagnostic workflow for the efficient use of biomarkers, filling the evidence gap

on biomarker prioritisation with a formal Delphi consensus procedure. This abstract reports the preliminary results as of April 2022.

Methods: A modified Delphi method was used to create consensus. Group members participated in virtual Delphi rounds and voted on specific questions regarding the diagnostic workup of neurocognitive patients, based on their experience and evidence from the literature. Consensus was reached at a threshold of 70% agreement, or 50%+1 when a question required rediscussion.

Results: Six rounds have been completed so far. Panelists agreed on the clinical workspace of the workflow (specialist outpatient service), the stage of application (prodromal and mild dementia), and the patient age window (biomarker use strongly encouraged below 70 years and of limited usefulness over age 85).
The workflow is patient-centred and features three levels of assessment (W): W1 defines eleven clinical profiles based on the integrated results of neuropsychology, MRI atrophy patterns, and blood tests; W2 describes the first-line biomarkers according to W1's clinical suspicion; and W3 suggests the second-line biomarker when the results of first-line biomarkers are inconsistent with the diagnostic hypothesis, uninformative or inconclusive. More specifically, CSF biomarkers are first-line in the suspect of Alzheimer's disease (AD) and when inconsistent neuropsychological and MRI findings hinder a clear diagnostic hypothesis; dopamine SPECT/PET for those leading to suspect Lewy body spectrum. FDG-PET is first-line for the clinical profiles leading to suspect frontotemporal lobar degeneration and motor tauopathies and is followed by CSF biomarkers in the case of atypical metabolic patterns, when an underlying AD etiology is conceivable.

Conclusions: The workflow will promote consistency in diagnosing neurocognitive disorders across countries, and rational use of resources. The initiative has an impact in preparing clinicians to work in the upcoming clinical space where etiological disease-modifying drugs are expected to be available.

1-P20

AN INVESTIGATION OF LONG-TERM MOTOR AND COGNITIVE OUTCOMES IN MS PATIENTS WITH SIGNS OF BRAIN GADOLINIUM RETENTION

Alessandra Scaravilli[1], Mario Tranfa[1], Giuseppe Pontillo[1,2], Fabrizia Falco[3], Chiara Criscuolo[3], Marcello Moccia[3], Serena Monti[4], Roberta Lanzillo[3], Vincenzo Brescia Morra[3], Giuseppe Palma[5], Maria Petracca[3,6], Enrico Tedeschi[1], Andrea Elefante[1], Arturo Brunetti[1], Sirio Cocozza[1]

[1]Department of Advanced Biomedical Sciences, University "Federico II", Naples, Italy. [2]Department of Electrical Engineering and Information Technology, University of Naples "Federico II", Naples, Italy. [3]Department of Neurosciences and Reproductive and Odontostomatological Sciences, University of Naples "Federico II", Naples, Italy. [4]Institute of Biostructure and Bioimaging, National Research Council, Naples, Italy. [5]Institute of Nanotechnology, National Research Council, Lecce, Italy. [6]Department of Human Neurosciences, Sapienza University of Rome, Rome, Italy

Objectives: Gadolinium (Gd) retention in the Dentate Nuclei (DN) of patients undergoing multiple Gd-based contrast agents (GBCA) administrations is a widely known and investigated phenomenon. Nevertheless, very little is known about the possible clinical impact of this retention.
Aim of this study was to investigate possible long-term effects of Gd retention on both motor and cognitive disability in patients with Multiple Sclerosis (MS).

Methods: In this retrospective study, relation between qualitative and quantitative MRI signs of Gd retention (namely, the presence of a DN T1-weighted hyperintensity and changes in longitudinal relaxation -R1- maps), previously described in a group of 74 MS patients (M/F=27/47; mean age=36.1±10.1) were probed with possible changes in motor and cognitive scores.
Motor evaluation was performed via the Expanded Disability Status Scale (EDSS) score at baseline and after a mean follow-up time of 7.6±0.6 years, while cognitive status was assessed administering the Brief International Cognitive Assessment for MS (BICAMS) battery in a 65 of the previously described 74 patients (M/F=26/39; mean age=36.5±10.1) at baseline, and in a subgroup of 32 subjects (M/F=13/19; mean age=45.9±10.5) after 7.5±0.7 years of follow-up.

Results: Patients with and without DN hyperintensity on T1-weighted images did not differ in terms of motor nor cognitive status (p=0.14 and 0.92, respectively).
When comparing patients with and without motor worsening, no difference emerged in terms of DN R1 (p=0.15). Similarly, no differences were found in terms of DN R1 between cognitive impaired and preserved patients (p=0.26). Finally, regression models including demographic, clinical and MRI features failed to find any relationships between DN R1 values and motor or cognitive symptoms (p=0.21 and 0.30, respectively).

Discussion: In our study, we confirmed the lack of correlation between MRI features of Gd retention in DN and significant clinical counterparts in MS patients. These results are in line with most of the available literature that fails to find a significant association between Gd retention and motor or

cognitive alterations. Furthermore, our study expands the current knowledge, by providing one of the first evidence about long-term counterparts of Gd retention, although future studies are warranted to confirm these results.

Conclusions: These findings suggest that Gd retention in the DN, indirectly assessed via qualitative and quantitative MRI parameters, seems to be unrelated to long-term motor or cognitive impairment in MS patients.

Keywords: Gadolinium retention, dentate nuclei, multiple sclerosis

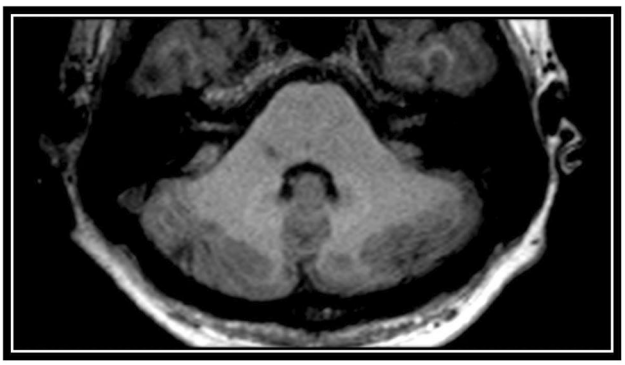

FIGURE 1
Axial T1-weighted MR image shows increased dentate nuclei hyperintensity in a 37-year-old MS female patient. The patient previously underwent 15 MR examinations with administrations of gadolinium-based contrast agents.

DEMYELINATING / INFLAMMATORY

1-P21

BLACK HOLE EVALUATION IN MULTIPLE SCLEROSIS: THE IMPACT OF DIFFERENT SEQUENCES IN CLINICAL PRACTICE AND A POSSIBLE ISSUE OF REPRODUCIBILITY

Mario Tranfa[1], Alessandra Scaravilli[1], Giuseppe Pontillo[1,2], Chiara Pastore[1], Alfredo Montella[1], Antonio Carotenuto[3], Roberta Lanzillo[3], Vincenzo Brescia Morra[3], Maria Petracca[3,4], Arturo Brunetti[1], Sirio Cocozza[1]
[1]Department of Advanced Biomedical Sciences, University of Naples "Federico II", Naples, Italy. [2]Department of Electrical Engineering and Information Technology, University of Naples “Federico II”, Naples, Italy. [3]Department of Neurosciences and Reproductive and Odontostomatological Sciences, University of Naples “Federico II”, Naples, Italy. [4]Department of Human Neurosciences, Sapienza University of Rome, Rome, Italy

Introduction: In the neuroradiological evaluation of Multiple Sclerosis (MS) patients, reporting T1-weighted (T1w) hypointense lesions (Black Holes-BH) provide useful information to the clinician. These lesions, defined as an area with a signal intensity comprised between gray matter and cerebrospinal fluid on T1w Spin-Echo (SE) sequences, represent irreversible axonal and neuronal loss and significantly correlate with patients' clinical status. Nevertheless, SE-T1w have been recently widely replaced by Gradient-Echo (GrE) T1w sequences, providing increased spatial resolution and a more pronounced tissue contrast. Hypothesizing that these features might influence BH evaluation, we aimed to compare the rate of BH detected on SE-T1w and GrE-T1w, and evaluate the different impact of these sequences on intra-reader variability.

Methods: Brain MRI scans were collected from 87 relapsing-remitting MS patients (M/F=22/65; mean age=36.3±10.4years). The acquisition protocol included a SE-T1w acquired with 3mm slice thickness and a 1mm isotropic GrE-T1w sequence, from which a 3mm thick MPR was computed. The three sequences (SE-T1w, 1mm-GrE-T1w and 3mm-GrE-T1w) were evaluated independently by a trained reader blinded for any clinical or demographic information. After a wash-out period of 30 days, the reader evaluated the same images in different order and with a different identification code to assess the intra-observer intra-class coefficient (ICC).

Results: The mean number of BH detected on 1mm-GrE-T1w was significantly higher compared to that obtained evaluating SE-T1w (4.6±7.3vs2.2±3.4, $p<0.0001$), with a similar difference, although less pronounced, that was proved when 3mm-GrE-T1w images were evaluated (4.6±7.3vs3.5±4.9, $p=0.005$). The ICC analysis showed that the evaluation of the SE-T1w images proved the be the most reliable (ICC=0.98), followed by the 3mm-GrE-T1w (ICC=0.91), while the 1mm-GrE-T1w sequence proved to have lower ICC values (ICC=0.87), suggesting that the evaluation of the latter was less reliable than those achieved using SE-T1w and the 3mm-GrE-T1w sequences.

Discussion: This study showed that applying the widely accepted definition of BH, GrE-T1w is prone to a greater variability compared to SE-T1w, probably due to both higher tissue contrast and spatial resolution, also in the light of the results found when the 3mm-GrE-T1w reformatted sequence was evaluated.

Conclusions: The detection of BH is crucial in the neuroradiological workup of MS patients, but their current definition might lead to an overestimated lesion load when GrE-T1w are evaluated, along with a lower reproducibility. For these reasons, an updated definition and standardization of how to evaluate BH on GrE-T1w is needed in the future.

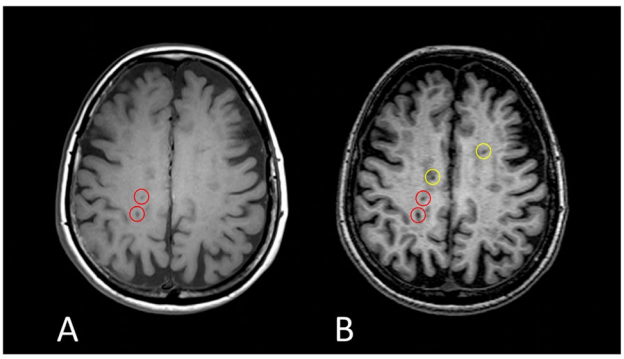

Brain MRI scans of a 58-year-old woman with Multiple Sclerosis. On the left (A), a SE-T1w image showing the presence of 2 *black holes* (red circles), while on the GrE-T1w image (B) two additional lesions (yellow circles) were classified as *black holes*.

1-P22

MRI PORTUGUESE NATIONAL SCREENING FOR THE FOLLOW-UP OF MS PATIENTS UNDER NATALIZUMAB

Joana Barata Tavares[1,2], Lidiane Pereira[3], Catarina Flores[4]
[1]Hospital da Cruz Vermelha Portuguesa, Lisbon, Portugal. [2]Hospital da Luz - Clinica de Odivelas, Lisbon, Portugal. [3]HealthTeam, Lisbon, Portugal. [4]Biogen, Lisbon, Portugal

Introduction: Progressive Multifocal Leukoencephalopathy (PML) is a rare but potentially fatal demyelinating disease caused by the reactivation of the John Cunningham (JC) virus. This virus is common and normally harmless; however, it can lead to PML in people whose immune system is weakened.
Natalizumab is a monoclonal antibody approved for the treatment of adults with highly active multiple sclerosis (MS). The risk of developing PML is increased in patients treated with natalizumab for more than 2 years, positive for anti-JC virus antibody and with previous use of immunosuppressants.
Magnetic resonance imaging (MRI) detects PML in the asymptomatic phase, allowing early treatment and improved prognosis.
Annual surveillance MRI is performed to assess MS lesions. Patients at high risk of developing PML, in addition to annual MRIs, should undergo more frequent examinations with an abbreviated protocol in which the goal is not to assess the progression of MS lesions but to detect PML in the asymptomatic phase.

Methods: The authors developed an MRI Portuguese National Screening for the follow-up of MS patients under natalizumab. An MRI with an abbreviated protocol was performed every 4 months in patients with JC positive antibodies and that had been taking natalizumb for more than 18 months. The abbreviated protocol included: Sagittal FLAIR 3mm, Axial FLAIR 3mm, Axial T2 and Axial DWI. Several main Portuguese Public hospitals were included and patients were enrolled by the attending neurologist. Private MR centers in Braga, Coimbra, Lisbon, Evora and Faro were contracted to do the MRIs and a teaching session to standardize the protocols was undertaken. The screening has been enrolling patients since 2020.

Results: Seven MRIs have been performed so far. Four patients are enrolled: one has already had three examinations and three others one each. So far, no PML lesions were reported.

Discussion: PML lesions typically involve the subcortical U-fibers and may present small "granular" or "microcystic" foci on T2-weighted images. These differ from MS lesions that are typically juxtacortical, periventricular or infratentorial and present no "microcystic" lesions.
MS patients under natalizumab rarely present new MS plaques, therefore a new FLAIR hyperintense lesion should always be screened to rule out a PML lesion.
So far, no highly suspicion lesions for PML were depicted.

Conclusion: National Screening Programs help standardize protocols and actively follow-up patients at risk.
Our program enables neurologists to be more reassured that their at-risk patients are being carefully monitored.

1-P23

DESCENDING DIFFUSION RESTRICTION IN THE CORTICOSPINAL TRACT AFTER RADIOTHERAPY. COULD IT BE RELATED TO SUBACUTE DEMYELINATING PROCESSES? CASE REPORT

MUHAMMED FATİH GOC[1], EZEL YALTIRIK BILGIN[1], OZKAN UNAL[2]
[1]SBU ANKARA ONCOLOGY TRAINING AND RESEARCH HOSPITAL, ANKARA, Turkey. [2]SBU ANKARA ONCOLOGY TRAINING AND RESEARCH HOSPI, ANKARA, Turkey

Demyelination is a very rare subacute complication of radiation therapy and is important to distinguish from tumor progression due to implications on management.(1-2-3)In our case, corticospinal tract lesions occurred subacutely in lower isodose zones ranging from 10-30 Gy,8 weeks after completing radiation.Demyelination went on progressively in distal pyramidal tracts on follow-up MR diffusion images.

Case Report: A 67-year-old female patient who was operated on with the preliminary diagnosis of who grade 2

diffuse astrocytoma in the left temporal lobe.[Fig 1.A and 1.B]No definitive diagnosis was made in the postoperative pathology report. After the operation,10 fractions of 30 gy radiotherapy was applied.Left leg and arm weakness occured during the treatment.In the MRI examination taken 8 weeks after the completion of the radiotherapy treatment,diffusion restriction in the left corticospinal tract is detected.Diffusion restriction went on propressively in distal pyramidal tracts on follow-up MR diffusion images.Diffusion restriction was observed in the posterior leg of the capsule interna in the first examination,in the mesencephalon in the second examination,and in the bulbus in the third examination.[Fig 2]In addition,radiation necrosis and residual tumour are also observed in the patient.The diffusion restricting area in the pyramidal tract showed different characteristics with the remaining tumor tissue;eg low perfusion,no contrast enhancement and different T2W intensity.These features further supported radiation induced treatment changes consistent with demyelination.Her baseline imaging before starting radiation did not demonstrate any demyelinating lesions. The patient did not have typical findings of demyelinating disease e.g. optic neurit,transvers myelitis.Biopsy was not required because there were no tumor findings in the patient.

Discussion: Radiation therapy is a common treatment and prophylactic modality for brain tumors, however,can have detrimental effects on the central nervous system resulting in neurological complications.The response of cerebral tissue to radiation is dynamic,and extending beyond the targeted tumor volume and influencing neural structures directly or indirectly.(4-5)Radiation-induced demyelination may be the cause of early-delayed neurological symptoms that occur between two week and 3 to 4 months of RT.We saw it in our patient 8 weeks later.6-7 Mechanisms of the late effects of radiation necrosis include vascular damage,white matter injury,and coagulation necrosis.Demyelination,inflammation and breakdown of the blood-brain barrier are among the main neurotoxic effects 10 observed in primates, dogs, rats and mice brain exposed to radiation.There are limited data from clinical studies on radiation-induced changes of neuroanatomical.(8-9-10)

Although there was no tissue obtained to pathologically verify demyelination, the radiographic features coupled with the sustained neurologic and radiographic response to steroids strongly supported demyelination as the diagnosis. For patients with symptomatic lesions and imaging that is concerning for pseudoprogression or true tumor growth, or when imaging is not clear for an etiology, a representative biopsy can clarify the diagnosis and assist in management.12-13

The classically described risk factors associated with radiation relating to toxicity include radiation with greater than 2 Gy per fraction, total dose greater than 60 Gy, large volume of radiation, and hypofractionated course of radiation. Neurotoxicity is greatest after treatment with parallel-opposed radiotherapy fields encompassing the temporal lobes, brainstem, and central white matter of the brain. Additionally, older age and concomitant comorbidities including diabetes mellitus or cerebrovascular disease also increase the risk of radiation-induced injury. Lastly, concurrent chemotherapy used as a radiation sensitizer and tumor specific factors including Methylguanine-DNA-methyltransferase (MGMT) promoter methylation also increase the risk of radiation relating to toxicity.13-14

Although rare, radiation relating to demyelination is a potential complication in brain tumor patients. If the demyelination is asymptomatic and was diagnosed solely as an isolated radiographic finding, it can be monitored with surveillance imaging. However, if it causes neurologic symptoms, it can be successfully managed with steroids. Demyelination, albeit rare, should be on the differential diagnosis for new distant enhancing lesions with typical radiographic features following radiation in the primary brain tumor population, not to be mistaken for tumor progression.

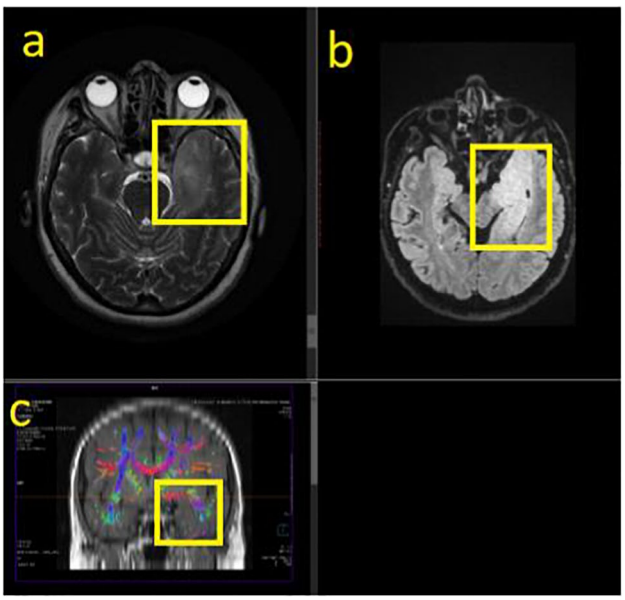

Figure 1a. 1b. The preliminary diagnosis of of who grade 2 diffuse astrocytoma in the lef temporal lobe.
Figure 1c. The mass pushed tracts aside.

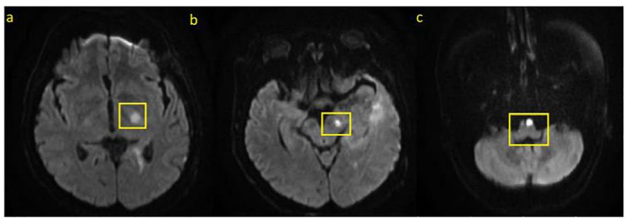

Figure 2a. First imaging performed 8 weeks after raiotherapy. Diffusion restriction in observed in the posterior leg of the capsula interna. There is no diffusion restriction in the mesencephalon and bulbus.
Figure 2b. Second imaging performed 16 weeks after raiotherapy. Diffusion restriction in the posterior leg of the capsule interna continues and new diffusion restriction is observed in the mesencephalon.
Figure 2c.Third imaging performed 24 weeks after raiotherapy. Diffusion restriction in the posterior leg of the capsule interna continues and mesencephalon, new diffusion restriction is observed in the bulbus.
As seen in these reviews demyelination went on propressively in distal pyramidal tracts on follow-up MR diffusion images.

1-P24
MOG-IGG-ASSOCIATED DISEASE: TWO PARANEOPLASTIC PRESENTATIONS

Henrique Queirós[1], Carolina Cunha[2], Inês Correia[2], Ricardo Veiga[1]
[1]Functional Area of Neuroradiology, Medical Imaging Department, Centro Hospitalar e Universitário de Coimbra, Coimbra, Portugal. [2]Neurology Department, Centro Hospitalar e Universitário de Coimbra, Coimbra, Portugal

Introduction: Myelin oligodendrocyte glycoprotein (MOG)-IgG-associated disease (MOGAD) represents a spectrum of inflammatory demyelinating disorders of the central nervous system with various phenotypes.

Methods: We present two cases of patients with paraneoplastic MOGAD and a brief literature review.

Results: Case 1: 56-year-old female with adenosquamous carcinoma of the lung, under Osimertinib, presented with visual loss and dyschromatopsia, fundoscopy revealed papilledema; MRI showed signal changes (mainly hyperintensity in T2/FLAIR) in the left half of optic chiasm, multiple lesions intracranially (left thalamus, pons, right middle cerebellar peduncle, both cerebellar hemispheres and vermis) and mild T2 hyperintensity in conus medullaris. Serum testing for MOG-IgG (1:100) was positive. Acute management with intravenous methylprednisolone, plasma exchange and intravenous immunoglobulin was highly effective.

Case 2: 43-year-old male with Hodgkin lymphoma, presented with leg monoparesis, dorsal level hypoesthesia, sphincter dysfunction and diplopia, four months after autologous hematopoietic stem cells transplantation. MRI showed T2 hyperintense lesions in mesencephalon bilaterally and mild medullary T2 hyperintensity longitudinally from D5 to D8. Serum testing for MOG-IgG (1:100) was positive. Acute management with intravenous methylprednisolone and posteriorly with intravenous immunoglobulin was highly effective.

Discussion: To this date, this is the first reported case of MOGAD coincident with Hodgkin lymphoma and the second with concomitant lung cancer.
The MRI lesions in MOGAD are usually larger, with scattered distribution, and found mainly in the pons, midbrain, grey matter, juxtacortical white matter and cerebellum, on both T2 and FLAIR images.
Disappearance or significant improvement of the lesions on follow-up MRI is noted in most cases.

Conclusion: Although no single set of diagnostic criteria is universally accepted, we want to draw attention to clinical, radiologic and immunological findings that may help physicians in diagnosing and managing MOGAD as a potential paraneoplastic manifestation.

Keywords: Myelin oligodendrocyte glycoprotein (MOG) antibody; MOG-IgG-associated disease; Lung cancer; Hodgkin lymphoma; Malignancy

1-P25
MAGNETIC RESONANCE IMAGES ASSESSMENT OF GRAY MATTER VOLUME AND CORTICAL THICKNESS REDUCTION IN NEUROMYELITIS OPTICA SPECTRUM DISORDERS ASSOCIATED WITH COGNITIVE IMPAIRMENT

Jitsupa Wongsripuemtet[1], Tharinee Sirithanasart[1], Chanon Ngamsombat[1]
[1]Radiology Department, Siriraj Hospital, Mahidol University, Bangkok, Thailand

Background: In neuromyelitis optica spectrum disorders (NMOSD), inflammation and neurodegeneration are important pathological processes of accumulation of disability and cognitive impairment but the study of regional grey matter involvement and its relationship with cognitive function in patients with Neuromyelitis optica spectrum disorder (NMOSD) remains scant and unclear.

Objective: To compare grey matter volume and cortical thickness between cognitively impaired and cognitively preserved NMOSD patients, as well as healthy controls by

using brain magnetic resonance imaging (MRI) data and to relate these imaging changes to cognitive function.

Materials and methods: This retrospective imaging study of 66 NMOSD patients (37 with cognitive impairment [CI] and 29 with preserved cognition [CP]) and 66 healthy controls (HCs) was conducted from October 2017 to October 2020 at Siriraj hospital. High-resolution 3D T1-weighted MRI gray matter volume and cortical thickness were evaluated in each clinical group.

Results: Results show a widespread reduction of gray matter volume and cortical thickness in NMOSD patients as compared with HCs and more extension of areas of brain involvement in NMOSD with CI. The areas of significantly decreased gray matter volume and cortical thickness were demonstrated at cortices of bilateral cerebral hemispheres, more pronounced at frontal lobes, temporal lobes, cingulate gyrus, and deep gray nuclei. NMOSD with CI showed a significantly greater reduction of gray matter volume over the right thalamic region in comparison with NMOSD with CP ($p = 0.037$), whereas no significant difference in the cortical grey matter was found between the two subgroups of NMOSD patients. Moreover, pronounced reduction of grey matter thickness was only significant in the right lateral occipitotemporal gyrus between both subgroups of NMOSD patients.

Conclusion: Widespread gray matter volume and cortical thickness reduction were found and more severe in patients with NMOSD with CI. Significant right thalamic volume reduction was displayed in NMOSD with CI when compared with the CP subgroup.

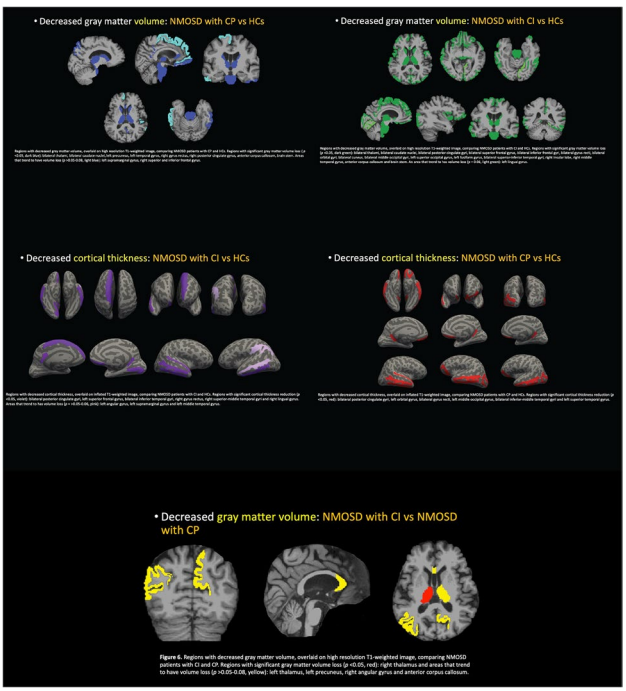

1-P26

EXPANDING THE CLINICAL-RADIOLOGICAL SPECTRUM OF MOG ANTIBODY-ASSOCIATED DISEASE

Liliana Igreja[1], João Moura[2], Eduarda Pinto[1], José Sá Silva[1], Vasco Sousa Abreu[1], João Tarrio[1,3], Raquel Samões[2,4], Sónia Figueiroa[5], Ana Martins da Silva[2,4], Sofia Pina[1], Ernestina Santos[2,4]

[1]Department of Neuroradiology, Centro Hospitalar Universitário do Porto, Porto, Portugal. [2]Department of Neurology, Centro Hospitalar Universitário do Porto, Porto, Portugal. [3]Hospital Central do Funchal, Funchal, Portugal. [4]Unit for Multidisciplinary Research in Biomedicine (UMIB), Instituto de Ciências Biomédicas de Abel Salazar (ICBAS), Universidade do Porto, Porto, Portugal. [5]Department of Pediatric Neurology, Centro Materno Infantil do Norte/Centro Hospitalar Universitário do Porto, Porto, Portugal

Introduction: Myelin oligodendrocyte glycoprotein antibody-associated disorder (MOGAD) is a novel CNS demyelinating disease with distinctive features from other immune-mediated neurological conditions. Knowledge on its clinical and neuroimaging profile has been expanding. Our goal was to characterize the imagiological features of the MOGAD cohort from a tertiary referral center.

Methods: We retrospectively analyzed a group of 20 MOGAD patients followed in our center. Demographic, clinical and neuroimaging investigation data were collected.

Results: We identified 20 patients with clinically suspected CNS demyelination and positive anti-MOG IgG antibodies, 55% females, 40% had the first outbreak between 40-59 years-old and 30% had pediatric-onset. Mean age at diagnosis was 48 (IQR) years old. The most frequent presenting clinical syndromes included myelitis in pediatric-onset disease (67%) and optic neuritis (50%) in the adult-onset subgroup. From 11 patients with ON involvement, 27% presented with bilateral affection and 27% showed involvement restricted to the anterior segment of the ON.

From all the supratentorial lesions, white matter T2/T2-FLAIR hyperintensities were the most common findings, 50% periventricular and/or subcortical with frontal predominance. The thalamus (25%) and brainstem (40%) were also frequently involved. Spine MRI revealed LETM in 35%, with patchy signal abnormalities typically involving central areas. Enhancement was observed in 30% of the myelitis attacks.

A multiphasic course was present in 55%, with a median number of events of 3 (2–5). Eight patients were on maintenance immunosuppressive treatment, with a current median follow-up of 6 years (IQR).

Discussion: Our findings of deep grey matter affection and frequent brainstem lesions were in agreement with the current literature on MOGAD patterns. There were no small children in our cohort which explains the absence of ADEM-like phenotypes.
Periorbital enhancement of the ON was only found in 1 patient which may be related to the timing when the MRI was performed.
Spinal cord lesions were typically dorsal affecting mainly the grey matter. Follow-up imaging revealed spine atrophy in one patient.
The MRI findings fulfilled the McDonald's 2010 dissemination in space criteria in 45%, highlighting the challenge differentiating this condition from other demyelinating diseases.

Conclusion: The clinical-radiological phenotypes of MOGAD show overlapping features with MS and NMOSD with anti-AQP4 antibodies. Neuroimaging features can be sufficiently suggestive to fit in a described pattern but can also be highly unspecific. However, they can have diagnostic and prognostic implications, since MOGAD generally responds well to immunotherapy and has a good functional prognosis.

CLINICAL FEATURES	FREQUENCY
AGE DISTRIBUTION OF SYMPTOMS ONSET	
○ 12-18 years-old	6/20 (30%)
○ 18-39 years-old	3/20 (15%)
○ 40-59 years-old	8/20 (40%)
○ >60 years-old	3/20 (15%)
ONSET NEUROLOGICAL SYNDROME	
Isolated Optic Neuritis	6/20 (30%)
Isolated Myelitis	10/20 (50%)
Optic Neuritis + Myelitis	3/20 (15%)
Brainstem Syndrome	1/20 (5%)
TREATMENT	
Steroids	20/20 (100%)
Plasma exchange	2/20 (10%)
Intravenous immunoglobulins	1/20 (5%)
Azathioprine	7/20 (35%)
Rituximab	1/20 (5%)
RELAPSES	11/20 (55%)
NUMBER OF RELAPSE-EVENTS	
○ 2	4/11
○ 3	5/11
○ 4	1/11
○ 5	1/11
OLIGOCLONAL BANDS IN CSF	3/20 (15%)
MEDIAN FOLLOW-UP	6 YEARS
OTHER AUTOIMMUNE DISEASES	2/20 (10%)

Table 1. Summary of the clinical features of the 20 patients of our cohort.

NEUROIMAGING FINDINGS	FREQUENCY
OPTIC NEURITIS	11/20 (55%)
Unilateral	8/11
Bilateral	3/11
+ Optic Chiasm Involvement	2/11
○ Anterior Segment of ON	3/11
○ Posterior Segment ON	2/11
○ Longitudinally Affected ON	6/11
• Atrophy	7/11
• Enhancement	1/11
SUPRATENTORIAL LESIONS	14/20 (70%)
Juxtacortical	3/20
Lateral periventricular	10/20
Subcortical white matter	11/20
Internal capsules	2/20
Thalamus	5/20
Basal Ganglia	2/20
Corpus Callosum	3/20
• Enhancement	3/20
• Restricted Diffusion	1/20
Absent	6/20
INFRATENTORIAL LESIONS	9/20 (45%)
Brainstem	8/20
Pons	7/8
Cerebellum	2/20
Middle cerebellar peduncles	3/20
• Enhancement	1/20
• Restricted Diffusion	1/20
Absent	11/20
MYELITIS	10/20 (50%)
LETM	7/10 (70%)
STM	3/10 (30%)
○ Cervical Spine	4/10
○ Dorsal Spine	6/10
○ Entire length of the spine	2/10
• Atrophy	1/10
• Enhancement	3/10

Table 2. Summary of the imaging findings in the investigation of the 20 patients of our cohort.
LETM, longitudinal extensive transverse myelitis; ON, optic nerve; STM, short-segment transverse myelitis;

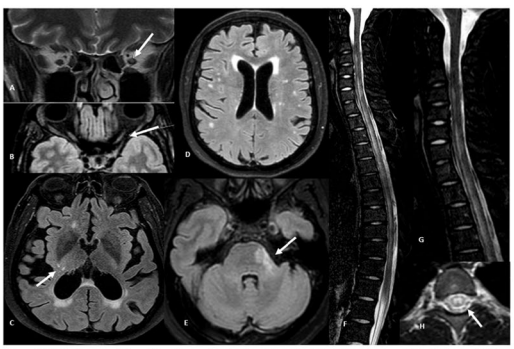

Figure 1. (A) Brain coronal T2 weighted image showing hyperintensity of the left optic nerve (ON). (B) Brain axial T2-FLAIR demonstrating atrophy of the anterior segment of the left ON. (C-E) Brain axial T2-FLAIR hyperintensities involving the right thalamus and internal capsule (C), the bilateral subcortical and periventricular white matter (D), as well as the protuberance and left middle cerebellar peduncle (E), in three patients. (F and G) Spine sagittal STIR showing longitudinal extensive patchy lesion spaning from cervical to thoracic cord. (H) Spine axial T2 with hyperintense "H" sign outlining the central gray matter of the spinal cord.

1-P27

CENTRAL NERVOUS SYSTEM MANIFESTATIONS OF ERDHEIM - CHESTER DISEASE. MRI FINDINGS

Zoe Papoutsou[1], Christina Aslanidi[1], Sofia Athanasiou[1], Stavroula Lyra[1], Vasileios Varsos[1], Antonios Tsanis[1]
[1]Athens General Hospital "Korgialenio-Benakio" H.R.C., Athens, Greece

Introduction: Erdheim-Chester disease (ECD) is a non-familial, multisystemic disease that belongs to the non-Langerhans histiocytoses. Patients present with non-specific symptoms, and the clinical course may vary from mild to a life-threatening disease, depending on the site and extent of involvement. The central nervous system (CNS) is involved, in approximately 30% of cases, with endocrine dysfunction being the most common neurological manifestation. The purpose of this poster is to discuss the spectrum of CNS manifestations of ECD and their key imaging findings.

Findings: The most affected intracranial location is the hypothalamic-pituitary axis with thickening of the infundibulum or an enhancing suprasellar mass with high T2 signal intensity on MR imaging. The mass may extend to the hypothalamus or cavernous sinus. The posterior pituitary bright spot on T1-weighted images may be absent. Supratentorial extra-axial lesions are also common in histiocytoses and include pachymeningeal thickening or dural-based masses hypo- or isointense on T1 and T2- weighted images with marked contrast enhancement. Supratentorial intra-axial lesions are not common but periventricular and basal ganglia T2-hyperintense areas or ependymal enhancement in the lateral ventricles have been reported in the literature. Involvement of the cerebellum (dentate nucleus) or the pons is depicted as high T2 signal intensity (Fig. 1a) with no mass effect and with (Fig.1b) or without contrast enhancement. Lesions of the spinal column may be extradural lesions or intramedullary with single or multiple T2 hyperintense areas. The orbits may also be affected with low T1 and T2 signal intensity retro-orbital lesions that may exhibit a mass effect on the optic nerve. Lesions of the maxillofacial bones and the skull include bilateral thickening of the paranasal sinuses' walls or the skull with a hypointense signal on T1 and T2 weighted images. Polypoid thickening or soft-tissue opacification of the paranasal sinuses is also reported in the literature.

Conclusion: The diagnosis of ECD is based on clinical, imaging, and histopathological findings. Knowledge of the diverse clinical and imaging findings of ECD by the radiologist is necessary to include it in the differential diagnosis. This will lead to a further pathological investigation for the appropriate markers, essential to make the correct diagnosis and guide therapeutic treatment.

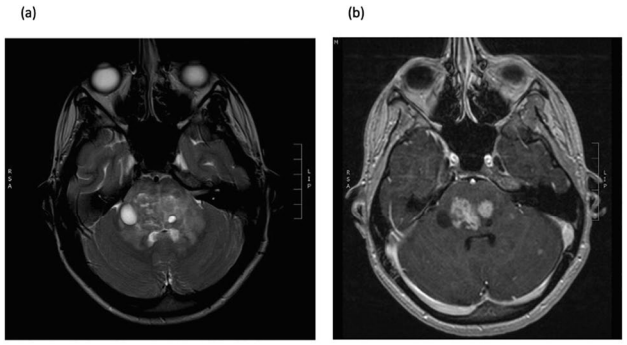

Figure 1. MR images of a patient with ECD and infratentorial involvement depict high signal intensity on T2-weighted images with small cystic components (a) and heterogeneous enhancement on contrast-enhanced T1 weighted images (b).

1-P28

IMAGING REVIEW OF AUTOIMMUNE ENCEPHALITIS: OVERLOOKED DIAGNOSIS

Laila Zitan Saidi[1], Jesus Prieto Casado[1]
[1]Torrecardenas University Hospital, Almeria, Spain

Keywords: Autoimmune encephalitis, Central nervous system, Limbic encephalitis, MRI

Introduction: Autoimmune encephalitis (AE) refers to a group of immune-mediated disorders that involve the central nervous system (CNS). Alteration of mood, behavior, and memory, decreased level of consciousness, and seizures occur in most types of AE. It occurs most often in young adults. Several paraneoplastic associations have been made and more recently patients with AE after viral infections have been reported.
The purpose of this review is:
To understand the many signs, symptoms and types of AE .
To review the main antibodies that have been identified and their patterns of CNS involvement and their typical anatomical distributions due to relative concentration of target proteins
To highlight the characteristic MR imaging findings associated with AE, with a specific emphasis on the role of neuroimaging in the diagnostic work-up.
To describe a case of AE associated with Covid 19.

Methods: In this review based on cases from our database, we expose the radiological manifestations of the various types of AE. All the cases were confirmed by detection in serum or CSF of specific antineuronal antibodies and each patient received treatment based on high doses of steroids and immunoglobulins, with a favorable clinical course.

Discussion and results: Antibody-associated disorders of the CNS are generally divided into two groups. The first group includes the classic paraneoplastic disorders in which there is a systemic anti-tumoral immune response against intracellular antigens by both B and T cells. The second group is characterized by formation of auto-antibodies which are primarily pathogenic. These antibodies target cell surface proteins, ion channels, or receptors. There is a third group which represents diseases caused by auto-antibodies to intracellular synaptic proteins
Common radiological features of limbic AE are:
Hyperintense signal involving the mesial temporal lobes on T2 weighted and FLAIR imaging,
A normal initial study is presented in 20-40% of patients.
The most common locations of AE lesions are the hippocampus, amygdala, cingulate gyrus, piriform cortex, subfrontal cortex, and insula.
In addition to the common characteristics, we have to know the most specific findings of each of the types of AE.

Conclusions: Due to its growing prevalence, autoimmune encephalitis should always be considered in an acute conduct disorder, decreased level of consciousness or cognitive dysfunction, especially in young patients. To know the imaging findings of AE is important to an early diagnosis and timely treatment that contributes to a favorable evolution of patients.

A 34-year-old female was admitted in the emergency department with generalized tonic-clonic seizure and behavioral disorders. A brain MRI showed FLAIR bilateral hyperintensities in mesial temporal lobes, bilateral hippocampi, right insula and caudate, as well as bilateral frontal hyperintensities. The images were consistent with limbic encephalitis. (figure 1)

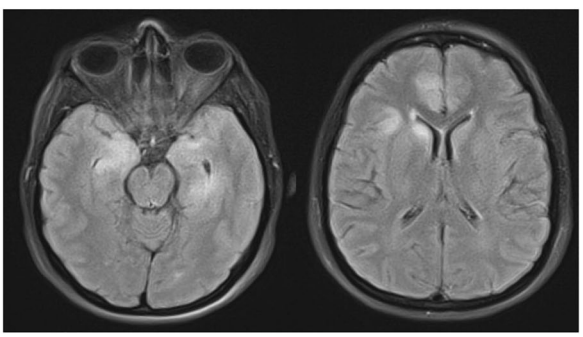

INFECTIOUS

1-P29

MACROSTRUCTURAL CHANGES IN COVID-19: RESULTS FROM A RETROSPECTIVE MR-NEUROIMAGING COHORT

Dariya Dryga[1,2], Tetiana Babkina[1]
[1]Shupik National Healthcare University of Ukraine, Kyiv, Ukraine. [2]"Dobrobut" medical care, Kyiv, Ukraine

We aimed to report on the frequency and type of neuroradiological findings in COVID-19 using MRI.

COVID-19 has multisystemic involvement due to the virus binding to the cellular receptor for angiotensin-converting enzyme 2 (ACE2), which is found in multiple cells of the human body, including neuronal cells. The virus accesses neuronal cells by a retrograde neuronal pathway or hematogenous dissemination, which explains the neurological symptoms: disturbed consciousness, paresthesia, anosmia, and headache. From August 2020 to March 2022, 126 brain MRI-studies was performed on the Siemens Magnetom Solo 1,5 T using standard clinical coilswere for SARS-CoV-2-positive patients (confirmed by RT-PCR test)
A total of 126 patients were included in the study and the mean age was 53±17,5 years; 56% of the patients were male.
- 58 patients(46%) had cerebral disorders, other 68(34%) had no visible structural changes.
- 30 out of patients (51,7%)were having an acute brain insult, 24(44,8%) of them had ischemic insult and 6(6,9%) patients had hemorrhagic insult.
- 24(41,3%) patients had microbleeds, SWI sequence was helpful.
- 3(5,1%) patients presented with venous thrombosis.
- 1(1,7%) patient had abnormal signal intensity in the olfactory bulbs and findings consistent with hypoxic-ischemic encephalopathy.

Conclusion: In hospitalized adults with COVID-19 undergoing MR-neuroimaging, vascular and inflammatory changes are common.
The most popular complication is brain insult (51,7%), the incidence of ishemic/haemorrhagic insult tends to 4\1.More than 1\3 of patients (41,3%) had microbleeds. Venous thrombosis(5,1%) and damage of olfactory bulbs (1,7%) are less common.

1-P30

MR ASSESSMENT OF BRAIN ALTERATIONS IN POST-COVID COGNITIVE SYNDROME

Miguel Yus-Fuertes[1,2], María Díez-Cirarda[3,2], Jordi A Matias-Guiu[3,2], Lidia Gil-Martinez[1,2], Natividad Gomez-Ruiz[1,2], Carmen Polidura-Arruga[1,2], Cristina Delgado-Alonso[3,2], Ulises Gomez-Pinedo[3,2], Manuela Jorquera-Moya[1,2], Jorge Matias-Guiu[3,2], Juan Arrazola-Garcia[1,2]
[1]Department of Radiology. Hospital Clínico San Carlos, Madrid, Spain. [2]Health Research Institute "San Carlos" (IdISCC). Universidad Complutense de Madrid, Madrid, Spain. [3]Deparment of Neurology. Hospital Clínico San Carlos, Madrid, Spain

Introduction: Brain alterations have been reported in post-acute phase in patients after SARS-Cov-2 infection. However, limited literature exists about brain alterations in post-COVID syndrome after several months from the acute phase. We aimed to investigate the brain structural and functional changes in post-COVID cognitive syndrome.

Methods: 86 patients with subjective cognitive complaints and 36 healthy controls were enrolled and studied under a protocol approved by the hospital ethics committee. Patients were scanned using a 3.0T Magnet (GE Signa Architect) and a 48-channel head coil. 3D T1-weighted images, T2 FLAIR, diffusion tensor images and resting-state fMRI were acquired in a single session. In addition, participants underwent a comprehensive cognitive assessment. Neuroimaging analyses were carried out in SPM12 for grey matter volume analysis, white matter integrity was evaluated in FSL and functional connectivity in CONN toolbox.

Results: Patients with post-COVID cognitive syndrome showed reduced grey matter in cerebellar, limbic and cortical areas, including frontal, temporal, parietal and occipital areas compared to controls. White matter alterations were also found, showing post-COVID syndrome patients reduced axial and medial diffusivity in the callosal body, fornix minor, bilateral uncinate fasciculus, bilateral superior longitudinal fasciculus, and bilateral inferior fronto-occipital fasciculus compared to the healthy control group. Patients showed functional connectivity alterations, both hyperconnectivity, and hypoconnectivity. Grey matter volume loss showed significant associations with cognitive dysfunction, mostly between the parahippocampal area and attention and working memory deficit (Figure 1).

Discussion & Conclusion: Patients with post-COVID syndrome showed reduced grey matter volume that was accompanied with reduced widespread diffusivity and functional connectivity alterations. These changes showed associations with cognitive dysfunction. Findings help in the better understating of the pathophysiology of post-COVID syndrome.

Keywords: Post-COVID syndrome; Brain alterations; MRI; rs-fMRI

Figure 1: Brain alterations in post-COVID syndrome compared to controls

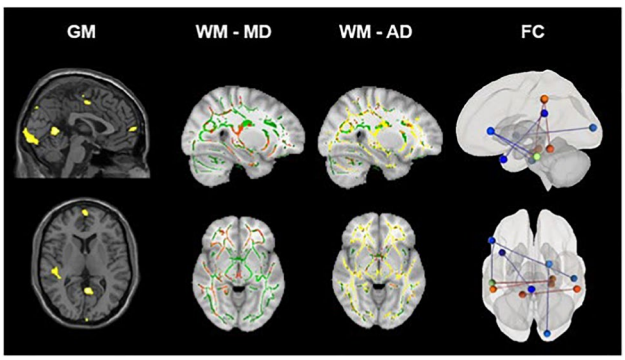

1-P31

RECURRENT HYPERTROPHIC PACHYMENINGITIS – A MANIFESTATION OF MYCOBACTERIUM LENTIFLAVUM CNS INFECTION

Diogo Marques[1], Filipa Castelão[1], Francisca Batista[1], Ricardo Silva[1], Cristina Rios[1]
[1]Hospital Garcia de Orta, Almada, Portugal

Introduction: Idiopathic hypertrophic cranial pachymeningitis is a rare inflammatory disease which the definitive diagnosis is difficult to establish.

Clinical Case: A 8 year old male patient, diagnosed with Global Development Delay and Attention Deficit Hyperactivity Disorder (in probable relation with duplication of chromosome 6p), who presented subacute onset of recurrent bilateral frontal headache, associated with occasional vomiting and bilateral hypoacusis. Physical examination at admition describes right palpebral ptosis, limitation of right globe abduction, reduced visual acuity in the right eye with homolateral impairment of direct fotomotor reflex and neck stiffness.

The MRI showed hypersinal T2/STIR with intense contrast enhancement of right medial rectus muscle and optic nerve, as well as posterior extension to the lateral wall of cavernous sinus and anterior wall of middle cranial fossa. It was identified the presence of oligoclonal bands on CSF. Corticotherapy was maintained for two months, with clinical relapse after withdrawn.

On the follow up MRI, there was resolution of intra-orbital findings with lateral and posterior extension of the pachymeningitis previously documented. The meningeal biopsy showed granulomatous infiltration suggestive of mycobacterial infection; the blood and CSF cultures were negative. Six month after, there was escalation of the imagiological findings.

A 6-month antimycobacterial treatment was initiated, without clinical-imagiological response.

In the fifth year follow up MRI, there was some mild imagiological fluctuation that motivated the chronic use of imunossupressant therapy. However, due to erroneous therapy compliance and concurrent symptomatic improvement, the medication was suspended. The CSF evaluation was repeated, and identified the presence of Mycobacterium lentiflavum. Antimycobacterial therapy was restarted and maintained for 1 year, with no signs of progression on the imaging follow up.

Conclusion: The present case intends to demonstrate the complexity and difficulty in obtain a definite diagnosis in patients with recurrent hypertrophic pachymeningitis.

1-P32

MRI IN CEREBELLAR SCHISTOSOMIASIS: A CASE REPORT

Marina Fick[1], Viviana Loureiro[2], Iandra Pacheco[1], Samuel Pereira[1]
[1]Federal University of Viçosa, Viçosa-MG, Brazil. [2]Hospital Israelita Albert Einstein, São Paulo-SP, Brazil

Introduction: Schistosomiasis is an endemic infection found in tropical countries [1]. It is caused by worms of the genus *Schistosoma* that affects mainly liver and intestine and can occasionally reach the central nervous system (CNS) [2]. According to the WHO, more than 700 million people live in endemic areas [3] and approximately 258 million were infected in 2014 [4]. Despite these numbers, cases of neuroimaging with cerebellar involvement by the parasite are rare. It is estimated that the present report is the fifth in literature to demonstrate this disorder caused by *S. mansoni* by magnetic resonance imaging (MRI).

Case: A 21 years old male, with a headache for 60 days, presented nystagmus and ataxia at physical examination. His first cranial MRI (**Figure 1**) showed edema of the right white cerebellar substance with an expansive effect. After gadolinium injection, micronodular leptomeningeal enhancement was noted in the sulcus of the vermis and right cerebellar hemisphere. The radiological aspect considered neurossarcoidosis, requiring further investigation.

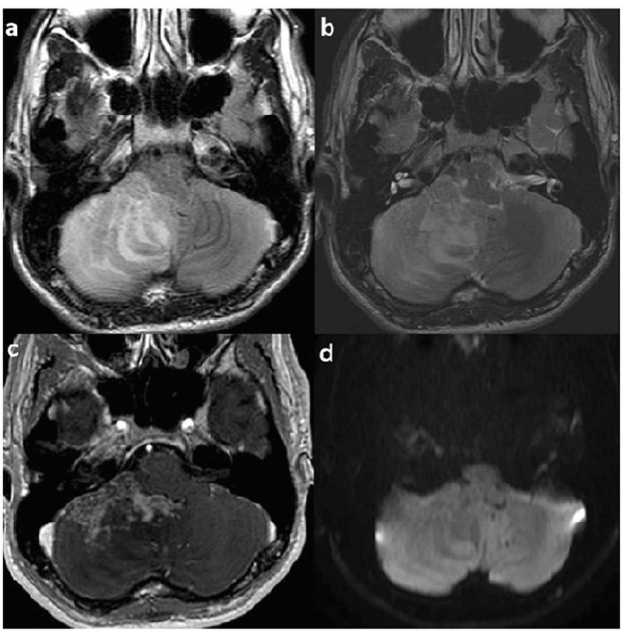

Fig. 1 - Cranial MRI, axial sections, T2-weighted (a) and FLAIR (b) showing hypersignal in the right cerebellum; contrast-enhanced T1-weighted (c) showing micronodular leptomeningeal enhancement in the sulcus between the

folium of vermis and right cerebellar hemisphere; DWI sequence (d) unrestricted

The histopathological study evidenced epithelioid granulomas, viable and degenerate eggs of *Schistosoma mansoni*, coexisting lymphoplasmocytic inflammatory infiltrate. Schistosomal Granulomatous Cerebellitis was diagnosed. After 6 months of treatment, a new cranial MRI was performed (**Figure 2**). It was observed a reduction of edema, absence of postcontrast meningeal enhancement and a remaining hypotrophy and gliosis of the right cerebellar hemisphere and peduncle.

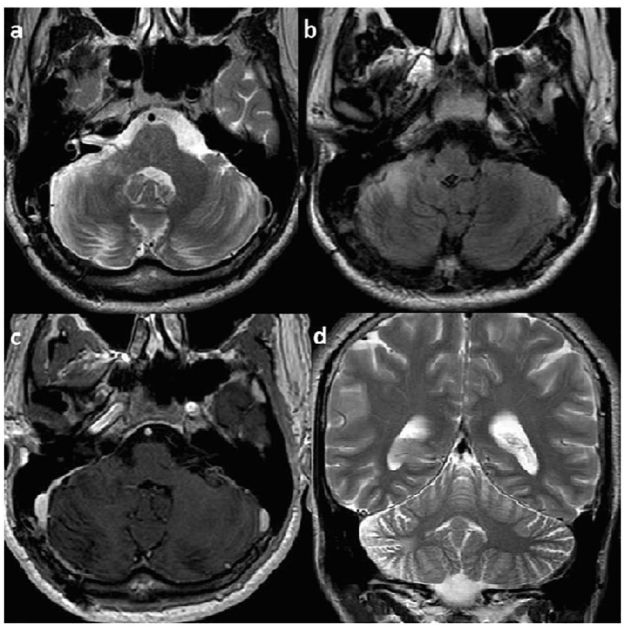

Fig. 2 - Cranial MRI, axial sections, T2-weighted (a) and FLAIR (b) showing hypersignal in the anterior region of the right cerebellar hemisphere; contrast-enhanced T1-weighted image (c) without enhancement; coronal T2-weighted section (d) showing hypotrophy of the right cerebellum

Discussion: It is estimated that up to 30% of those infected by *S. mansoni* may have CNS injury [5,2]. However, exact details on cerebellar involvement are scarce, supposedly justified by low diagnostic suspicion. Recognizing an image pattern like this can help potentiate diagnosis, direct treatment and avoid unnecessary surgery.

Conclusion: Considering the large number of infected and so that other cases do not go unnoticed, it is necessary to disclose this form of involvement and insert it as a differential diagnosis in etiologies with cerebellar manifestations, either in endemic regions or where there is import of cases.

1-P33

NEUROIMAGING IN SARS-COV-2 INFECTION

Umberto Rozzanigo[1]
[1]Ospedale Santa Chiara, Trento, Italy

Objectives: Discuss the pathogenetic mechanisms underlying the damage to the nervous system. Illustrate the CT and MRI imaging patterns more frequently noticed during the acute-subacute phase in hospitalized patients. Identify chronic brain outcomes attributable to Coronavirus disease in long-Covid follow-up.

Introduction: Covid-19 patients are often suffering from neurological disorders, but imaging in acute phase is performed only in a minority of cases, due to the need for isolation: plain CT is the first examination, in some cases associated with CT-Angiography, while MRI is reserved for the most severe cases. During follow-up can be difficult to relate the neuroradiological findings to the previous COVID-19 infection, being the majority of MRI examinations performed for long-Covid negative or non-specific.

Discussion: The main pathogenetic mechanisms are three: 1) Direct damage of the virus to the CNS 2) Post-infectious autoimmunity phenomena 3) Complications of hypoxia, anticoagulants or others treatments (drugs, dialysis ...). Vascular complications, mostly ischemic and to a lesser extent haemorrhagic, are identified with brain CT and CT-angiography examinations and prevail in the acute-subacute phase. MRI may show reversible white matter changes, encephalo-myelitis or CNS vasculitis-like patterns if performed early in the symptomatic patient. In the chronic phase MRI may show post-inflammatory demyelinating changes, microhemorrhagic pattern with peculiar involvement of the corpus callosum in severe ARDS patients or diffuse white matter gliosis similar to delayed post-hypoxic leucoencephalopathy (DPHL) in intensive care unit ventilated patients.

Conclusions: The neuroradiologist must learn to recognize the typical imaging pictures of SARS-CoV-2 infection both in hospitalized patients and during follow-up.

TUMORAL

1-P34
LONG-TERM EPILEPSY-ASSOCIATED TUMORS

Maria Inês de Sá[1], Guilherme Matins[1], Joana Freitas[1], Ângelo Dias[1], Carlos Morgado[1]
[1]Hospital de Santa Maria, Centro Hospitalar Universitário Lisboa Norte, Lisboa, Portugal

Introduction: Long-term epilepsy-associated tumors (LEATs) are the second most common cause of drug-resistant epilepsy, following focal cortical dysplasia in children and hippocampal sclerosis in adults. These tumors are mostly benign, with neocortical and temporal lobe localization and occur mostly in children and young adults. LEATs are primarily associated with medically refractory epilepsy, therefore, in many cases, epilepsy surgery is the ideal treatment, and, in most cases, it has a good response.

Methods: We retrospectively collected and analyzed data from patients submitted to resective epilepsy surgery with histopathological diagnosis of some type of LEATs, dating from 1992 until the start of 2021. Those patients belong to the reference center for epilepsy surgery of Centro Hospitalar Universitário Lisboa Norte (CHULN), the GCE-HSM (epilepsy surgery group from Hospital Santa Maria). The variables analyzed were age group, gender, median age of onset of seizures, median age at the time of surgery and type of tumor. A pictorial review of the most common finding LEATs was also performed, illustrating their most typical imaging presentation.

Results: From a total of 260 patients submitted to resective surgery, 49 (18.8%) had histological diagnosis of some type of LEATs. Of these, 10 (20.4%) were children and 39 (79.6%) were adults, 28 (51.1%) were male and the remaining 21 (42.9%) were female. The median age of onset of seizures was 14.0 (IQR 20.3, mean of 19.0) and the median age at the time of surgery was 34.0 (IQR 28, mean of 34.2). The most frequent type of tumor in our series was the Dysembryoplastic neuroepithelial tumor (DNET) which accounted for 36.7%, followed by Gangliogliomas (14.3%) and Pilocytic astrocytomas (12.2%). We also had cases of Gangliocytomas and Pleomorphic xanthoastrocytomas.

Conclusion: Ganglioglioma is described to be the most common LEATs. In our analysis, Ganglioglioma was the second most common, following DNET. Long-term epilepsy-associated tumors are the second most common cause of drug-resistant epilepsy. knowing the different types of LEATs and understanding their differences in imaging, is crucial for diagnosis and therefore the correct treatment.

1-P35
PRIMARY CENTRAL NERVOUS SYSTEM LYMPHOMA SHOWING "LYMPHOMATOSIS CEREBRI" PATTERN: AN UNCOMMON CAUSE OF DIFFUSE WHITE MATTER SIGNAL ABNORMALITY

Gonçalo Borges de Almeida[1], Rui Carvalho[1]
[1]Department of Neuroradiology, Centro Hospitalar e Universitário de Lisboa Central, Lisbon, Portugal

Introduction: Primary Central Nervous System Lymphoma (PCNSL) is a rare and aggressive type of extranodal non-Hodgkin lymphoma, accounting for approximately 2% of all Central Nervous System (CNS) tumors. About 95% of all PCNSL are diffuse large B-cell lymphomas (DLBCL), which usually present as a solitary focal space-occupying mass lesion with predilection for the periventricular white matter. Nonetheless, PCNSL may rarely show diffuse infiltrative lesions, an imaging pattern which has been termed "Lymphomatosis Cerebri" (LC).

Methods: We report the case of an adult male patient with histologically-proven DLBCL and LC pattern on Magnetic Resonance Imaging (MRI) of the brain.

Results: A 58 year-old male patient with unremarkable medical history was brought to our hospital due to transient loss of consciousness following head trauma. Neurological examination revealed left lower limb paresis. A Computed Tomography (CT) scan of the brain did not show traumatic lesions, although a hypodense subcortical lesion was seen on the left superior frontal gyrus. A subsequent MRI of the brain revealed a total of 3 subcortical T2/FLAIR hyperintense lesions in both superior frontal gyrus and in the right internal parietal lobe, with mild linear and punctate enhancement of both lesions in the right cerebral hemisphere. None of the lesions caused visible mass effect.
Due to suspicion of vasculitis, an extensive laboratorial work-up was performed but did not support an underlying autoimmune, infectious or paraneoplastic etiology. One month later, a control MRI showed slight increase of the aforementioned lesions and brain biopsy favored the diagnosis of vasculitis due to the presence of perivascular inflammatory infiltrates, although no abnormalities were present on cerebral Digital Subtraction Angiography (DSA).
Four months later the patient's motor impairment worsened and a new brain MRI revealed significant increase in the size of lesions, extending to the corpus callosum and cerebral cortex, as well as increased choline, decreased N-acetylaspartate (NAA) and presence of lactate peak on spectroscopy. Brain biopsy was repeated and showed significant B-cell infiltrates with CD20 and BCL2 immunoreactivity, consistent with DLBCL.

Discussion & Conclusion: LC is a rare imaging pattern seen in PCNSL with only a few dozen of cases reported in the literature. Since its imaging features are non-specific and may mimic other lesions of different etiologies, this case highlights the need to perform a complete work-up to reach the correct final diagnosis and initiate appropriate treatment.

1-P36

SEARCHING FOR A DIAGNOSTIC TOOL DERIVED FROM MRI PARAMETERS IN SOLITARY FOCAL CEREBRAL LESIONS DIFFERENTIATION (GLIOBLASTOMA MULTIFORME VS METASTASIS)

Fabio Marconi[1], Fabiola Cappella[2], Vittorio Marconi[3], Giorgio Robuffo[1], Serena Lisi[2], Serena Campa[1], Luana Regnicolo[4], Mauro Dobran[4], Gabriele Polonara[1]
[1]Radiology Department, Università Politecnica delle Marche, Ancona, Italy. [2]Neurosurgery Department, Università Politecnica delle Marche,, Ancona, Italy. [3]Centre of Epidemiology and Biostatistics,Università Politecnica delle Marche, Ancona, Italy. [4]Radiology Department, Ospedali Riuniti, Ancona, Italy

Scope: In patients over 50 without history of a neoplastic disease, a single cerebral lesion differential diagnosis could result in similar probability of being primary or metastatic in nature.
Our original work strived to find MRI quantitative parameters that could be helpful to differentiate Glioblastoma Multiforme (GBM) from solitary brain metastasis. We quantified total perilesional hyperintensity volume in T2w/FLAIR images and total volume of the lesion in post-gado T1w images. Then derived the ratio between these two parameters and explored its diagnostic value.

Materials and methods: In this single center study we retrospectively evaluated 101 MRI scans of patients without history of malignancy with a single cerebral lesion that subsequentially was histologically proven to be either Glioblastoma multiforme (GBM) or metastasis (M). Volumes of total T2w/FLAIR perilesional hyperintensity and total post gado T1w lesional volume were calculated by hand-drawing the contour of the pathologic signal, then the ratio R=Total hyperintensity in T2w/FLAIR / Total tumoral volume in post gado T1w was derived for each patient. Statistical analysis was conducted using "Mann-Whitney U test" to compare between non-parametric variables (average values). ROC curves were used to evaluate differential potential power of our test and finding area under the curve with its relative confidence interval and threshold of R.

Results: Mann-Whitney U test shows two statistically different distributions for GBM R value = 2.96 and metastasis R value = 4.52 with p=0.003. Area under the ROC curve = 0.669 (rang 0.563 -0.776) with threshold = 1.58.

Conclusion: Area under curve demonstrates a significant contribution to parameter "R=hyperintensity volume in T2w/FLAIR / Total tumoral volume in post-gado T1w" to differentiate solitary brain lesions in patients without history of malignancies. Even though its contribution to the diagnosis is weak if considered alone it could be an useful implementation in view of radiomics contribution in radiologic practice.

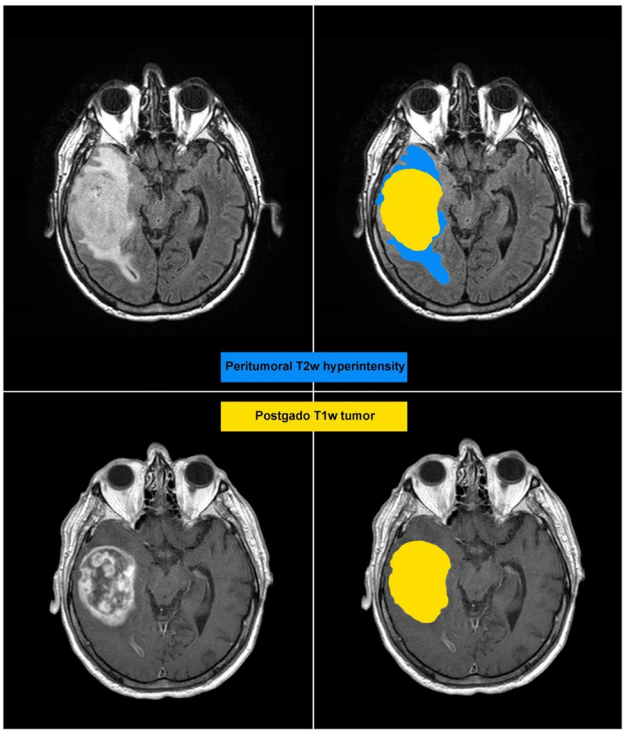

1-P37

BRAIN TUMORS AS INCIDENTAL FINDINGS IN PATIENTS WITH MULTIPLE SCLEROSIS

Manuela Vaneckova[1,2], Michaela Andelova[3,2], Tomas Uher[3,2], Dana Horakova[3,2], Eva Kubala Havrdova[3,2]
[1]Department of Radiology, General University Hospital, Prague, Czech Republic. [2]First Faculty of Medicine, Charles University, Prague, Czech Republic. [3]Department of Neurology, General University Hospital, Prague, Czech Republic

Introduction: Multiple sclerosis (MS) patients are usually annually monitored by MRI, to monitor disease activity such as new active lesions and brain atrophy. We investigated occurrence of brain tumors as a secondary finding in MS patients and how often they are missed by radiologists during MRI monitoring of MS.

Methods: We searched for patients with brain tumors, including meningeal and cranial nerve tumors, in a database of MRI monitored MS patients from January 2016 to April 2022 (4754 MS, 20993 scans). We also retrospectively reviewed previous MRI scans to assess whether tumors were evident before they were finally described by a radiologist. The MRI protocols used varied only minimally and always included FLAIR (mostly 3D FLAIR), 3D T1WI and DWI. A contrast agent was administered to 4 patients.

Results: We found 38 patients with 40 intracranial neoplasms (two patients had duplicity). The most frequent tumors were meningioma in 25 cases (62.5%), followed by 6 vestibular schwannomas (15%), 3 metastases (7.5%), 2 glioblastomas (5%), 1 oligoastrocytoma, 1 astrocytoma (grade II, recurrence 4 years after surgery when the tumor was grade IV) 1 hemangiopericytoma, and 1 primary CNS plasmacytoma. Only 15 tumors (27.5%) were not retrospectively visible on previous MRIs. The longest interval between tumor description on MRI and the first visible findings on MRI was 11 years (this was a very small meningioma of the falx).

Discussion: We identified the following main reasons for delays in tumor diagnostics.1) Focusing only on detection of MS activity. 2) An effect of previous incorrect MRI description. 3) Lower quality 1.5T MR images, mainly in 2D FLAIR in the infratentorial region; automatic co-registration and subtraction was not always available. 4) Tumor location- missed meningiomas in the vertex region. 5) Misinterpretation of findings - a patient with low grade glioma was initially described as an atypical tumefactive demyelinating lesion. 6) The MRI protocol was highly sensitive for MS, but not for other pathologies. 7) The radiologist noted suspected secondary pathology and requested a clinician's order for a new diagnostic MRI (sometimes involving delay). 8) Clinical symptoms possibly misinterpreted as symptoms of MS.

Conclusion: Intracranial tumors may occur without clinical presentation or be misinterpreted as MS symptoms and the radiologist should therefore be very careful when characterizing patients being monitored for MS and other neurological diseases. The use of automatic co-registration and subtraction methods may increase their early detection.

1-P38

SINGLE BRAIN METASTASIS VERSUS GLIOBLASTOMA MULTIFORME: A VOI-BASED MULTIPARAMETRIC ANALYSYS FOR DIFFERENTIAL DIAGNOSIS

Francesco Dellepiane[1], Andrea Romano[1], Giulia Moltoni[1], Serena Palizzi[1], Allegra Romano[1], Valentina Frezza[1], Guido Trasimeni[1], Alessandro Bozzao[1]
[1]La Sapienza University, Sant'Andrea Teaching Hospital, Rome, Italy

Purpose: The authors purpose was to create a valid multiparametric MRI model for the differential diagnosis between Glioblastoma and solitary Brain Metastasis.

Materials and methods: Forty-one patients (twenty glioblastomas and twenty-one brain metastases) were retrospectively evaluated. MRIs were analysed with Olea Sphere® 3.0. Lesions Volumes of interest (VOIs) were drawn on enhanced 3D T1 MP-RAGE, and projected on ADC and rCBV co-registered maps. Another 2 VOIs were drawn in the region of hyperintense cerebral oedema, surrounding the lesion, respectively within 5mm around the enhancing tumor and into residual oedema. Perfusion curves were obtained and the value of signal recovery (SR) was reported. A Two sample T-Test was obtained to compare all parameters of GB and BM groups. Receiver operating characteristics (ROC) analysis was performed.

Results: According to ROC analysis, the area under the curve was 88%, 78% and 74% respectively for mean ADC VOI-values of the solid component, the mean and max rCBV values in the perilesional edema and the PSR. The cumulative ROC curve of these parameters reached an area under the curve of 95%.Using perilesional max rCBV>1,37, PSR>75% and mean lesional ADC<1x10 -3 mm 2 s -1 GB could be differentiated from solitary BM (sensitivity and specificity of 95% and 86%).

Conclusion: Lower values of ADC in the enhancing tumor, a higher percentage of signal recovery in perfusion curves, and higher values of rCBV in the peritumoral edema closed to the lesion, are strongly indicative of GB than solitary BM.

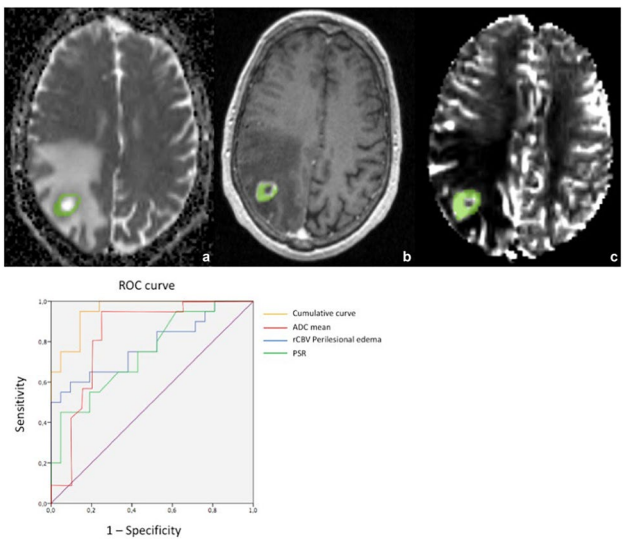

1-P39

INTRALABYRINTHINE SCHWANNOMA: AN UNCOMMON ENTITY

Inês Freire[1], Luís Baptista[2], Pedro Calvão Pires[1], Joana Barata Tavares[3], Pedro Vilela[3], Pedro Soares[1]
[1]Department of Neuroradiology, Centro Hospitalar Lisboa Ocidental – Hospital de Egas Moniz, Lisbon, Portugal. [2]Department of Otorhinolaryngology, Centro Hospitalar Lisboa Ocidental – Hospital de Egas Moniz, Lisbon, Portugal. [3]Department of Neuroradiology, Hospital da Luz – Clínica de Odivelas, Lisbon, Portugal

Keywords: intralabyrinthine schwannoma, intracochlear schwannoma, vestibulocochlear nerve

Introduction: Vestibulocochlear schwannoma is a benign nerve sheath tumor and is the most common neoplasm of the internal auditory canal (IAC) and cerebellopontine angle (CPA). These tumors most often arise from the vestibular division of the vestibulocochlear nerve. Intralabyrinthine schwannomas develop primarily from the terminal ends of the vestibulocochlear nerve within the membranous labyrinth: cochlea, vestibule, or semicircular canals.
An intracochlear schwannoma is the most frequent subtype of intralabyrinthine schwannomas that is exclusively confined to the cochlea. Based on their location, intralabyrinthine schwannomas can be further classified into intravestibular, intravestibulocochlear, transmodiolar, transmacular, tympanolabyrinthine, and transotic.
Their diagnosis is largely based on magnetic resonance imaging (MRI) and has been increasing together with the progress of imaging techniques and resolution.

Methods: The authors reviewed the MRI performed for hearing loss from January 2017 to May 2022 to depict the cases of intralabyrinthine schwannomas. Of all intralabyrinthine schwannomas, five were intracochlear and one was transmodiolar.
After bibliographic review, we focused mainly on their most frequent imaging findings on MRI.

Results: Magnetic resonance imaging was performed in these patients with high-resolution T2-weighted and enhanced T1-weighted sequences. In the first case presented here, the MRI revealed a hypointense filling defect within the basal turn of the left cochlea on T2WI with corresponding homogeneously enhancing mass on T1WI C+, corresponding to a probable intracochlear schwannoma (fig. 1 - arrows).

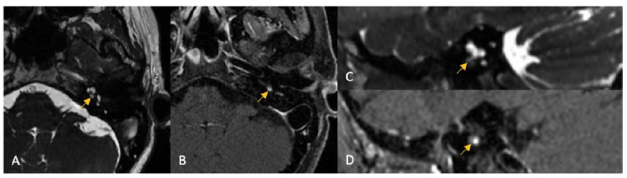

Figure 1. A, Axial high-resolution T2-weighted MR image. B, Axial enhanced T1-weighted MR image. C, Oblique sagittal high-resolution T2-weighted MR image. D, Oblique sagittal enhanced T1-weighted MR image.

In the second case there was a mass extending from the left cochlea to the internal auditory canal and the cerebellopontine angle cistern, being hypointense on T2WI with corresponding enhancement on T1WI C+, corresponding to a transmodiolar schwannoma (fig. 2 - arrows).

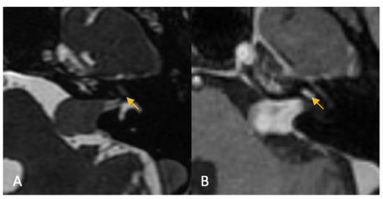

Figure 2. A, Axial high-resolution T2-weighted MR image. B, Axial enhanced T1-weighted MR image.

Discussion: Intralabyrinthine schwannoma is an uncommon lesion of the inner ear, increasingly diagnosed with advancements in MRI technology.
The most common symptoms of the patients presented in this work were sensorineural hearing loss followed by tinnitus. All of them had a normal otoscopy.
On MRI, intracochlear schwannomas typically appear as a small intracochlear nodular lesion in the modiolus, appearing isointense on T1-weighted images and hypointense on T2-weighed images with homogeneous enhancement after gadolinium administration. Gadolinium administration optimizes the recognition of these small lesions. The most important differential diagnosis is labyrinthitis.
The treatment of these tumors is variable and not all patients require surgery.

Conclusion: Magnetic resonance imaging plays a vital role in the diagnosis, classification, and follow-up of intralabyrinthine schwannomas.

1-P40

PITUITARY ADENOMA "PNEUMO-APOPLEXY": A RARE ENTITY

Luísa Sampaio[1,2], José Maria Sousa[1], Sofia Vedor[1], Ana Isabel Almeida[1]
[1]Department of Neuroradiology, Centro Hospitalar e Universitário de São João, E.P.E., Porto, Portugal. [2]Faculty of Medicine, Oporto University, Porto, Portugal

Introduction: Pituitary tumor apoplexy is a clinical syndrome that results either from infarction or hemorrhage of a pituitary tumor. Pneumocephalus has been only occasionally described in the literature in cases of pituitary adenoma, out of which gas confined to the sellar/supra-sellar region is rare. Most commonly, pneumosella has been described in association with postsurgical states (typically occurring immediately after surgery) or rarely as a sequel of radiation. We present a case of pituitary macroadenoma apoplexy associated with a large volume of intra-tumoral gas.

Case report: A 74-year-old man with a nonfunctioning pituitary macroadenoma was submitted to transsphenoidal and frontoparietal partial resection followed by radiotherapy thirteen years ago (with secondary panhypopituitarism), showing imagiological stability for the last six years.
He presented to emergency department with impaired consciousness, left hemiparesis, visual acuity deterioration, headache and fever. Head CT, CT angiography and perfusion CT ruled out an ischemic event. Head CT and brain MRI revealed a large sellar and suprasellar lesion, that extended from the floor of the sphenoid sinus to the optic chiasm, containing a small hemorrhagic area and a large collection of air - findings compatible with pituitary tumor "pneumo-apoplexy". A right thalamo-capsular ischemic lesion was also identified, probably resulting from the regional mass effect of the lesion. Although the absence of apparent rhinorrhea, a sellar floor defect due to previous surgeries was depicted and empiric antibiotic therapy was initiated.
Given the gradual consciousness recovery and focal neurological deficits improvement, an initial conservative approach was adopted; two weeks later a transsphenoidal surgical revision of sellar floor was done, without detection of evident CSF leakage points. Subsequent head CTs showed no surgical complications and a progressive reabsorption of the air and blood components inside the lesion. The patient was discharged with a mild motor deficit.

Conclusion: We present a case of a pituitary tumor "pneumo-apoplexy", a pneumosella with simultaneous findings of tumor apoplexy. Given previous sellar floor defect, we consider the hypothesis of an arachnoid breach occluded by the tumor as a "plug" preventing a CSF leak. The tumor shrinkage from apoplexy may have developed a transient CSF leak with an associated pneumosella. To our best knowledge, this is only the second report of this entity but, even rare, it should be considered in patients with compatible clinical findings, mainly if they have a history of transsphenoidal pituitary region surgery.

Keywords: Pneumosella; Pneumocephalus; Apoplexy; Adenoma; Pituitary.

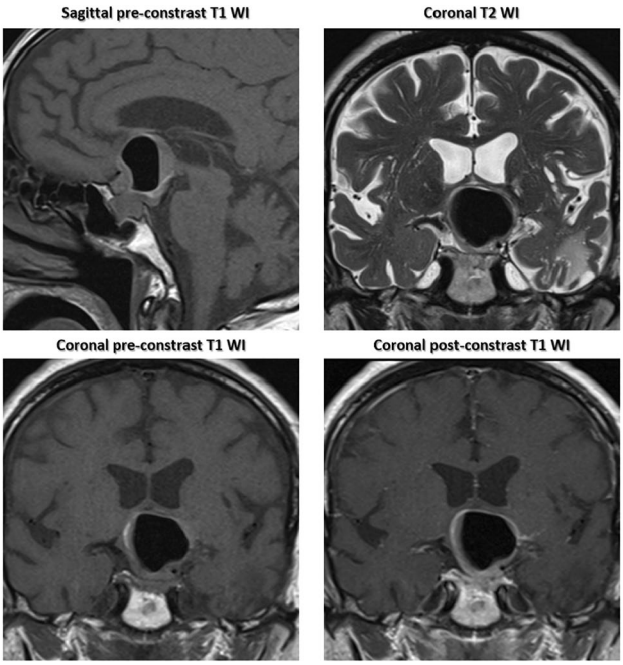

1-P41

DURAL TAIL SIGN AND MIDDLE MENINGEAL ARTERY HYPERTROPHY IN PATIENTS WITH GLIOBLASTOMAS. IT IS A RARITY?

Serena Palizzi[1], Andrea Romano[1], Giulia Moltoni[1], Allegra Romano[1], Francesco Dellepiane[1], Valentina Frezza[1], Antonella Blandino[1], Andrea Grossi[1], Alessandro Bozzao[1]
[1]Sapienza Università di Roma, Facoltà di Medicina e Psicologia, Dipartimento NESMOS U.O.C. Neuroradiologia Azienda Ospedaliero-Universitaria "Sant'Andrea", Rome, Italy

Introduction: Dural tail sign and enlarged external carotid artery (ECA) branches (middle meningeal artery, MMA) on MRI are highly suggestive of meningioma. Unlike meningiomas, GBMs are highly vascular and aggressive lesions, with a blood supply deriving from pial vasculature. The aim of this study is to verify the prevalence of dural tail sign and enlarged MMA in a large cohort of patients affected by intra-axial GBM, as the identification of these findings could have a great impact in pre-surgical planning.

Materials & Methods: We retrospectively evaluated 180 patients affected by GBM (88 males, 92 females; mean age 65 years ±9,5 years) in the last 10 years, considering the location of GBM (deep or superficial), the presence of dural tail sign and an enlarged MMA located close to the tumor. Consequently, the prevalence of both dural and vessel sign was estimated.

Results: The cohort of patients was divided in two groups according to GBM location (84 deep location, 96 superficial location). In our analysis, only superficial GBMs were considered. Dural tail sign was detectable in 29 GBMs (30% of 96 patients). In 18 patients (all of them with dural tail sign) was evident an enlarged MMA (19% of 96 patients). The neurosurgeons reported the tumor with the enlarged MMA as blood vessels-rich mass. Also, intraoperative findings demonstrated numerous capillary vessels connecting the dura and the tumor, leading to easily and abundant bleeding.

Discussion & Conclusion: Dural tail sign and enlarge MMA in GBM are more common than we expected. Also, the presence of an enlarged MMA represents a potential bleeding risk factor during surgery and its recognition by radiologists is a crucial condition.

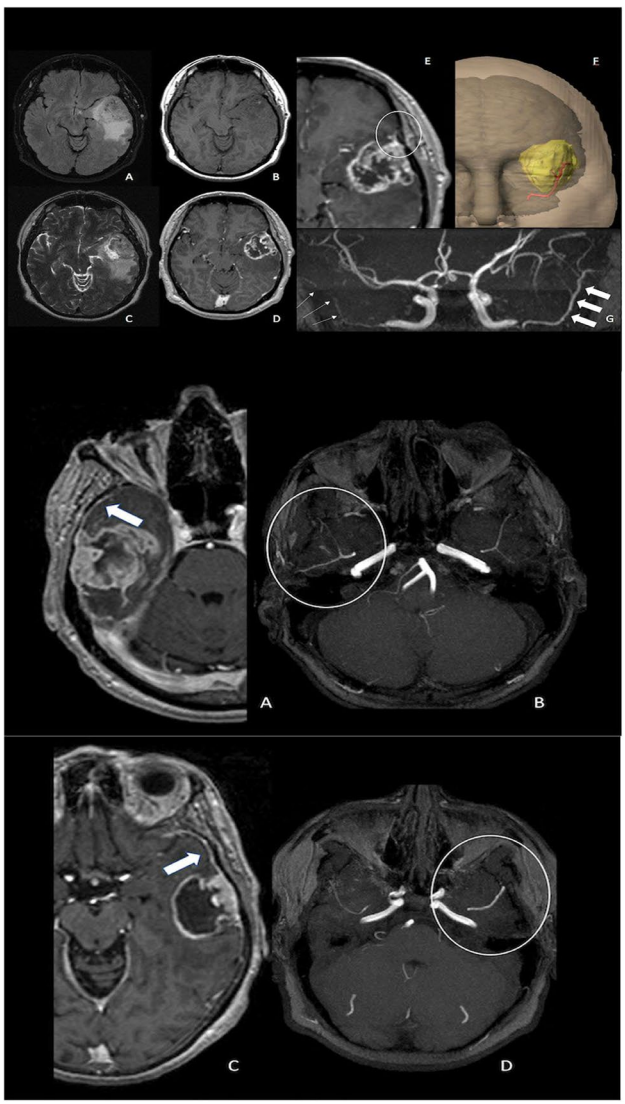

Captions

Figure 1 (A-G). Patient 3. Left temporal glioblastoma (A-D). Intralesional flow-voids (A and C) and hemorrhagic components (B) are evident. In E, dural enhancement (dural tail) is appreciable (circle). Time of Flight sequence shows an asymmetric representation of middle meningeal artery, better visible on the left side (G, thickened arrows), ipsilaterally to glioblastoma. A three-dimensional reconstruction confirms the proximity of the vessel to the tumor (F).

Figure 2 (A-B) (C-D). Patient 1 (A-B), Patient 2 (C-D). In both cases the dural tail sign (arrows) and the middle meningeal artery hypertrophy (circles) are appreciable.

1-P42

IT IS A GIANT ONE! – A SYMPTOMATIC COLLOID CYST

Sofia Vedor[1], Ana Isabel Almeida[1], Gonçalo Alves[1], Rita Figueiredo[1]

[1]Department of Neuroradiology, Centro Hospitalar e Universitário São João, Porto, Portugal

Introduction: Colloid cysts are benign epithelial lined cystic lesions, mainly located in the anterior part of the third ventricle, with characteristic imaging features. Although usually asymptomatic, their location at the level of the roof of the third ventricle, near the foramina of Monro, can occasionally result in sudden obstructive hydrocephalus. Giant colloid cysts are extremely rare, with only few cases reported in the literature. They may develop in the presence of some anatomical variations, that allow unusual large sizes with an asymptomatic growth. This finding is secondary to a vertical growth of a retro-foraminal colloid cyst through anatomical windows devoid of the mechanical restraint of the forniceal structures. Furthermore, they may present with fluid-fluid levels, depending on the amount of gelatinous material within the tumor.

Case report: We report a case of a 59-years-old male with unremarkable medical and psychiatric history, who presented with one month history of progressive gait disturbances and left lower-limb muscle weakness. Head CT and brain MRI revealed a giant well-circumscribed intraventricular lesion at the level of the right foramen of Monro, occupying the virtual space between the two leaves of the septum pellucidum. The tumor had two components: an anterior isointense on T1-weighted sequence and hyperintense on T2/FLAIR; and a major posterior component, isointense on T1 and T2-weighted images and hyperintense on T2/FLAIR, without restricted diffusion, suggesting the presence of proteinaceous components. The perfusion study did not show any elevation on

the relative cerebral blood volume (rCBV). There were no areas of contrast enhancement, with the exception of a slight prominence of peripheral vascular structures, probably corresponding to septal veins. The lesion measured approximately 31 x 27 x 26 mm, justifying a noticeable supratentorial hydrocephalus, with prominent dilatation of the right lateral ventricle and signs of interstitial edema. The patient underwent complete macroscopic resection of the lesion and the final diagnosis of colloid cyst of the third ventricle was confirmed by the pathology.

Conclusion: The authors report a giant colloid cyst with a curious fluid-fluid level appearance. Even though the clinical and imaging characteristics of colloid cysts are already well documented, the etiology and factors responsible for their typical radiological features continue to be a subject of debate. It is important to recognize these unusual variants, to establish a more adequate differential diagnosis.

Keywords: Third ventricular cyst, colloid cyst, obstructive hydrocephalus, fluid-fluid level

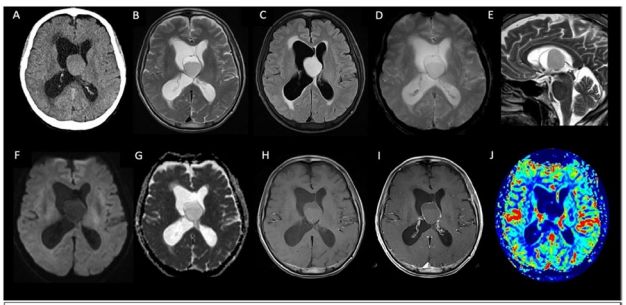

Fig 1. CT (A) and MRI showed a giant intraventricular cyst, displacing the two leaves of the *septum pellucidum,* with proteinaceous content, drawing a fluid-fluid level (B-E). There was no restricted diffusion (F-G), contrast enhancement (H-I) or elevated rCBV (J).

1-P43

DIFFERENTIATION OF GLIOBLASTOMA, BRAIN METASTASES AND CENTRAL NERVOUS SYSTEM LYMPHOMAS USING AMOUNT OF VASOGENIC EDEMA AND DIFFUSION MR IMAGING OF TUMOR CORE AND PERITUMORAL ZONE- SEARCHING FOR A PRACTICAL APPROACH

Ezel Yaltırık Bilgin[1], Özkan Ünal[1]
[1]Dr. Abdurrahman Yurtaslan Ankara Oncology Training and Research Hospital, Ankara, Turkey

Introduction: We aimed to evaluate the differences of the amount of edema and the diffusion characteristics of the tumor core-peritumoral zone between glioblastoma, brain metastasis and central nerve system lymphoma cases.

Materials and Methods: 39 patients (13 central nerve system lymphoma, 13 glioblastoma and 13 brain metastases) were included in the study. ADCmin values of the lesion and peritumoral region were calculated from the ADC maps in Brain Magnetic Resonance Imaging. Also the largest diameter of the vasogenic edema-mass complex was measured in T2 sequences. In contrast-enhanced series, the largest diameter of the metastatic lesion was measured, and the edema-mass ratio was calculated by proportioning the diameter of the edema mass complex to the diameter of the mass.

Results: There was a statistically significant difference in edema-mass ratio according to tumor type ($p<0.01$). According to the Bonferroni analysis, it was determined that this difference was caused by glioblastoma. Compared to patients with lymphoma and brain metastases, EMR was found to be lower in lesions diagnosed with glioblastoma. A statistically significant difference was found in the ADC-min value measured from the lesion according to the tumor type ($p<0.05$). It was determined that the ADCmin values were lower in lesions with central nevre system lymphoma compared to glioblastoma.

Conclusion: Lesional and perilesional ADC values measured by diffusion-weighted examination, and edema mass ratio measurements may increase the accuracy of differential diagnosis. In order to support the findings, studies with larger series should be combined with clinical practice.

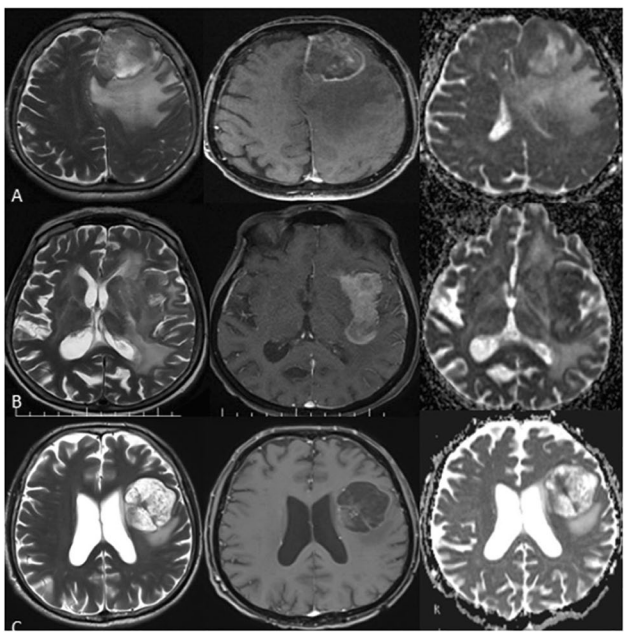

1-P44

COMMUNICATING HYDROCEPHALUS ASSOCIATED WITH MENINGIOMA SURGERY: A TREATABLE THREAT

Fátima Hierro[1], Ana Isabel Almeida[2], Sofia Vedor[2], Carina Reis[2], Sara De Carvalho[2]
[1]Hospital Pedro Hispano, Matosinhos, Portugal. [2]Centro Hospitalar e Universitário São João, Porto, Portugal

Introduction: Meningioma is the most common primary intracranial tumor, especially prevalent in the elderly population and often incidentally diagnosed. Active surveillance, surgical removal and in some cases radiotherapy are the management options. Common complications after surgical management of skull base meningiomas include cranial nerve deficits, pituitary dysfunction, cerebrovascular events, infection, and cerebral hemorrhage or contusion. The development of communicating hydrocephalus after surgical management of meningiomas is a rare, not yet fully understood, but well-established phenomenon.

Case report: We present a case of a 56-year-old male who underwent subtotal removal of a left sphenopetroclival meningioma (WHO 1), followed by radiotherapy. One year later, the patient presented with with inability to walk and bilateral reduced visual acuity. Physical examination revealed mydriatic pupils were found, without direct or consensual photomotor reflex on the left eye, and bilateral papillary edema. MR imaging of the brain revealed ventricular system dilatation, without evidence of obstruction and no white matter changes. A ventriculoperitoneal shunt was placed, and after 10 days there was visual improvement in the right eye and improved balance in orthostatism.

Discussion: The development of communicating hydrocephalus after surgical management of meningiomas is a rare phenomenon, however not yet fully understood. There are multiple hypotheses for its occurrence, such as an increased in CSF protein content, subarachnoid hemorrhage, or infection. Additionally, the presence of tumor cell aggregates in the CSF has been described, raising the hypothesis that hydrocephalus could be caused by their obstruction to CSF reabsorption.,n most cases described in the literature, this complication occurs after surgical approach, and most commonly in skull base meningiomas. Also, the association between adjuvant radiotherapy in meningiomas and communicating hydrocephalus has been described, in patients who develop radiation leukoencephalopathy.

Conclusion: The postoperative development of communicating hydrocephalus can dramatically alter the clinical course of a patient with a meningioma, as well as the necessary therapeutic interventions. Thus, the recognition of this entity allows for early ventricular shunting in order to avoid symptomatic progression, permanent neurological damage or even death.

Keywords: Communicating hydrocephalus, Skull base meningioma, Post-surgical complication

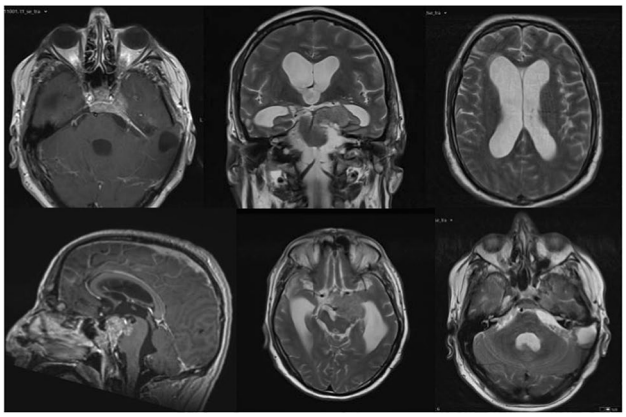

1-P45

A CASE OF PARASELLAR MENINGIOMA WITH INTRASELLAR EXTENSION MIMICKING PITIUTARY MACROADENOMA

Makbule Çaylak[1], Özkan Ünal[1]
[1]Sağlık Bilimleri Üniversitesi Dr. Abdurrahman Yurtaslan Onkoloji Eğitim ve Araştırma Hastanesi, Ankara, Turkey

Introduction: Meningiomas account for 34.7% of all primary intracranial tumors observed in adults, the majority of which are benign. Suprasellar/parasellar meningiomas are seen in 5%-10% of all intracranial meningiomas. Pituitary adenomas are the most prevalent sellar and suprasellar masses, contributing to about 90% of all cases. Meningiomas constitute only 1% of the sellar masses. Sellar/suprasellar meningiomas can mimic both clinically and radiologically any of the other non-hormone secreting sellar region masses, in particular the non-functioning pituitary adenoma. Previous studies have dealt with sellar/suprasellar meningiomas but used a broad definition of the "sellar area", including mainly parasellar lesions.

Case Report: A 55-year-old female patient was admitted to the neurology clinic due to headache and recent onset of visual dysfunction on the left eye. MRI examination revealed the presence of a large parasellar mass with intrasellar extension and the normal pituitary gland could not be distinguished as a separate structure. All hormone levels of the patient were normal. Because of the tumour firmness, cavernous sinus invasion and close relationship with the optic tract and optic nerve, the mass could not be resected

totally.Histopathological result was WHO grade 1 meningioma. The patient applied to our hospital after the operation. In our hospital stereotactic radiotherapy (SRT) was applied for residual tumour and one year radiological follow-up after SRT the mass remained stable .

Discussion/Conclusion: Differentiating between suprasellar or parasellar meningiomas that grow downward into the pituitary fossa and pituitary macroadenomas that arise within the sella turcica and extended superiorly is difficult because of their overlapping imaging findings.However, correct preoperative identification of these two tumours is useful because they have different surgical approach most of the time. Some MRI characteristics may be helpful for differential diagnosis like contrast enhancement patern, tumour epicenter, dural tail sign, visibility of the pituitary gland or sellar enlargement. In this report, we aimed to present a case of parasellar meningioma that can be confused with pituitary macroadenoma.

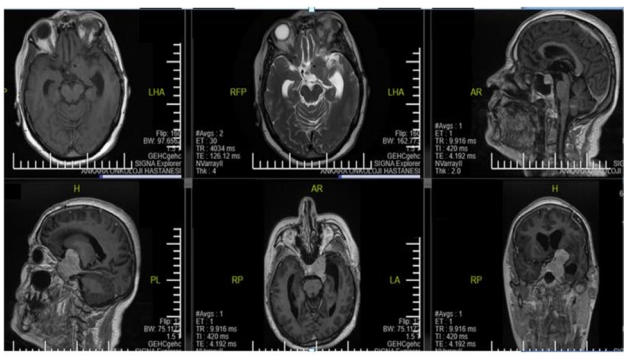

Left parasellar mass lesion with inrasellar extension :Tumour is isointens on T1 and T2 weighed images, showing marked homogeneous contrast enhancement and dural tail sign. The mass completely invades the left cavernous sinus . There is also encasement of the left internal carotid artery and middle cerebral artery by the tumour.The optic chiasm and left optic nerve slightly displaced to the right. The normal pituitary gland could not be distinguished as a separate structure.

1-P46

GENETICS AND RADIOMICS IN ONCOLOGICAL IMAGING: A SYSTEMATIC REVIEW OF THE GENETIC VALIDATION DATA USED IN RADIOMICS STUDIES REGARDING BRAIN TUMORS

Anne Rix Arildskov[1], Frederik Jager Bruun[1], Lotte Harries Hasselbach[1], Kristine Bærentz Holst[1], Sine Hvid Rasmussen[1], Rebeca Mirón Mombiela[1]
[1]Radiology Derpartment, Herlev og Gentofte Hospital, Copenhagen, Denmark

Background: Radiogenomics is motivated by the concept that biomedical images contain information that reflects underlying pathophysiology. This review focused on studies that used genetics to validate radiomics models and outcomes in brain tumors and assessed their contribution to the radiomics field.

Methods: Literature search included all original research articles with the words radiomics and genomics in English and performed in humans up to 31 January 2022; studies were identified in Medline and Embase. Study quality was assessed with Radiomic Quality Score (RQS) and the Cochrane recommendation for diagnostic accuracy study Quality Assessment 2.

Results: 15 studies addressing brain tumors were included in our systematic review with a mean RQS of 12 (range 5-19). The majority used MGMT-methylation and IDH status as genetic validation. The genetic data also included clustering, metagenes, gene subgroups and genes with association to specific tissue processes. The studies addressed various types of gliomas and their association with radiomics features and the genetic profile. All studies focused on survival prediction.

Conclusions: We found that radiomics are a promising clinical tool for noninvasive diagnostics regarding brain tumors.

Keywords: Brain tumors, radiomics, genetics.

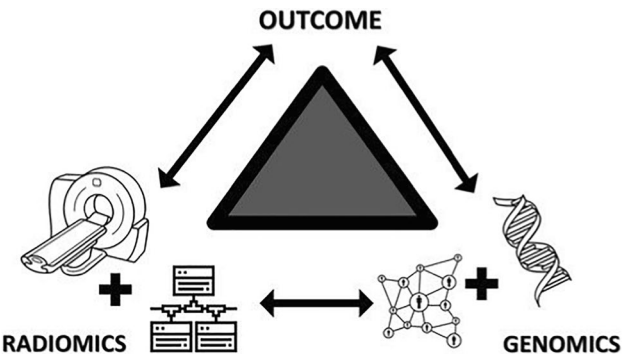

1-P47

RUPTURED INTRACRANIAL DERMOID CYSTS – RADIOLOGICAL FINDINGS OF A RARE ENTITY

Sara de Carvalho[1], Sofia Vedor[1], João Meira[2], Carina Reis[1]
[1]Neuroradiology Department, Centro Hospitalar e Universitário São João, Porto, Portugal. [2]Neurosurgery Department, Centro Hospitalar e Universitário São João, Porto, Portugal

Introduction: Intracranial dermoid cysts account for approximately 0.5% of all primary intracranial neoplasms and their rupture represents an uncommon event. Nonetheless, association with serious complications due to rupture can occur, such as chemical meningitis, cerebral infarcts, hydrocephalus, and even potential death. In this setting, neuroimaging plays a significant role in diagnostics, since both ruptured and unruptured intracranial dermoid cysts present

with typical CT and MRI findings, commonly leading to a straightforward diagnosis.

Methods: A pictorial review of ruptured intracranial dermoid cysts, with resort to both CT and MR images. Data was collected from patients with evidence of ruptured intracranial dermoid cysts on a radiological assessment performed at our center, Centro Hospitalar e Universitário de São João, and registered in our database, since January 2014 until May 2022.

Results: We found six patients who met the inclusion criteria. Except for one patient, all lesions were supratentorial, mainly in a paramedian/median location. All dermoids presented typical signal characteristics on brain CT and MRI, except for a slight peripheral enhancement detected in four patients at post-contrast T1-weighted sequences. Fat droplets with blooming artifacts within the ventricular system were found in two patients and in the subarachnoid spaces across all examinations. Radiological signs of chemical meningitis were the only complication associated with the rupture of a dermoid cyst, reported in two patients.

Discussion: Intracranial dermoid cysts have a typical midline location. Imaging features on head CT are very characteristic – these lesions are well-circumscribed, with a central hypodensity consistent with lipids/sebum and may show calcified edges/capsule. On brain MRI, a dermoid cyst appears as an hyperintense mass on T1, with heterogenous signal intensity on T2 and signal suppression on fat saturation sequences, with no restricted diffusion on DWI/ADC map and, although rare, contrast uptake has been described. Furthermore, chemical shift and/or blooming artefacts, in both ruptured and unruptured dermoid cysts can be observed. When ruptured, the classical feature of fat droplets in the subarachnoid spaces and/or ventricular system can be noticed. Moreover, a leptomeningeal reaction with contrast enhancement can be demonstrated.

Conclusion: Fat droplets in the subarachnoid space and/or ventricular system, together with blooming artefacts in these locations, form classical imaging features of ruptured intracranial dermoid cysts. Comprehension of these specific neuroimaging patterns, prompts an accurate diagnosis, allowing for appropriate treatment referral.

Keywords: Ruptured dermoid cyst, fat droplets, blooming artefacts

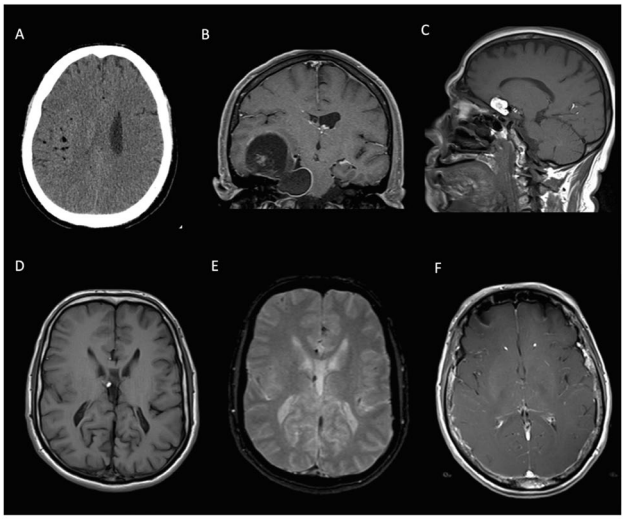

Figure 1. Characteristic imaging features of ruptured intracranial dermoid cysts.
Head CT (axial) (A) showing hypoattenuating fat droplets in the subarachnoid space along frontal and parietal sulci, after head trauma, in a patient with a dermoid cyst located in the right anterior temporal region. Brain MRI. (B) T1 (SE) post-gadolinium (coronal view) - slight peripheral enhancement of the lesion's capsule after rupture of a dermoid cyst, in the same patient as figure A. (C) Dermoid cyst at the right lateral aspect of the *planum sphenoidale* showing hyperintense signal on sagittal T1 (SE) weighted imaging and fat droplets within the subarachnoid space, along the parieto-occipital sulcus, in a patient presenting with headache. (D) Fat droplets within the III ventricle on axial T1 SE with blooming artifacts (E) in axial T2 gradient echo sequence, in a patient with an incidental right frontal-basal dermoid cyst. (F) Leptomeningeal enhancement in axial T1 SE post-gadolinium due to chemical meningitis, as complication of dermoid cyst rupture, in another patient presenting with headache.

VASCULAR

1-P48

MULTIMODAL CT CLOT CHARACTERISTICS AND SUCCESS OF ENDOVASCULAR THROMBECTOMY IN ACUTE ISCHEMIC STROKE

Naphon Assawagumtorn[1], Krittanon Lertutsahakul[1], Ketsuda Jakchairoongruang[1]
[1]King Chulalongkorn Memorial Hospital The Thai Red Cross Society, Bangkok, Thailand

Introduction: Endovascular thrombectomy plays an important role in treatment for acute large arterial ischemic stroke. CT and CT angiography (CTA) have high sensitivity, specificity, and are informative for acute occlusive thrombus. Conflicting results of the thrombus characteristics and revascularization outcome after endovascular thrombectomy (EVT) have been debated for a decade. We aimed to evaluate the association between the clot heterogeneity and clot characteristics on multi-modal CT and EVT outcome in acute anterior-circulation ischemic stroke.

Methods: Non-contrast CT and multi-phase CTA brain of 59 acute anterior-circulation ischemic stroke adult patients who underwent EVT in our institution from November 2019 to June 2021 were reviewed. The clot characteristics including the most proximal clot location, clot length, clot burden score (CBS), distance from distal internal carotid artery (DT), clot heterogeneity, mean clot attenuation, relative mean clot attenuation to contralateral artery, and clot perviousness were assessed. Standard deviation (SD) of the measured clot attenuation was used to represent clot heterogeneity. At least mTICI2b on post-thrombectomy cerebral angiography was considered successful revascularization. Descriptive and analytic statistical analysis between these clot characteristics and EVT outcome were obtained with $p<0.05$ considered significant. The duration of treatment, thrombectomy method, number of attempts, and immediate complication were also reviewed.

Results: Fifty two of 59 cases (88.1%) had successful thrombectomy. Aspiration thrombectomy was the most used method (47/59 cases, 79.7%). DT was significantly shorter in successful group (8.5±9.1 mm) versus unsuccessful group (16.4±13.2 mm) with p=0.046. Association between DT and successful outcome did not reach statistical significance (OR=0.94; 95%CI=0.87-1.00; p=0.061). The clot heterogeneity and other clot characteristics showed no difference and no association with the revascularization outcome. There was excellent agreement in assessment of clot location, CBS, clot length, and DT, while moderate agreement for clot heterogeneity.

Discussion: Our results showed significantly shorter DT in successful group than unsuccessful group, while other characteristics were not different and showed no association with EVT outcome, which were concordance with some priors. We focused on clot heterogeneity assessment, which has not been studied, using SD of the clot attenuation. Unlike prior histology study of clot heterogeneity, CT clot heterogeneity showed no association with EVT outcome.

Conclusion: Non-contrast CT and multi-phasic CTA were suitable and reliable non-invasive imaging method for accurate assessment of the occlusive thrombus. Distance of the clot from terminal ICA was significantly shorter in the successful EVT group. Further assessment of clot heterogeneity and EVT outcome should be sought.

1-P49

STURGE-WEBER SYNDROME WİTH BRAIN SURFACE ENHANCEMENT

Özkan Ünal[1], Onur Simsek[1]
[1]Dr Abdurrahman Yurtaslan Ankara Oncology Training and Research Hospital, Ankara, Turkey

Purpose and Learning Objectives: To provide a review of contrast surface enhancement on post-contrast Fluid Attenuated Inversion Recovery (FLAIR) images in the light of current literatüre. To describe the common and distinctive features of our case with previously described surface enhancement cases. To discuss possibble Blood-Brain Barrier (BBB) changes in Sturge-Weber Syndrome (SWS)

Approach: Literature search was conducted with the following keywords:
Post-contrast FLAIR, Contrast leakage, Contrast surface enhancement, Pericortical enhancement, Leptomeningeal enhancement, Sturge-Weber Syndrome, CSF enhancement, Classical features of SWS and surface enhancement were discussed in light of the current literature.

Background: The Sturge–Weber syndrome, encephalofacial angiomatosis, is a neurocutaneous disorder characterized by leptomeningeal vascular abnormalities and a port-wine stain on the face (1). Pericortical contrast enhancement on delayed postcontrast FLAIR imaging is a marker for focal loss of BBB integrity (2). In previous studies, CSF enhancement on post-contrast FLAIR was found related to varying neurological diseases (2). Some studies also associated this imaging phenomenon with higher ages (2).

Conclusion: Although vascular malformations are significant at SWS's pathophysiology, BBB abnormalities are not well known as imaging findings. This exhibit represents a young SWS patient with surface enhancement on post-contrast FLAIR.

References: Shirley MD, Tang H, Gallione CJ, et al. Sturge-Weber syndrome and port-wine stains caused by somatic mutation in GNAQ. N Engl J Med. 2013;368(21):1971-1979. doi:10.1056/NEJMoa1213507
Freeze WM, van der Thiel M, de Bresser J, et al. CSF enhancement on post-contrast fluid-attenuated inversion recovery images; a systematic review. Neuroimage Clin. 2020;28:102456. doi:10.1016/j.nicl.2020.102456

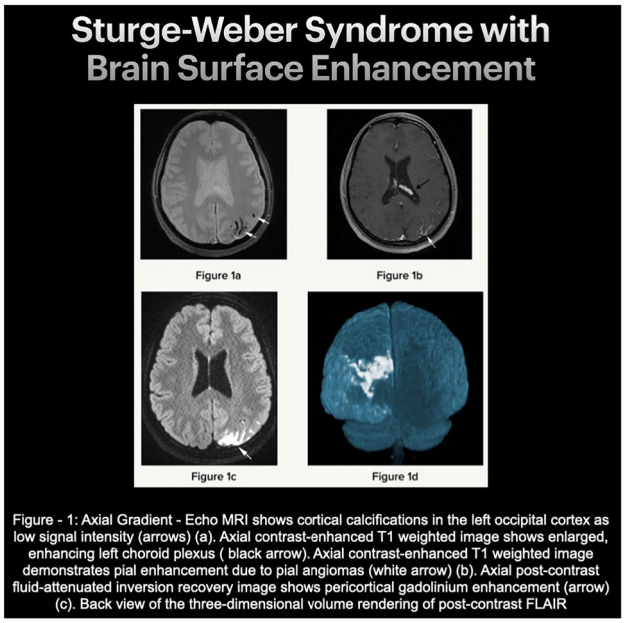

Figure - 1: Axial Gradient - Echo MRI shows cortical calcifications in the left occipital cortex as low signal intensity (arrows) (a). Axial contrast-enhanced T1 weighted image shows enlarged, enhancing left choroid plexus (black arrow). Axial contrast-enhanced T1 weighted image demonstrates pial enhancement due to pial angiomas (white arrow) (b). Axial post-contrast fluid-attenuated inversion recovery image shows pericortical gadolinium enhancement (arrow) (c). Back view of the three-dimensional volume rendering of post-contrast FLAIR

1-P50

SUPERIOR CEREBELLAR ARTERY DISSECTION IN A COVID-19 RECOVERED PATIENT DIAGNOSED WITH REVERSIBLE CEREBRAL VASOCONSTRICTION SYNDROME: A CASE REPORT

Tiago Pedro[1], Rúben Maia[1], Rafaela Costa[2,3], Pedro Abreu[2,3], Pedro Castro[2,3,4], Ricardo Soares-dos-Reis[5,3,6]
[1]Department of Neuroradiology, Centro Hospitalar Universitário de São João, E.P.E, Porto, Portugal. [2]Department of Neurology, Centro Hospitalar Universitário de São João, E.P.E, Porto, Portugal. [3]Department of Clinical Neurosciences and Mental Health, Faculty of Medicine of University of Porto, Porto, Portugal. [4]Cardiovascular Research and Development Unit, Faculty of Medicine of University of Porto, Porto, Portugal. [5]Department of Neurology, Centro Hospitalar Universitário de São João, E.P.E., Porto, Portugal. [6]i3s - institute for research and innovation in health, University of Porto, Porto, Portugal

Introduction: Arterial dissection is an uncommon complication of reversible cerebral vasoconstriction syndrome (RCVS). To our knowledge, this is the first case reported of RCVS associated with dissection of the superior cerebellar artery (SCA) in a patient who recently recovered from COVID-19.

Objectives: We describe a 35-year-old woman with a history of migraine who presented with recurrent thunderclap headaches and focal neurological signs, including right hemiataxia. Her current medications included sumatriptan PRN for migraine and a progestin contraceptive implant. She had been diagnosed with COVID-19 infection two weeks earlier.

Methods: Diffusion-weighted (DWI) magnetic resonance imaging (MRI) showed right cerebellar hemisphere restricted diffusion consistent with acute cerebellar ischemia and MRI vessel wall imaging (VWI) after gadolinium administration showed a long SCA hyperintense filling compatible with arterial dissection and intramural thrombus. MRI angiography revealed multifocal stenosis of the posterior circulation arteries and stenosis of the prepontine segment of the right superior cerebellar artery followed by fusiform dilatation of the arterial lumen.

Discussion: Superior cerebellar artery dissection is a rare entity with only a few cases previously described. Dissection is more common on the proximal arterial segment and exhibits a young female predominance. RCVS may raise the likelihood of arterial dissection by increasing intraluminal pressure after the stenosis, but the intima dissection can also release vasoactive substances capable of inducing vasospasm. COVID-19 infection may trigger an inflammatory response with consequent endothelial damage and intimal vessel disruption.

Conclusion: The interplay between COVID-19 infection, RCVS, and arterial dissection requires further investigation.

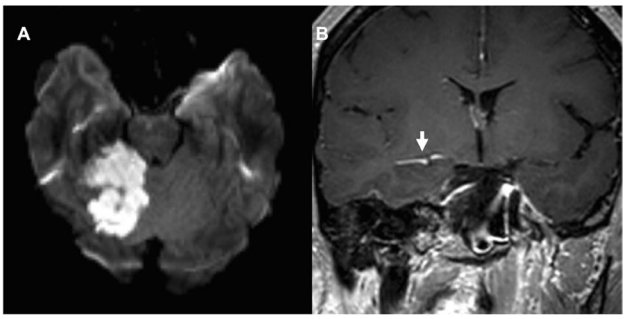

1-P51

CAROTID WEB: AN UNDERRECOGNIZED CAUSE OF STROKE

Guilherme Ribeiro Martins[1], Maria Inês de Sá[1], David Berhanu[1,2], Hugo Cadilha[1], Lia Neto[1,2]
[1]Department of Neurologic Imaging, Hospital Santa Maria, Centro Hospitalar Lisboa Norte, Lisboa, Portugal. [2]Anatomy Department, Lisbon School of Medicine, Lisboa, Portugal

Introduction: Up to one-third of all patients presenting with ischemic strokes lack an identifiable cause. Carotid

web (CW) is a very rare vascular disease of the internal carotid artery suspected to be an underdiagnosed cause of cryptogenic strokes. We aim to report the clinical and imaging findings of a group of patients with CWs and its relation with acute stroke/TIA.

Methods: We retrospectively reviewed computed tomography angiography (CTA) reported has having CW (April 2019 - April 2022). Carotid webs were defined as a linear filling defect in the posterior internal carotid artery bulb, on oblique sagittal section CTA. All images were reviewed by three blinded neuroradiologists, including a neurovascular intervention specialist. Interobserver agreement was calculated using Chone's kappa coefficient. For the selected patients, demographics, imaging findings, treatment and clinical outcomes were analyzed.

Results: We found 22 CTAs describing CW. After our evaluation, 11 (50%) were true webs according to our definition. The agreement between the observers was substantial (Cohen's kappa coefficient 0.66). Median age was 63 (43-83) years, and 7 (64%) were male. The majority of the patients had at least one vascular risk factor. Nine (82%) patients had acute stroke/TIA in the vascular territory of the CW, 73% confirmed by CT or MRI. Only 2 patients out of 9 (22%) had the CW identified on Doppler ultrasound and 6/6 patients confirmed the web on Digital Subtraction Angiography (DSA). Three (27%) patients had history of recurrent stroke/TIA involving the territory of the web. Regarding treatment, 3 (38%) patients had carotid endarterectomy, 5 were medically treated and 3 patients were transfer to another institution and lost for follow-up. Carotid web was assumed as the cause of the ischemic assault in 7 (64%) patients and the remaining (36%) had more than one possible etiology (undetermined etiology TOAST).

Conclusion: Carotid webs represent an underrecognized etiology for primary and recurrent stroke and TIA. In our cohort it was the cause of 55% of the acute ischemic lesions. Head and neck CTA and DSA are reliable imaging methods to detect CWs, being superior to ultrasonography in our series. There are no current guidelines concerning the best management of CWs and further studies are needed in order to define the optimal imaging method and treatment of this condition.

Keywords: Carotid web; CT angiography; Stroke; TIA

1-P52

AN UNUSUAL CASE OF AN INTRACEREBRAL HEMORRHAGE IN A NON-HYPERTENSIVE YOUNG PATIENT

Sara Rosa[1], Carolina Guerreiro[1], Jorge Ferreira[1], Carolina Pinheiro[1], João Reis[1]
[1]Centro Hospitalar Universitário de Lisboa Central, Lisbon, Portugal

Introduction: Intracerebral hemorrhage represents 15% of all strokes. Lenticulostriate artery aneurysms are infrequent vascular abnormalities and, contrary to popular belief, only 25% are associated with a diagnosis of hypertension. We present a case of an external capsule hemorrhage where a lenticulostriate artery aneurismatic formation was found.

Case: A 34-year-old male patient, with no relevant past medical history besides active smoking, presented to the emergency department with obtundation after suffering head trauma in the context of a car crash. At the time of the accident, he was under the influence of alcohol. The patient displayed no other symptoms or other signs on neurological examination.
Head CT revealed an acute intraparenchymal hemorrhage involving the right external capsule and a slit-like sequela image, isodense with the cerebrospinal fluid, occupying the contralateral external capsule. CT Angiography showed a grossly spherical contrast enhancing image (vascular dilation versus "spot sign" signal) within the hemorrhage. Conventional cerebral angiography confirmed the right lenticulostriate artery 1,5 mm ruptured aneurysm.
No interventional treatment was performed and the patient remained clinically stable throughout his hospital stay. Etiological investigation did not reveal any predisposing aneurysm formation factor - besides active smoking.

Conclusion: Albeit rare, lenticulostriate artery aneurysms are a possible cause of striatocapsular hemorrhage which should be sought out, particularly in young patients with no history of hypertension. This case poses an intriguing etiological challenge, especially given the aforementioned slit-like sequela image found on head CT in a patient with no previous neurological symptoms.

Keywords: Lenticulostriate Artery Aneurysm; Ruptured Aneurysm; External Capsule Hemorrhage; Non-hypertensive Aneurysm.

1-P53

REMOTE CEREBELLAR HAEMORRHAGE - THE RARE POST-SURGICAL PHENOMENON

Francisca Sena Batista[1], Diogo Marques[1], Filipa Castelão[1], Rosa Couto[1], Mariana Cardoso Diogo[2], Lígia Neves[1], Cristina Rios[1]
[1]Hospital Garcia de Orta, Lisbon, Portugal. [2]Hospital Garcia de Orta, Almada, Portugal, Lisboa, Portugal

Introduction: Remote Cerebellar Haemorrhage (RCH) is a rare post-operative complication of supratentorial craniotomies and, less frequently, of spinal surgeries or lumbar punctures. We present the case of RCH in a middle-aged man, hours after craniotomy for removal of a supratentorial meningioma, as well as a review of imaging presentations of this entity.

Case Report: 56 years-old man underwent craniotomy for resection of a large fronto-parietal meningioma. There were no intrasurgical complications, however in the first hours post-operation, the patient developed aphasia and agitation. Head CT revealed an acute bilateral cerebellar haemorrhage, with typical blood layering the cerebellar folia - *zebra sign*. Patient was treated conservatively, showing progressive improvement of the symptoms.
RCH may occur after a variety of supratentorial procedures, spinal surgery and even lumbar puncture. Most cases occur within hours of the procedure, but some cases have been reported up to 1 week after.
The aetiology of this rare post-surgical complication is probably related do CSF hypovolemia, leading to downward displacement of cerebellar hemispheres and tearing of bridging veins. The majority of patients are asymptomatic, being an incidental finding in early CT/MR postoperative scans. When symptomatic, reduced level of consciousness with delayed wakening from anaesthesia is the most common manifestation. Some patients develop motor and cerebellar symptoms.
RCH can be bi- or unilateral, ipsi- or contralateral to the site of surgery. Prognosis is good, but related to haemorrhage severity. Obstructive hydrocephalus is the most severe complication and has to be promptly identified. Otherwise, this phenomenon is self-limited and does not require additional investigation.

Discussion & Conclusion: RCH is a type of Remote Site Haemorrhage in the cerebellum occurring post-surgery. Although rare, it should be promptly recognised by neuroradiologists in order to avoid costly aetiological investigations or inappropriate interventions. We present a case of immediate post-surgical RCH and propose an overview of this pathology in order to raise awareness for this entity. Knowledge of its imaging features is essential for both radiologists and neurosurgeons.

1-P54

HEMORRHAGIC PATTERNS, OUTCOMES, AND ADDITIONAL INVESTIGATION IN PATIENTS WITH ANGIONEGATIVE SUBARACHNOID HEMORRHAGE ADMITTED IN A TERTIARY CENTER

Miguel Serôdio[1], Tiago Lorga[2], Inês Freire[2], Carla Reizinho[3]
[1]Neurology Department, Centro Hospitalar Lisboa Ocidental, Lisboa, Portugal. [2]Neuroradiology Department, Centro Hospitalar Lisboa Ocidental, Lisboa, Portugal. [3]Neurosurgery Department, Centro Hospitalar Lisboa Ocidental, Lisboa, Portugal

Introduction: Up to 15% of subarachnoid hemorrhages (SAH) are angionegative, in which no vascular malformation is determined in the first angiography. The majority of these SAH are in a perimesencephalic distribution. Many studies report its better outcome when compared to aneurysmal SAH. Alternative causes ought to be excluded, but there seems to be wide differences regarding the diagnostic and therapeutic approach to these patients.
The aim of this work is trying to identify hemorrhagic distribution patterns of angionegative SAH which are suggestive of a worse prognosis and existing subjacent pathology.

Methods: We conducted a retrospective study of patients admitted in Centro Hospitalar Lisboa Ocidental with angionegative SAH, between 01/01/2010-31/12/2020. Patients were grouped by hemorrhagic distribution patterns of SAH: radionegative (diagnosis via xanthochromia in lumbar puncture – type I), interpeduncular (type II), extension to posterior fosse cisterns (type III), extension to anterior and lateral cisterns (type IV) and convexity (type V).
Statistical analyses were made regarding clinical, radiological, and prognostic characteristics.

Results: We included 75 patients. 2 (2,7%) had type I SAH, 18 (24,0%) type II, 13 (17,3%) type III, 33 (44,0%) type IV, and 9 (12,0%) type V SAH.
Type III and IV had more frequently higher mFisher classification, as well as more frequently higher WFNS and Hunt & Hess scales. Globally, 12 (16,0%) had vasospasm, 14 (18,7%) had hydrocephalus on admission and 68 (90,7%) a good functional outcome (modified Rankin Scale ≤ 2) on discharge. The hemorrhagic pattern correlated with presence of vasospasm (p=0,017), hydrocephalus on admission (p=0,012) and good functional outcome (p=0,043), with type IV having more vasospasm and hydrocephalus than other types, and less frequently good functional outcome.

72 (96,0%) had CTA+DSA as initial screening and 60 (80,0%) repeated vascular imaging. 3 (3,8%) had a final alternative diagnosis (cavernomas in type II and type V; posterior aneurysm in type IV).

Discussion: Patients with type IV SAH appeared to have greater probability of complications and worse prognosis. A relevant percentage of patients showed vascular pathology on second vascular image, in which a posterior circulation aneurysm was documented on a patient with type IV SAH, therefore showing the need of image repetition and search for underlying pathology.

Conclusion: Our proposed classification of angionegative SAH by its hemorrhagic distribution might help select patients who benefit additional investigation and surveillance.

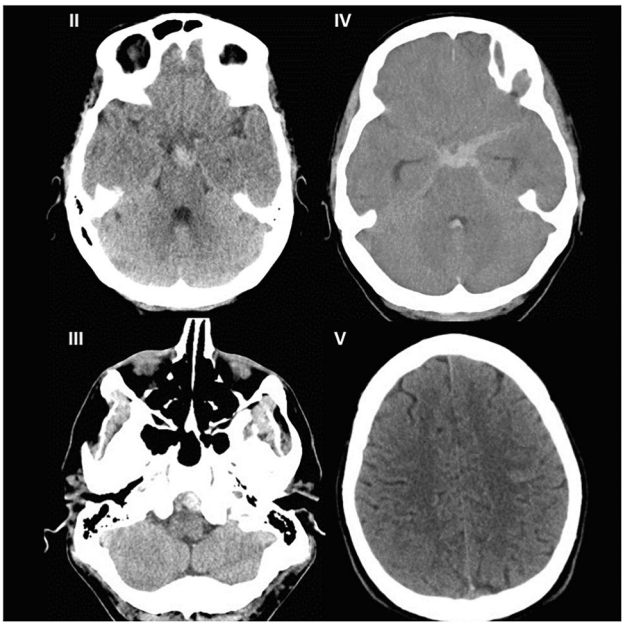

1-P55

IMAGING FINDINGS IN PATIENTS OF NON-TRAUMATIC SUBARACHNOID HAEMORRHAGE WITH INITIAL NEGATIVE CEREBRAL CT ANGIOGRAPHY

Harsha M T[1], Sameer Vyas[1], Chirag Ahuja[1], Vikas Bhatia[1], Ashish Agarwal[1]
[1]Postgraduate Institute of Medical Education and Research (PGIMER), Chandigarh, India

Introduction: CTA is widely used in detecting cerebral aneurysms in a patient with subarachnoid haemorrhage (SAH). However, it is unable to determine a cause for SAH in 5% to 30% of patients. As a result, DSA is done regularly in patients with SAH with a negative CTA diagnosis. Our aim was to analyse the initial CT pattern of SAH, and to investigate the diagnostic yield of DSA in non-traumatic SAH with negative initial CT angiography.

Methods: In this prospective study, total of 50 adult patients with SAH who were negative in Cerebral CT angiography evaluation at presentation were included from July 2020 to December 2021 in which all the. Follow up CTA was performed in cases when the DSA examination was inadequate because of subtle abnormalities or moderate to severe vasospasm.

Results: The patients were divided into 2 categories based on the pattern of SAH initial NCCT: (I) perimesencephalic subarachnoid haemorrhage (PMSAH), (II) non-perimesencephalic subarachnoid haemorrhage (nPMSAH). nPMSAH accounted for 60% of the cases, while PMSAH for 40%. DSA revealed a cause of the hemorrhage in eight (16%) patients with CTA-negative ntSAH, all of whom presented with a nPMSAH pattern. With a p-value of 0.015, there was a significant association between the site of SAH according to this method and DSA positive patients. DSA revealed that none of the patients (n-23) with mFischer grade 1& 2 were positive. DSA was found to be positive in 8 patients with mFischer grade III& IV. With a p-value of 0.005 in the Fisher exact test, there was a significant correlation between the grade of SAH according to this approach and DSA positive patients.

Conclusion: DSA identified a causative lesion in 16% of patients with CTA-negative ntSAH, but only in patients with nPMSAH and all were Fischer grade III and IV. These results suggest that DSA can help to diagnose aneurysms in nPMSAH and immediate DSA is suggested in all patients with CTA-negative ntSAH with nPMSAH or mFischer grade III/IV SAH on initial NCCT and Clinical follow up is recommended in PMSAH patients or mFischer grade I/II SAH

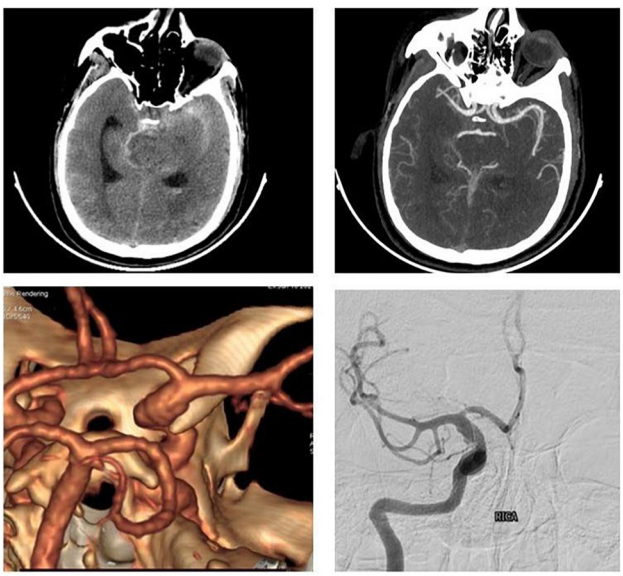

1-P56

EVALUATION OF FINAL INFARCT VOLUME IN PATIENTS WITH CROSSED CEREBELLAR DIASCHISIS: A RETROSPECTIVE STUDY

Ana Maria Braz[1], Denil Tribovane[1], João Oliveira[1], Pedro Vilela[1]
[1]Hospital Beatriz Ângelo, Loures, Portugal

Introduction: Crossed cerebellar diaschisis (CCD) in middle cerebral artery (MCA) stroke refers to attenuated blood flow and energy metabolism in the contralateral cerebellar hemisphere to the infarcted cerebral tissue. CCD is associated with an interruption of cerebro-cerebellar tracts, but the precise mechanism is unknown. We hypothesized that in patients with MCA territory infarcts, CCD might indicate severe hemodynamic impairment and tissue damage, translating into worse outcomes.

Material and Methods: We retrospectively analyzed patients with MCA ischemic stroke admitted within 24 h of ictus between January and December 2021 who underwent AIS imaging protocol. Patients with posterior or bilateral strokes, stroke mimics, haemorrhagic lesions, high-grade carotid stenosis and poor-quality data were excluded. CT Perfusion (CTP) analysis was performed in order to establish the coexistence of CCD. Follow-up imaging evaluation was performed within 1 week after onset and final infarct volume was quantified. The effects of the occurrence of CCD on supratentorial cerebral ischemia and final established infarct volume were analyzed and compared using the Alberta Stroke Program Early CT Score (ASPECTS).

Results: Among 401 patients selected who underwent AIS imaging protocol, 93 patients had acute MCA stroke and 14 (15.1%) patients demonstrated CCD on CTP and underwent follow-up imaging within 1 week. Quantitative final infarct volume was performed in 28 patients divided into two groups: CCD-positive (n=14) and a selected CCD-negative control group (n=14). The mean age was 74.8 (SD=8) vs 75.0 (SD=9) years (p=0.7, two-sample t-test). The mean time from symptoms onset and admission NIHSS was also similar between groups (p=0.7 and p=0.4, two-tailed Mann-Whitney U, respectively). The occurrence of CCD was related to a reduction in cerebral blood volume (CBV), cerebral blood flow (CBF) and prolongation of time parameters. The final infarct volume and imaging follow-up was assessed and correlated with the occurrence of CCD, which was associated with worse imaging outcomes when compared with the age-matched control group without CCD (p=0.03).

Conclusion: CCD was detectable by CTP in acute supratentorial ischemic stroke by processing the cerebellum volume. CCD can have an association with functional impairment and final infarct volume may have an adverse effect on functional outcomes during the subacute rehabilitation phase of stroke.

1-P57

HOW TO INTERPRET POST MECHANICAL THROMBECTOMY BRAIN IMAGING – A PRACTICAL GUIDE TO CORRECT DIAGNOSIS

Christina Aslanidi[1], Sofia Athanasiou[1], Zoe Papoutsou[1], Vasilios Mamalis[1], Sofia Mylona[1], Arhontakis Eftichios[1], Antonios Tsanis[1]
[1]Red Cross Hospital, Athens, Greece

Introduction: Mechanical thrombectomy (MT) has become the preferred treatment option for selected patients with acute ischemic stroke (AIS) secondary to large vessel occlusions. Patients are assesssed routinely after MT with CT scanning in order to detect hemorrhagic transformation (HT), evaluate arterial patency and final infarct extent. Follow-up brain imaging findings differ in patients who underwent MT due to the arterial injection of iodine contrast in the target vessel, direct clot manipulations and intracranial catheterization. Knowledge of specific MT-related complications and their radiographic features is essential in order to reduce errors or missed diagnoses.

Imaging Findings: Intracerebral HT is one of the major complications of AIS and it typically occurs in reperfused yet infarcted parenchymal regions. A key issue after MT is differentiating iodine contrast staining from HT on non-contrast CT in order to avoid misdiagnosis resulting in a delay of necessary treatments. The phenomenon of contrast staining is a consequence of multiple factors resulting in an increase of the blood-brain barrier permeability. Contrast agents tend to be re-absorbed within 24-48hours whereas blood remains in the extravascular space and thus should be hyperdense for more than 48hours on CT.
Subarachnoid hemorrhage (SAH) can be detected after MT in early (<6 hours) CT scans usually ipsilater to the treated vessel. There are no specific imaging characteristics than can help differentiate between SAH and contrast extravasation. Thus, the persistence of hyperdensities in the subarachnoid space for more than 24-48hours indicate SAH rather than contrast staining. Final infarct volume is critical as it directly relates to the clinical outcome. Ischemic changes in initially healthy brain territories may be also be detected on post-MT patients due to thrombus fragmentation and distal emboli to new brain regions.

A variety of complications in patients undergoing MT have been described. Intracranial arterial perforation is a rare, life-threatening complication of MT and it is associated with poor clinical outcome. It can be caused during blind maneuvering of the microguide wire/microcatheter or when retrieving the stent. Iatrogenic arterial dissection is another less-common complication of MT and it is more frequent in the extracranial arteries.

Conclusion: MT alters the clinical and imaging course of AIT secondary to large vessel occlusions. Appropriate understanding of post-MT imaging manifestations linked to arterial contrast injection and clot manipulations as well as specific complications is crucial in order to optimize patient management and care-related decisions.

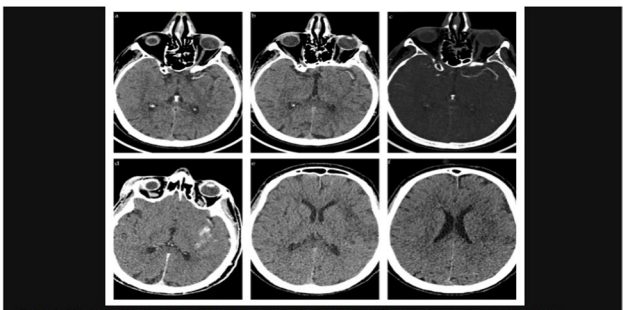

Figure 1. 60 year old male admitted with right hemiparesis.Non enhanced CT(a,b)performed on admission shows a hyperdense left middle cerebral artery,indicating acute thrombus as demonstrated in the CTA(c). NECT (d)performed right after MT reveals spontaneous hyperdensity in the left insular region,no longer visible at 48h post -MT (e,f) , indicating contrast staining. Also note the hypoattenuating regions (e,f) within the periventricular white matter extending into the left corona radiata indicating subacute infarction.

1-P58

CEREBRAL VENOUS THROMBOSIS: A CHALLENGING DIAGNOSIS. A NEW COMPUTED TOMOGRAPHY STANDARDIZED SEMI-QUANTITATIVE METHOD

Valentina Frezza[1], Andrea Romano[1], Giulia Moltoni[1], Allegra Romano[1], Serena Palizzi[1], Francesco Dellepiane[1], Francesca Tari Capone[1], Alessandro Bozzao[1]
[1]Sapienza Università di Roma, Facoltà di Medicina e Psicologia, Dipartimento NESMOS, U.O.C. Neuroradiologia, Azienda Ospedaliero-Universitaria "Sant'Andrea", Rome, Italy

Objectives: We propose a standardized, semiquantitative and easy-to-evaluate method to assess cerebral venous sinus thrombosis (CVST) on non-contrast CT scans in adult and pediatric patients.

Methods: We retrospectively selected 41 children and 36 adults with confirmed CVST and two age-matched control groups with comparable initial symptoms. Two blinded experienced readers evaluated the images placing 4 small circular ROIs in standardized regions of the brain dural venous system. Mean and maximum HU values were considered from each ROI and relative percentage variations were calculated (mean % variation and maximum % variation). We compared the highest measured value to the remaining three HU values through an ad-hoc formula based on the assumption that the thrombosed sinus has higher attenuation than the healthy sinuses. Percentage variations were employed to reflect how the attenuation of the thrombosed sinus deviates from the unaffected counterparts.

Results: We found that, in both pediatric and adult groups, the attenuation of the affected sinus was increased in patients with CVST, and consequently both mean % and maximum % variations were increased. A mean % variation value of 12,97 and a maximum % variation value of 10,14 were found useful to distinguish patients with CVST from healthy subjects, with high sensitivity and specificity.

Conclusion: Increased densitometric values are present in the site of venous thrombosis. A systematic, blind, evaluation of the brain venous system can assist the radiologist in identifying patients who need or do not need further imaging.

1-P59

RADIOMICS SIGNATURE IN ACUTE ISCHEMIC STROKE: REVIEW

Alexandra Rodrigues[1,2], Tiago Machado[3], João Gonçalves[1,2], Catarina Perry da Câmara[1]
[1]Neuroradiology Department, Centro Hospitalar Universitário de Lisboa Central, Lisboa, Portugal, Lisboa, Portugal. [2]Unidade de Neurorradiologia, Hospital Central do Funchal, Funchal, Portugal, Funchal, Portugal. [3]Laboratório de Farmacologia Clínica e Terapêutica, Faculdade de Medicina da Universidade de Lisboa, Lisboa, Portugal

Introduction: The celerity of algorithmic decisions is essential to a favourable prognosis in acute ischemic stroke (AIS). A new radiomic approach to medical imaging data extraction and sophisticated analysis methods, such as machine learning and deep learning, allow the assessment of large quantitative features and the generation of predictions that are beyond the reach of the current clinical practice. By combining both neuroimaging features and clinical variables, there is an increasing expectation that radiomics will assist neuroradiologists in delivering more accurate and prompt responses in the management of AIS.
This review aims to summarize the current evidence on the potential of neuroimaging radiomics in predicting factors related to prevention, diagnosis, treatment and outcomes in AIS.

Methods: The MEDLINE (PubMed) database was searched for studies published between January 2012 and May 2022 using the following keywords: ("radiomics" OR "texture analysis" OR "textural features" OR "texture features") AND ("stroke" OR "brain ischemia"). Additionally, we performed forward citation searching of relevant articles. Identified studies were screened and assessed based on the eligibility criteria.

Results: Forty eligible studies were included and categorized into five groups: diagnosis, treatment, management, prognosis and prevention. 78% of the studies were published since 2020. Most studies were based on retrospective samples, while ten examined prospective cohorts. Predictions about the diagnosis and prognosis of AIS were the most reported findings, often built upon imaging and clinical variables. In this review, we summarized the selected imaging modalities, number and classes of radiomic features, and the applied validation methods.

Discussion & Conclusion: Radiomic signature holds promise across the whole spectrum of AIS. It may allow the identification of patients at higher risk of events, the detection of new lesions and their onset, and may predict complications, such as haemorrhagic transformation or malignant brain oedema. The efficacy of the created models depends on the quality of the underlying data, hence we discuss recommendations for radiomic-based studies to produce more reproducible pipelines. New clinical tools may be developed in the near future, reinforcing the need to validate the algorithms in real world settings.

Keywords: Acute ischemic stroke, radiomics, review.

1-P60

PURE ARTERIAL MALFORMATIONS – A CASE SERIES

Pedro S. Brandão[1], Sofia Bettencourt[1], Gonçalo Gama Lobo[1], Carla Conceição[1], João Jacinto[1]
[1]Neuroradiology Department, Centro Hospitalar Universitário de Lisboa Central, Lisbon, Portugal

Introduction: The recognition of tortuous, dilated vessels on brain imaging is not always a manifestation of arteriovenous malformations or fistulas. Less common cerebrovascular disorders should also be considered, including pure arterial malformations (PAMs). Defined as dilated, overlapping, and tortuous arteries with a coil-like appearance and/or a mass of arterial loops in the absence of any venous components, most reported cases of PAMs were incidentally diagnosed. There is still debate on the optimal management, but conservative treatment has been proposed as these lesions are generally asymptomatic and stable.
We report 8 cases of PAMs and discuss their distinguishing features.

Methods & Results: We retrospectively collected cases of patients with PAMs and reviewed the demographic and clinical characteristics, imaging findings, and follow-up data.
Eight patients met the inclusion criteria. Six (75%) were female. The mean age at diagnosis was 5 years (patients aged between 2 months and 10 years). The symptoms and reason for imaging varied, with 6 patients (75%) presenting with segmental infantile hemangiomas and/or congenital anomalies, later confirmed PHACE syndrome; 1 with headache; and 1 with fine postural tremor and suspected developmental delay. Involvement of the posterior cerebral artery and posterior communicating artery was the most common (7 lesions affecting at least one of these arteries). The supraclinoid internal carotid artery was involved in 3 cases; in 2 cases each the anterior cerebral artery and the superior cerebellar artery; and the middle cerebral artery in 1 case. An associated aneurysm was present in two patients, both located in the posterior cerebral artery. None had intracranial hemorrhage or infarction attributed to the PAMs. Endovascular treatment was attempted in one patient with unsuccessful aneurysm embolization. Five patients had available follow-up MR imaging that showed no changes.

Discussion & Conclusion: PAMs are rare cerebrovascular disorders that can affect any intracranial artery and may be associated with aneurysms. Often incidental findings and mostly diagnosed in young women, its etiopathogenesis remains unclear. Distinction from other vascular abnormalities and accurate characterization of the PAMs' architecture are mandatory, avoiding unnecessary invasive procedures. Given their benign natural history, it has been proposed that patients with PAMs should be managed conservatively with serial imaging. However, according to the literature, endovascular treatment could be considered when local aneurysms are present. Further investigation on this topic is needed to address and better elucidate the etiology, clinical course, and management of these probably underdiagnosed entities.

1-P61

Impact of an advanced stoke imaging protocol for patients not receiving thrombectomy

Sirindrha Suepiantham[1], Grant Mair[2,3]
[1]Medical School, University of Edinburgh, Edinburgh, United Kingdom. [2]Centre for Clinical Brain Sciences, University of Edinburgh, Edinburgh, United Kingdom. [3]Department of Clinical Neurosciences, NHS Lothian, Edinburgh, United Kingdom

Introduction: Advanced stroke imaging protocols (for example, CT angiography and CT perfusion in addition to non-enhanced CT) are now commonly acquired in many centres to identify and triage potential candidates for thrombectomy. However, the impact of this change on patients who are not offered thrombectomy is unknown.
We aimed to assess whether treatment for acute ischaemic stroke (other than thrombectomy) differed before and after the introduction of an advanced stroke imaging protocol in one comprehensive stroke centre.

Methods: We retrospectively reviewed routinely-collected data for all patients who presented with possible ischaemic stroke to the Royal Infirmary of Edinburgh over two equivalent two month periods, one before (2019) and one after (2021) the introduction of an advanced CT imaging protocol for thrombectomy. For patients within these cohorts who received (2021) or would have received (2019) advanced imaging according to the thrombectomy protocol, we then compared the proportion of patients receiving standard treatments including antiplatelets, thrombolysis or supportive care only. We used Chi-square tests to compare proportions and Mann-Whitney U tests to compare non-parametric ordinal or continuous data. We considered a p-value <0.05 significant.
The local Caldicott Data Guardian approved this analysis as an evaluation of a change in practice.

Results: Over a total of four months, we identified 95 patients given a final diagnosis of ischaemic stroke: 53 males [56%], median age 76 years (interquartile range 67-84.5), median baseline National Institutes of Health Stroke Scale 6 (4-11.5), median time from symptom onset to CT 2.4 hours (1.8-4.9). These variables did not significantly differ between 2019 and 2021 cohorts, nor between those in 2021 who received advanced imaging (n=14) and those in 2019 who would have received advanced imaging (n=14). There were also no significant differences in standard treatment offered before and after the introduction of the advanced imaging protocol; antiplatelets (6/14, 43% in 2021 vs 5/14, 36% in 2019), thrombolysis (7/14, 50% in 2021 vs 8/14, 57% in 2019), supportive care only (1/14, 7% in both groups).

Discussion & Conclusion: Following the introduction of an advanced CT imaging protocol designed to identify candidates for thrombectomy following ischaemic stroke, we found no difference in the use of standard treatments including antiplatelets and thrombolysis. Our analysis is limited by small patient numbers but might provide confidence that advanced stroke imaging does not seem to be detrimental to patients unsuitable for thrombectomy.

1-P62

PREVALENCE OF ACUTE DIZZINESS AND VERTIGO IN CORTICAL STROKE

Oi Yean Wong[1], Yuk Man Chan[2], Diego Kaski[2]
[1]Lysholm Department of Neuroradiology, National Hospital for Neurology and Neurosurgery, London, United Kingdom. [2]Centre for Vestibular and Behavioural Neuroscience, Institute of Neurology, University College London, London, United Kingdom

Background and purpose: In posterior circulation stroke, vertigo can be a presenting feature. However, whether isolated hemispheric strokes present with vertigo is less clear, despite a few single case reports in the literature. Here, (a) the prevalence of vertigo/dizziness in acute stroke is explored and (b) the cortical distribution of the lesions in relation to both the known vestibular cortex and the evolution of the symptoms, are considered.

Methods: Structures interviews were conducted in 173 consecutive unselected patients admitted to the hyperacute stroke unit at the University College London Hospitals. Interview was used to evaluate whether the patient was suffering from dizziness and/or vertigo before the onset of the stroke and at the time of the stroke (acute dizziness/vertigo), and the nature of these symptoms.

Results: In all, 53 patients had cortical infarcts, of which 21 patients reported acute dizziness. Out of these 21, five patients reported rotational vertigo. Seventeen of the total 53 patients had lesions in known vestibular cortical areas distributed within the insular and parietal opercular cortices.

Conclusions: The prevalence of vertigo in acute cortical strokes was 9%, with no single locus of lesion overlap. There is growing evidence supporting a lateralised vestibular cortex, with speculation that cortical strokes affecting the right hemisphere are more likely to cause vestibular symptoms than left hemispheric strokes. A trend was observed for this association, with the right hemisphere affected in four of five patients who reported spinning vertigo at the onset of the stroke.

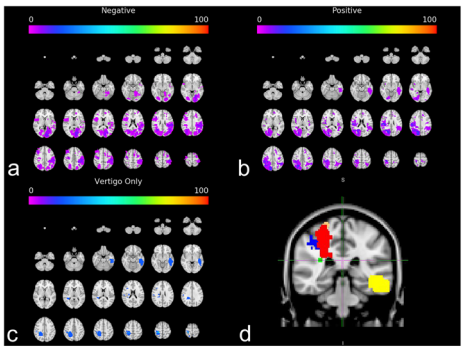

Lesion overlay map showing the locations of acute cortical infarcts in 53 patients on 2 mm MNI brain atlas. Of these, (a) 32 patients did not report symptoms of dizziness, (b) 21 patients were positive for symptoms of acute dizziness and (c) five patients reported rotational vertigo. The colour scale represents the percentage of subjects that had a lesion in the represented area on the map. All three groups had lesions widespread across the cortex, with no clear correlation between vertigo symptoms and involvement of the vestibular cortex. (d) A composite of lesion distribution of the five patients with vertigo. Each patient is represented by a different colour. Four out of five patients had predominantly right-sided lesions.

1-P63

IMAGING REVIEW OF CEREBRAL VENOUS THROMBOSIS: MISSED DIAGNOSIS AND POTENTIAL PITFALLS AND MIMICS

Jesús Prieto Casado[1], Leila Zitan Saidi[1]
[1]HU Torrecardenas, Almería, Spain

Keywords: cerebral venous thrombosis, CT scan, MRI.

Introduction: Cerebral venous thrombosis (CVT) is a rare, but clinically relevant cause of stroke in young adults. CVT is frequently missed or diagnosed late because it can mimic other acute neurological conditions and can only be recognised with optimal and timely brain imaging. The purpose of this statement is to provide an overview of Cerebral Venous System's anatomy, to review the main imaging findings of CVT and to highlight the potential pitfalls in Cerebral Venous Thrombosis.

Methods: We reviewed the relevant literature with an emphasis on reports published in the last 10 years. We searched for the clinical features, diagnosis, and specially imaging findings. Based on the results of the bibliographic search, we collect the most representative cases from our database.

Discussion and results: Unenhanced CT is usually the first imaging investigation performed given the nonspecific clinical presentation in these cases. We can find a subtle finding on CT images, relying on hyperdensity of the sinus being identified (only present in 33% of cases). Potential findings include: cord sign and dense vein sign as direct signs, and vasogenic edema and venous hemorrhage as indirect signs.With contrast administration, especially with a CT venogram, a sinus filling defect is sought. Signs on contrast CT include: empty delta sign, gyral enhancement and prominent intramedullary vein. The main direct sign on conventional MR sequences is an absence of normal flow void inside the affected venous structure and an increased collaterality. The main false negatives are often due to incorrect timely brain imaging. We should know that chronic thrombi are less hyperdense on Unenhanced CT than acute ones, and sometimes there may be enhancement of the thrombus due to the formation of capillaries inside. The main false positives are due to false hyperdensity on unenhanced CT due to dehydration or elevated hematocrit, a potential pitfall is interpreting the distal superior sagittal sinus as being hyperdense near the torcula herophili. Arachnoid granulations and asymmetries in the size of the venous sinuses can simulate filling defects on contrast CT. Possible artifacts must be known of flow in the MR sequences.

Conclusions: CVT is a rare and difficult diagnosis to make. Imaging plays a crucial role in diagnosis and management, follow-up and detection of acute and late complications of this disease, so every radiologist should be familiarized with key imaging features in various modalities.

1-P64

UNILATERAL MASTICATORY MUSCLE ATROPHY DUE TO BRAIN STEM INFARCTION: CASE REPORT

Filip Samardžić[1], Radmila Perić[1], Nikola Anđelić[2], Jasmina Boban[3]
[1]Center for Radiology, Clinical Center of Vojvodina, Novi Sad, Serbia. [2]Center for Imaging diagnostics, Oncology Institute of Vojvodina, Sremska Kamenica, Serbia. [3]Center for Imaging diagnostics, Oncology Institute of Vojvodina, Novi Sad, Serbia

Introduction: Unilateral trigeminal motor neuropathy (UTMN) is characterized by paralysis of the motor branch of the trigeminal nerve with atrophy of masticatory muscles, caused by infection, tumor, trauma, stroke or idiopathic.

Case report: An 86-year-old woman, with long-standing hyeprtension, was referred to brain MRI due to left temporomandibular joint pain, dizziness and leaning to left side. MRI showed a focal lesion at the level of the pons towards the middle cerebellar peduncle on the left side, corresponding to a chronic ischemic lesion, localized in the area of the pontine left trigeminal nerve nucleus (Figure 1a). There was striking left sided fat atrophy of the masticatory muscles (temporalis, masseteric, medial and lateral pterygoid muscles; Figure 1b), without any other focal pathologic findings. Additionally, imaging showed diffuse dilatation of perivascular (Virchow-Robin) brain spaces, global cerebral parenchymal atrophy and few lacunar infarctions of the basal ganglia, mostly thalamic, bilaterally.

Discussion & Conclusion: Unilateral involvement of masticatory muscles with fat atrophy is the most common sign of UTMN. These muscles are innervated by the ipsilateral

trigeminal motor branch, coming from the non-decussating nerve fibers stemming from the pontine nucleus. Pure form of UTNM is affection of motor branches, without involvement of sensory branches of the trigeminal nerve or other cranial nerve. Magnetic resonance imaging and neurophysiological measurements are commonly used to confirm UTMN and to exclude other causes such as tumors or infections. Differential diagnosis should be made if other cranial nerves are involved. Since there are no clear guidelines for treatment of UTMN, therefore determining the etiology should be of the highest priority. The available treatment options for different causes are surgical or pharmaceutical, aiming to relief symptoms and limit the spread of the underlying cause.

Conflict of Interests: We have no conflicts of interest to disclose.

Keywords: Unilateral trigeminal motor neuropathy; MRI; brain stem infarction;

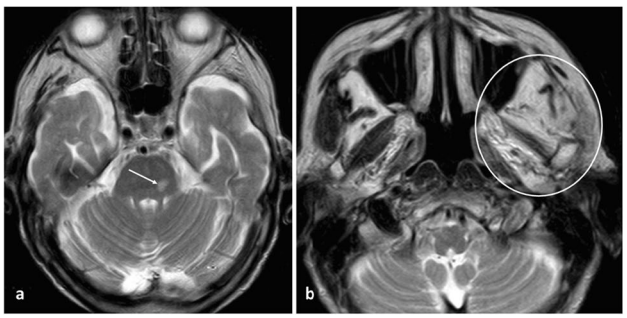

1-P65

A CASE OF PRES ASSOCIATED WITH FOLFOX FOR GASTRIC ADENOCANCER

Şahap Törenek[1], Ezel Yaltirik Bilgin[1], Özkan Ünal[1]
Ankara OncologyTraining and Research Hospital, ANKARA, Turkey

Posterior reversible encephalopathy syndrome (PRES) is a rare disease in which various neurological symptoms should be evaluated together with radiologic findings .It should be kept in mind in case of new neurological symptoms in patients using chemotherapy. We aimed to present a rare case of PRES associated with gastricadenocancer and the use of FOLFOX (folinicacid fluorouracil and oxaliplatin) theraphy with magnetic resonance imaging (MRI).
44-years old male patient with diagnosis of gastric adeno cancer underwent total gastrectomy .After three cures of FOLFOX treatment, visual disturbances and headache complaints occurred in the patient. Neurological examination and blood plessure were normal. MRI showed hyperintense areas in the left temporal, bilateral occipital lobes, right cerebellar hemisphere and bilateral insular subcortical areas in FLAIR images.(Figure) There was no enhancement after postcontrast studies and was not accompanied by diffusion restriction. Control MR images were normal three weeks later and visual impairment and headache were recovered.
PRES is a syndrome in which clinical and radiological findings are seen together, first described by Hincey et al. . A wide variety of neurological symptoms such as confusion, seizures, decreased visualacuity, headache have been reported.
Although the etiology of the disease is not fully known, autoregulation mechanisms and endothelial dysfunction due to hypertension are thought to be effective. Interestingly, however, hypertension was not reported in 20 % of the patients. In our patient, blood pressure was also normal.
Typical MR imaging findings are hyperintensities corresponding to areas of vasogenic edema in subcortical white matter of the occipital and parietal lobes on T2 and FLAIR sequences. In the literature, the occipital and parietal lobes were most frequently involved localization followed by the frontal and temporal lobes. . In addition, cerebellum involvement differentiated our patient from other patients in the literature.
In the literature, a case of PRES has been reported after the use of FLOT regimen due to gastric adenocancer, but no case of PRES has been reported after theuse of FOLFOX for gastric adeno carcinoma. Our patient is also the only PRES case in the literature due to FOLFOX treatment in gastric adenocarcinoma
There are a few PRES cases in the literature after the use of FOLFOX. PRES should be kept in mind in the sudden onset of neurological symptoms in cancer patients using chemotherapeutic drugs and diagnosis should be made with imaging methods.

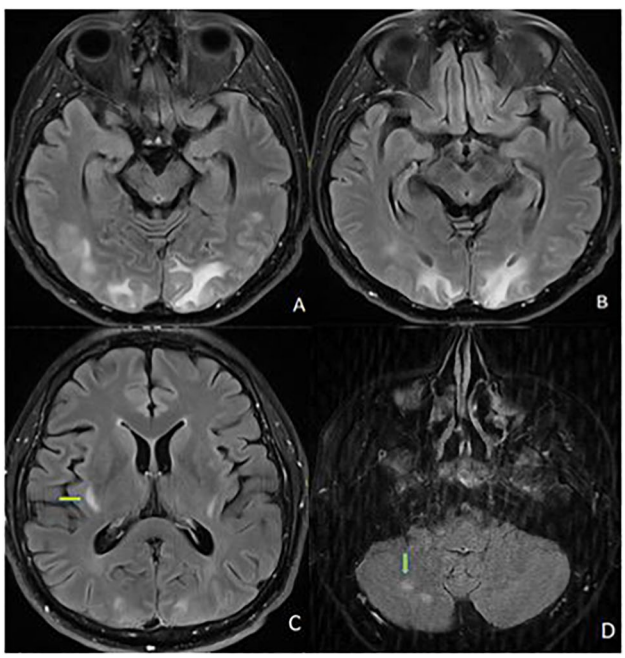

1-P66

CHASING THE STROKE – ANALYSIS OF A SINGLE CENTER EXPERIENCE WITH MULTIMODALITY STROKE IMAGING

Ivana Jevtic[1], Nataliya Toncheva[2], Ronald Antulov[1]
[1]Department of Radiology and Nuclear Medicine, Hospital South West Jutland, Esbjerg, Denmark. [2]Department of Neurology, Hospital South West Jutland, Esbjerg, Denmark

Introduction: Stroke is the second leading cause of death and the third cause of disability worldwide. Acute ischemic stroke (AIS) patients are candidates for reperfusion therapy (RT) which includes intravenous thrombolysis and endovascular treatment in the case of a large vessel occlusion (LVO). Nowadays, different imaging modalities are available to facilitate the decision-making process for RT, but in order to avoid delays in providing the optimal imaging modality for AIS detection, applying a selection criteria based on the assessment of patients done by a neurologist in the emergency department (ED) of a hospital could facilitate the choice of the imaging modality for AIS detection. The National Institutes of Health Stroke Scale (NIHSS) could be a useful LVO prediction instrument. Based on the WAKE-UP trial, patients who awoke with stroke symptoms or have unclear onset of symptoms can be treated with RT based on the DWI-FLAIR mismatch concept. We analyzed the impact of such assessments on the outcomes of our multimodality stroke imaging protocol.

Methods: Our study population included patients with suspected AIS assessed at the ED of our hospital during a period of 10 months. There were 135 patients with a CT examination of the head and 15 patients that had an MRI examination of the head because they were classified as wake-up stroke or stroke with unknown onset.

Results: Of the 135 patients which had a CT examination of the head there were 49 (36%) patients with a NIHSS<6, 56 (41%) patients with NIHSS ≥6, while the rest were not scored. Of the 56 patients with NIHSS ≥6 there were 20 patients without acute findings, 29 patients with acute ischemic changes and 7 patients with acute bleeding. Of the 29 patients with acute ischemic changes, 12 patients underwent endovascular treatment for a LVO. Of the 49 patients with a NIHSS<6, there were 36 patients without acute findings, 10 patients with acute ischemic changes, 1 patient with acute bleeding and 2 patients with other findings like tumors. No patients underwent endovascular treatment in the NIHSS<6 group. Of the 15 patients which were classified as wake-up stroke or stroke with unknown onset, 6 (40%) had a confirmed DWI-FLAIR mismatch on the MRI.

Discussion & Conclusion: Applying an assessment of patients based on NIHSS before multimodality stroke imaging and introducing MRI for patients with wake-up stroke or stroke with unknown onset improves the decision-making process for RT.

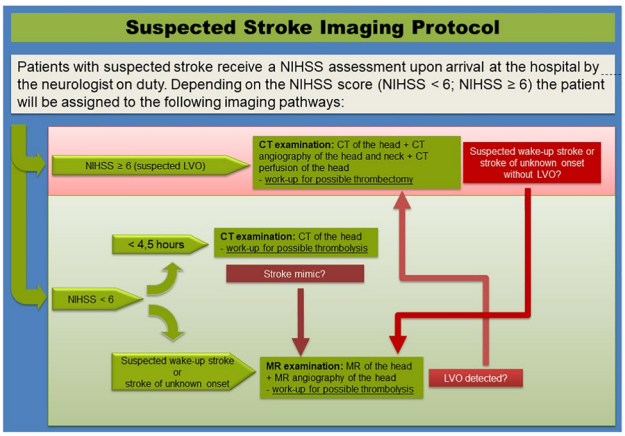

VARIOUS

1-P67

HEADACHES DURING PREGNANCY: THE ROLE OF NEUROIMAGING

Rosa Couto[1], Francisca Sena Batista[1], Filipa Castelão[1], Diogo Marques[1], Ana Cristina Rios[1], Mariana Diogo[1]
[1]Hospital Garcia de Orta, EPE, Almada, Portugal

Headache is a common yet challenging symptom during pregnancy. Whereas women of reproductive age have an increased likelihood of developing primary headache disorders orchanges in their character, frequency or severity, a secondary headache can be diagnosed in up to one third of women during gestation. Secondary headaches are common manifestations of pregnancy complications, like intracranial hypertension, preeclampsia and eclampsia, or reversible cerebral vascular syndrome, that should be swiftly excluded or addressed. When evaluating pregnant women for headache, a detailed history and a complete neurological examination are critical in order to recognize red flags as pregnant women are at increased risk of acute neurologic events. It can be just as relevant to perform adequate and timely image studies, most MR imaging, whenever available. The aim of this presentation is to present illustrative cases of imaging findings of pregnant patients presenting with headache, cerebral venous and sinus thrombosis, posterior reversible encephalopathy syndrome, reversible cerebral vasoconstriction syndrome, haemorrhagic or ischemic stroke, idiopathic intracranial hypertension, and pituitary apoplexy. Pearls and pitfalls will be presented. We will also

briefly discuss key points in the radiologist's decision making in the sometimes thin balance between risk and benefit of exams in this patients. The aim of this work is to critically correlate brain imaging findings of pregnant women who sought medical observation for headaches with non-reassuring features.

1-P68

ENTORHINAL CORTEX ATROPHY SCORE'S INTER-OBSERVER AGREEMENT

Marcos Rosa-Junior[1], Isabela Dutra[1], Fernanda Ferreira[1], Karen Dias[1]
[1]Hospital Universitário Cassiano Antônio Moraes da Universidade Federal do Espírito Santo, Vitória, Brazil

Introduction: Alzheimer's Disease (AD) definitive diagnosis is a challenge, especially on early stages. In radiology, this effort is pursued by ERICA Score (ES), a method based on visual stratification of atrophy at the Entorhinal Cortex, implied as the first topography compromised by AD. Aiming the validation of this tool, the present study analyses the interobserver agreement (IA) of ES in a Brazilian center.

Methods: This retrospective study analyzed the two hemispheres of all MRI brain images obtained with the volumetric T1-SPGR sequence before contrast in our service between 2016 and 2017 on Philips Achieva 1.5T. Each exam was independently graded by two examiners using the ES. Results were compared using linearly weighted Kappa (K).

Results: On both hemispheres, moderate interobserver reliability was found. Right hemisphere: K = 0,4785; CI 95% [0,2420; 0,7151]; statistically different from zero, reliability = 72,5%. Left hemisphere: K = 0,5526; CI 95% [0,3330; 0,7723]; statistically different from zero, reliability = 78,4%.

Discussion: Despite the scarce evidence about ES in the literature, a moderate IA on this study supports its potential in clinical practice. Although the agreement was only moderate in the analysis of the ES from 0 to 3, when we grouped patients into two groups - ES 0 and 1 (normal volume) x ES 2 and 3 (atrophy compatible with AD) the evaluators agreed in all cases, which reinforces its use for diagnosis. Still, the absence of accurate diagnostic tools or biomarkers for AD limits its application.

Conclusion: The ERICA Score had a satisfactory IA performance, with moderate reliability results. Hence, the adoption of this tool in medical schools should be encouraged for further validation.

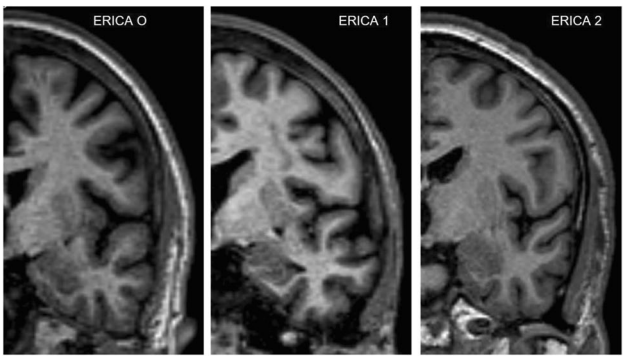

1-P69

USE OF REAL-LIFE SAFETY DATA FROM INTERNATIONAL PHARMACOVIGILANCE DATABASES TO ASSESS THE IMPORTANCE OF SYMPTOMS ASSOCIATED WITH GADOLINIUM EXPOSURE (SAGE)

Imran Shahid[1], Alvin Joseph[2], Eric Lancelot[3]
[1]Guerbet, London, United Kingdom. [2]Guerbet, Princeton, USA. [3]Guerbet, Villepinte, France

Objective: Recent scientific publications have reported cases of patients who complained from a variety of symptoms after they received a gadolinium-based contrast agent (GBCA). The aim of this study was to appreciate the importance of these clinical manifestations in the overall population by assessing the weight of "symptoms associated with gadolinium exposure" (SAGE) among the bulk of safety experiences reported to major health authorities.

Materials and Methods: SAGE symptoms were identified from a review of the scientific literature, and the corresponding preferred terms (PTs) were searched in each system organ class (SOC) category recorded in the European and North American pharmacovigilance databases, EudraVigilance (EV) and FDA Adverse Event Reporting System (FAERS), respectively. The numbers of SAGE symptoms per PT, and cumulatively per SOC, were recorded and their weights in the overall spectrum of AEs was determined for each GBCA.

Results: The literature search led to identify 11 articles from which the most prevalent symptoms of "gadolinium deposition disease" (GDD) were selected. The extraction and analysis of such AEs in EV and FAERS revealed a significantly higher SAGE weight for gadobenate dimeglumine (EV: 25.83%, FAERS: 32.24%) than for gadoteridol (EV: 15.51%; FAERS: 21.13%), and significantly lower SAGE weights for gadobutrol (EV: 7.75%; FAERS: 13.31%) and gadoterate meglumine (EV: 8.66%; FAERS: 12.99%). The SOCs "skin and subcutaneous tissue disorders", "musculoskeletal and

connective tissue disorders", "general disorders and administration site conditions" and "psychiatric disorders" were consistent with this ranking, with gadoteridol showing alternately a SAGE profile aligned on the linear GBCA or on the other macrocyclic GBCAs.

Conclusion: This study showed that SAGE symptoms represent a significant percentage of the bulk of adverse events reported to the health authorities for each GBCA. It provided real-life arguments suggesting that SAGE symptoms may be more prevalent with linear than macrocyclic GBCAs, and that gadoteridol may present a higher SAGE risk than the other macrocyclic contrast agents.

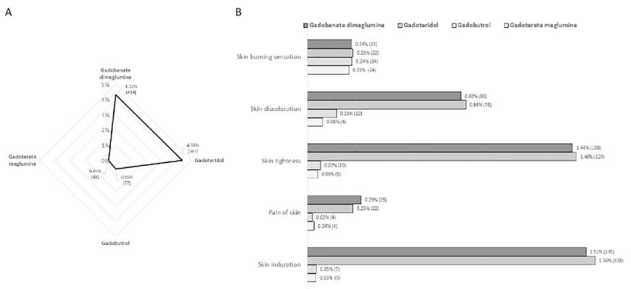

1-P70

NEWLY EMERGING ARTEFACTS IN MODERN NEURORADIOLOGY MR-EXAMS

Catalin George Iacoban[1], Benedikt Sundermann[1], Christian Mathys[1]
[1]Evangelisches Krankenhaus Oldenburg, Medical Campus University of Oldenburg, Oldenburg, Germany

Introduction: With the advent of new generation MR sequences and their practical implementation in routine neuroradiological studies, novel artefacts are being increasingly encountered and should not be mistaken for pathology.

Methods: Educational case series based on our institutional practical experience and on review of the current literature regarding modern MR-sequences and acceleration techniques.

Results: 3D-sequences are nowadays highly beneficial to brain imaging protocols, allowing good lesion detection and providing excellent topographic information as well as an excellent basis for follow-up imaging and intraoperative navigation. Among them, 3D-FLAIR has gained a pivotal role in imaging protocols of many diseases such as multiple sclerosis. Movement in 3D-FLAIR can cause small signal fluctuations and mimic cortical lesions, therefore requiring an adaptation phase for appropriate reporting. 3D "black blood" T1-weighted imaging is a core sequence of vessel wall imaging, for example in vasculitis. Slow flow in superficial veins can however cause hyperintensity and may be mistaken for arterial vessel wall pathology. Dixon techniques have gained ground both in spinal as well as in head/neck imaging providing a relatively homogeneous fat suppression. They allow calculation of both fat-saturated and non-fat-saturated images from a single acquisition and can be applied to a wide range of basic sequences (e.g. T1, T2, PD, etc.), being available both for 2D as well as for 3D-sequences. The Dixon fat suppression technique is susceptible to "computational" artefacts, such as the so-called "fat-water-swap" artefact. Acceleration techniques such as simultaneous multi-slice imaging are prone to "slice leakage" artefacts as well as cross-talk phenomena, depending on the applied acceleration factor, the number of slices and the field of view shift factor.

Conclusion: (Neuro-)radiologists should become familiar with and correctly assess novel artefacts encountered in recently implemented MR-sequences and modern acceleration techniques.

Keywords: MR artefacts, 3D-sequences, Dixon technique, acceleration techniques

1-P71

TEXTILOMAS SINGLE-CENTER CASE REVIEW: A DIAGNOSTIC CHALLENGE

Gonçalo Gama Lobo[1], Danila Kuroedov[1], João Gonçalves[1], Dalila Forte[2], Amets Sagarribay[2], Carla Conceição[3]
[1]Neuroradiology Department, Hospital de São José, Centro Hospitalar Lisboa Central, Lisbon, Portugal. [2]Pediatric Neurosurgery Department, Hospital Dona Estefânia, Centro Hospitalar Lisboa Central, Lisbon, Portugal. [3]Neuroradiology Department, Hospital Dona Estefânia, Centro Hospitalar Lisboa Central, Lisbon, Portugal

Introduction: Textilomas are defined as expansile inflammatory/granulomatous lesions that arise in the surgical bed as a response to hemostatic material. Textiloma formation in a tumor-resected area can be alarming and lead to invasive unnecessary procedures. Therefore, even though they are extremely rare, this diagnosis is of uttermost importance with dramatic changes to the approach, preventing invasive procedures.

MRI can help differentiating textiloma from a true tumor residue or recurrence based on its characteristics: lower T2 signal, lack of restricted diffusion and a "ring and bubble" enhancing pattern. A conservative and watchful approach with close follow-up will reveal a progressively decreasing lesion with eventual spontaneous resolution.

Methods: We reviewed the resected tumors data base from our pediatric tertiary center from the last 10 years to identify the cases that matched these imaging characteristics.

Results: In the aforementioned period, we found 3 cases of post-tumor resection textilomas that occurred in the last trimester of 2020. We hereby describe these clinical cases and their MR findings that are in accordance with the literature. All the 3 cases were closely followed-up and revealed progressive resolution.

Discussion & Conclusion: Textilomas in a tumor-resected area are a very rare entity but represent a potential harm for patients when misinterpreted. Its diagnosis can change the medical approach and prevent unnecessary invasive procedures.
When retrospectively reviewing our resected tumors database we found 3 cases of post-tumor resection textilomas, all happening in a recent time, without any prior case in the other past 10 years. After investigating we found that the surgical oxidized cellulose and hemostatic gel brands had been replaced just before the surge of these cases. In our understanding, even though we could not confirm in which patients the new material had been used, this material change might be the cause of the sudden occurrence of textilomas, which to our knowledge had never happened before. The decrease and progressive resolution in all our cases highlight the importance of a conservative watchful and non-invasive approach.

1-P72

TEMPORAL ENCEPHALOCELES AND DRUG RESISTANT EPILEPSY: IS THERE RADIOLOGICAL CORRELATION WITH THE EPILEPTOGENIC FOCUS?

Aleix Jareño Badenas[1], Mario Matute González[1], Fernando Diego Choque Chávez[1], Tomas Fernández Rovira[1], Alex Gil Ordoñez[1], Àngel Castillo Fortuño[1], Valeria Richart Sierra[1], Antonio Morales Rosa[1], Núria Bargalló Alabart[1], Santiago Medrano Martorell[1], Sofía González Ortiz[1]
[1]Hospital Clinic de Barcelona, Barcelona, Spain

Introduction: Encephaloceles are protrusions of cerebral tissue through a skull defect. They are a possible cause of epilepsy, although their actual epileptogenic potential has not been assessed yet. Lately, with the improvement of MRI imaging, the identification of encephaloceles in patients with drug resistant epilepsy (DRE) has increased. The purposes of this study are:
To correlate the location of encephaloceles with the epileptogenic focus in patients with DRE.
To evaluate their characteristics and to correlate them with their epileptogenicity.

Methods: We performed a retrospective analysis of the MRI and neurofunctional studies of patients of our epilepsy unit with DRE and an MRI diagnosis of encephalocele.
We evaluated the correlation between the encephalocele's location and the epileptogenic focus, as well as their characteristics (number, location, size and presence of gliosis).
The location and characteristics of the encephaloceles were evaluated in the 3T MRI studies with a specific epilepsy protocol.
The epileptogenic focus was evaluated in our epilepsy unit after the evaluation of different neurofunctional techniques (video-EEG, PET/SPECT and SEEG).

Results: We had a study population of 11 patients (7 women and 4 men) with a mean age of 24.6 years.
Six (55%) patients had correlation between the epileptogenic focus and the location of the encephalocele, whilst in the other 5 (45%) they were not matching.
67% of the patients with correlation showed gliosis and a mean encephaloceles volume of 0.25cc, while 40% of patients without correlation presented gliosis and a mean volume of 0.33cc.

Conclusions: Our results show that encephaloceles have to be considered as potentially epileptogenic lesions in patients with DRE. Gliosis may be an indicator of higher epileptogenicity. In our group of patients, the smaller encephaloceles were more epileptogenic, which is inconsistent with previous literature.

Patient	Gliosis	Volume (cc)
Patients with correlation (55%)		
2	NO	0,64
4	YES	0,22
6	YES	0,14
7	NO	0,03
9	YES	0,04
11	YES	0,12
TOTAL	4/6 67%	0,25
Patients without correlation (45%)		
1	YES	0,49
3	NO	0,16
5	YES	0,45
8	NO	0,42
10	NO	0,14
TOTAL	2/5 40%	0,33

1-P73

EVALUATION OF CENTRAL NERVOUS SYSTEM INVOLVEMENT IN PATIENTS UNDERGOING CAR-T THERAPY BY MAGNETIC RESONANCE IMAGING

Fernando Diego Choque Chavez, Aleix Jareño Badenas, Mario Matute Gonzalez, Tomas Fernandez Rovira, Marta Español Rego, Mariona Pascal, Daniel Benitez-Ribas, Laura Oleaga Zufiria
Hospital Clinic of Barcelona, Barcelona, Spain

Introduction: Immune effector cell-associated neurotoxicity syndrome (ICANS) can occur in patients following Chimeric Antigen Receptor (CAR) T-cell therapy. Imaging findings are fully established. Our purposes are:
To list the clinical manifestations ICANS associated to CAR T-cell therapy.
To identify the Magnetic Resonance Imaging (MRI) findings in CAR-T neurotoxicity.

Methods: Retrospective analysis of the MRI studies performed in 18 patients treated with CAR-T therapy and neurological symptoms after the therapy. Five cases were discarded from the analysis due to the presence of other non-related brain pathology in prior examinations.
We evaluated a neurological symptoms scale to assess severity, duration of symptoms, baseline brain MRI and a post-therapy MRI (performed in cases with neurological clinical manifestations after the CAR-T therapy).
MRI studies were performed on a 1.5T and 3T units. The protocol included T1W, T2W, FLAIR, SWI, DWI and T1W post gadolinium sequences. Images were analyzed to evaluate: 1) presence of T2/FLAIR increased signal in the white matter, dorsal midbrain, medulla, and basal ganglia; 2) transient lesions of the splenium of the corpus callosum; 3) presence of diffuse punctate deposits of hemosiderin distributed in white matter; and 4) presence of leptomeningeal enhancement.

Results: The final number of cases analyzed were 13 (9 men, 4 women) with a mean age of 40.7 years. Six patients with acute lymphoblastic leukemia and 7 patients with lymphoma.
Neurological symptoms after therapy included: fever in nine cases, disorientation in five cases, tremor in four cases, seizures in two cases, nystagmus in one case and hypoesthesia in one case. Severity of the symptoms was: grade 1 in three cases, grade 2 in five cases, grade 3 in three cases and grade 4 in two cases.
We found one case of diffuse bilateral symmetric leukoencephalopathy and one case with punctate deposits of hemosiderin diffusely distributed in the white matter. In one case, we demonstrated a concurrent bilateral human herpesvirus 6 encephalitis.

Discussion & Conclusion: Imaging findings in ICANS are present in less than one third of patients (24% in our series) and are not fully understood. MRI findings are unspecific, but we should look for white matter alterations and hemosiderin deposits. Although not found in our series, leptomeningeal enhancement, cerebral edema, intracranial hemorrhage, and cortical diffusion restriction should be considered.
MRI may help in the development of new preventive strategies and guide therapeutic approaches.

Table 1: Patient demographics and Clinical Features

Characteristic	No. of Patients (*n* = 13)
Age (years)	40,7
Sex	
Male	9 (69%)
Female	4 (31%)
Malignancy	
Acute lymphoblastic leukemia	6 (47%)
Primary mediastinal lymphoma	2 (15%)
DLBCL	2(15%)
Folicular lymphoma	1 (8%)
Mantle Cell Lymphoma	2 (15%)
Anti-CD19 CAR T-cell product	
ARI-0001	6 (47%)
Yescarta	5 (38%)
KTE-X19	2 (15%)

1-P74

MRI ALTERATIONS IN PATIENTS WITH PSYCHOGENIC NON-EPILEPTIC SEIZURES: PREVALENCE, DISTRIBUTION AND CLASSIFICATION OF THE FINDINGS

Sofía González-Ortiz[1], Martio Matute[1], Fernando Diego Choque[1], Tomás Fernandez Rovira[1], Luis Pintor[1], María Centeno[1], Estefanía Conde[1], Núria Bargalló Alabart[1], Aleix Jareño Badenas[1]
[1]Hospital Clinic, Barcelona, Spain

Introduction: Psychogenic non-epileptic seizures (PNES) are paroxysmic episodes that mimic an epileptic crisis without an electroencephalographic translation. A conversive psychiatric origin is attributed to this kind of episodes. However, beyond this psychiatric perspective, the possible neurobiological basis of the pathology has not received much attention. Some studies have documented structural and functional alterations in these patients, but without consistent results to support a causative hypothesis. The objectives of this study are:
To evaluate the MRI findings in patients with PNES
To classify the results
To evaluate a possible structural basis of these episodes

Methods: We performed a retrospective analysis of the MRI studies conducted on patients of our epilepsy unit with a confirmed diagnosis of only PNES or epilepsy and PNES.

A descriptive study of the findings in both groups was performed and compared with the incidental findings in the general population obtained from literature.
The radiologic findings were classified into: vascular, tumoral, posttraumatic/gliotic, small vessel, cortical, hippocampal sclerosis, unspecific or normal studies, as well as into epileptogenic and non-epileptogenic.

Results: Our study population was formed of 60 patients with a confirmed diagnosis of PNES and 16 patients with epilepsy and PNES (75% women, 25% men, mean age at diagnostic of 41 years).
55% of the patients with PNES had a pathologic finding, and 13% had a finding considered epileptogenic, whilst in the group with PNES and epilepsy, 81% showed a pathologic finding, and 31% were considered epileptogenic.
The most frequent findings in the PNES group were unspecific, vascular and hippocampal sclerosis in this order, whilst in the epilepsy and PNES group were unspecific, hippocampal sclerosis and small vessel.

Conclusions: Patients with PNES have a higher prevalence of abnormalities in MRI than the general population (around 18% according to existing literature) and this prevalence is even higher when associated with epilepsy.
There is a higher prevalence of PNES among women.

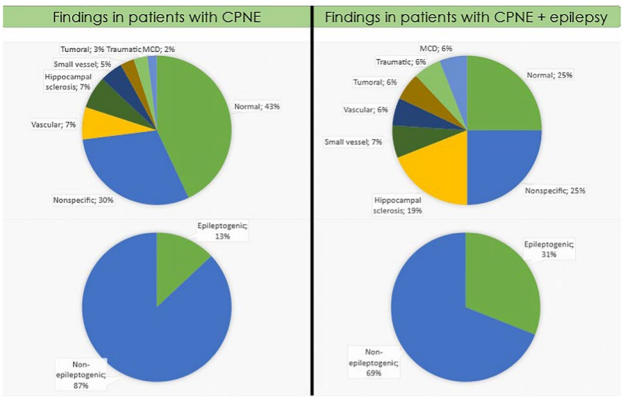

1-P75

CRANIAL NERVE ENHANCEMENT - SINGLE-CENTER CASE REVIEW

João Gonçalves[1,2], Gonçalo Gama Lobo[1], Danila Kuroedov[1], Roberto Carranca[1], Carolina Pinheiro[1]
[1]Neuroradiology Department, Hospital de São José, Centro Hospitalar Lisboa Central, Lisbon, Portugal. [2]Unidade de Neurorradiologia, Hospital Central do Funchal, Funchal, Portugal

Introduction: Cranial nerve enhancement on MRI is seen in a myriad of entities that cause disruption of the blood-brain barrier, resulting in leakage and accumulation of contrast in the perineurium. Infection, inflammation, neoplasm, hereditary diseases and iatrogenic causes are some of the various etiologies of this imagiologic pattern.

Method: We retrospectively reviewed the cranial nerve enhancement cases from our center and provide a pictorial review depicting the key clinical and imaging findings that can help narrow down the differential diagnosis.

Results: In these series we describe 6 cases of cranial nerve enhancement including Miller Fisher Syndrome, Chronic inflammatory Demyelinating Polyneuropathy, Ramsay-Hunt Syndrome, Lyme Disease, Lymphoma and Meningeal Carcinomatosis.

Conclusion: Cranial nerve enhancement is a generic MRI pattern that may be the first imaging finding of an undiagnosed disease. The enhancing pattern together with other imagiologic findings, as well as the clinical history, patient examination and laboratory results, might help us in the right diagnostic workup.

Keywords: Cranial, Nerve, Enhancement, MRI.

1-P76

EFFICACY AND SAFETY OF GADOPICLENOL FOR CENTRAL NERVOUS SYSTEM (CNS) MAGNETIC RESONANCE IMAGING (MRI): RESULTS FROM THE PHASE III PICTURE TRIAL

Christoph Groden[1], Anna Pichiecchio[2], Balint Kolumban[3], Gabor Hutoczki[4], Katarzyna Dziadziuszko[5]
[1]Department of Neuroradiology, Universitätsmedizin Mannheim, University of Heidelberg, Mannheim, Germany. [2]IRCCS Mondino Foundation, Pavia, Italy. [3]Department of Neurosurgery, University of Pécs, Pécs, Hungary. [4]Department of Neurosurgery, Faculty of Medicine, University of Debrecen, Debrecen, Hungary. [5]II Department of Radiology, Medical University of Gdańsk, Gdańsk, Poland

Introduction: Gadopiclenol is a high relaxivity GBCA, developed by Guerbet and currently under review by regulatory authorities. This study aimed to demonstrate the non-inferiority of gadopiclenol at 0.05 mmol/kg to gadobutrol at 0.1 mmol/kg for CNS MRI.

Methods: This international, randomized, double-blind, controlled, cross-over study included 256 patients with CNS lesions. The patients were randomized to undergo two MRIs with gadopiclenol then gadobutrol or vice versa (interval of 2 to 14 days). The primary criterion was lesion visualization, based on 3 parameters (border delineation,

internal morphology and contrast enhancement), assessed by 3 independent off-site blinded readers. Overall diagnostic preference was assessed in a global matched-pairs fashion by 3 additional blinded readers. Adverse events (AEs) were collected up to one day post-second MRI.

Results: For all readers, and all visualization co-criteria, the difference in mean of scores showed the non-inferiority of gadopiclenol to gadobutrol (lower limit of 95% CI ≥-0.06, above the non-inferiority margin [-0.35], p<0.0001).
Blinded readers preferred images with gadopiclenol in 44.8% to 57.3% of evaluations, reported no preference for 21.6% to 40.7% of evaluations, and preferred images with gadobutrol in 14.5% to 24.1% of evaluations (p<0.001).
AEs were reported similarly after MRI with gadopiclenol (14.6%) and gadobutrol (17.6%). AEs considered related to gadopiclenol (4.9%) and to gadobutrol (6.9%), were mainly injection site reactions, and none of these AEs was serious.

Conclusion: MRI with gadopiclenol at 0.05 mmol/kg is non-inferior to gadobutrol at 0.1 mmol/kg for CNS lesion visualization. Gadopiclenol showed a good safety profile.

1-P77
EXPLORING THE DEPTHS IN NEUROIMAGING FOR DEEP BRAIN STIMULATION PLANNING

Ricardo Pires[1], Pedro Monteiro[2], Ricardo Pereira[2], Daniela Pereira[1]
[1]Functional Unit of Neuroradiology, Department of Medical Imaging, Coimbra Hospital and University Centre, Coimbra, Portugal. [2]Department of Neurosurgery, Coimbra Hospital and University Centre, Coimbra, Portugal

Introduction: Deep brain stimulation (DBS) has been approved for treatment of refractory movement disorders and medically refractory epilepsy and is used for neuropsychiatric indications in recent trials. The role of neuroimaging in successful and consistent DBS results is critical. Neuroimaging is used for preoperative selection of patients and to identify landmarks which help accurately localize target nuclei.

Methods: Brief review and pictorial description of the role of MRI techniques in DBS planning process.

Results: T1-weighted imaging is commonly employed due to its ability to produce thin slice, high resolution acquisitions within short periods. T2-weighted MRI can better visualize subcortical structures with high metal concentration. FGATIR combines benefits from both, being a short scan time with consistent high contrast and high resolution. DTI data generates imaging maps that correspond to the potential orientation of white matter tracts.

Discussion: Although still limited by the generally inadequate resolution for the small target structures and complex surrounding anatomy, as well as motion artifacts, imaging plays a central role on the preoperative evaluation and selection of patients who are candidates for DBS. In some cases, abnormalities such as atrophy, leukoencephalopathy, or multiple lacunae, may preclude the procedure. The next step is then the accurate determination of the target location, ideally direct localization on structural MRI sequences, like T1w 3D-MPRAGE and T2w imaging (particularly useful for the subthalamic nucleus). Inversion-recovery sequences, like FGATIR, represent an interesting complementary tool at the subcortical level (internal globus pallidus, anterior thalamic nucleus) due to its high contrast between grey and white matter. The integration of DTI tractography imaging in the presurgical MRI allows a better understanding of the structure of white matter, including pathways that may be targeted, used to infer the localization of the target structure, or that need to be avoided. Stereotactic coordinates of the target are obtained relative to a stereotactic frame positioned on the patient's head – this can be done in MR alone or using an MRI/stereotactic-CT dataset co-registration for anatomic localization. The implantation trajectory can then be adequately planned.

Conclusions: DBS is an actively developing field, with a rapidly increasing number of patients and many emerging new targets and new applications. Neuroimaging is crucial in the preoperative, perioperative, and postoperative context. Further research is required to improve on the current limitations of imaging techniques and validate the use of more novel sequences in clinical practice.

1-P78
THE STRANGE CASE OF MATRIOSKA

Caterina Bombardieri[1], Kurt Pardatscher[2], Claudio Ceccotti[3]
[1]Neuroradiology Unit, Azienda Ospedaliera Universitaria "Mater Domini", Catanzaro, Italy. [2]Retired Full Professor of Neuroradiology, Catanzaro, Italy. [3]Retired Chief of Neurosurgery, Catanzaro, Italy

Introduction: Chronic calcific subdural hematoma is rarely seen, accounting for 0.3-2.7% of subdural hematomas. It is found more frequently in children than in adults. When the exclusive and uniform calcification of the periphery of the hematoma, with a gelatinous internal content, is obtained, we speak of a chronic "ossified" subdural hematoma (1). This image is defined in international literature as "matryoshka head" (2), matryoshka skull, or "armored brain" (3), armored brain.

Methods: We present the case of a patient suffering from the so-called "matryoshka skull", who was able to evaluate twelve years with different methods, CT and MRI, for a long period of time.

Discussion: We discuss the etiology, the pathophysiological mechanism, the neuroradiological picture, the clinical aspect, the prognosis, the therapeutic options and any differential diagnoses of this singular condition found for the first time, during an autopsy, in 1844 by the Bohemian pathologist Carl von Rokitansky.

Conclusions: Chronic "ossified" subdural hematoma, in which a skull appears to be present in the skull, is a rare condition, with varied clinical manifestations, which requires thoughtful evaluation, as it poses many problems in case of surgical treatment (3).

References: 1 - Turgut M, Akhaddar A, Turgut AT. Chronic calcified or ossified subdural hematoma: a systematic review of 114 cases reported in the past century with a demonstrative case report. World Neurosurgery 2020. 134: 240-263. 2 - Sgaramella E, Sotgiu S, Miragliotta G et al. “Matryoshka head”. Clinical case of chronic calcified subdural hematoma. J Neurosurgery Sc 2002. 46: 28-31. 3 - Petraglia AL, Moravan MJ, Jahromi BS. Armored brain: a case report and literature review. Surgic Neurol Intern 2011. 2: 120. Keywords: Matryoshka head, armored brain, bilateral calcified chronic subdural hematomas

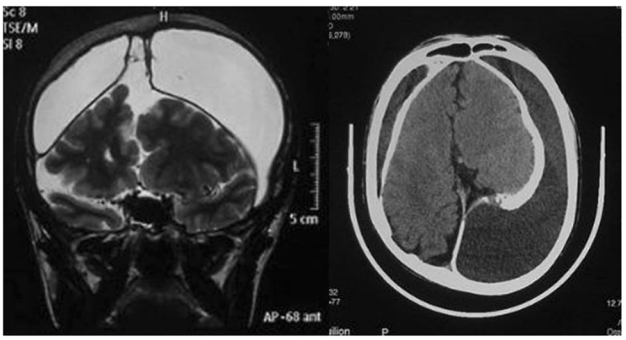

1-P79

CYTOTOXIC LESIONS OF THE CORPUS CALLOSUM, ABOUT TWO CASES

Cesar Zabaleta[1], Alejandro Boero[2]
[1]Rossi Center, Buenos Aires, Argentina. [2]Chief Rossi Center Imaging Unit – Finochietto Sanatorium, Buenos Aires, Argentina

We report two cases of a 27 and 38 years old male with magnetic resonance findings of cytotoxic lesions in the corpus callosum no previous medical history.

Cytotoxic lesions of the corpus callosum are secondary lesions associated with various entities including viral illness, drug toxicity, seizures, malignancy, subarachnoid hemorrhage and metabolic disturbances. Are non-specific findings on brain Magnetic Resonance Imaging (MRI) associated with reversible neurological signs, such as behavior changes.

The involvement of the corpus callosum typically shows one of three patterns: A small round or oval lesion located in the center of the splenium, a lesion centered in the splenium but extending through the callosal fibers laterally into the adjacent white matter, or a lesion centered posteriorly but extending into the anterior corpus callosum. On diffusion-weighted magnetic resonance (MRI) images, manifest as areas of low difusión, lack enhancement on contrast material enhanced images, tend to be midline, and are relatively symmetric.

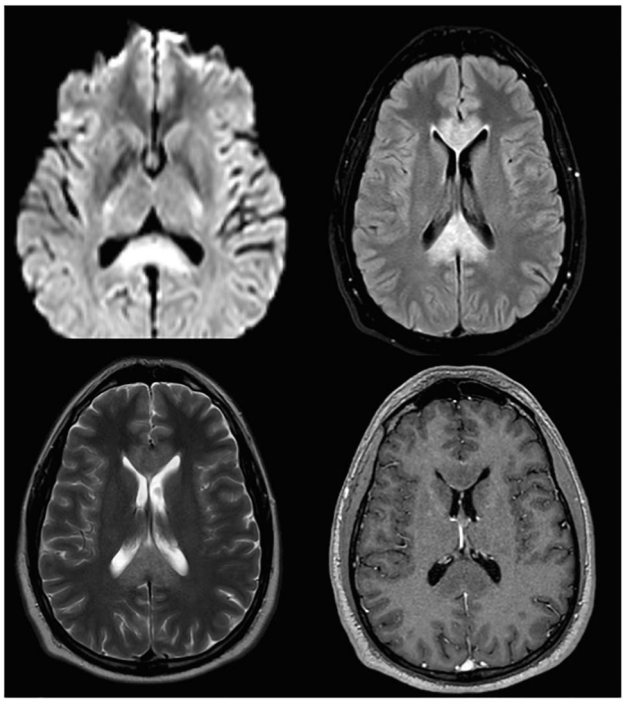

1-P80

VOXEL-BASED AND SURFACE-BASED MORPHOMETRY STUDY OF THE EARLY-STAGE OF CARBON MONOXIDE POISONING-INDUCED PARKINSONISM

Yanli Zhang[1], Junqiang Lei[1], Shunlin Guo[1], Tianhong Wang[1]
[1]The first hospital of Lanzhou university, Lanzhou, China

Purpose: Gray matter (GM) volume change in carbon monoxide poisoning (COP)-induced parkinsonism have been investigated in previous studies. However, a combining

analysis of voxel-based morphometry (VBM) and surface-based morphometry (SBM) is still lacking.

Methods: Eighteen CO-induced parkinsonism patients and 22 healthy controls (HCs) were enrolled in this study. All MRI scans were performed within 3 months after COP, and the datas were measured with a combination of VBM and SBM. Relationships between structural changes and clinical scores were detected with partial correlation analysis.

Results: VBM analysis showed reduced GM volumes in the bilateral frontal, temporal, anterior cingutate (ACC), amygdala, olfactory, striatum, thalamus, and cerebellum (FDR corrected $P < 0.001$), and it also showed a trend of white matter atrophy of the anterior cerebral and medial mesencephalon but swelling of the posterior cerebral and motor cortex area (uncorrected $P < 0.001$) in the patients group. SBM analysis showed widespread cortical thinning extended beyond frontotemporal regions and involved occipitoparietal areas, meanwhile, regional shallow sulcal depth in left supramarginal gyrus in the patients (FWE corrected $P < 0.05$). The motor severity was correlated with GM atrophy in the medial orbital superior frontal gyrus (SFG), ACC, caudate, thalamus, and caudal middle frontal gyrus, while nonmotor disorders was associated with GM atrophy in the SFG, ACC, thalamus, amygdala, and crus I of cerebellum (all $P < 0.05$).

Conclusion: Early-stage COP-induced parkinsonism patients are characterised with widespared GM atrophy. A combination analysis of VBM and SBM contribute to reveal the imaging pathological feature.

2. INTERVENTIONAL

ANEURYSMS

2-P1

DIFFERENT RESCUE APPROACHES OF MIGRATED WOVEN ENDOBRIDGE (WEB)-DEVICES: AN ANIMAL STUDY

Andreas Simgen[1]
[1]Department of Neuroradiology, Saarland University, Homburg/Saar, Germany

Purpose: Treatment of wide-necked intracranial aneurysms using the Woven Endobridge (WEB) device has become widely used. Feared complications with the potential of increased poor clinical outcome include dislocations and migration of the device. We sought to determine the effectiveness of a variety of different strategies to rescue migrated WEB devices.

Methods: In a porcine model, WEB devices of different sizes (SL 3.5x2 and SL 4.0x3, SL 8x5 and SLS 8) were placed into both the subclavian and axillary arteries. A total of 32 rescue maneuvers (8 per rescue device) were performed. Small WEBs were rescued using reperfusion catheters (RCs) (SOFIA Plus and JET 7), larger WEBs were rescued using dedicated rescue devices (Microsnare and Alligator). Rescue rates, times, attempts and complications were assessed.

Results: Rescue attempts of migrated WEBs were successful in all cases (100%). Rescue time (p= 0.421) and attempts (p= 0.619) of small WEBs using RCs were comparable without significant differences. Sole aspiration of larger WEBs was not successful. Rescue of larger WEBs was slightly faster (122.75 ± 41.15 sec vs. 137.50 ± 54.46 sec) with fewer attempts (1 vs. 1.37) when using the Microsnare compared to the Alligator device. Complications such as entrapment of the WEB in the RCs, vasospasm, perforation, or dissection were not observed.

Conclusions: Rescue of migrated WEB devices is a feasible and effective method. One hundred percent rescue rates and appropriate rescue times can be achieved for small WEBs using RCs and for larger WEBs using dedicated rescue devices (Microsnare and Alligator).

2-P2

SURGICAL TREATMENT FOR UNRUPTURED ANTERIOR COMMUNICATING ARTERY ANEURYSM.(RESULT OF ENDOVASCULAR TREATMENT AS THE 1ST LINE TREATMENT)

Masaru Hirohata[1]
[1]Kurume University Hospital, Kurume, Japan

Objective: We report the results of endovascular surgery as the first-line treatment for unruptured anterior communicating artery aneurysms.

Methods: Fifty-seven patients (F:M, 30:27; mean age, 65.5 years) underwent surgery for unruptured anterior communicating artery aneurysms in our hospital between January 2017 and January 2021.

Results: The mean aneurysm dome size was 5.29 mm (2–22 mm), and the mean aneurysm neck size was 3.2 mm (1.5–7 mm). Coil embolization was performed for fifty-four patients using various adjunctive techniques (simple, 7; double catheter, 15; balloon neck remodeling, 7; stent-assisted, 26

(LVIS Jr., 12; ATLAS, 14). Neck clipping was performed in 3 cases. The surgical results revealed complete coil embolization in 27, neck remnant in 26, and dome filling in 1 patient(s). The reason for 3 patients treated with neck clipping are patient's preference in one, associated with severe Middle cerebral artery stenosis needed TSA MCA anastomosis on one, and difficulty of embolization in one patient. Postoperative thrombotic complications were observed in 1 patient. The modified Rankin scale scores were 0 in 32 (96.5%) patients, 3 in 1 (1.7%) patient, and 6 in 1 (1.7%) patient. Follow-up was performed in 55 patients, with an average duration of 29.5 months (3–45 months). However, one patient underwent re-aneurysm embolization for major recanalization of aneurysm dome, none of them suffered from rupture of treated aneurysm.

Conclusion: Endovascular surgery may be the first choice of treatment for unruptured anterior communicating artery aneurysms.

2-P3

FLOW RE-DIRECTION ENDOLUMINAL DEVICE (FRED) FOR THE TREATMENT OF INTRACRANIAL ANEURYSMS: 6 YEARS CLINICAL RESULTS

Thais Takamura[1], Ana Carolina Felipe Da Silva[1], Lorena Maria Dering[1], Matheus Kahakura Pedro Franco[1], Joel Fernando Sanabria Duarte[1], Murilo Souza Meneses[1], Ricardo Ramina[1], Andre Giacomelli Leal[1]
[1]Instituto de Neurologia de Curitiba, Curitiba, Brazil

Introduction: Flow redirectors are one of several models of metallic spirals used in the endovascular treatment of intracranial aneurysms (IAs). This therapy consists in redirecting blood flow, consequently causing thrombosis and endothelial growth inside the IA. The FRED (Flow Re-direction Endoluminal Device) is a model of flow redirector available in medical practice that stands out for being a two-layer braided spiral that helps to reconstruct the blood vessel wall.

Objective: Report the experience of the use of the FRED dispositive, also investigate the safety and efficacy, in the endovascular treatment of IAs at a tertiary hospital in Brazil.

Methods: This retrospective and single-center observational study evaluates the use of FRED or FRED Jr from July 2016 to April 2022. Patients were included if they were older than 18 years; and were excluded if the implant did not occur for some complication or if they didn't perform a control cerebral angiography after the procedure. Dual antiplatelet therapy (acetylsalicylic acid and clopidogrel) was managed 5 days before and 6 months after the procedure and acetylsalicylic acid was used for another 6 months.

The data were collected from the medical records: patient's sex and age, number and location of IAs, complications, morbidity and level of IA occlusion – following the O'Kelly Marotta (OKM) classification scale. The follow-up of patients was carried out 6 and/or 12 months after the procedure with a digital subtraction angiography.

Results: 191 patients were screened, which 31 met exclusion criteria and 135 were female. The mean age was 53 years. A total of 198 AIs were treated – 178 of them in the internal carotid artery, mainly in the ophthalmic segment. Patient and aneurysm characteristics are shown in Table 1.
Following the OKM scale for occlusion of IAs, 61% fulfilled category D; while C, B and A were observed in, respectively, 11%, 7% and 6%. 28 patients had not undergone control angiography at the time of the study, but were not excluded because there was still time for follow-up. The morbidity rate was 16% (mainly headache). No deaths were reported.

Conclusions: IAs are more common in females, with the highest incidence after 50 years old. In this study, the occlusion rate was seen in 70% of the cases, a value that can still increase as follow-ups are concluded. Thus, high efficacy in the use of FRED in the endovascular treatment of IAs is suggested.

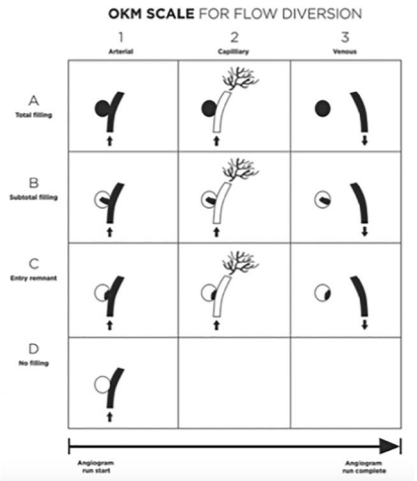

Figure 1: The OKM grading scale describes the degree of the aneurysm filling after treatment. A – persistence with filling > 95% ; B – persistence with incomplete filling, between 5 - 95%; C – partial filling occlusion < 5%; D – complete occlusion.

2-P4

A STRANGE CASE OF SAH

Simona Corraine[1], Ledda Valeria[1], Nicola Desogus[2], Laura Aste[2], Antonio Ferrari[1], Federica Schirru[1], Federico Fusaro[1], Marco Erta[1], Simone Comelli[1]
[1]Neuroradiology - ARNAS Brotzu, Cagliari, Italy. [2]Neurosurgery - ARNAS Brotzu, Cagliari, Italy

Introduction: While the frequency of cerebral aneurysms is ranged from 0.2% to 10%, pituitary tumors are a common intracranial pathology with a prevalence of 10 - 15% in the population. In particular, the incidence of aneurysms in

patients with pituitary tumors has been estimated between 2.3 and 5.4% of patients.

Methods: A concomitant cavernous-clinoid carotid aneurysm and giant prolactinoma was managed by a minimally invasive endovascular treatment and a medical therapy based on Cabergoline. After-treatment follow-up was made, every 6 months, by Digital Subtraction Angiography (DSA) and Magnetic resonance imaging (MRI).

Results: We report a case of a 61year-old female with a giant pituitary adenoma and cavernous-clinoid carotid aneurysm, presented with severe headache. Computer tomography scan showed a destructive skull base mass and cisternal subarachnoid hemorrhage. MRI revealed hemorrhagic necrosis of an infiltrative macroadenoma characterized by sellar, suprasellar and bilateral cavernous extension with a concomitant large cavernous-clinoid aneurysm of the left internal carotid artery. After a multidisciplinary discussion, we decided to proceed with a preventive aneurysm repair procedure and, subsequently, with the tumor treatment. Starting from 3 days before the procedure, the patient was premedicated with dual antiplatelet therapy and then the woman underwent endovascular treatment to reconstruct the parent artery with Pipeline Flex 4,75x30 mm (Medtronic); the woman was maintained on double antiaggregation therapy for 1 month followed by aspirin in the next 5 months. After endovascular procedure, it was introduced medical therapy with Cabergoline to treat the prolactinoma. DSA and MRI follow-up showed a complete resolution of aneurysm after 18 months and at the same time it was observed a significant decrease of tumor mass. Surgical treatment has not yet been performed.

Conclusion: This case report suggests that concomitant treatment of cerebral aneurysms and pituitary adenomas requires a knowledge of up-to-date medical, surgical and endovascular therapeutical options for each pathology, as well as an accurate consideration of the timing and sequence of intervention.

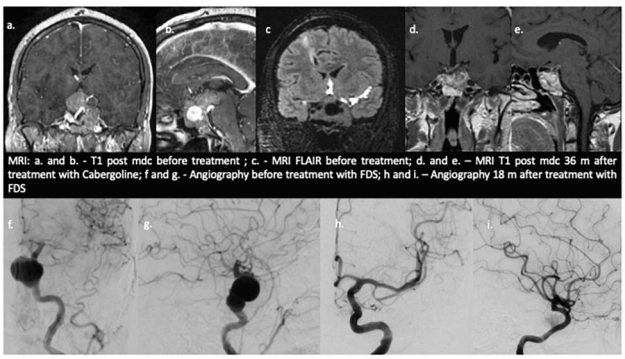

BRAIN AVM / DURAL AVF

2-P5
ODD LOOKING AVM BRAIN HOW WE TREAT

Umair Rashid[1]
[1] Neuroradiology Department, Lahore General Hospital, Lahore, Pakistan

Objective: Endovascular embolization of brain arteriovenous malformations (AVMs) is widely utilized, often used in conjunction with micro – and/or radiosurgery. To report the clinical experience by using a liquid embolic agent Squid/ Onyx or glue for embolization of Odd Looking Brain AVMs.

Materials and Methods: This study was conducted from June 2017 to December 2021 at the Department of Neuroradiology, Lahore General Hospital/Post Graduate Medical Institute, Lahore. A total of 100 patients with AVM at Infra and Supratentorially including deep seated AVMs were treated of both genders. Clinical presentation seizures 20 patients with hemorrhage 70 patients and 10 with motor weakness. The procedures were performed under biplane Artis ZEE DSA Siemens.

Results: Out of 200 patients, there were 80 males and 120 female patients. Their age ranged from 14 - 45 years. The maximum numbers of patients were in their early twenties. In hemorrhagic AVMs, the rupture point when recognized is endovascularly occluded, while the complete cure of the AVM is postponed after the expected clinical improvement.
In our study targeted, complete or partially embolization or targeted embolization was done in these patients, 60 to 85% size reduction was achieved with no significant complication.

Conclusion: Embolization of Odd Looking AVM varies case to case particularly where the access of nidus is not possible. Our experience favours selection of the embolizing material Squid 12/ Onyx 18 or glue both remain feasible, safe penetration with easy accessibility and embolization of different compartments of AVM, particularly for deep seated.

2-P6

TRANS-VENOUS ENDOVASCULAR TREATMENT OF A DAVF INVOLVING AN ISOLATED SEGMENT OF THE SUPERIOR SAGITTAL SINUS THROUGH RECANALIZATION OF THE OCCLUDED SINUS: CASE REPORT AND REVIEW OF THE LITERATURE OF ALL THE CASES OF THE DAVFS INVOLVING AN ISOLATED SEGMENT OF THE SUPERIOR SAGITTAL SINUS

Emilio Lozupone[1], Alfredo Pauciulo[1], Adriana Paladini[1]
[1]Vito Fazzi Hospital, Lecce, Italy

Introduction: Cerebral DAVFs of an isolated segment superior sagittal sinus have usually aggressive clinical presentation. Furthermore, the treatment can be challenging due to the tortuous anatomy of arterial feeders and the venous route can be precluded due to the SSS occlusion.

Methods: We describe a case of a 75-year-old man who presented with bilateral frontal hematomas due to a dural arteriovenous fistula (DAVF) involving an isolated segment of the superior sagittal sinus (SSS). After an unsuccessful attempt of trans-arterial endovascular embolization of the DAVF, the DAVF was occluded using a trans-venous approach through the recanalization of the occluded SSS.
An extensive review of the literature was performed in order to identify clinical, angioarchitettural data and treatment approaches of the DAVFs involving an isolated segment of the superior sagittal sinus.

Results: 6 cases were reported in the literature, including our case. Three cases presented with hemorrhage, 2 cases cognitive impairment and 1 case with paraparesis. All DAVFs belong to Borden type III, all presented venous hypertension in the brain parenchyma tributary to the SSS. MMA was always involved while AMA, STA and OA were respectively involved in the DAVF of anterior, mid and posterior thirds of the SSS. 4 trans-venous and 2 trans-arterial approach were performed; 3 treatments were performed in combination with surgery.

Conclusion: The treatment of cerebral DAVFs of an isolated segment superior sagittal sinus can be challenging. Recanalization of the occluded SSS can be feasible in order to reach the foot of the vein when trans-arterial approach is ineffective. Combined surgical approach should be reserved for those cases in which trans-arterial and trans-venous routes are precluded.

2-P7

THE DIAGNOSTIC PERFORMANCE OF CT ANGIOGRAPHY IN THE IDENTIFICATION OF DURAL ARTERIOVENOUS FISTULAS IN PATIENTS WITH INTRA CRANIAL HEMORRHAGE: A SINGLE-CENTER RETROSPECTIVE STUDY

Laura Gemini[1], Mario Tortora[1], Gianvito Pace[2], Mariarosaria Giardiello[2], Gemma Taglialatela[2], Fabrizio Fasano[2], Carmine Sicignano[2], Valeria Piscitelli[2], Francesco Somma[2], Vincenzo D'agostino[2], Alberto Negro[2]
[1]Università Di Napoli "Federico Ii", Napoli, Italy. [2]Ospedale Del Mare, Napoli, Italy

Purpose: To evaluate the accuracy and diagnostic performance of intracranial CT angiography in the identification and characterization of dural arteriovenous fistulas (DAVFs) in patients with intracranial hemorrhage (ICH), compared to 3D DSA.

Methods and Materials: The study was conducted on 27 patients with ICH associated with DAVFs. Demographic, clinical and radiological information at onset (location and extension of ICH, location and grading of DAVF) were considered. The CT angio findings examined are: dilated and asymmetrical arterial power supplies; dilated and turgid cortical veins; "Breast results"; vascular canals available transcalvaria. The accuracy of Angio CT was assessed by contingency table and standard statistical analysis.

Results: In patients (76% male, mean age 55 years), the most frequent onset symptomatology was headache (73%). Parenchymal hemorrhage was the most common cerebral form of bleeding (76%). The tentorial site (75%) was the most popular for DAVFs. The 3D DSA based on the Cognard classification identified: 5 DAVF type IIa / IIb; 12 type III; 10 type IV. The CT angio study allowed the identification of DAVF with a diagnostic sensitivity, specificity and accuracy of 61%, 100% and 92%.

Conclusions: The Angio CT study can represent an alternative diagnostic method to 3D DSA for the study of DAVF in the initial preliminary diagnostic approach phase, especially in emergency / urgent situations. In fact, it is a rapid, inexpensive, non-invasive and accessible study, unlike DSA, allowing to obtain the information necessary for identification, classification and therapeutic planning of DAVFs.

2-P8

CAVERNOUS SINUS DURAL FISTULA TREATED BY TRANSVENOUS EMBOLIZATION THROUGH DIRECT PUNCTURE OF THE SUPERIOR OPHTHALMIC VEIN

João Madureira[1], Manuel Correia[1], Gonçalo Basílio[1], Inês Leitão[1], Luísa Biscoito[1]
[1]Hospital de Santa Maria, Lisboa, Portugal

Purpose: Based on a procedure performed at our center, we will review the vascular anatomy of the orbit and cavernous sinus (CS) and demonstrate the required steps for embolization of a carotid cavernous fistula (CCF) by direct puncture of the superior ophthalmic vein (SOV) with a combined approach.

Background: Transvenous catheterization of the cavernous sinus through the inferior petrosal sinus (IPS) is the first-line approach for CS dural fistula embolization in most cases. The SOV route is an alternative route when inferior petrous sinus (IPS) is inaccessible. We depict the case of a 66 years-old woman with a right indirect dural fistula of the CS with feeders from both internal and external carotid arteries bilateral. Venous access through both IPS and facial vein was not possible.

Findings: The procedure was performed under general anesthesia with biplane fluoroscopic guidance in the neuroangiosuite. A diagnostic catheter was placed in the right common carotid artery for control. Exposure of the SOV was performed by the plastic surgeon by a medial upper eyelid crease incision and dissection of the planes of the orbicularis oculi muscle and orbital septum. Direct puncture of the right SOV was attained using an 18G abbocath. The interventional neuroradiologist catheterized the SOV with a 1.7 F microcatheter and embolized the cavernous sinus with coils with the exclusion of the fistula. At 3-months follow-up there was an improvement in symptoms related to the CS dural fistula.

Conclusion: Transvenous catherization of the cavernous sinus through the SOV is a safe and effective technique that benefits from a multidisciplinar team. It is an alternative when access when more common routes are not possible.

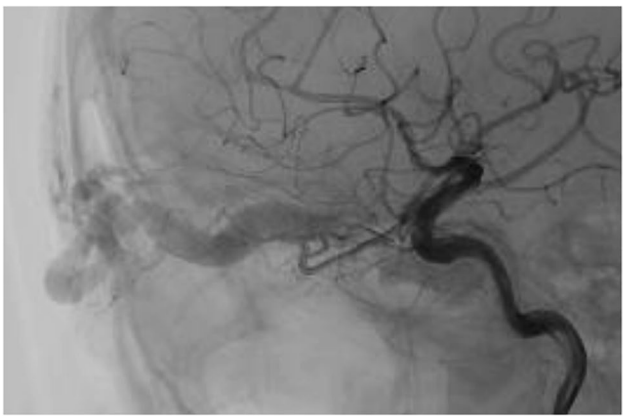

2-P9

ALTERNATIVE PATHS OF TRANSVENOUS EMBOLIZATION OF INTRACRANIAL DURAL ARTERIOVENOUS FISTULAS: THE EXPERIENCE OF OUR DEPARTMENT

Sofia Athanasiou[1], Zoe Papoutsou[1], Christina Aslanidi[1], Vasilios Mamalis[1], Antonios Tsanis[1], Eftichios Arhodakis[1]
[1]Red Cross Hospital, Athens, Greece

Objectives: To present the results of embolization of dural arteriovenous fistulas (dAVF) with an emphasis on the different routes of transvenous approach, identifying the incidence, characteristics and management strategies.
To evaluate the efficacy and safety of this treatment, outlining the possible complications and limitations.

Material and methods: We retrospectively collected data from patients who were diagnosed with dAVF and were treated with transvenous embolization from March 2019 to May 2022 at our department. Retrospective chart analysis and radiographic studies were performed in 21 patients (aged 23-78 years) with a dAVF treated with percutaneous transvenous embolization in the past three years. Lesions were located in the anterior cranial fossa, cerebellar tentorium, transverse-sigmoid sinus and cavernous sinus. The dAVFs were treated with detachable platinum coils via different transvenous approaches.

Results: Various routes to achieve transvenous access were used. Transvenous access can be established through the ipsilateral or contralateral internal jugular vein (16 patients), intracavernous plexus (2 patients), surgical superior ophthalmic venous access (2 patients) or direct puncture to affected sinus with craniotomy (1 patient). In situations of a trapped or thrombosed sinus/vein, the transvenous approach was very challenging. In these cases, access was achieved by crossing or recanalisation of a closed venous segment. Complete occlusion was obtained in 20 (95,2%) patients. Sub-total occlusion was obtained in 1 (4,8 %) patient. Clinical outcomes during follow-up were complete recovery in 20 patients and intermittent tinnitus in 1 patient.

Conclusion: Transvenous embolization is an effective treatment of dAVFs with high occlusion and low complication rates. Understanding the regional venous anatomy of the craniocervical junction, the number of feeding arteries, the fistula connection point, the venous drainage pathways and the direction of venous flow are crucial for targeting fistulous sites and selecting the appropriate route for transvenous approach.

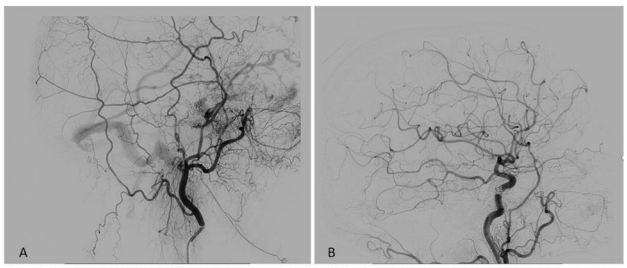

A. Pre-embolization digital subtraction angiography reveals dAVF type II from bilateral ICA, ECA branches and drains into the vein of Labbe and the left superior opthalmic vein. B. Through transvenous approach the right inferior petrosal sinus was revascularised. Then, through the intracavernous plexus, the fistula was embolized successfully with detachable platinum coils.

STROKE

2-P10

FEASIBILITY AND SAFETY OF ADAPT IN ACUTE DISTAL POSTERIOR CEREBRAL ARTERY OCCLUSIONS

Frederik Boxberg[1], Katharina Melber[1], Hauke Wensing[1], Katharina Schulz[1], Heinrich Lanfermann[2], Martin Schlunz-Hendann[1], Dominik Grieb[1,2]
[1]Department of Radiology and Neuroradiology, Sana Kliniken Duisburg, Duisburg, Germany. [2]Department of Diagnostic and Interventional Neuroradiology, Medical School Hannover, Hannover, Germany

Background: The direct aspiration first pass technique (ADAPT) is an effective and safe endovascular treatment (EVT) for distal medium vessel occlusions (DMVO) of the anterior circulation. Data about ADAPT in the distal posterior circulation is limited. We evaluated feasibility, safety and efficacy of ADAPT with distal access catheters (DAC) as the primary method for EVT of acute distal posterior cerebral artery occlusions (PCAOs).

Methods: We retrospectively identified all patients between 2017 and 2021 with an acute ischemic stroke due to distal PCAOs (P2-/P3-segment), either isolated or combined with proximal large vessel occlusions, that underwent thrombectomy using ADAPT with DACs as frontline therapy. We analyzed demographic data, angiographic recanalization rates and procedural safety.

Results: 18 consecutive patients with distal PCAOs (P2: 15/18; P3: 3/18) were included. Ten presented with an isolated distal PCAO, eight harbored distal PCAOs in combination with a basilar artery occlusion (BAO) or distal ICA occlusion and dominant PcomA. In all cases, the distal PCAO could be reached with the DAC. Successful revascularization (mTICI $\geq$ 2b) with ADAPT alone was achieved in 72% of cases (13/18) with mTICI 3 achieved in 61% (11/18). No complications related to distal PCA aspiration thrombectomy occurred.

Discussion: Initial results of EVT in DMVOs of the posterior circulation are promising. Our retrospective analysis of acute distal PCAOs treated with ADAPT demonstrated good revascularization rates which are in line with these previously published studies. Moreover, we encountered no procedural complications in our cohort. A low complication rate is essential for a reliable evaluation of different thrombectomy techniques, particularly in the challenging field of DMVOs.

Conclusion: ADAPT with DACs appears to be feasible and safe for acute distal PCAOs in the setting of different occlusion patterns. Further studies are needed to investigate clinical effectiveness of distal PCA thrombectomies and to better delineate eligible patients.

Figure: Middle-aged female patient with a residual left distal PCAO (P3-segment) (arrows in A, D) after recanalization of an acute BAO (NIHSS 13). ADAPT with a SOFIA 5F DAC (single pass) led to mTICI 3 (arrows in B, E indicate DAC tip). NIHSS 0 at discharge; mRS 0 at 90 days.

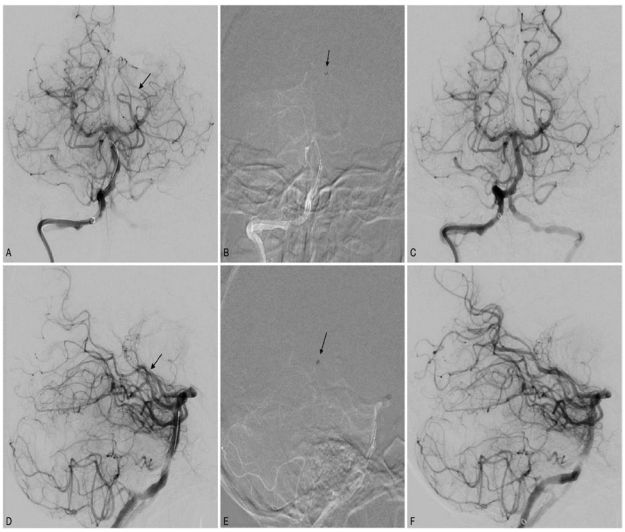

2-P11

VERTEBRAL ARTERY DISSECTING ANEURYSM AND SPINAL HEMORRHAGE – AN EXTREMELY RARE AND YET UNEXPLAINED CONNECTION

Tiago Lorga[1], Joana Tavares[1], Ana Luís[1], Gabriel Branco[1], Cristina Branco[1]
[1]Hospital de Egas Moniz, Lisboa, Portugal

Introduction: Vertebral artery dissecting aneurysm (VADA) is a rare entity that commonly presents with cervical pain, ischemic stroke and subarachnoid hemorrhage. Due

to its high risk of rebleeding and associated poor clinical outcome, it is necessary to treat a ruptured VADA as soon as possible.
The advent of modern endovascular treatment brought an alternative to occlusion of the parent vessel and neurosurgical approach. In cases of ruptured VADA, endovascular treatment is the preferred strategy due to its safety and efficiency, especially in cases of pseudo-aneurysm, flow restriction and contra-indication for anticoagulation.
Treatment options vary accordingly to every specific case, as coiling and stenting may, in some cases, be preferred over flow-diverter. The point of emergence of PICA, instability of the lesion and the caliber of the VA are factors to consider when planning an intervention.
The aim of this work is to review the particular pathological and radiological characteristics of VADAs, current endovascular treatment options and to present 2 cases of spinal hemorrhage contemporaneous to ruptured VADAs.

Methods: We reviewed cases of ruptured VADAs and analyzed the endovascular strategies used. Two of these cases revealed spinal hemorrhages (lumbar SAH and cervico-dorsal epidural hematoma).

Results: Case 1: A 31-year-old female suffered from sudden-onset and intense right cervicalgia. In the next hours, the patient noticed progressively decreased muscular force and sensitivity of the lower limbs and abdomen. Cervico-dorsal CT revealed an acute ventral epidural hematoma, extending from C1 to D9. Emergent surgical decompression was performed. Afterwards, DSA showed a VADA on the V3 segment of the right VA, that was promptly treated using two telescope stents.
Case 2: A 46-year-old female presented with left cervicalgia that evolved to intense low back pain. Brain CT did not reveal acute SAH. A lumbar MRI was performed few days later and showed spinal SAH, which the lumbar puncture confirmed. The patient was submitted to a DSA that revealed a left V4 VADA. A stent and a coil were used to successfully treat the aneurysm.

Discussion: VADA are a cause of SAH and ischemic stroke. There are few recorded cases in the literature of ruptured VADA and spinal hemorrhage. The underlying mechanisms are not well understood and either contempt spinal extension of SAH and perivascular bleeding for the epidural hematoma formation.

Conclusion: It is critical to be acquainted with the importance of treatment of ruptured VADA and its very rare manifestations such as spinal hemorrhage.

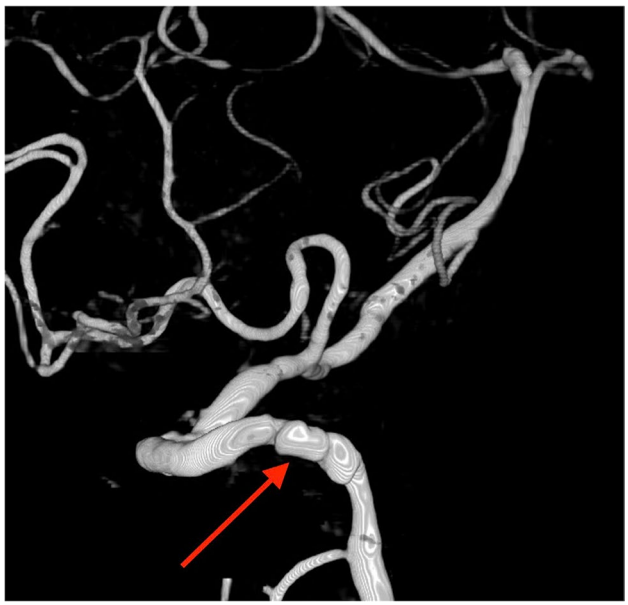

SPINE

2-P12
PREDICTION OF EPIDURAL BLOOD PATCH EFFICACY IN SPONTANEOUS INTRACRANIAL HYPOTENSION USING FOLLOW UP MRI

Hung-Chieh Chen[1,2], Yu-Wei Wang[1], Jyh-Wen Chai[1], Po-Lin Chen[3], Chih-Cheng Wu[4]
[1]Department of Radiology, Taichung Veterans General Hospital, Taichung, Taiwan. [2]School of Medicine, National Yang-Ming Chiao-Tung University, Taipei, Taiwan. [3]Department of Neurology, Taichung Veterans General Hospital, Taichung, Taiwan. [4]Department of Anesthesiology, Taichung Veterans General Hospital, Taichung, Taiwan

Objectives: Epidural blood patching (EBP) is the mainstay treatment for spontaneous intracranial hypotension (SIH). MRI is used for evaluating spinal CSF leakage. Post-EBP MRI is shown to be effective in predicting EBP efficacy. However, there are few reports on how post-EBP MRI findings may change with time. The aim of this study was to evaluate the relationship between post-EBP MRI findings at different time points and the corresponding effectiveness of EBP.

Methods: We retrospectively reviewed 63 SIH patients who had received target EBP. All patients received MRI follow-up within 10 days (post-EBP MRI) and at 3 months after EBP (3-month MRI). Sub-group analysis was performed according to different post-EBP MRI time points (0–2, 3–6, and 7–10 days). The relationships

between the post-EBP MRI findings and the EBP effectiveness were evaluated.

Results: Thirty-five (55.56%) patients were EBP-effective and 28 (44.44%) were EBP non-effective group according 3-month MRI. Compared to the EBP non-effective group, the EBP-effective group had significantly lower numbers of spinal CSF leakage in the post-EBP MRI (4.49 vs. 11.71; p = 0.000) and greater numbers of leakage improvement (7.66 vs. 2.96; p = 0.003). For patients with post-EBP MRI on 0–10, 0–2, 3–6, and 7–10 days, the cutoff values of numbers spinal CSF leakage for predicting EBP failure were 4, 6, 4, and 5, respectively, with AUC above 0.77.

Conclusion: Numbers of spinal CSF leakage identified in post-EBP MRI could predict EBP failure in SIH patients accurately.

2-P13

FEASIBILITY OF PERCUTANEOUS TRANS-SACRAL HIATUS PUNCTURE OF THE LUMBOSACRAL SUBARACHNOID CISTERN IN SPINAL MUSCULAR ATROPHY PATIENTS. AN INITIAL NEUROIMAGING MORPHOMETRIC STUDY

Siddhant Dhawan[1,2], Tarik Massoud[1,2]
[1]Division of Neuroimaging and Neurointervention, Department of Radiology, Stanford University School of Medicine, Stanford, USA. [2]Stanford Initiative for Multimodality neuro-Imaging in Translational Anatomy Research (SIMITAR), Stanford, USA

Introduction: Lumbar puncture (LPs) can be challenging, and imaging guidance is often necessary. However, a standard fluoroscopic LP may be impossible in presence of severely distorted lumbar spines or surgical hardware and fusion, e.g. in patients with spinal muscular atrophy (SMA) requiring intrathecal nusinersen therapy. There are case reports of intrathecal spinal anaesthesia via the sacral hiatus. It was also previously reported that despite the curvature of the sacrum in normal subjects (Norms), there usually exists a straight trajectory in the lower sacral canal that theoretically could allow image-guided percutaneous trans-sacral hiatus puncture and access to the lumbosacral cistern. Here we test the potential feasibility of this approach in SMA patients (SMAp) by initial morphometric analysis of curvature of their sacra and sacral canals compared to Norms. We hypothesized that if sacra in SMAp are relatively straighter than in Norms, this might facilitate unhindered trans-sacral hiatus passage of a standard spinal needle for intrathecal puncture.

Methods: We retrospectively analyzed lumbosacral spine midsagittal CTs or CT-myelogram images of 19 SMAp and 19 age and sex-matched Norms. We digitally measured sacral curvature using two methods (with a lower angle signifying a straighter sacrum). We also measured midsagittal sacral canal surface areas, levels of lumbosacral thecal sac terminations, and distances from sacral hiatus to the most caudad aspect of the thecal sac ('needle distances'). We measured statistical correlations between morphometrics, age, and sex, with significance set at $p<0.05$.

Results: Norms and SMAp had a mean age of 33.2 and 31.2 years, respectively, with dural sacs terminating at similar levels. The mean values for morphometrics were: (a) Midsagittal surface area of sacral canal for Norms = 701.2 mm2, and for SMAp = 601.5 mm2 (ns). (b) Full sacral curvature for Norms = 61.89°, and SMAp = 35.69° (p = 0.0009). (d) Width of sacral hiatus for Norms = 14.9 mm, and SMAp = 15.0 mm (ns). (e) 'Needle distance' for Norms = 54.7 mm, and SMAp = 49.9 mm (ns). There were no significant correlations between age or sex, and sacral curvature or width of the sacral hiatus or 'needle distance' for Norms and SMAp.

Discussion & Conclusion: Despite sacral curvature observed in Norms, a straight trajectory of the lower sacral canal points to the theoretical feasibility of percutaneous trans-sacral hiatus puncture of the lumbosacral SAS. SMAp have significantly straighter sacra compared to Norms, which theoretically renders them even more amenable to this technique.

2-P14

FEASIBILITY OF IMAGE-GUIDED PERCUTANEOUS S1 TRANSLAMINAR PUNCTURE OF THE SACRAL SUBARACHNOID CISTERN AS AN ALTERNATIVE TO LUMBAR PUNCTURE. AN INITIAL NEUROIMAGING MORPHOMETRIC STUDY

Siddhant Dhawan[1,2], Tarik Massoud[1,3]
[1]Division of Neuroimaging and Neurointervention, Department of Radiology, Stanford University School of Medicine, Stanford, USA. [2]Stanford Initiative for Multimodality neuro-Imaging in Translational Anatomy Research (SIMITAR), Standord, USA. [3]Stanford Initiative for Multimodality neuro-Imaging in Translational Anatomy Research (SIMITAR), Stanford, USA

Introduction: Alternative image-guided procedures may be considered for difficult lumbar punctures. Previous reports described percutaneous thoracolumbar transosseous translaminar puncture, or use of a purported midline dorsal sacral 'foramen' between S1 and S2 to puncture the lumbosacral cistern. Hence, we studied if favorable anatomy would allow possible percutaneous S1 translaminar puncture of the sacral dural sac. We morphometrically assessed two potential approaches for needle access: Transosseously through thinned S1 dorsal laminae, or through uncharacterized S1 foramina or clefts that may exist in these laminae.

Methods: We analyzed lumbosacral spine CT-myelogram images of 38 subjects. On axial images we measured the thinnest anteroposterior width of S1 and S2 laminae close to the base of their spinous processes. We then noted presence and size of any near-midline bony clefts or foramina in fused bone between S1 and S2 spinous processes, or extending off midline into S1 laminae. We defined clefts as laminar defects <3mm wide, and clefts >3mm as foramina. Full clefts and foramina completely traversed laminae to connect the dorsal sacrum to the central spinal canal, whereas partial clefts incompletely crossed the lamina. We measured statistical correlations between morphometrics, age, and sex, with significance at $p<0.05$.

Results: Mean age of subjects was 45.4 years. Most dural sacs ended between low S1 and low S2. S1 laminae were significantly thicker than S2 laminae at means 6.4mm and 3.4mm ($p=0$), respectively, with no age or sex correlations. There were no midline bony defects between S1 and S2 spinous processes. However, 21 subjects had a cleft or foramen at the S1 spinous process base, extending laterally into either lamina when wide. There were 7 foramina (mean width 7.1mm), 5 full clefts (2.8mm), and 9 partial clefts (1.9mm). The bony defects were left-sided in 15 subjects, and on the right in 6 ($p=0.054$); more commonly found in females (68%) than males (28.6%) ($p=0.029$). There were no significant correlations between age and defect widths.

Discussion & Conclusion: Alternative image-guided percutaneous translaminar routes for puncture of the sacral cistern through the dorsal sacrum are possible theoretically. If considering puncture of a low dural sac, the S2 lamina is sufficiently thin to more easily breach with a bone biopsy coaxial system than at higher spinal levels. Moreover, presence of hitherto undocumented but commonly observed bony clefts and foramina in S1 laminae could provide a new, less invasive route for unobstructed dorsal percutaneous needle access to the dural sac.

VARIOUS

2-P15
BILATERAL STEREOTACTIC ABLATION OF THE NUCLEUS ACCUMBENS INDUCES REMOTE CHANGES IN THE VENTRAL TEGMENTAL AREA

Rodrigo Ferrone Andreiuolo[1,2], Ricardo de Oliveira-Souza[2]
[1]Grupo Fleury, Rio de Janeiro, Brazil. [2]D'or Institute of Research and Education, Rio de Janeiro, Brazil

Background: Charcot and Turner (1852) and von Monakow (1914) were the first to describe respectively the neuroanatomical and functional changes in neural structures remote from the original seat of injury but anatomically connected with it through fiber tracts. Crossed cerebro-cerebellar atrophy is the neuroanatomical change most consistently reported in the current neuroimaging literature. In this communication, we report a case of damage to the ventral tegmental area (VTA) as an acute distant effect of bilateral injury of the nucleus accumbens (NAcc).

Case Report: A 28-year-old man, with a history of pharmaco-resistant polysubstance abuse underwent bilateral radio frequency ablation of the bilateral nucleus. One month later, bilateral restricted diffusion of the VTA was seen in a follow-up magnetic resonance study.
Acute changes in the VTA due to a discrete bilateral injury of the NAcc have not so far been described in the literature. These changes are most probably related to remote excitatory cytotoxicity. Further studies will be carried out to see the degree to which they survive the immediate postoperatory period and if they contribute to the behavioral results of the surgery.

Conclusion: Discrete bilateral injury of the NAcc may induce remote changes in the VTA, a paramedian midbrain region which sustains massive connections with the NAcc via the medial forebrain bundle.

Keywords: Nucleus accumbens (NAcc), ventral tegmental area (VTA), radio frequency (RF) ablation, addiction, magnetic resonance iImaging (MRI).

Conflict of Interest: The authors report no competing interests.

2-P16
DIAGNOSTIC YIELD AND OUTCOMES OF REPEAT LATERAL DECUBITUS DIGITAL SUBTRACTION MYELOGRAMS FOLLOWING PRIOR NEGATIVE EXAMS

Dong Kun Kim[1], Michael Oien[1], Ajay Madhavan[1], Jason Little[1], John Benson[1]
[1]Mayo Clinic, Rochester, USA

Background and purpose: CSF venous fistulas (CVF) are increasingly recognized cause of spontaneous intracranial hypotension, and lateral decubitus digital subtraction myelogram (LDDSM) can detect the exact location of the fistula to direct targeted treatment. However, detection of CVF requires active leakage at the time of exam, prompting repeat exams in patients with high clinical suspicion for CVF with negative exams. We report our experience on repeat LDDSMs performed for prior negative exams.

Materials and Methods: A retrospective review was performed on patients who underwent repeat LDDSM following negative, diagnostic quality LDDSMs from 5/1/2019 to 5/1/2022. Examinations were excluded if the repeat exams were due to poor image quality on prior exams, concern for leaks on previously not included level, or recurrent symptoms following definitive treatment (surgery or embolization) for positive findings on prior LDDSMs.

Results: Total of 312 patients underwent LDDSM during the study period for clinical suspicion for CSF leak, and 34 patients underwent repeat LDDSM following negative diagnostic quality LDDSMs. Of those, 9 patients underwent 3rd LDDSMs after negative 2nd set, and among the 9 patients, one underwent 4th and 5th sets of LDDSMS.
Of the 34 patients who underwent 2nd DSM, 6 (18%) patients had positive findings on the 2nd DSM. 3 of the 6 patients underwent nerve root ligation, and the other 3 patients underwent transvenous CVF embolization procedure. Of the patients who underwent surgery, one had sustained resolution of symptoms, one did not benefit initially but improved after 2nd surgery, and one had pain relief for 1 month, but symptoms recurred. Of the 3 patients who underwent embolization procedure, one had 50-60% improvement at 1 month, one minimally worsened despite partially improved brain MRI finding, one improved at 1 month but symptoms recurred at 7 months.
Of the 9 patients who underwent 3rd sets of LDDSMs, 2 (22%) were positive for CVFs. Both patients underwent transvenous embolization. One minimally improved (25% improvement) and the other developed rebound hypertension which has been waxing and waning.
The patient who underwent 5 sets of LDDSMS had all negative exams.

Conclusion: Repeat LDDSM diagnostic yield following prior negative LDDSM is lower than the reported initial LDDSM diagnostic yield. Moreover, CVF found in subsequent exams following prior negative LDDSM may have lower rate of treatment response compared to the ones found in initial exams.

3. PEDIATRIC

ADVANCED TECHNIQUES

3-P1
DYNAMIC MRI IN ASSESSING VELOPHARYNGEAL INSUFFICIENCY DURING PHONATION

Marta Gómez-Chiari[1], Emili Inarejos Clemente[2], Anna Maria Demestres[2], Miguel Bejarano[2], Sara Cardelus[2], Agueda Diaz Anadon[2], Francisco Parri[2], Josep Rubio-Palau[2], Monica Rebollo[2], Jordi Muchart[2], Mireia Riba[2], Manuel Gómez Ponce[2], Ignasi Barber[2], Teresa Maristany[2], Josep Munuera del Cerro[2]
[1]Hospital Sant Joan de Déu, Barcelona, Spain. [2]Hospital Sant Joan de Deu, Barcelona, Spain

Introduction: Velopharyngeal insufficiency (VPI) results in speech disorders, due to soft palate and pharyngeal walls structural and neuromuscular involvement, affecting normal functions of the velopharyngeal (VP) sphincter mechanism. The diagnostic methods includes a perceptual assessment by logopaedist followed by instrumental evaluation with nasopharyngoscopy, fluoroscopy, and magnetic resonance imaging (MRI).

Methods: A 2– year retrospective study from January 2020 to May 2022 was performed at our Institution. We included 30 patients (15 girls and 15 boys). Patients age ranged from 6 to 17 years (mean age 10.8+/-4.5). We have reviewed structural imaging findings without movement and on dynamic MRI phonation using anatomic and fast sequences with cine mode in a 3T scanner, in patients with VPI. During dynamic phonation sequence we used paradigms according to logopaedist and Otorhinolaryngologists (ORL)
We evaluated VP opening, length of soft and hard palates, posterior wall thickness, VP depth, anatomy of the levator veli palatini (LVP) and palatopharyngeal muscle, quantifying adenoid and tonsillar tissue sizes without movement. On dynamic MRI we evaluated VP movements (movement of velum toward posterior pharynx, medial movement of lateral pharyngeal walls, and anterior movement of posterior pharyngeal wall). Movements after palatoplasty were also evaluated.

Results: A total of 30 patients with VPI (20 without pharyngoplasty and 10 with posterior pharyngeal flap and sphincter pharyngoplasty) were evaluated. In operated patients, 2 have lower attachment of posterior pharyngeal flap, 2 presented posterior flap disinsertion and 1 showed construction of sphincter pharyngoplasty with unilateral muscle disinsertion. In non-operated patients we found a gap > 1cm2 with a predominance of sagittal and circular closure, due to anomaly position of muscles, submucosal cleft, soft and hard palates shorts, deep posterior pharyngeal.

Discussion: MRI provided additional information about anatomic structures during rest and speech, by showing sphincter movements followed with dynamic pictures on three planes; findings showed abnormal position or structure of LVP muscle, asymmetric movement of the lateral pharyngeal walls that could not be depicted by videofluoroscopy or measurement and evaluation some blind points in endoscopic examination, help to selection of surgical procedure. MRI evaluated postoperative characteristics and failures possible of pharyngoplasty.

Conclusion: MRI is a non-invasive and radiation free technique very useful in identifying and predicting patients who need surgery. It also evaluates the efficacy in follow-up after treatment of VPI providing a view of the exact plane of closure without the depth-distortion effect seen in nasopharyngoscopy

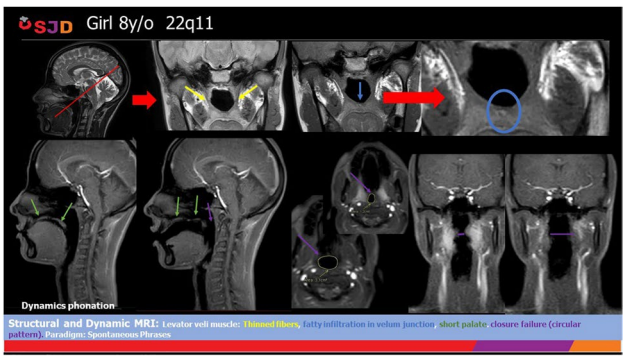

3-P2

EVALUATION OF AUDITORY PATHWAY WITH DIFFUSION TENSOR IMAGING IN PEDIATRIC COCHLEAR IMPLANT CANDIDATE

Direnç Özlem Aksoy[1], Yeşim Karagöz[1], Kemal Furkan Kaldırımoğlu[1], Abdullah Soydan Mahmutoğlu[1]
[1]Istanbul Training and Research Hospital, Istanbul, Turkey

Keywords: auditory pathway, diffusion tensor imaging, pediatric deafness, cochlear nerve area

Purpose: Auditory neural network texture could change when the stimulus is interrupted, and we aimed to investigate whether those changes could be noticed via Diffusion Tensor Imaging (DTI) in children with hearing loss.

Material and Method: In this retrospective study, 54 cochlear implant candidate cases (108 sides) and 47 normal hearing controls (94 sides) were included. All participants were under 18 years old and had DTI images gained by 1.5T scanner. Fractional anisotropy (FA), radial diffusivity (RD), apparent diffusion coefficient (ADC) maps were generated. We placed two regions of interest (ROI) bilaterally on Cochlear Nucleus (CN), Superior Olivary Nucleus (SON), Lateral Lemniscus (LL), Medial Geniculate Body (MGB), Auditory Radiation (AR), Heschel Gyrus (HG), Inferior Fronto-Occipital Fascicle (IFOF), Superior Longitudinal Fascicle (SLF) and an ROI on the splenium of the corpus callosum (CCS) in the midline. (Figure 1,2,3) The area of the cochlear nerve in the distal internal auditory canal was measured.(Figure 4) DTI metrics, children ages, and cochlear nerve area were compared in control and patient group.

Results: ADC and RD values of patients are significantly higher than control group, in all places except RD values of MGB. FA values of patient group are significantly lower than control group at LL, AR, HG, IFOF, SLF and CCS. (Table 1, Figure 5,6,7)
There is a positive correlation between FA and age in both deaf and control groups, for all locations. (Table 2)
The cochlear nerve area is lower in-patient group (0.88 ± 0.29) than control group 1.18±0.14 (p=0.000). The cochlear nerve area has a positive correlation with age in patient group (p=0.000) but has not in control group. (Table 1)
The cochlear nerve area has a positive correlation with FA values of all locations except FA values of MGB. (Table 3)

Conclusions: The alterations of DTI metrics on auditory pathway are reflection of the microstructural changes of white matter tracts, in deaf children. The change of DTI parameters with age supports the temporal development of white matter tracts. The correlation of cochlear nerve diameter with DTI metrics suggests that axonal deterioration in hearing loss may also affect the cochlear nerve.

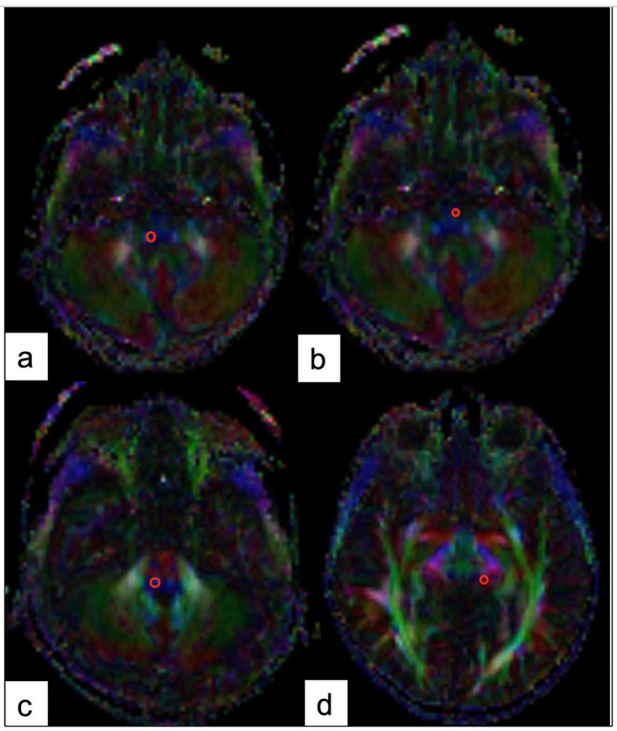

Figure 1. The ROIs on the Cochlear Nucleus (CN) (a), Superior Olivary Nucleus (SON) (b), Lateral Lemniscus (LL) (c), Medial Geniculate Body (MGB) (d) on color-coded maps.

3-P3

DEFINING THE NORMAL RANGE OF PAEDIATRIC CEREBELLAR METABOLITE RATIOS ACQUIRED BY PROTON MAGNETIC RESONANCE SPECTROSCOPY AND IDENTIFYING TRENDS WITH AGE

Vartan Balian[1], Santosh Mordekar[2], Paul Armitage[3], Ruth Batty[1], Helen McQuillan[1], Marios Hadjivassiliou[4], Daniel Connolly[1]

[1]Sheffield Children's Hospital NHS Foundation Trust, Sheffield, United Kingdom. [2]Department of Paediatric Neurology, Sheffield Children's Hospital NHS Foundation Trust, Sheffield, United Kingdom. [3]Academic Unit of Radiology, University of Sheffield, Sheffield, United Kingdom. [4]Academic Department of Neurosciences, Sheffield Teaching Hospitals NHS Foundation Trust, Sheffield, United Kingdom

The diagnostic role of proton magnetic resonance spectroscopy (1H-MR spectroscopy) is well established in adults, particularly for identifying metabolic changes in cerebellar pathology. In children this has not occurred due to difficulty in obtaining normative data. We aim to define a range of normal paediatric cerebellar metabolite ratios and identify any trends between these ratios and age.

Children undergoing MRI imaging as part of routine clinical practice were included between November 2018 to December 2020. Metabolite ratios of n-acetylaspartate (NAA)/creatine (Cr), n-acetylaspartate (NAA)/creatine (Cr) (height), choline (Cho)/creatine (Cr), and n-acetylaspartate (NAA)/choline (Cho) were acquired over the superior vermis and right cerebellar hemispheric cortex using long TE 1H-MR single voxel point-resolved spectroscopy (PRESS) at 3T, and statistical analysis carried out.

99 children were included. Metabolite ratios for NAA/Cr, NAA/Cr (h) and NAA/Cho increased between birth to around the age of 3 to 4 years, and thereafter followed a more stable pattern. There was a statistically significant difference in NAA/Cr, NAA/Cr (h), and NAA/Cho over both the superior vermis and right cerebellar hemispheric cortex ($p < 0.001$) when comparing children aged between 4 months to 3 years with those aged between 3 to 16 years.

We have shown for that the paediatric range of normal cerebellar metabolite ratios NAA/Cr, NAA/Cr (h) and NAA/Cho acquired by long TE 1H-MR spectroscopy increase between 4 months to around the ages of 3 to 4 years, and that there is a significant difference in these when comparing children under the age of 3 with those over the age of 3.

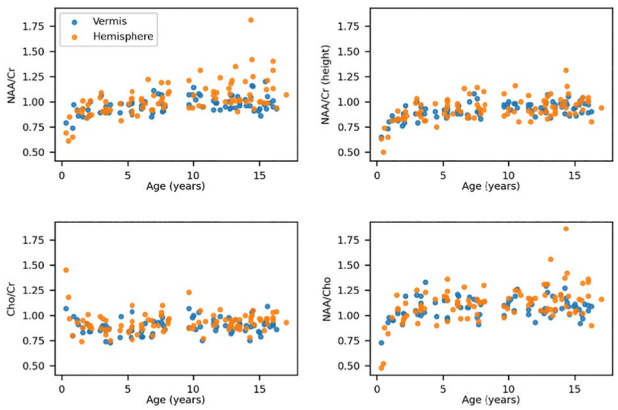

Fig. 1 Age (in years, n=99) against cerebellar metabolite ratios for both superior vermis (blue) and right cerebellar hemispheric cortex (orange)

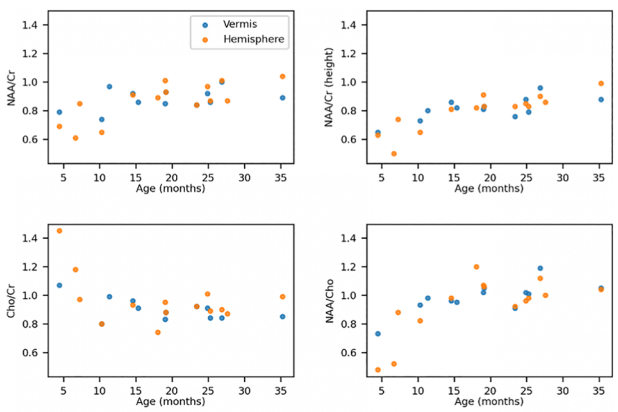

Fig. 2 Age (in months) for under 36 months (n=16) against cerebellar metabolite ratios for superior vermis (blue) and right cerebellar hemispheric cortex (orange)

3-P4

A FAST PEDIATRIC WHOLE-BRAIN MR SEQUENCE WITH PARAMETRIC MAPS AND SYNTHETIC WEIGHTED IMAGES

Mary Kate Manhard[1], Amol Pednekar[1], Nehal Parikh[1]
[1]Cincinnati Children's Hospital and Medical Center, Cincinnati, USA

Keywords: Quantitative MRI, synthetic images, rapid acquisition

Introduction: The overall goal of this work was to investigate a multi-inversion multi-echo spin and gradient echo whole-brain (MI-SAGE) MRI brain acquisition in children. The accelerated MI-SAGE approach allows full brain coverage in under 2 minutes, reducing the sensitivity to motion and consequently the need for sedation. Here, an MI-SAGE acquisition was optimized for robust parametric mapping and subsequent synthetic multi-contrast image generation in children.

Methods: The MI-SAGE sequence was implemented on a 3T Philips system and evaluated in 17 awake 3- to 8-year-olds subjects. A non-selective adiabatic inversion pulse was followed by the single-shot EPI acquisition of all slices, resulting in a different inversion time (TI) for each slice. Slice ordering was shuffled over repetitions, acquiring adequate range of TIs for fitting T1 relaxation. Each slice was imaged with a SAGE approach acquiring both gradient echos as well as asymmetric spin echo readouts, to allow for both T2 and T2* fitting. Simultaneous multi-slice with multiband RF pulses and blipped-CAIPI was incorporated to further improve the time efficiency of the scan. The images were acquired with an in-plane acceleration factor of 3 and multiband factor of 2, 1.2x1.2x4mm^3 resolution, 32 slices, and a total scan time of 61 seconds.
Image contrasts were fit together using a dictionary matching approach to the signal evolution on a voxel-by-voxel basis. Relative proton density (PD) maps were then found from the normalized difference between the dictionary fit and the data signal evolution. The quantitative maps were used to create synthetic images using the sequence parameters of standard T1 and T2 weighted and FLAIR images.

Results: Images were visually assessed for artifacts and image quality. Quantitative T1, T2, T2*, and PD maps were estimated for all subjects along with synthetic T1-, T2-, T2*-weighted, and T2-FLAIR images. Representative image contrasts from two slices in one 3-year-old subject are shown in Figure 1, and image quality was similar to traditional images in most subjects. MI-SAGE provided motion artifact free images and EPI related artifacts were limited to inferior slices, below the cerebellum.

Conclusion: In this cohort of 3-8 year old children, T1w, T2w, T2*w and FLAIR images with full brain coverage and reasonable image quality were synthesized from a 1 minute MI-SAGE acquisition. Additionally, T1, T2, T2*, and PD parameter maps were also generated.

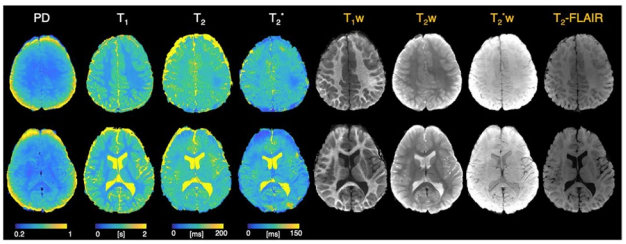

CONGENITAL

3-P5

A MULTICENTRE PICTORIAL REVIEW OF POSTERIOR FOSSA MALFORMATIONS IN FETAL MRI

Pedro Bem[1], André Miranda[2], Joana Nunes[3], Carla Conceição[4], Ana Filipa Geraldo[2]
[1]Unidade Local De Saúde Matosinhos – Hospital Pedro Hispano, Porto, Portugal. [2]Centro Hospitalar Vila Nova Gaia/Espinho, Gaia, Portugal. [3]Unidade Local De Saúde Matosinhos – Hospital Pedro Hispano, Gaia, Portugal. [4]Centro Hospitalar Universitário Lisboa Central – Hospital Dona Estefânia, Lisboa, Portugal

Introduction: Posterior fossa malformations (PFM) represent a large and frequent group of pathologies in pediatric neuroradiology, and it is essential for neuroradiologists to be familiarized with the main imaging findings of these entities in fetal MRI.

Methods: Our goal is to systematize the main PFM and how they present in fetal MRI and to correlate the imaging findings with post-natal MRI, autopsy results, genetic studies, and clinical outcomes, when available.
A total of 818 fetal MRIs, performed between January 2012 and September 2021, from two Portuguese Hospital Centres (Centro Hospitalar de Vila Nova de Gaia – Espinho and Centro Hospitalar Lisboa Central – Hospital Dona Estefânia) were reviewed.

Results: MR findings were divided into five different groups: 1) predominantly vermian involvement, 2) global cerebellar involvement, 3) unilateral cerebellar involvement, 4) cerebellar and brainstem involvement and 5) predominantly brainstem involvement and representative cases from the distinct categories were selected for pictorial review.

Discussion & Conclusion: Recognition of the main PFM and their main imaging features on fetal MRI as well as their associated neurological prognosis is paramount for an early and accurate prenatal diagnosis and counseling.

Keywords: Fetal, Posterior Fossa, malformation, cystic lesions.

3-P6

TUBA1A MUTATION: FROM PRENATAL FETAL MRI TO POSTMORTEM AUTOPSY AND GENETICS CONFIRMATION

Vasco Sousa Abreu[1], Mariana Santos[2], Sofia Almeida Xavier[2], Carla Conceição[3]
[1]Neuroradiology Department, Centro Hospitalar Universitário do Porto, Porto, Portugal. [2]Neuroradiology Department, Hospital de Braga, Braga, Portugal. [3]Neuroradiology Department, Hospital Dona Estefânia, Centro Hospitalar Universitário de Lisboa Central, Lisboa, Portugal

Introduction: fetal MRI is a widely used technique to confirm, complement or exclude questionable prenatal ultrasound (US) findings and plays an essential role in evaluating fetuses with suspected US findings and /or positive family history. Kinked brainstem is a rare finding in fetal neuroimaging, typically seen in association with other CNS abnormalities.

Clinical case: a 26-year-old woman with a history of endometriosis, prolactinoma and ovarian teratoma, with no previous pregnancies and no history of inbreeding undergoes prenatal US evaluation at 21 weeks and 4 days of gestation with evidence of microcephaly and multiple central nervous system (CNS) malformations. Three days later fetal MRI is performed, showing a complex CNS malformation, characterized by kinked brainstem, marked hypoplasia of the cerebellum, complete agenesis of the corpus callosum, cavitation of the ganglionic eminences, malformation of the midbrain-diencephalic junction and microcephaly with delayed sulcation and gyration pattern. α-dystroglycanopathy, X-linked hydrocephalus, tubulinopathy or lissencephaly with cerebellar hypoplasia were considered as the main differential diagnosis.
At 22 weeks and 6 days of gestation she was hospitalized for medical termination of pregnancy, and the postmortem anatomopathological examination confirmed the imaging findings. Genetic study identified a mutation involving the TUBA1A gene (c.601G>A).

Conclusion: prenatal identification of a kinked brainstem should prompt evaluation of the multiple possible associated CNS malformations, allowing an attempt to distinguish between main possible diagnosis, such as X-linked hydrocephalus (L1CAM mutation), tubulinopathy (TUBA1A mutation) or α-dystroglycanopathies (e.g., Walker-Warburg syndrome).
Although definitive diagnosis depends on genetic confirmation, fetal MRI provides the necessary resolution to detect complex CNS malformations, to further assist genetic evaluation, management, and counseling.

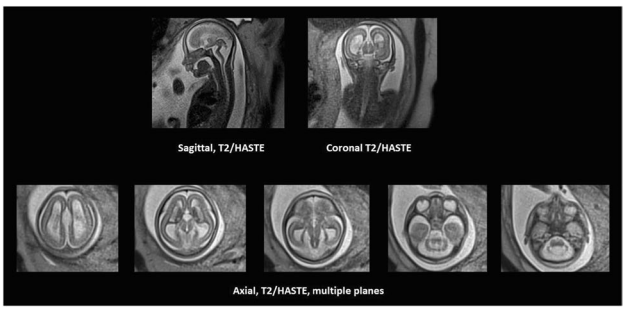

3-P7

UNUSSUAL PRESENTATION OF DUPLICATION OF THE PITUITARY GLAND-PLUS SYNDROME

Vesna Stokanovic[1], Ivana Markovic[2], Zoran Radovanovic[1,3], Dragan Stojanov[1,3], Milena Trandafilovic[3]
[1]Center for radiology, Clinical center Nis, Nis, Serbia. [2]Department of Radiology and Molecular Imaging, Sultan Qaboos University Hospital, Muscat, Oman. [3]Faculty of medicine, University of Nis, Nis, Serbia

Duplication of the pituitary gland (DPG) is a very rare developmental anomaly. Just over 50 cases are reported in the literature with different combinations of associated anomalies. We performed MR head exam of the three-year-old, male patient with duplication of pituitary gland-plus syndrome, and here we present the findings.
The patient had duplication of pituitary gland, sella and infundibulum associated with several other anomalies, such as: duplication of basilar artery, nasal dermoid cyst with dermal sinus, absent olfactory bulbs, callosal corpus dysgenesis, hypothalamic pseudohamartoma, broadening of the optic chiasm, persistent nasopharyngeal canal and persistent median basal canal. Patient also had cleft palate and cystic formation within the nasopharynx.
The case presented has multiple malformation commonly associated with DPG. Rarely described associations include duplication of facial features, absent olfactory bulbs, neuronal migration abnormalities, duplication of odontoid process, supernumerary teeth and clival encephalocele. Dermoid mases have been described in five cases, none of them was nasal dermoid cyst which is unique to our case.

DPG is an extremely rare malformation resulting from splitting of the rostral notochord and prechordal plate during blastogenesis. The term DPG-plus syndrome has been proposed for duplication of the pituitary gland in combination with other craniofacial anomalies.

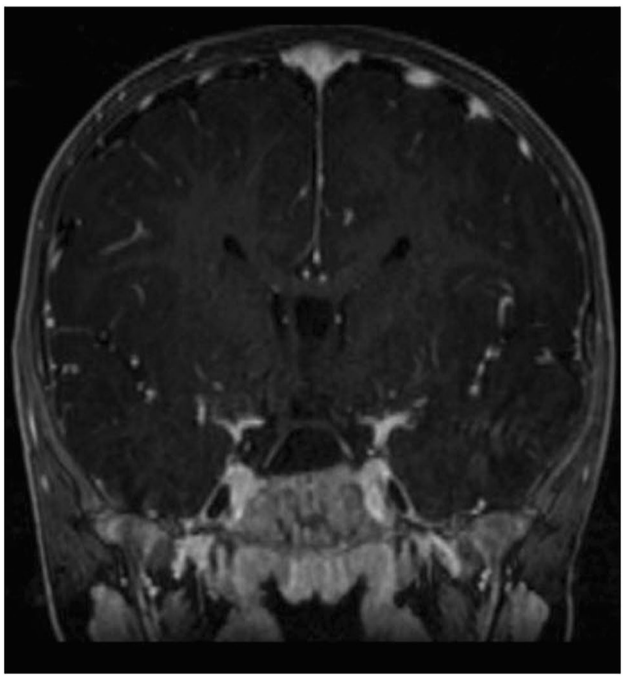

INFECTIOUS

3-P8
ORBITAL AND INTRACRANIAL COMPLICATIONS OF ACUTE RHINOSINUSITIS IN CHILDREN – A REVIEW OF THREE CASES

Ana Carolina Chaves[1], Carolina Maia[1], Cristina Moura[1], César Nunes[1]
[1]Centro Hospitalar e Universitário de Coimbra, Coimbra, Portugal

Introduction: Acute rhinosinusitis is a common disease in children, characterized by acute inflammation of the paranasal sinus mucosa. It has been reported that between 4% and 20% of acute rhinosinusitis can be complicated, being orbital cellulitis the most common complication, followed by intracranial disease. These are challenging complications, as they carry the potential to become a source of significant morbidity and mortality.

Methods: Descriptive analysis of clinical presentation, imaging, microbiological aspects, therapy, disease course, and outcomes. We report 3 patients with complicated acute rhinosinusitis, admitted between October 2021 and May 2022 in our institution.

Results: The mean age was 14 years-old, and all patients were female. All patients presented with fever and headache, one had seizure episodes and drowsiness, while the other had palpebral edema and proptosis. MR imaging was extensively used and was superior to CT in diagnosis. Two patients had intracranial empyema, one epidural and the other subdural. Another patient had subperiosteal orbital and intracranial abscess formations. All patients received intravenous antibiotics and underwent endoscopic sinus surgery, one patient received antiepileptic medication and neurosurgical epidural drainage, while other had surgical drainage of subperiosteal orbital abscess. Mean hospital stay was 30.1 days (minimum 22 days and maximum 46 days). Only one patient had a microorganism isolated, namely *S. intermedius*. Overall, neurologic outcome was excellent.

Conclusion: Orbital and intracranial complications of acute rhinosinusitis are rare but potentially harmful. Diagnosis and management of orbital and intracranial complications are challenging, and close collaboration among different specialties is required. Early imaging is critical to establish diagnosis and prognosis can be favorable by using a combination of medical and surgical interventions.

Keywords: acute rhinosinusitis; complicated rhinosinusitis; orbital complication; intracranial complication.

3-P9
"PADS, PAWS AND CLAWS" – CAT SCRATCH DISEASE ASSOCIATED PEDIATRIC OSTEOMYELITIS

Gonçalo Alves[1], Fátima Hierro[2], José Maria Sousa[1], Carina Reis[1], Sara de Carvalho[1]
[1]Neuroradiology Department, Centro Hospitalar e Universitário São João, Porto, Portugal. [2]Neuroradiology Department, Unidade Local de Saúde de Matosinhos, Matosinhos, Portugal

Introduction: Cat scratch disease (CSD) is a common zoonosis, caused by Bartonella henselea, usually associated with a history of a scratch, bite or contact with cats. Osteomyelitis represents a rare manifestation of this entity, with preferential involvement of the axial skeleton. Superficial lymphadenitis, considered the hallmark of CSD, is less common in children affected by this atypical presentation, delaying an accurate diagnosis.

Methods: We report a case of a 10-year-old girl diagnosed with osteomyelitis and paravertebral abscesses, due to confirmed Bartonella henselea infection.

Results: A 10-year-old girl presented with a 2-week history of right-lateral lumbar pain and fever for 3 days. Past medical history was uneventful. At physical examination, spinal flexion was limited by pain and no lymphadenopathies were noted. Blood analysis revealed elevated systemic inflammatory markers. Lumbar MRI showed a spinal infiltrative process, along with vertebral canal and right paravertebral expression. There were areas of bone erosion, cortical discontinuity, signal changes and gadolinium uptake of the L2 vertebral body, suggestive of an infectious or tumoral etiology. Diagnostic workflow included a whole-body SPECT, revealing foci of intense hypermetabolism at the L2 vertebral body and right L2 and L3 pars articularis. Although under ceftriaxone, clindamycin and vancomycin for 24, 6 and 15 days, respectively, fever persisted. This being, CT-guided aspiration was performed, demonstrating an inflammatory process. Lumbar MRI was repeated, showing disease progression: increased right paravertebral edema, including psoas abscesses extending from L1 to L3 level, invasion of the ipsilateral L1 to L3 intervertebral foramina and vertebral canal, with slight epidural expression; greater extension of L2 bone involvement with marked contrast uptake. Afterwards, polymerase chain reaction forBartonella was positive, on pus and bone samples from another CT-guided aspiration/biopsy, and retrospectively on the material collect in the first procedure. At this point, a new medical history revealed the girl had had a kitten, 6 months previously. Antibiotherapy was switched to rifampicin and doxycycline for 12 days, and after fever and systemic inflammatory markers normalized, the child was discharged with complete resolution of the initial complaints.

Discussion and conclusion: CSD is a rare cause of pediatric osteomyelitis. Nevertheless, this entity should be considered when an infiltrative bone disease is suspected, to prompt an early diagnosis and timely therapeutic implementation. It can be included as a differential diagnosis, along with Ewing's sarcoma and tuberculosis, since unfortunately, the ability of imaging techniques to accurately distinguish them is limited.

Keywords: Cat scratch disease, Osteomyelitis, Pediatrics

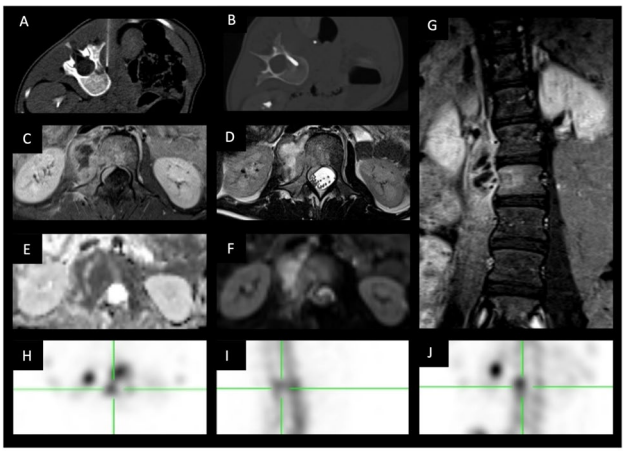

Figure 1. CT-guided needle aspiration **(A)** and bone biopsy **(B)** of L2 vertebral body. Lumbar MRI. **(C)** Axial T1-Turbo Spin Echo (TSE) fat saturation post-gadolinium and T2 TSE **(D)** sequences showing marked signal changes and contrast enhancement of the vertebral body and pedicle of L2, along with an anterior/right-lateral epidural collection; additionally, right psoas abscesses are present and depicted on DWI b50 **(E)**/ADC map **(F)**. **(G)** Coronal T1-TSE fat saturation post-gadolinium demonstrating the extension of the abscesses. Bone SPECT **(H)**, **(I)**, **(J)** on axial, sagittal and coronal views revealing foci of intense hypermetabolism at the L2 vertebral body and L2 and L3 *pars articularis*.

METABOLIC

3-P10

MRI DIAGNOSTIC CLUE OF HEREDITARY LEUKODYSTROPHY IN NEXT GENERATION SEQUENCING ERA

Seung-Koo Lee[1]
[1]Department of Radiology, College of Medicine, Yonsei University, Seoul, Korea, Republic of

Purpose: Hereditary leukodystrophy syndrome is rare disorders with diverse clinical and radiologic features. Next generation sequencing (NGS) enables more precise diagnosis of leukodystrophy by analyzing genetic feature. The purpose of this study was to re-organize MRI findings of leukodystrophy according to NGS, not clinical manifestations.

Method: From 2015 to 2022, total 22 patients (M:F=15:7, mean age=6.5) diagnosed to have leukodystrophy syndrome were retrospectively reviewed. NGS was performed for all patients. Location and extent of dysmyelination, enhancement pattern and diffusion restriction were reviewed according to responsible gene abnormality.

Results: Eight patients were confirmed to have adenosine triphosphate-binding cassette subfamily D (ABCD)

member 1 gene mutation and they showed uniform and typical appearance of peritrigone dysmyelination with linear enhancement zones (Fig. 1). Six patients showed arylsulfatase A (ARSA) gene mutation and they showed diffuse dysmyelination without zone preference and preservation of subcortical u-fibers. Three patients had proteolipid protein 1 (PLP1) gene mutation and showed diffuse dysmyelination, involvement of brain stem, subcortical u-fibers. More severe and extensive dysmyelination was seen in megalencephalic leukodystrophy (MLC1) gene (n=1) and galactosylceramidase (GALC) gene mutation (n=2). Diffusion restriction was noted in white matter involvement of Charcot Marie Tooth disease (n=1) and thalassemia (n=1) (Fig. 2).

Conclusion: NGS provides precise genetic diagnosis of leukodystrophy syndrome. Zone preference, extent of dysmyelination, severity of white matter involvement can be assessed according to each gene mutation and will be helpful for differential diagnosis of various leukodystrophy syndrome.

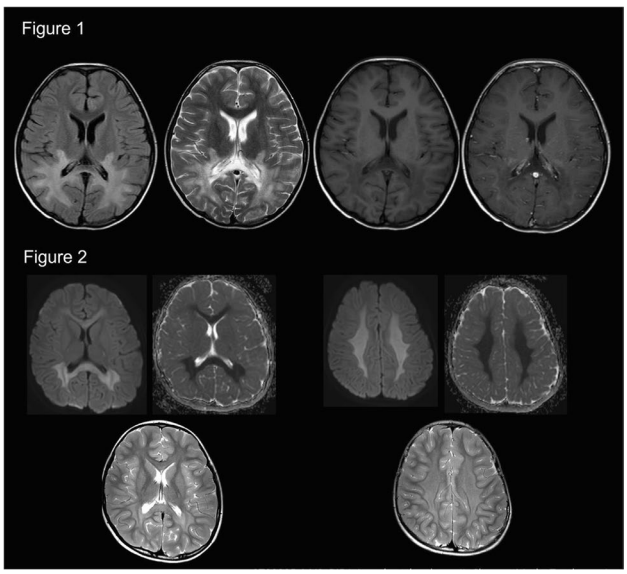

3-P11

ALEXANDER DISEASE- AN UNUSUAL CAUSE OF HYDROCEPHALUS DIAGNOSED PRENATALLY

Ioana Mihaela Pop[1], Mariana Constanta Coman[1], Veronica Maria Marcu[1], Catalin Cirstoveanu[1]
[1]Emergency Pediatric Hospital M.S. Curie, Bucharest, Romania

Purpose or Learning Objective: To evaluate the imaging modalities in diagnosing Alexander disease (AxD) and learn about the role of MRI.

To be able to recognize the different forms of the disease and assess its severity and evolution.

Methods or Background: Alexander disease is a rare and progressive leukoencephalopathy that is caused by a gain-of-function mutation in GFAP gene, resulting in protein aggregates (Rosenthal fibers) that cause astrocyte dysfunction.
AxD has been divided traditionally in 4 subtypes (neonatal, infantile, juvenile and adult).
Our department was confronted for the first time with a case of neonatal AxD, the diagnosis challenge starting with fetal MRI; genetic testing being conclusive.

Results or Findings: Unlike the classic radiological features that, corroborated with clinical aspects can guide to the diagnosis of AxD, diagnosing neonatal form is challenging.
Seizures and signs of raised intracranial pressure are sometimes the prerequisite, with onset within the first month of life and rapid progression leading to severe disability or death within the first 2 years of life.
In neonatal form, fetal MRI can show infiltrating white matter lesions in the brainstem and hydrocephalus, other studies even showing slightly swollen fornices.
After birth, transfontanellar ultrasound is used as a monitoring tool for ventriculomegaly and progression of the white matter abnormalities.
Regarding imaging, MRI is the only modality that can thoroughly characterize the white matter lesions, being required 4 out of the 5 criteria that were described by van der Knaap et.al. and constitute the landmarks of AxD diagnosis:
-extensive cerebral WMA with a frontal preponderance
-presence of a periventricular rim of decreased signal intensity on T2-weighted images and elevated signal intensity on T1-weighted images;
-abnormalities of the basal ganglia and thalami (swelling + elevated T2 signal intensity or atrophy+ elevated/decreased T2 signal intensity)
-brain stem abnormalities
-contrast enhancement involving one or more of: ventricular lining, periventricular rim of tissue, white matter of the frontal lobes, optic chiasm, fornix, basal ganglia, thalamus, dentate nucleus, and brain stem structures.
Late onset AxD disease is mainly characterized by progressive atrophy of the medulla oblongata and upper cervical spinal cord, with hyperintensities on T2WI being predominant.

Conclusion: Imaging diagnosis of rare genetic diseases in utero is highly challenging; hence, they are mostly detected

in the neonatal period. Associated findings of hydrocephalus and WMA could suggest AxD but genetic testing is deciding.

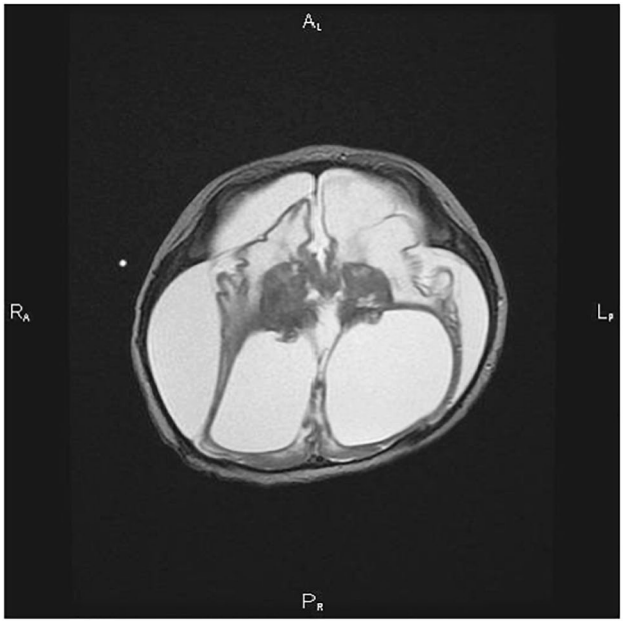

TUMOR

3-P12

MAGNETIC RESONANCE FEATURES OF H3 K27M ALTERED DIFFUSE MIDLINE GLIOMAS IN CHILDREN

Elzbieta Jurkiewicz[1], Jedrzej Sarnecki[1], Malgorzata Goluch[1], Paulina Opyrchal[1], Monika Drogosiewicz[1], Ewa Swieszkowska[1], Joanna Trubicka[1], Wieslawa Grajkowska[1]
[1]The Children's Memorial Health Institute, Warsaw, Poland

Introduction: Pediatric diffuse midline glioma PDMG is considered one of the pediatric-type diffuse high-grade gliomas, described as CNS WHO grade 4 with poor prognosis. The most common location is the pons although the tumor may occupy any the midline structures: thalamus, brainstem, spinal cord. Independently of the location, the prognosis of PDMG is poor, with a 2-year survival rate of <10%. Due to molecular markers these tumors are defined in CNS WHO classification 2021 as a diffuse midline glioma, H3 K27-altered.The overexpression of EZHIP, or an EGFR mutation are also observed. Surgical resection is often highly limited, due to the involvement of critical brain structures. Radiation or chemotherapy is standard.
The present study included 16 patients, aged from 3 and 4/12 to 17 y.; median age was 9 years.

Methods: All patients were examined on 1.5 T scanner with protocol including T2/FLAIR images, diffusion-weighted sequence (DWI) and T1-weigted images without and with contrast injection.
We characterized the structural MR imaging features of these tumors, gadolinium enhancement patterns, calcifications, haemorrhage, necrosis and cyst formation.
Biopsy was performed in all patients.
Pathologic/microscopic and molecular characteristics were also performed.

Results: Tumors were located in pons in 12 patients (in 4 of them additionally cerebellum was involved) and in thalamus in 4 children. All tumors were hypointense on T1- and heterogeneously hyperintense on T2/FLAIR images. Contrast enhancement was seen in 7 patients (punctate or rim), restriction diffusion in 4. Exophytic component was noted in one child. Hydrocephalus was present in 4, necrosis in 3, and haemorrhagic component in 1 patient.
The mutations c.83A>T H3F3A were recognized in 14 children and mutations c.83A>T HIST1H3B (H3C2) in 2 patients.

Conclusion: We found that midline gliomas with histone H3 K27M mutation centered within the thalamus and brainstem were solid with infrequent exophytic component and haemorrhage.

3-P13

DIFFUSE LEPTOMENINGEAL GLIONEURONAL TUMORS IN CHILDHOOD: A CASE SERIES BASED REVIEW

Mario Tortora[1], Carmela Russo[2], Domenico Cicala[2], Federica Mazio[2], Maria De Liso[2], Pietro Spennato[3], Lucia Quaglietta[4], Eugenio Maria Covelli[2], Giuseppe Cinalli[3]
[1]Department of Advanced Biomedical Sciences, University of Naples "Federico II", Naples, Italy. [2]Department of Neurosciences, Division of Neuroradiology, Santobono-Pausilipon Children's Hospital, Naples, Italy. [3]Department of Neurosciences, Division of Neurosurgery, Santobono-Pausilipon Children's Hospital, Naples, Italy. [4]Unit of Pediatric Neuro-Oncology, Santobono-Pausilipon Children's Hospital, Naples, Italy

Introduction: The aim of this study is to show the clinical, radiological and histological features of diffuse leptomeningeal glioneuronal tumors (DL-GNT) in order to increase awareness of this pathology and facilitate rapid diagnosis in affected patients. Furthermore, we try to hypothesize about possible correlations between genotype and phenotype. These tumors are a relatively new entity (WHO2016), typical of the pediatric age. In 2018, two different molecular

subgroups (DLGNT-MC-1 and DLGNT-MC-2) with distinct molecular and clinical characteristics were proposed.

Methods: We retrospectively reviewed the medical and radiological records of all patients referred to our institution who were finally diagnosed with DL-GNT. Four patients are then analyzed: two male and two female children aged between 1 and 14 years. These subjects underwent MR imaging of the brain and spinal cord at 1.5 T with T2-weighted sequences, FLAIR, T1 pre- and post-gadolinium, and DWI / ADC. All MR imaging studies were independently reviewed by 2 pediatric neuroradiologists. All cases underwent biopsy and histopathological analysis.

Results: Our case history is similar to that reported in the literature in terms of frequency of typical findings. In particular, leptomeningeal thickening with intracranial (4/4, 100%) and intraspinal (3/4, 75%) nodular enhancement are the most frequent findings. This finding is often associated with small cystic-like lesions, which do not take contrast, intracranial (2/4, 50%) and intraspinal (1/4, 25%) and with hydrocephalus phenomena, sometimes marked. In addition, these tumors may have atypical features, such as a solitary mass of the spinal cord (1/4, 25%). Also reported calcifications. Histopathology demonstrated strong reactivity for OLIG2, MAP2 and S-100, with variable expression of glial fibrillar acid protein and synaptophysin. Molecular evaluation is required to search for the 1p ± co-deletion 19q loss, the 1q increase and the hyperexpression of BRAF, NTRK and RAF1> MAPK / ERK.

Discussion & Conclusion: There should be high suspicion for DL-GNT when typical findings are observed in the absence of clinical and laboratory signs of infection (e.g. tuberculosis or neurocysticercosis) and when a dominant neural axis mass is absent or disproportionately small or indolent in comparison to the degree of leptomeningeal disease. When the diagnosis is suspected, a timely biopsy should be performed to obtain a definitive diagnosis and institute the most appropriate treatment.

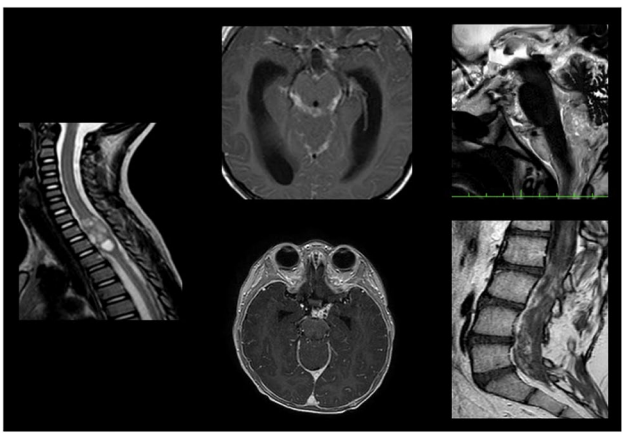

3-P14

DIFFUSE PEDIATRIC CEREBELLAR GLIOMA: IDENTICAL IMAGING PHENOTYPES OF AN EXTREMELY RARE ENTITY WITH DISPARATE PATHOLOGY

Aden Mclaughlin[1], Rahul Lakshmanan[1], Jason Dyke[2,3], Richard Warne[1], Snigdha Saha[4], Christopher Lind[4], Michael Bynevelt[5,6]

[1]Perth Children's Hospital Department of Medical Imaging, Nedlands 6009, Perth, Western Australia, Australia, Perth, Australia. [2]PathWest Neuropathology, Royal Perth Hospital, Perth 6000, Western Australia, Australia, Perth, Australia. [3]School of Medicine and Pharmacology, University of Western Australia, Crawley 6009, Western Australia, Australia, Perth, Australia. [4]Perth Children's Hospital Department of Neurosurgery, Nedlands 6009, Perth, Western Australia, Australia, Perth, Australia. [5]Perth Children's Hospital Department of Medical Imaging, Nedlands, 6009, Perth, Western Australia, Perth, Australia. [6]Neurological Intervention and Imaging Service of Western Australia (NIISwa), Nedlands, 6009, Perth, Western Australia, Australia, Perth, Australia

Introduction: Although the posterior fossa is a common location for pediatric brain tumours, diffuse cerebellar glioma is an extremely rare entity. Only two cases of isolated diffuse paediatric cerebellar glioma are reported in the English language. Only one of these cases had a similar imaging phenotype to ours. Although similar to Lhermitte-Duclos; the appearances are distinct from other neoplasms of the pediatric posterior fossa. Presented here are two diffuse cerebellar gliomas in children under the age of 3 with near identical imaging phenotypes demonstrating differing histological and molecular genetic profiles.

Cases: Case 1 is a 2-year-old male undergoing MRI brain during investigation for global developmental delay and macrocrania. MRI demonstrated diffuse expansile high T2 signal abnormality centred on the cerebellar vermis extending into the medial cerebellar hemispheres and the middle cerebellar peduncles bilaterally and sparing the brain stem (figure 1 A – D). There was associated mass effect with effacement of the fourth ventricle and basal cisterns, obstructive hydrocephalus and tonsillar decent. There was no diffusion restriction or enhancement. Biopsy was performed and the integrated pathological diagnosis was diffuse glioma not elsewhere classified, favour histological WHO grade II; IDH, BRAF, FGFR, NTRK, H3K27M, MYB and MYBL intact/wild-type.

Case 2 is a 4month old male presenting to our Emergency Department (ED) with parental concerns regarding increasing head circumference, which was on the 97th centile on presentation. Cranial US was performed demonstrating

severe hydrocephalus. MRI brain (figure 1 E – H) demonstrated diffuse expansile signal abnormality centred on the cerebellar vermis extending into the medial cerebellar hemispheres and the middle cerebellar peduncles bilaterally, sparing the brain stem. The mass effect and hydrocephalus was more advanced than case 1. There was no diffusion restriction or enhancement. Biopsy was performed and the integrated pathological diagnosis was diffuse cerebellar anaplastic astrocytoma, WHO grade III, IDH wild-type with PDGFRA mutation.

Conclusion: Only two cases of diffuse paediatric glioma isolated to the cerebellum have been reported in the English language and only one of these cases had a similar imaging phenotype to ours. Despite the identical location and MRI appearance, our cases had differing histopathology and molecular profiles with the associated implications for treatment and prognosis. Diffuse paediatric cerebellar glioma should be considered in the differential diagnosis in the setting of diffuse signal abnormality in the cerebellum with imaging features not typical of the usual posterior fossa tumours and clinical findings not supportive of entities such as rhombencephalitis.

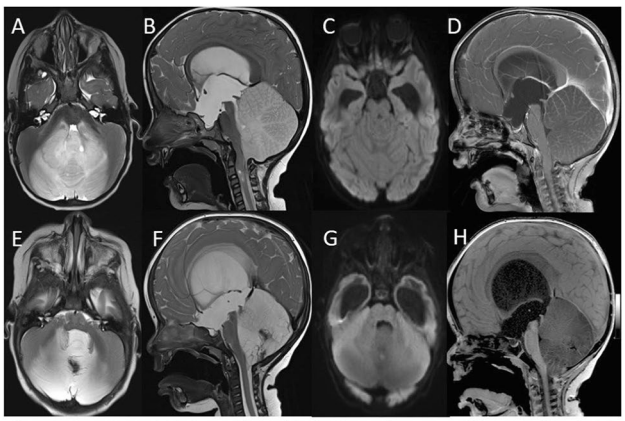

Fig. 1. Case 1 A-D; Case 2 E-H. A,E: Axial T2-weighted sequence demonstrates diffuse expansile region of increased T2 signal involving the vermis and medial aspects of the cerebellar hemispheres extending into the middle cerebellar peduncles. There is cerebellar tonsillar descent in both cases and a small syrinx at C2/3 in case 1 B,F. Compression of the 4th ventricle is more marked in Case 2. Small focus of susceptibility inferiorly in Case 2, presumably reflects haemorrhage. B,E,F: Sagittal T2-weighted sequence demonstrates diffuse expansion of the cerebellar vermis. Compression of the 4th ventricle and distension of the third and lateral ventricles is noted in both cases - more marked in Case 2. Small focus of susceptibility inferiorly again noted in Case 2. C,G: No restricted diffusion on DWI. D,H; Midline Post Contrast T1-weighted sequence revealing absence of tumour enhancement. Ventricular changes are again noted.

3-P15

WILD TUMOR OF BRAIN: BITHALAMIC DIFFUSE PEDIATRIC-TYPE HIGH-GRADE GLIOMA

Begumhan Baysal[1], Fatih Calis[2], Mahmut Bilal Dogan[1]
[1]Istanbul Medeniyet University Goztepe Prof Dr Suleyman Yalcin City Hospital, Department of Radiology, Istanbul, Turkey. [2]Istanbul Medeniyet University Goztepe Prof Dr Suleyman Yalcin City Hospital, Department of Neurosurgery, Istanbul, Turkey

Introduction: Primary thalamic tumors are rare, constituting only 1.5% of all brain tumors. About a quarter occur in children. Bilateral thalamic gliomas (BTGs) are extremely rare subtypes known to have a poor outcome.

Diffuse pediatric-type high-grade gliomas, H3-wild-type and IDH-wild-type are high-grade pediatric tumors included in the classification by the latest WHO brain tumor classification, 5th Edition (2021). It is evaluated under the title of pediatric-type diffuse high-grade gliomas. It is usually located supratentorial (over 80%) (1). In this case, we present a rare case of bithalamic diffuse pediatric-type high-grade gliomas, H3-wild-type and IDH-wild-type.

Methods: A 1-year-old 8-month-old male patient applied to the emergency department with complaints of subfebrile fever, loss of balance and gait disturbance. On physical examination, pupils were bilateral isochoric, light reflex and globe movements were normal, extremity motor examination was normal, and Babinski test was negative.

Results: Cranial Computed Tomography scan showed bilaterally enlarged, heterogeneous thalamus. In MRI examination, diffusely expanding signal increases in T2 and FLAIR sequences in bilateral thalamus, pathological signal changes in the periaqueductal area in the thalamomesencephalic junction and superior mesencephalon are observed. In diffusion MR examination, there is a patchy form of diffusion restriction area in the dorsal part of the left thalamus. There are occasional diffusion restrictions in the posterior part of the right thalamus. Linear subtle enhancement is seen within the lesion.
In addition, dilatation is observed in both lateral ventricles. In the third ventricle, there is posterior compression and focal dilatation in the anterior section.
In the multi voxel MR spectroscopic evaluation, a decrease in NAA values, an increase in the choline peak and a significant increase in the choline/creatinine ratio are remarkable. A lactate peak is seen in the spectral analysis. The described findings were thought to be compatible with bithalamic glioma.

Discussion & Conclusion: Primary bilateral (as opposed to unilateral) thalamic tumors, especially IDH and H3K27 wild type, are incredibly rare. There are only a few case reports in the literature, and information on radiological findings is limited (2).
These tumors often do not show contrast enhancement, appearing hypo-isointense on T1-weighted images and hyperintense on T2-weighted images. The radiological differential diagnosis of BTGs includes lymphomas, other brain tumors such as teratoma, vascular infarcts, toxic and metabolic disorders, and infections (such as encephalitis,

Creutzfeldt-Jakob disease) (3). Diffuse midline gliomas may have similar radiological findings and may require tissue biopsy for definitive diagnosis.

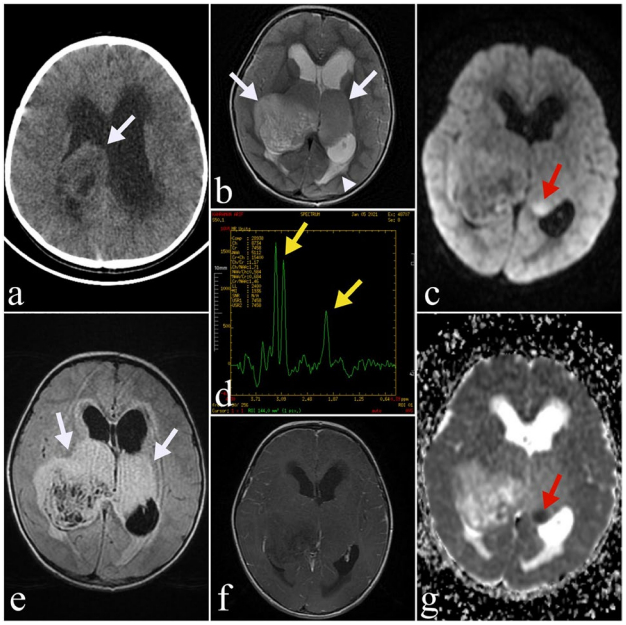

VASCULAR

3-P16
EVALUATION OF PREVALENCE OF PUNCTATE WHITE MATTER LESIONS IN A HEALTHY VOLUNTEER NEONATAL POPULATION

Saminderjit Kular[1], Daniel Connolly[1]
[1]Royal Hallamshire Hospital, Sheffield, United Kingdom

Background: Neonatal hypoxic-ischemic injury (HIE) is the commonest of neonatal encephalopathies, ahead of infection, metabolic disorder and trauma. HIE may occur in significantly preterm or term infants. HIE can manifest on MRI with deep-grey nuclei, cortical or watershed injury. Punctate white-matter lesions (PWML's) are hyperintense on T1-weighted imaging and iso-/hypointense on T2-weighted imaging, and have been described in association with HIE . We have reviewed a normal volunteer population to assess prevalence of neonatal PWML's who did not manifest clinical signs of HIE.

Methods: Neonatal subjects were scanned on a 3-Tesla (3-T) magnetic resonance imaging (MRI) scanner. Included cases had T2-weighted imaging with either one/both standard T1-weighted spin-echo or T1-volumetric sequences. Image review was performed on normal volunteers imaged as part of the 'Firefly' 3 Tesla MRI scanner project evaluation. Images were reviewed by consultant paediatric neuroradiologists involved in the initial study.

Results: 52 subjects were recruited, however 12 had no T1-weighted imaging therefore 40 cases were evaluated for PWML. Of 40 subjects, one(2.5%)had a solitary T1-weighted PWML. No pre-/peri-natal injury had occurred, thus the presentation had unknown aetiology but was highly unlikely due to perinatal asphyxia.

Conclusion: Our findings support the premise that PWML's have a very low incidental prevalence in healthy neonates and supports the association with HIE. In the extremely small prevalence of infants deemed healthy, who are identified with a PWML (only 1 case in our study), the infant is likely to be developmentally normal.

3-P17
PEDIATRIC STROKE IMAGING - A SMALL POPULATION, A GREAT CHALLENGE

Inês Carneiro[1,2], Joana Freitas[1,2], David Berhanu[1,3], Joana Coelho[4], Gonçalo Basílio[1], Luísa Biscoito[1], Sofia Reimão[1], Graça Sá[1]
[1]Neuroradiology Department, Centro Hospitalar Universitário de Lisboa Norte, Lisbon, Portugal. [2]Clínica Universitária de Imagiologia da Faculdade de Medicina da Universidade de Lisboa, Lisbon, Portugal. [3]Instituto de Anatomia da Faculdade de Medicina da Universidade de Lisboa, Lisbon, Portugal. [4]Pediatric Neurology Unit, Department of Pediatrics, Centro Hospitalar Universitário de Lisboa Norte, Lisbon, Portugal

Background: Stroke is a recognized worldwide health problem causing substantial morbidity and mortality. Pediatric stroke is a distinct, less common and less understood clinical entity, not only due to its unique set of etiologies but also for being an important cause of acquired brain injury throughout childhood, with high morbimortality. Stroke can be divided into hemorrhagic and ischemic subtypes, the latter including arterial ischemic stroke and venous infarction caused by cerebral sinus or cortical vein thrombosis. The lower prevalence of pediatric stroke often precludes physicians from considering this diagnosis and symptoms can be subtle and mimic other more frequent pathologies in this age group. The diagnosis is therefore challenging and often delayed. Neuroimaging (computed tomography, magnetic resonance imaging and angiography) is a key tool in the identification of stroke, in the study of the underlying etiology and in guiding therapeutical interventions.

Objectives: To characterize the pediatric population and the patterns of ischemic stroke, hemorrhagic stroke, or cerebral

venous thrombosis in a Portuguese tertiary center and to provide updates on their etiologies, analyzing the imaging characteristics and the correlation with clinical data.

Methods: A retrospective analysis was conducted using medical records of patients admitted to the Pediatric Neurology Unit of Hospital de Santa Maria in Lisbon, from January 2012 to May 2022. Perinatal stroke patients and patients with findings directly related to head trauma or brain tumors were excluded; readmissions were not included. Demographic and clinical data were obtained, and relevant neuroimaging findings were drawn.

Discussion: Eighty-four patients were included, comprising 40 female and 44 male individuals. There were 45 cases (54%) of hemorrhagic stroke, 29 (34%) of ischemic stroke and 10 (12%) of cerebral venous thrombosis. There were an average of eight admissions per year. No patient with ischemic stroke was submitted to thrombectomy. Four patients died, of which three had a hemorrhagic stroke. Neuroimaging findings were crucial for the diagnosis, etiological and prognostic definition and to guide therapy. We revised the concept of pediatric stroke in a thorough manner to raise awareness to the recognition of this less expected disease and its causes in this age group. Prompt diagnosis, transfer to specialized centers and treatment in a timely manner are essential for preserving brain function and improving prognosis. The challenges posed by pediatric stroke can be partially mitigated by a multidisciplinary approach in a centre that thoughtfully applies diagnostic imaging, which contributes to improving survival and functional outcomes.

3-P18

MOYAMOYA WITHIN THE PAEDIATRIC COHORT

Shweta Samanta[1], Heena Chotai[1], Fiona Dickinson[1], Ahmed Sharaf[1], Motahare Yadegarfar[1]
[1]University Hospitals Leicester, Leicester, United Kingdom

Introduction: Moyamoya is a progressive vasculopathy characterised by gradual stenosis of the major proximal intracranial arteries; predominantly the anterior circulation. Collateral arteries hypertrophy in response to the progressive stenosis giving rise to the moya moya 'puff of smoke' appearance on angiography. Clinical presentation is variable and includes symptoms of transient ischaemic attacks, seizures and headaches.

Aim: The pattern of Moyamoya can occur as a standalone entity when idiopathic, known as Moyamoya disease (MMD). However Moyamoya syndrome (MMS) are cases where the pattern arises in association with other conditions. This case report compares the differences between MMD and MMS and includes one of the key associations; Down syndrome. We will demonstrate the importance of considering all possible aetiologies for diagnosis.

Methods: We retrospectively analysed two patients' journeys from presentation to diagnosis to analyse the differences seen in MMD vs MMS.

Results/Discussion: Four year old with complex medical history including Down Syndrome, presented generally unwell and dehydrated. Neurological findings included right facial droop with reduced left sided power at 3-4/5, positive plantars and exaggerated knee reflex. Imaging revealed narrowed bilateral supraclinoid internal carotid arteries (ICAs) with extensive right MCA infarction. Differentials included vasculitis and neurovascular MDT suggested treatment with bilateral extracranial-intracranial bypass.
Seven year old presented with a two month history of worsening and increasing frequency of headaches, vomiting, tiredness and decreased responsiveness. Imaging revealed a structurally normal brain with multiple collateral vessels demonstrated involving the thalamostriate and thalamoperforator vessels. No acute infarction was demonstrated. The patient was discharged on medication and educated about MMD.
The most common age of onset in the paediatric population is the first decade of life which both our patients fall into. MMD however has bimodal manifestation, with onset again in the fourth decade of life. Our two patients show the variation in presentation along with the differences in medical history, imaging features and treatment. Despite this, both demonstrated the same core imaging characteristics of bilateral supraclinoid ICA narrowing.

Conclusion: As a rare and progressive disease, symptomatic relief along with revascularisation to the brain is key to long term management. Symptoms of Moyamoya can be easily masked by patients with associated conditions such as Down syndrome as there are many other causes of stroke in Down syndrome. For example congenital heart disease such as atrioventricular septal defects. A high degree of suspicion is therefore needed for the diagnosis of Moyamoya.

3-P19

CLINICAL AND IMAGIOLOGICAL FOLLOW-UP OF CEREBRAL VASCULAR ANOMALIES TREATED WITH MULTIPLE CRANIAL BURR HOLE SURGERY, AN INDIRECT REVASCULARIZATION TECHNIQUE

Sofia Almeida Xavier[1], Vasco Sousa Abreu[2], Mariana Santos[1], Amets Sagarribay[3], Carla Conceição[4]
[1]Neuroradiology Department, Hospital de Braga, Braga, Portugal. [2]Neuroradiology Department, Centro Hospitalar

Universitário do Porto, Porto, Portugal. [3]Neurosurgery Department, Hospital Dona Estefânia, Centro Hospitalar Universitário de Lisboa Central, Lisboa, Portugal. [4]Neuroradiology Department, Hospital Dona Estefânia, Centro Hospitalar Universitário de Lisboa Central, Lisboa, Portugal

Introduction: Vascular anomalies are localized defects secondary to errors in vessels morphogenesis that can lead toprogressive steno-occlusive disease, leading to impaired cerebral blood flow (CBF). Several surgical revascularization techniques have been adopted to restore adequate CBF, being indirect techniques suitable in younger children whose small-caliber vessels make direct anastomosis difficult. The multiple cranial burr hole (MCBH) surgery has been adopted as a sole procedure with excellent clinical results: drilling multiple holes through the skull stimulates anastomotic angiogenesis from branches of the external carotid artery (ECA).

Methods: We present two pediatric cases with cerebral steno-occlusive disease treated with MCBH technique with a special focus on their clinical and associated imaging evolution.

Results: A 7-month-old male presented with myoclonus and jerking movements of the left hemibody and left-sided hemiparesis. Brain MRI showed ischemic lesions involving the right middle and posterior cerebral arteries' territories. MRA showed marked stenosis of the distal internal carotids arteries (ICAs) and of the top of the basilar trunk, with concomitant marked hypertrophy of the perforating branches, suggesting a moya-moya pattern. Follow-up MRI, seven months later, revealed new recent ischemic lesions on both hemispheres. After DSA characterization, surgical revascularization with MCBH was performed. During a 6-years follow-up there was no new ischemic events, persisting a mild residual left hemiparesis and poor motor coordination. Later control neuroimaging showed hypertrophy of the ECA branches bilaterally, in relation to the neo-vascular recruitment through the multiple burr holes. MRI-perfusion showed no abnormal hypoperfused parenchymal areas.
A 9-year-old male was admitted for right-sided hemiparesis. Brain MRI revealed an acute ischemic lesion in the territory of the left medial cerebral artery (MCA) and other bilateral lesions from different timepoints. MRA showed associated cervical and intracranial vascular malformations, better characterized by DSA: bilateral occlusion of the ICAs and vertebral arteries, with CBF mainly supplied through the anterior spinal artery. Four days later he was submitted to MCBH, with good post-surgical clinical evolution. During a 2-years follow-up there was no new ischemic events, and the patient was clinically stable only with a mild right hemiparesis. Later MRIs confirmed multiple vascular anastomoses between branches of the ECA and leptomeningeal vessels through the burr holes, leading to an evident improvement in the intracranial perfusion profile.

Conclusion: Indirect revascularization techniques represent a valuable therapeutic tool to manage vascular steno-occlusive syndromes and neuroimaging is essential for diagnosis, detailed characterization of the cerebrovascular anatomy and post-surgical follow-up.

VARIOUS

3-P20
TYPICAL AND ATYPICAL MRI FINDINGS IN STURGE WEBER SYNDROME IN INFANTS

Chika Egbeama[1], Nash Laura[1], Richa Sinha[1], John Cain[1]
[1]Lancashire Teaching Hospitals NHS Foundation Trust, Preston, United Kingdom

Introduction: Present a pictorial review of the variety MRI imaging findings associated with Sturge Weber syndrome in infants from a tertiary neuroscience centre.

Methods: Review of MRI finding from the intuitional PACS for patients with diagnosis of Sturge Weber syndrome performed prior to the age of 2 over the last 10 years and collate imaging findings in an educational presentation.

Results: Present multiple cases for in Sturge Weber syndrome in infants and the associated MRI findings. Including differing appearances of pial angiomatosis. Accelerated myelin maturation of affected hemisphere (see image). Choroid plexus hypertrophy, early cortical/subcortical calcifications, associated venous abnormalities. Extra cerebral findings including orbital Choroidal hemangiomas.

Presented cases will include both initial presentation scans and subsequent follow-up imaging to demonstrate the chronology of MRI changes. Will present the natural history of the condition. Advise on suggested MR protocol to ensure all pertinent findings are recognised.

Discussion & Conclusion: The aim of the presentation is to alert the reader to the variety of MR finding associated with Sturge Weber syndrome in infants and increase confidence in making this diagnosis and aid in protocoling of MR scan requests.

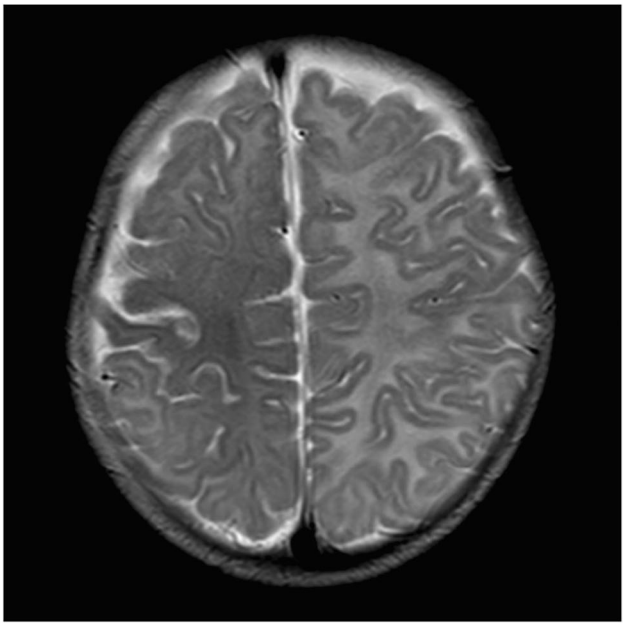

3-P21

THE EFFECTS OF OBSTRUCTIVE SLEEP DISORDERED BREATHING ON COGNITIVE PERFORMANCE, CORTICAL STRUCTURE, AND WHITE MATTER INTEGRITY IN CHILDREN IN THE ABCD COHORT

Jeannette Mathieu[1], Leo Sugrue[1]
[1]University of California, San Francisco, San Francisco, USA

Introduction: Sleep disordered breathing encompasses a spectrum of behaviors during sleep that range from primary snoring, defined as snoring without apneic events or desaturations, to obstructive sleep apnea. Sleep disordered breathing affects up to 10% of children and has been previously associated with adverse cognitive, behavioral, and psychosocial outcomes such as poor academic performance, hyperactivity, aggression, executive function deficits, anxiety, and depression. Sleep disturbances have also been associated with observable changes in brain structure and function in children, although many of these effects have been described in studies that are limited by either small sample size and/or heterogeneous imaging protocols. The goal of this study was to perform a population-wide analysis to investigate how sleep disordered breathing affects intelligence, cortical area and thickness, and white matter structural integrity.

Methods: The Adolescent Brain Cognitive Development Study (ABCD) includes more than 12,000 normally developing American children over multiple sites across the country. Data collected on study participants includes high resolution volumetric T1 and diffusion weighted brain MRI imaging, NIH Toolbox Cognition Battery (NIHTBXCB) composite scores for fluid and crystallized intelligence, and surveys about sleep habits including sleep duration and the presence and frequency of obstructive symptoms. Linear mixed effects models were performed on the ABCD to relate sleep duration and snoring with cognitive performance, vertexwise cortical morphology, and white matter structural integrity, with fractional anisotropy serving as a proxy.

Results: Always snoring, compared to never snoring, and decreased sleep duration (<7 hours vs. >9 hours) were associated with statistically significant decreased fluid and crystallized intelligence ($p < 0.01$). Furthermore, both reduced sleep duration and snoring were associated with differences in brain morphology (cortical area and thickness), but with different regional distributions; for instance, daily snorers had decreased cortical area in the left medial orbitofrontal cortex and right greater than left precuneus. Finally, children who always snore had decreased FA values along critical white matter tracts within the language dominant left hemisphere including the left superior longitudinal fasciculus, left arcuate fasciculus, and left uncinate fasiculus.

Discussion & Conclusion: Sleep disordered breathing has measurable negative effects on childhood brain development, with both cortical and white matter structure affected. Interestingly, snoring appeared to affect the left hemisphere white matter tracts, particularly tracts involved in language and learning functions. These observations might help explain observed differences in fluid and cognitive intelligence.

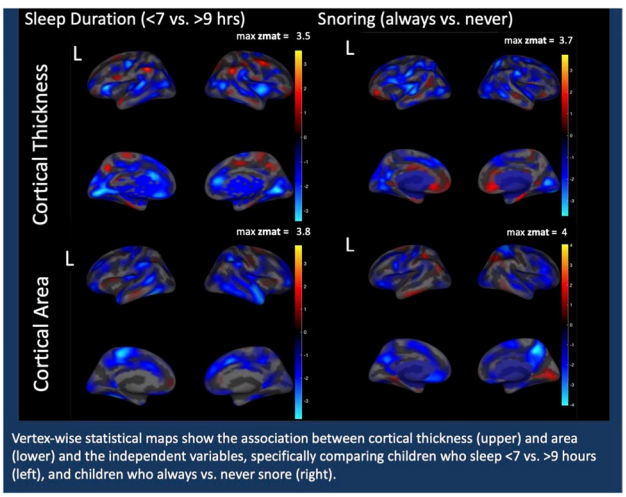

Vertex-wise statistical maps show the association between cortical thickness (upper) and area (lower) and the independent variables, specifically comparing children who sleep <7 vs. >9 hours (left), and children who always vs. never snore (right).

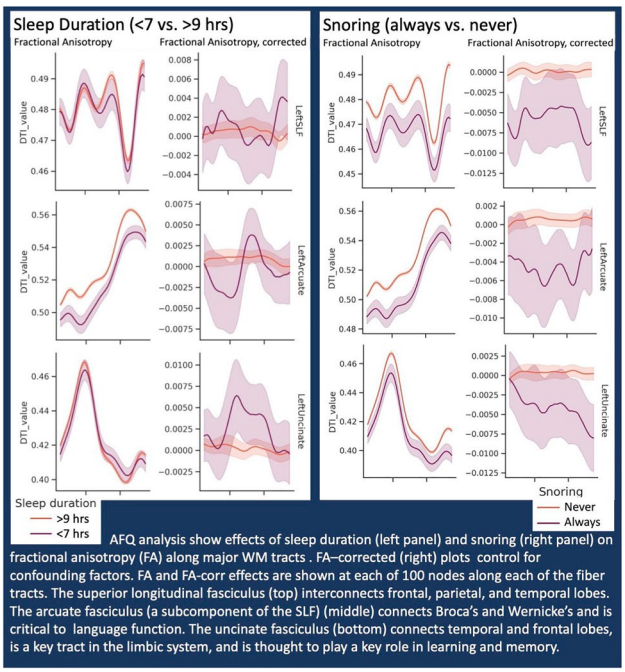

AFQ analysis show effects of sleep duration (left panel) and snoring (right panel) on fractional anisotropy (FA) along major WM tracts . FA–corrected (right) plots control for confounding factors. FA and FA-corr effects are shown at each of 100 nodes along each of the fiber tracts. The superior longitudinal fasciculus (top) interconnects frontal, parietal, and temporal lobes. The arcuate fasciculus (a subcomponent of the SLF) (middle) connects Broca's and Wernicke's and is critical to language function. The uncinate fasciculus (bottom) connects temporal and frontal lobes, is a key tract in the limbic system, and is thought to play a key role in learning and memory.

3-22

PEDIATRIC IDIOPATHIC INTRACRANIAL HYPERTENSION: A CASE SERIES FROM ONE INSTITUTION (2011-2021)

Suely Fazio Ferraciolli[1,2], Caroline Pereira Boginho[2], Aline Sgnolf Ayres[1], Lais Fajardo Ramin[1], Luziany Araujo[1], Katia Terumi[1], Laise Neri[1], Raquel Diogenes A Sindeaux[2], Gabriela Procopio M Oliveira[2], Jose Albino da Paz[2], Lisa Suzuki[3], Leandro Lucato[1], Claudia Leite[1]
[1]Inrad HCFMUSP, São Paulo, Brazil. [2]ICr - HCFMUSP, São Paulo, Brazil. [3]ICr HCFMUSP, São Paulo, Brazil

Introduction: Intracranial Idiopathic Hypertension (IIH) is characterized by signs and symptoms of intracranial hypertension, confirmed by increased CSF opening pressure and exclusion of secondary causes. It is rare in children, with an incidence of 0.6/100,000. Female sex and obesity are risk factors in post-pubertal children. Young children may be asymptomatic or have nonspecific clinical symptoms. In older children, the most common complaint is headache (57-78%), and the most important signs are papilledema, which is almost always present, and involvement of cranial nerves, especially the abducens nerve (10-17%).

Methods: A retrospective study based on medical records of pediatric patients diagnosed with IIH in our institution from September 2011 to July 2021 found 17 patients. All the patients had their medical records reviewed, with 6 cases excluded for not meeting the modified Dandy Criteria for IIH. The remaining 11 cases had their MRI analyzed.

Results: The mean age of patients at diagnosis was 10 years and 3 months. Of the eleven patients, eight were post-pubertal, and seven were female. Seven patients had endocrinological comorbidities (obesity, hypothyroidism), 1 had sickle cell anemia, and 1 had hemophilia A. On initial ophthalmological examination, all had papilledema, and five had abducens nerve involvement.
Seven patients had positive MRI findings:
Five patients (63,6%) presented dural sinus stenosis (all of them of the transverse sinus).
Four patients had "empty sella" (57%).
Six patients (85,7%) had optic nerve sheaths dilatation (bilateral in 4 cases) and flattening of the posterior sclera, with optic nerve tortuosity in 4 cases (57%) and preliminary post-contrast enhancement in 2 cases (29%).
Meckel cavity dilatation and subcutaneous fat accumulation in the head and neck were found in 2 cases (29%).
The specific finding of occipital emissary vein was present in 3 cases (42,8%).
No expansion of superior ophthalmic veins, pseudomeningoceles, skull base foramina dilatation, and ectopic cerebellar tonsils were found.

Conclusions: Although IIH is rare in pediatrics, in the face of an IIH syndrome, exclusion of secondary causes is essential for early diagnosis. As found in the literature, endocrinological comorbidities and female gender were associated with pediatric IIH in our institution. The main MRI findings described in the adult population are also present and prevalent in our pediatric cohort, which explicit the importance of MRI in the accurate diagnosis. Studies with larger casuistic, such as meta-analysis, may help us to evaluate patients' risk factors and clinical outcomes in this disorder.

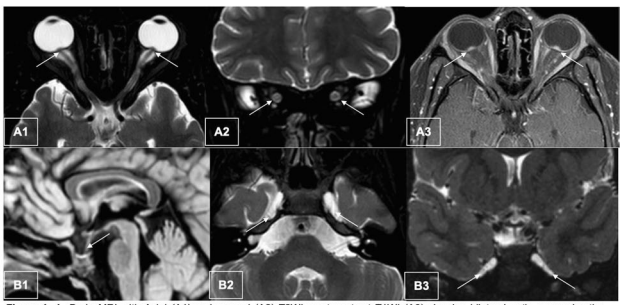

Figure 1. A. Brain MRI with Axial (A1) and coronal (A2) T2WI, post contrast T1WI (A3) showing bilateral optic nerve sheaths dilatation (arrows in A1 and A2) with protrusion of the optic papilla and preliminary post-contrast enhancement (arrow in A3)
B. Sagital FLAIR image (B1) showing an empty sella. Axial (B2) and coronal (B3) T2WI showing bilateral Meckel cavity dilatation (arrows).

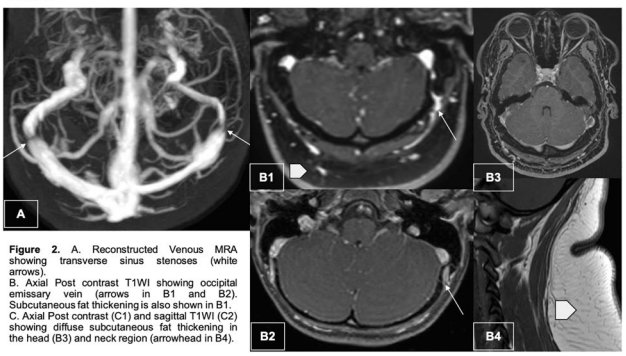

Figure 2. A. Reconstructed Venous MRA showing transverse sinus stenoses (white arrows).
B. Axial Post contrast T1WI showing occipital emissary vein (arrows in B1 and B2). Subcutaneous fat thickening is also shown in B1.
C. Axial Post contrast (C1) and sagittal T1WI (C2) showing diffuse subcutaneous fat thickening in the head (B3) and neck region (arrowhead in B4).

3-P23

PEDIATRIC PSEUDOTUMOR CEREBRI: CONCORDANCE OF CLINICAL AND IMAGING FEATURES

Begumhan Baysal[1], Mahmut Bilal Dogan[1], Fehim Esen[2], Ozlem Turkyılmaz[2], Elif Yuksel Karatoprak[3]
[1]Istanbul Medeniyet University Goztepe Prof Dr Suleyman Yalcin City Hospital Department of Radiology, Istanbul, Turkey. [2]Istanbul Medeniyet University Goztepe Prof Dr Suleyman Yalcin City Hospital, Department of Ophthalmology, Istanbul, Turkey. [3]Istanbul Medeniyet University Goztepe Prof Dr Suleyman Yalcin City Hospital, Department of Pediatric Neurology, Istanbul, Turkey

Introduction: The aim of this study was to determine the distinctive magnetic resonance imaging (MRI) findings of pediatric pseudotumor cerebri (PTC) and the relationship of these findings with the neurological and ophthalmological findings of the disease.

Methods: The history, clinical, laboratory, and imaging data of 15 pediatric patients with pseudotumor cerebri who were followed up in the ophthalmology and pediatric neurology department of a tertiary hospital were retrospectively analyzed. Ophthalmic findings (visual field, acuity, color vision, papilledema, and optical coherence tomography findings) and neurological examination (including cerebrospinal fluid pressure) results were recorded as clinical data. Dural sinus stenosis, flattening of the posterior sclera (Figure 1a), pituitary flattening, empty sella, optic nerve sheath dilatation (Figure 1b and c), and optic nerve tortuosity (Figure 1a) were evaluated with MRI brain and in some cases with MRI orbit. We investigated the sensitivity and specificity of these MRI findings for pseudotumor cerebri in children.

Results: Of the 15 patients included in the study, 5 were male and 10 were female. The mean age of the patients was 11.9±3.1 (5-16) years. The mean BMI was 22 (14-37). The most common risk factor was obesity in 3 patients. Headache was the presenting complaint in 12 (80%) of the patients. Vomiting was seen in 4 patients (27%) and is the second most common symptom. Papilledema was present in all patients and was seen in 9, 3, 1, and 2 patients from grades 1 to 4, respectively. Cerebrospinal fluid (CSF) pressure was present in 11 patients and was above 250 mmH2O in all of them. The average was 329 mmH2O. Dural sinus stenosis was not observed in any patient. Flattening of the posterior sclera was observed in 4 (27%) and pituitary flattening was observed in 2 (13%) patients. Optic nerve sheath dilatation was detected in 9 (60%) patients, and optic nerve tortuosity was detected in two patients (13%).

Discussion & Conclusion: Pseudotumor cerebri is rare in the pediatric population. According to our study, optic nerve sheath dilatation is the most common imaging finding in pediatric pseudotumor cerebri. It is more common in patients with high CSF pressure and Grade 4 papilledema.

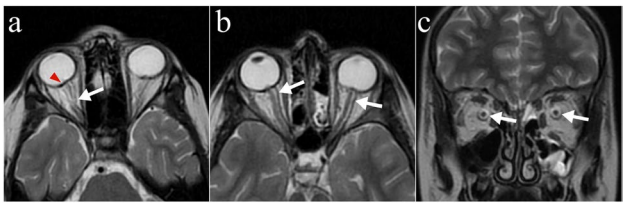

3-P24

THE ADDED VALUE BY FAT-SAT FLAIR SEQUENCE IN DEPICTION OF FRACTURES IN QUICK-MRI IN YOUNG CHILDREN HEAD TRAUMA

Mario Tortora[1], Filippo Arrigoni[2], Andrea Righini[2], Cecilia Parazzini[2], Chiara Doneda[2], Giana Izzo[2]
[1]Department of Advanced Biomedical Sciences, Neuroradiology Unit, University "Federico II", Naples, Italy. [2]Department of Pediatric Radiology and Neuroradiology, Children Hospital V. Buzzi, Milan, Italy

Introduction: In pediatric minor head trauma, Quick-MR imaging, based on single-shot T2-weighted sequences, is increasingly applied. Of this protocol, the ability to depict a calvarian fracture represents a substantial limitation. Therefore, it is customary to integrate the diagnostic work-up with plain film or low-dose CT. In this context, we tested an abbreviated version of fat-sat FLAIR sequence (40-50 sec. long) and verified whether a "dural thickening sign" could herald an associated fracture.

Methods: We reviewed our database for children under the age of 5 undergoing Quick-MRI for minor head trauma. We selected the cases that possessed the following inclusion criteria: a) shortened version of the fat-sat FLAIR sequence; b) Cranial plain film or low dose CT (to be used as a reference standard for fractures). Abbreviated version fat-sat FLAIR parameters were: TR/TE: 8000/120 msec, slice thickness 4 mm, 1mm2 in plane res. SENSE-factor 2, 1 nex, axial and coronal plane. Two pediatric neuroradiologists assessed blindly only fat-sat FLAIR images for representation of the fracture; two other evaluators only single-shot T2-weighted sections.

Results: A total of 21/53 cases met the inclusion criteria. Among them (M / F: 11/10; mean age: 12.6 months, min: 1 month, max: 60 months), cases with cranial plain film

or CT positive for calvary fractures were 13/21 (61.9%). Of these, 53.8% of cases were identified by the weighted single-shot sequence T2 (specificity: 57%; precision: 71%) for direct representation of the rhyme fracture. Instead 76.9% were identified by the "dural thickening sign" on fat-sat FLAIR sequence (specificity: 73%; accuracy: 86%). No fractures were reported in non-fractured patients at cranial plain film or CT, so both sequences did not show any false positives.

Discussion & Conclusion: Through identification of "dural thickening sign", abbreviated version of fat-sat FLAIR sequence appears to hold promise in highlighting fractures so that it could be used in addition to quick-MRI imaging in the trauma setting. The "dural thickening sign" could represent intradural edema / mild blood collection as a result of the underlying fracture. Therefore, it can overcome the spatial resolution and contrast limit of MR imaging in the direct representation of thecal discontinuity.

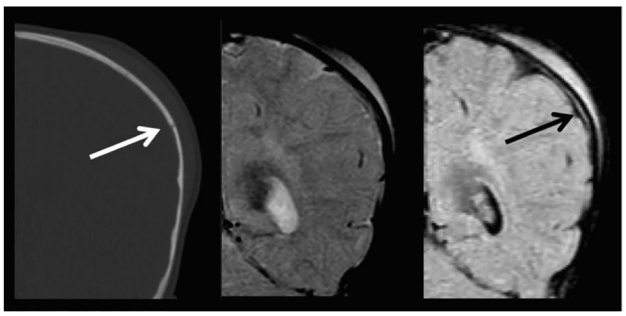

3-P25

CAN 3D CRANIAL ULTRASOUND BE USED TO SUCCESSFULLY RECONSTRUCT A 2D IMAGE WITHOUT COMPROMISING ON IMAGE QUALITY IN A NEONATAL POPULATION?

Joao Alves Rosa[1], Rachel Roberts[2], Sian Curtis[3], Adam Smith-Collins[3], Savvas Andronikou[4]
[1]North Bristol NHS Trust, Bristol, United Kingdom. [2]Oxford University Hospitals NHS Foundation Trust, Oxford, United Kingdom. [3]University Hospitals Bristol and Weston Foundation Trust, Bristol, United Kingdom. [4]Children's Hospital of Philadelphia, Philadelphia, USA

Introduction: Neonatal intensive care unit (NICU) patients often require cranial ultrasound (US). 2-dimensional (2D) US requires significant training whilst 3-dimensional (3D) US images are acquired automatically and do not need complex training but are not currently used in this setting.

If image quality was proven to be equal between 2D and 3D, these studies could be performed at remote sites, where 2D trained specialists are unavailable. The images could then be interpreted by specialists remotely.
The aim of this study was to compare the performance of 2D and 3D cranial US in the neonatal population.

Methods: Prospective study, approved by the Health Research Authority (IRAS 237123), funded by the Royal College of Radiologists of the United Kingdom.
Based on the current literature, 6 coronal and 5 sagittal views were defined as standard (Figure 1). Anatomical landmarks for each view were pre-determined (77 in total) and views were graded for quality.
For each patient, a 3D study was acquired automatically and a 2D study was performed immediately afterwards by an experienced operator, aiming to acquire the standard views. The 3D data was reconstructed by a research assistant into those same views.
Both data sets (2D and 3D) were analysed by 3 readers, blinded to the method of acquisition. The obtained views were assessed for the presence of anatomical landmarks and quality.

Results: 20 neonates were included, a total of 40 studies.
Overall, 3D scans identified more anatomical structures but a significant difference between 2D and 3D was only demonstrated for the frontal lobe (3D superior) and caudothalamic groove (2D superior) views.
No other significant difference was demonstrated for number of anatomical landmarks or view quality.
The presence of pathology significantly deteriorated quality for several of the standard views but this was similar to both types of study.

Discussion: The 3D acquired studies performed similarly to 2D in number of anatomical landmarks identified and view quality. The small differences are likely secondary to the mode of 3D acquisition, performed automatically in a swipe movement in the coronal plane. It is therefore feasible the 3D acquisition could perform better in more extreme sagittal views if parameters were adjusted.

Conclusion: This study demonstrated that 3D ultrasound of the neonatal brain performs similarly to the standard 2D. This could enable it to be performed at remote sites and images interpreted remotely by expert radiologists, avoiding long transfers of unwell neonatal patients.

Keywords: Neonatal, 3D, Ultrasound

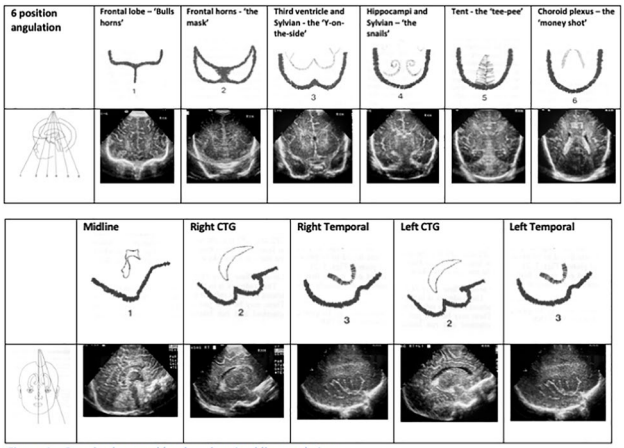

Figure 1 – Standard coronal (top) and sagittal (bottom) views

4. HEAD & NECK

CRANIAL NERVES

4-P1

DOES OLFACTORY CLEFT LENGTH ASSOCIATE WITH POST-COVID OLFACTORY DYSFUNCTION?

João Tarrio[1,2], Francisco Sousa[3], André Machado[3], Joana Costa[3], Catarina Pinto[1], Ana Pinto[3], Bruno Moreira[1]
[1]Centro Hospitalar Universitário do Porto, Neuroradiology Department, Porto, Portugal. [2]Hospital Central do Funchal Dr. Nélio Mendonça, Neuroradiology Department, Funchal, Portugal. [3]Centro Hospitalar Universitário do Porto, Otorhinolaryngology Department, Porto, Portugal

Introduction: Olfactory dysfunction (OD) is a very commonly reported symptom of coronavirus disease 2019 (COVID-19). To date, it remains unknown why some COVID-19 patients suffer from long-lasting OD, while others regain functionality after a few days. A potential link as recently been pointed in Literature concerning olfactory cleft (OC) configuration and persistent COVID-19 induced olfactory dysfunction (pCIOD).

Methods: Three subgroups were recruited from the Otorhinolaryngology consultation at a tertiary hospital: group A included patients with pCIOD, group B included patients without olfactory dysfunction following SARS-CoV2 infection and group C consisted in a control group without past history of SARS-CoV-2 infection. Olfactory perception thresholds (OPT) and visual analogue scale for olfactory impairment (VAS-olf) were obtained. Computed tomography scans were reviewed to obtain measurements of the OC. Results were subsequently compared between groups.

Results: A total of 55 patients were included with a mean age of 39 ± 10 years. No significant differences existed between groups concerning age, gender and comorbidities ($p>0.05$). OPT was significantly lower in pCIOD patients (group A: 4.2 ± 2.1 vs group B: 12.3 ± 1.8 and group C: 12.2 ± 1.5, $p < 0.001$). VAS-olf was significantly higher in pCIOD (group A: 6 ± 2.6 vs group B: 1.7 ± 1.6 and group C: 1.6 ± 1.5, $p < 0.001$). OC length was significantly higher in group A (42.8 ± 4.6) compared to group B (39.7 ± 3.4, $p= 0.047$) and C (39.8 ± 4, $p= 0.037$). The odds of pCIOD occurring after COVID-19 infection increased by 21% (95% CI [0.981,1.495]) for a one unit (mm) increase in OC length. Likewise, the odd of pCIOD occurring is 6.9 times higher when OC length > 40 mm than when OC length < 40 mm. No significant differences were observed regarding OC width between subgroups ($p=0.580$).

Conclusion: Higher OC length may associate with pCIOD, so that a longer OC may be a risk factor for pCIOD. This study should encourage further research on the OC morphology and its impact on olfactory disorders.

4-P2

NEURORADIOLOGICAL EVALUATION OF NEUROVASCULAR CONFLICT AS THE MOST COMMON CAUSE OF TRIGEMINAL NEURALGIA

Svjetlana Jefić[1], Daliborka Marić[2], Dalibor Vranješ[3]
[1]Polyclinic "Dr Al-Tawil", Radiology Department, Sarajevo, Bosnia and Herzegovina, Banja Luka, Bosnia and Herzegovina. [2]University Clinical Centre of the Republic of Srpska, Department of Radiology, Banja Luka, Bosnia and Herzegovina, Banja Luka, Bosnia and Herzegovina. [3]University Clinical Centre of the Republic of Srpska, Ear, Throat and Nose Department, Banja Luka, Bosnia and Herzegovina, Banja Luka, Bosnia and Herzegovina

Introduction: Conflict between cisternal segment of trigeminal nerve (TN) with a closely related artery is the most common cause of trigeminal neuralgia (TNA). The confirmation of neurovascular conflict of TN is a neuroradiological task that should be performed while following particular rules. Firstly, a clinically suggestive picture is necessary. It is estimated that there is no neurovascular conflict without positive clinical findings. Once faced with a clinically suggestive case of TNA, a neuroradiologist is obliged to apply adequate imaging protocol including heavily T2-weighted sequence as well as criteria for neurovascular conflict: 1. the contacting vessel must be identified as an artery, 2. the contacting nerve segment should be REZ (root entry zone), 3. signs of nerve displacement and/or compression should be identified.

Method: We present seven instructive cases of patients diagnosed with TNA that demonstrate neuroradiological procedure in such cases.
Case 1: 53 y.o. M: Surgically treated patient with NVC between left SCA and REZ of the left TN. Control exam shows the Teflon „pillow" between left SCA and TN.
Case 2: 63 y.o. F: Contact between SCA and TN on both sides, but on the right side the REZ of TN is in contact, whereas on the left side REZ is not compromised – this being in correlation with clinical picture of right-sided TNA.
Case 3: 52 y.o. F: Contact between SCA and TN nerve on both sides, but only on the left side there is compression and dislocation of TN – this being in correlation with clinical picture of left-sided TNA.
Case 4: 47 y.o. F: NVC between left AICA and TN.
Case 5: 47 y.o. F: NVC between right SCA and TN.
Case 6: 42 y.o. F: NVC between left SCA and TN.
Case 7: 86 y.o. F: An example of other pathology as a cause of TNA – as a reminder that despite the focused attention to pontine cisterns, dedicated analysis of all head regions is mandatory.

Results: The patient who had surgery has fully recovered. Other patients with neurovascular conflict are still on conservative therapy with different levels of therapeutical response. The patient with non-neurovascular conflict pathology is under oncologist's supervision.

Conclusion: The diagnosis of vascular conflict with TN can be made with a high degree of confidence by combining the clinical picture with certain diagnostic criteria. Dedicated analysis of the entire head region must not be forgotten.

Key words: Neuralgia nervi trigemini, MR imaging, diagnostic criteria

TEMPORAL BONE

4-P3
LONGTERM EVALUATION OF CT-SCANS IN OTOSCLEROSIS

Syam Satyavolu[1], Friedrich Götz[1], Frederic Bodmann[1], Martin Durisin[2], Athanasia Warnecke[2], Heinrich Lanfermann[1], Anja Giesemann[1]
[1]Institute for Diagnostic and Interventional Neuroradiology, Hannover, Germany. [2]Clinic for Otorhinolaryngeology, Hannover, Germany

Purpose: Otosclerosis is characterized by pathological bone remodeling of the otic capsule. It is a clinical diagnosis, CT sensitivity for lesions is up to 95%. Purpose of this study is to describe CT-morphology over a long period of time.

Method: 564 patients admitted for otosclerosis treatment were scanned for follow-up temporal bone CT's. 210 were found to have more than one CT and 35 of those had a time difference between the first and the last CT of over 5 years. 63 ears were analysed by two experienced neuroradiologists. Progression of extent and density of the lesions were evaluated in different localisations.

Results: The average age was 48.94 years. Time difference between first and last exam was an average of 100 months. Lesions were found in the following localisation: fissula ante fenestram 50/63 (79%); oval window 27/63 (42%); round window 21/63 (33%); IAC 8/63 (13 %); retrofenestral 20/63 (32%). An increase in local extent and density was found in 13% and 26% respectively. None of the cases showed an extension from fenestral to retrofenestral otosclerosis.

Discussion: Over a period of 5 to 14 years there was no significant progression of the lesions visible on CT scans. The results of our study were corroborated by Lee et al. Clinically there is a correlation between severity of hearing loss and severity of lesions. However according to Ishai et al. the majority of patients with otosclerosis do not show clinically significant progress of sensory neural hearing loss over a time-period of 10 years.

4-P4
RELATIONSHIP BETWEEN SUPERIOR SEMICIRCULAR CANAL DEHISCENCE AND THE INTEGRITY OF TEMPORAL BONE STRUCTURES

Yiken Karelys Ng Wong[1], Tortajada Juan Carlos[1], Sarria-Estrada Silvana[1], Rovira Àlex[1]
[1]Vall d'Hebron University Hospital, Barcelona, Spain

Keyword: Superior semicircular canal dehiscence, temporal bone CT, ear.

Introduction: The main purpose of this study is to determine the prevalence of superior semicircular canal dehiscence (SSCD) on CT scans of the temporal bone, and the relationship with other temporal bone structural abnormalities. Secondary objectives included association with clinical symptoms and audiometry findings.

Methods: We analyzed all consecutive temporal bone high resolution CT scans obtained over the course of one month in patients with clinical suspicious for vestibular disease. We assessed the presence of SSCD as well as dehiscence

in other temporal bone structures like the tegmen tympani, jugular bulb, and posterior and lateral semicircular canals. Demographics, clinical symptoms and type of hearing-loss were collected.

Results: We analyzed 82 ears from 41 patients (mean age of 53.32 years (SD 15,2); 63% (n=26) females). SSCD was found in 12 ears (14,6%), which was bilateral in four patients. Associated clinical findings included: vertigo (26.8%), tinnitus(26,8%), otorrhea (21.9%) earache/otitis (7.3%), plugged-ears (4.8%). Hearing loss was present in 82.9% of the patients: conductive (37%), sensorineural (11%) and mixed (22%).
Tegmen tympani dehiscence was found in 32 ears (39%), which was bilateral in 12 patients.
Tegmen tympani dehiscence and tinnitus were significantly more frequent in the presence of SSCD (34.4% vs 13.3%, $p<0.001$; 36.4% vs 13.3% $p<0.001$).

Conclusion: SCCD was found in roughly 15% of patients with ear complaints, and it was linked to tegmen tympani dehiscence, which could be explained by the fact that both structures share a common layer of external periosteum. In contrast to earlier research, our findings revealed a higher prevalence of tinnitus in patients with SSCD.

TUMOR

4-P5
HEAD AND NECK ANGIOSARCOMA WITH HYPEREOSINOPHILIC SYNDROME MIMICKING KIMURA DISEASE

Fátima Hierro[1], Pedro Bem[1], Inês Prisco[1], Rute Garcia[1], Joana Martins[1], Ana Reis[1]
[1]Hospital Pedro Hispano, Matosinhos, Portugal

Introduction: Angiosarcoma is a rare vascular neoplasm of endothelial origin that typically affects the skin and subcutaneous tissues of the head and neck, where it preferentially affects the face and scalp. Concomitant metastases are common at presentation, usually located in the lung or spleen. Cutaneous cases are usually associated with risk factors such as radiation exposure or chronic lymphedema. There is, however, an association between hepatic angiosarcoma and hemochromatosis. Cases of hypereosinophilia secondary to soft tissue sarcomas have been described.
Kimura disease is a benign inflammatory pathology, the definitive diagnosis being established by histopathology. It presents with pruriginous but painless subcutaneous masses in the head and neck, involving salivary glands and lymph nodes in the neck, associated with hypereosinophilia with increased serum IgE. It most often affects men in the 3rd to 5th decade of life, being more common in Asia.

Case report: A 70-year-old man presented with multiple swellings on his face and scalp. The lesions had been present for 3 months and were associated with pruritus but not pain. Upon inspection, they had a violet appearance and were centrally ulcerated. The patient had a medical history of hemochromatosis. In the analytical study, hypereosinophilia (7200/uL) with IgE hypergammaglobulinemia (6047 U/mL) was detected.
The imaging study detected multiple hypervascular expansive lesions located in the face, including the parotid gland, and scalp, and multiple homolateral jugulocarotid adenopathies. There was no bony erosion, intracranial extension or concomitant liver lesions detected.

Conclusion: We present a case whose clinical, laboratory and imaging presentation is compatible with Kimura disease. Only age and geographic location were against this diagnosis. A histological diagnosis of angiosarcoma was obtained, and the analytical findings of hypereosinophilia and hypergammaglobulinemia were interpreted as secondary to the soft tissue sarcoma.
Recognition of this constellation of symptoms, imaging and laboratory findings can assist in the timely guidance for histological characterization of these lesions.

Keywords: Kimura disease; angiosarcoma; head and neck

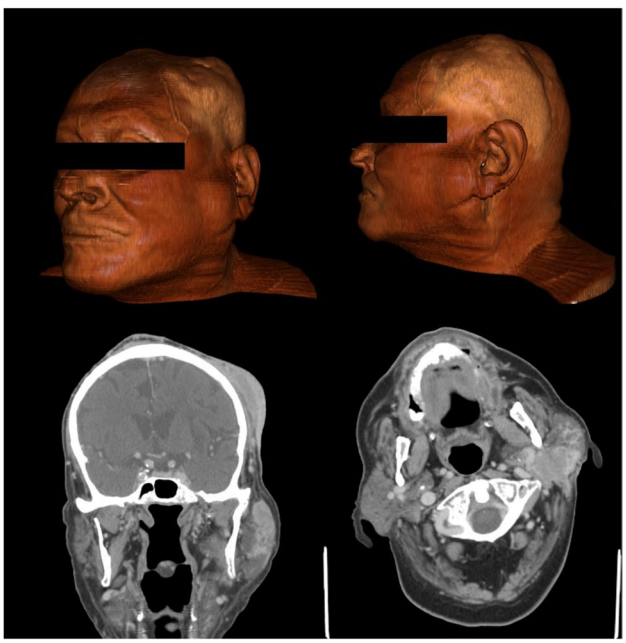

4-P6

SALIVARY GLAND MASSES: HOW TO ACCURATELY DIAGNOSE BY IMAGING

Silvia María Díaz de la Fuente[1], Adela Rodríguez Fuentes[2], Glenis Nieves Perdomo[2]
[1]Department of Radiology, Hospital Universitario de Canarias, San Cristóbal de La Laguna, Spain. [2]Department of Radiology, Neuroradiology, Hospital Universitario de Canarias, San Cristóbal de La Laguna, Spain

Introduction: The pathology of the salivary glands is wide and heterogeneous, especially tumour pathology.
The imaging characteristics may overlap widely between different tumours and there are no pathognomonic radiological signs to differentiate them. This makes radiological diagnosis difficult, requiring anatomopathological study for definitive assignment of tumour histology. Therefore, the main objective of imaging techniques is to provide information about extension and to detect signs of malignancy (invasion patterns, extension to deep planes, infiltration of soft tissues or perineural dissemination).

Objectives: To study the most frequent radiological characteristics of the different salivary gland pathologies and to determine if there is a pattern of behavior in the available imaging modalities for the most frequent pathologies.
To determine the incidence of salivary gland pathology in our hospital.

Methods: This is a retrospective study of salivary gland lesions analyzed in our hospital from January 2019 to December 2021. All lesions were studied by at least one imaging technique (US/CT/MRI) with definitive diagnosis by cytology and/or biopsy.
The following variables were studied: age, sex and radiological behavior in the different imaging techniques. The radiological characteristics evaluated were: solid-cystic nature, location, shape and margins, echotexture-signal-density, homogeneity, vascularization, number of lesions, laterality, lymph node enlargement, size and patterns of expansiveness and infiltration. Data were analyzed using SPSS statistical data processing package SPSS 25.0IBM Co.

Results: A total of 80 salivary gland lesions were studied; 74% parotid, 24% submandibular and 2% minor salivary glands. The majority were tumours (79%) most of them benign (n=46). Benign tumours included 22 pleomorphic adenomas (PA), 18 Warthin's tumours (WT), 2 cystadenomas and 5 from other subtypes. Malignant tumours (n=16) included 12 carcinomas, 2 lymphomas and 2 metastases.
The majority of APs and WTs had well-defined, rounded margins, while 50% of malignant tumours had ill-defined, irregular margins.
On MRI, WTs were predominantly heterogeneous in all sequences, with areas of necrosis/cystic degeneration and mild contrast enhancement.
Contrast enhancement on CT was moderate to intense in 39% of WTs versus 13.6% of APs.
Lymph node enlargement was detected in over 50% of WTs and malignant tumours.
The majority of WT were bilateral (66.7%) and multifocal (56%) lesions, a significantly higher rate than the rest of the pathologies.

Conclusion: Despite not having pathognomonic findings, the most common radiological findings in terms of shape, enhancement, homogeneity, multiplicity and laterality, combined with localization and clinical parameters, allow a more accurate radiological diagnosis.

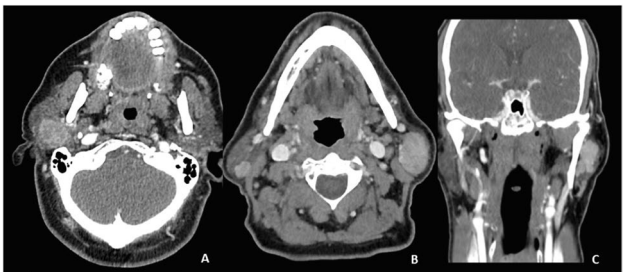

Contrast CT of parotid lesions. A. Pleomorphic adenoma with rounded, well- defined margins, with mild enhancement. B. Bilateral Warthin's tumour with rounded, well- defined margins, with moderate to intense homogeneous enhancement. C. Acinar cell carcinoma , with irregular, partly well-defined margins, with moderate to intense homogeneous enhancement

VARIOUS

4-P7

CHRONIC DIFFUSE SCLEROSING OSTEOMYELITIS: A DIAGNOSIS TO CONSIDER

Luís Augusto[1], Ana Isabel Almeida[1], Sofia Vedor[1], Luísa Sampaio[1,2], Jose Maria Matos Sousa[1]
[1]Department of Neuroradiology, Centro Hospitalar Universitário de São João, E.P.E., Porto, Portugal. [2]Faculty of Medicine, Oporto University, Porto, Portugal

Keywords: Osteomyelitis; Chronic infection; Bone sclerosis.

Introduction: Osteomyelitis describes an inflammatory process involving the bone and is subdivided in chronic and acute. Chronic diffuse sclerosing osteomyelitis

(CDSO) is the least known of the various types of chronic osteomyelitis, being a rare, insidious disease with cryptic pathophysiology, without age preference (described from 10 to 72 years old).
CDSO reflects a nonsuppurative inflammatory/infectious bone reaction with swelling of the overlying musculature/soft tissues, often presenting with insidious complaints of trismus and recurrent facial pain. CT scans show varying grades of hyperostosis and/or sclerosis, with or without foci of bony erosion. MRI further characterizes oedematous changes of the bone marrow and soft tissues.

Case Report: Patient history: A 22-year-old female was admitted to the emergency department reporting insidious onset of visual disturbances (diplopia and left ophtalmoparesis) during the previous weeks and complaints of trismus and masticatory difficulty with up to one year of duration. Her dental history revealed root canal surgery (teeth 2.7 and 2.8), with persistent pain in 2nd quadrant at least 2 years prior to admission.
Imaging Findings: Head CT revealed extensive endosteal sclerosis of the left sphenoid and zygomatic bones, including the pterygopalatine process and the inferolateral wall of the orbit, with moderately-preserved anatomy and cortical thickening. Areas of bone erosion were evident in the lateral maxillary wall, infraorbital canal and in the alveolar process of maxilla related with the roots of 2.8 tooth. Also, an enhancing soft tissue mass was noted in the left orbital floor (with displacement of orbital muscles and extension to the orbital apex) and in the retroantral fat.
MRI additionally depicted abnormal signal intensity of bone marrow in the affected areas, as well as oedema/enhancement of overlying musculature (including masseter, lateral and medial pterygoids and temporalis muscle).
Considering imagiological appearance and insidious clinical presentation, the diagnosis of CDSO was proposed.

Discussion: Owing to the rarity of CDSO as whole and its relative infrequency in the absence of mandibular involvement, the disease seldom features in differential diagnosis.
Combined CT and MRI evaluation is optimal, with accurate definition of sclerotic changes in CT and adequate definition of the extent of the inflammatory process with MRI. The literature describes hypertrophic and oedematous changes of the masseteric muscles as a distinctive feature of CDSO. It is suggestive of muscle hyperactivity, evoking chronic tendoperiostitis as an important etiological factor.

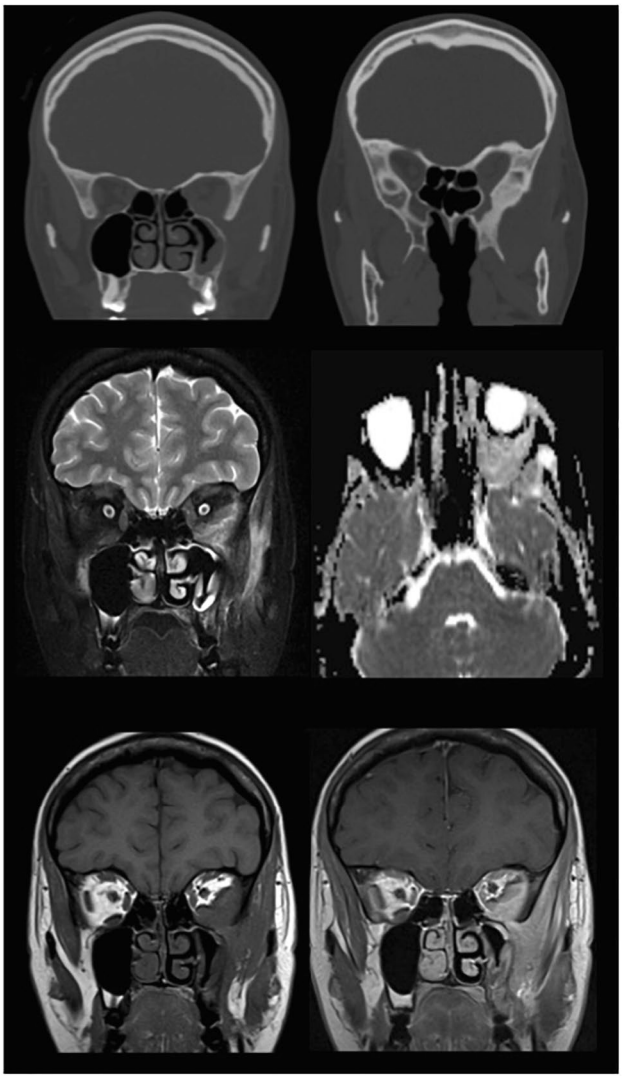

4-P8
ROTATORY SUBLUXATION OF AXIS-RADIOLOGICAL PICTURE AND PRESENTATION OF TWO CASES

Radmila Peric[1], Filip Samardzic[1], Jasmina Boban[2,3], Nikola Boban[1]
[1]Clinical centre of Vojvodina, Novi Sad, Serbia. [2]Oncology institute of Vojvodina, Novi Sad, Serbia. [3]Faculty of Medicine, Novi Sad, Serbia

Injuries to the atlantoaxial joint occur in one third of cases of cervical spine injuries. One of the types of injuries is atlantoaxial rotatory subluxation (AARS), which leads to instability of the atlantoaxial joint (AA), and can be traumatic or non-traumatic. They occur most often due to injury of the alar ligament by rotatory and flexion forces and are usually seen as part of isolated ligament lesions.

In the clinical picture, these patients have neck pain, a feeling of instability and the need to adhere to the head, torticollis, and a limited degree of mobility.
The radiological signs of AARS are discrete and must be interpreted as part of the clinical picture.
Depending on the age of the lesion, the radiological finding may show direct signs of trauma of the ligament apparatus (existence of edema, hematoma and post-contrast enhancement of signal intensity within inflammation and reparative changes). The described signs can be best assessed by MR examination. Indirect signs of AARS are disturbed relationships of bone structures - asymmetric dens position and the existence of dislocation of the articular surfaces of the lateral AA. These signs can be seen radiologically on X-ray and CT scans. Evaluating the relationship between bone and ligament structures of the AA joint can often be challenging given discrete radiological signs as well as the frequent existence of bilateral injuries; aggravating factors in adults may be degenerative changes.

Case report: The first of our two patients occurs after fresh traffic trauma with persistent pain and reduced range of motion in the neck; in this patient, MR examination showed an asymmetrically positioned dens axis relative to the lateral masses of the atlas with signs of acute injury of the left alar ligament. Another patient appears several months after the onset of symptoms that were not preceded by trauma; the MR finding also showed an asymmetric position of the dens axis; there were no signs of acute trauma on the side of the ligament lesion, while there were minor signs of trauma on the contralateral ligament structures.

Conclusion: Given the often nonspecific clinical picture, detailed radiological evaluation may be crucial for the diagnosis of AARS.

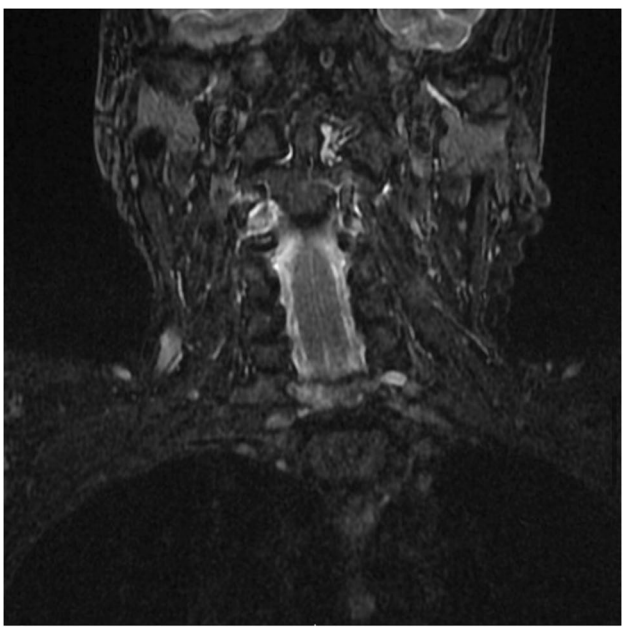

Keywords: atlantoaxial rotatory subluxation; cervical spine injury; cranio-cervical transition.

4-P9

INTRACRANIAL HYPERTENSION IN SCLEROSTEOSIS: THE FIRST ITALIAN FAMILY

Caterina Bombardieri[1], Francesco Bono[2]
[1]Neuroradiology Unit, Azienda Ospedaliera Universitaria, CATANZARO, Italy. [2]Headache Center, SOC Neurology, Azienda Ospedaliera Universitaria "Mater Domini", CATANZARO, Italy

Introduction: Sclerosteosis is a rare autosomal recessive disorder due to SOST gene mutation, resulting in loss of function of sclerostine protein which regulate osteoblastic bone apposition which lead to cranio-tubular hyperostosis with high density bone. Very few sporadic cases have been described around the world mainly in Africa and South America. Here we describe the first Italian family with sclerosteosis.

Case description: We present the case of two brothers of 45 and 36 years old with a history of chronic headache and nocturnal snoring. They presented macrocephaly and an enlarged mandible. In addition they complained unilateral visual acuity loss and unilateral deafness since adolescence. Moreover, the youngest one had a bilateral facial nerve palsy since childhood. The neurological examination of the youngest brother revealed mild bilateral exophthalmos, motu manu visual acuity in left eye and bilateral facial nerve palsy. Fundus oculi examination showed a bilateral mild optic disc swelling and pallor of left optic disc. The patient underwent to an audiometric examination which demonstrated a deep sensorineural impairment. Cranial CT showed a massive and sclerotic thickening of neurocranial and splanchnocranial bones, optic ducts stenosis, absence of mastoid pneumatisation bilaterally. Brain MRI and MR venography displayed partial empty sella, flattening of posterior aspect of the globes, distension of perioptic space, unilateral transverse sinus stenosis, presence of Chiari malformation. We performed 1-hour lumbar CSF pressure monitoring through spinal needle which gave evidence of an elevated intracranial pressure (opening pressure 370 mmH2O).

Conclusion: In the patient hyperostosis causes multiple cranial nerve palsy, as a result of encroachment of cranial nerve foramina. We speculate that hyperostosis of splanchnocranial bones causes intracranial hypertension and headache.

References:

W. Van Hul et al. Van Buchem Disease (Hyperostosis Corticalis Generalisata) Maps to Chromosome 17q12-q21. Am. J. Hum. Genet. 62:391–399, 1998

K. Staehling-Hampton et al. A 52-kb Deletion in the SOST-MEOX1 Intergenic Region on 17q12-q21 Is Associated With van Buchem Disease in the Dutch Population. American Journal of Medical Genetics 110:144–152 (2002)

Keywords: Sclerosteosis, headache, intracranial hipertension.

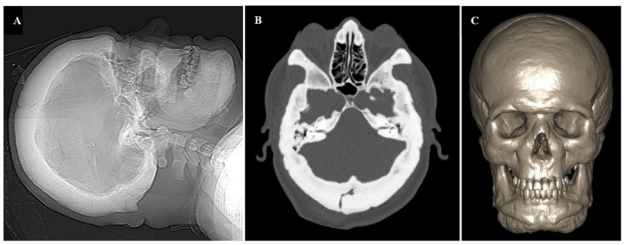

Figure 1: A) CT scanogram of the skull (lateral view) shows extensive sclerosis of the calvarium, maxillae and mandible. B) CT scan at the level of the posterior cranial fossa detects a marked thickening and sclerosis of the skull bones with narrowing of the internal auditory canals. C) 3D Volume Rendering of Spiral CT Data.

4-P10
LATERAL DECUBITUS CT CISTERNOGRAPHY TO IDENTIFY CSF LEAK – A CASE REPORT

João Saraiva[1], Sofia Xavier[1], Mariana Santos[1], João Fernandes[1], Jaime Rocha[1]
[1]Hospital de Braga, Braga, Portugal

Most cases of intracranial hypotension are caused by leakage of CSF somewhere along the neuraxis. A 33-year old woman presented with worsening orthostatic headaches, fever and seizures; she had intermittently complained of clear fluid otorhinorrhea and had been previously diagnosed with intracranial hypovolemic syndrome. Initial head computed tomography (CT) scan ruled out vascular/tumoral lesions or extra-axial collections. A lumbar puncture was not performed due to low-lying cerebellar tonsils, but a central nervous system infection was assumed and empirical antimicrobial therapy was started. Magnetic resonance imaging revealed signs of intracranial hypotension and fluid retention at the right petrous apex, and no evidence of cerebritis or abscesses. Bone-algorithm thin-slice head CT scan showed a bony defect at the posteromedial wall of the right petrous apex, immediately superior to the petroclival fissure. CT cisternography was performed with the iodinated contrast injected in intrathecal space after lumbar punction at L4-L5 level – there was an early contrast filling at the right petrous apex with leakage to the carotid canal and possible dehiscence of the carotid plate at the vertical portion of the petrous internal carotid artery, suggesting an osteodural defect of the temporal bone with cerebrospinal fluid (CSF) leakage. Despite no evidence of iodinated contrast in either the protympanum or the external auditory canal (EAC), there was contrast impregnation in a cotton bandage placed inside the patient's right EAC, supporting a diagnosis of CSF fistula and its relation with CSF otorrhea, intracranial hypotension, and meningitis. This case report highlights the additional benefits of CT cisternography in the detection of CSF leak.

4-P11
DETECTION OF VERTEBRAL ARTERY DISSECTION ON DUAL ENERGY CT

Halah Baqer[1], Kim-Son Nguyen[2]
[1]Westmead Hospital, NSW, Australia. [2]Bankstown Hospital, NSW, Australia

Background: Vertebral artery dissection is a difficult diagnosis that can be a dilemma for physicians. MRI is seen as the gold standard for diagnosis. However, MRI may not always be possible or available in a timely fashion.

Aim/Research Question: To see if there are features on dual energy CT that can aid in the detection of vertebral artery dissection

Methods/Study Design: Between September 2020 and May 2021, 4 patients presented to a mid-size hospital with neurological symptoms concerning for stroke and TIA. These patients had an initial CT angiogram of their neck and head. Due to both imaging findings and clinical concerns, these patients then had an MRI which confirmed the presence of vertebral artery dissection

Findings: 3 out of the 4 patients had both thickening of the vessel wall on curved MPR reconstructions and markedly reduced attenuation(>250HU) of the affected vertebral artery vs the unaffected side at the level of the occipital condyle on the 45keV mono energy reconstruction.
1 of the 4 patients had sections of occlusion/loss of contrast opacification along the affected vertebral artery that precluded vessel tracking to allow a curved MPR reconstruction but also demonstrated marked attenuation on the 45keV mono energy reconstruction at the level of the occipital condyle.

Outcomes: There were features on the dual energy CT angiogram, which included reduce attenuation on the affected side on the low energy mono energy reconstruction and vessel wall thickening on curved MPR reconstruction which could help in diagnosing vertebral artery dissection.

5. SPINE

DEGENERATIVE

5-P1

INTRAVOXEL INCOHERENT MOTION MRI: A NEW MARKER OF DEGENERATIVE CERVICAL CORD COMPRESSION?

Marek Dostál[1,2], Miloš Keřkovský[1,3], Tomáš Rohan[1,3], Andrea Šprláková-Puková[1,3], Petr Ouředníček[4,5], Josef Bednařík[6], Zdeněk Kadaňka[6], Zdeněk Kadaňka jr.[6]
[1]University Hospital Brno, Department of Radiology and Nuclear Medicine, Brno, Czech Republic. [2]Masaryk University, Faculty of Medicine, Department of Biophysics, Brno, Czech Republic. [3]Masaryk University, Faculty of Medicine, Department of Radiology and Nuclear Medicine, Brno, Czech Republic. [4]St. Anna University Hospital Brno, Department of Medical Imaging, Brno, Czech Republic. [5]Philips, Prague, Czech Republic. [6]University Hospital Brno, Department of Neurology, Brno, Czech Republic

Introduction: MRI is a key diagnostic tool in patients with degenerative cervical myelopathy (DCM). However, degenerative cervical cord compression (DCCC) can be found quite commonly also in asymptomatic subjects and intramedullary signal abnormalities may not be visible in all patients with symptoms of DCM. This clinical-to-imaging mismatch limits interpretation of MRI findings and their role in deciding about surgical treatment. Thus, novel MRI techniques are being sought to improve MRI diagnostics in patients with DCM. One of them is intravoxel incoherent motion (IVIM), which may reflect tissue perfusion through the advanced analysis of the water diffusion. The main aim of this pilot study is to evaluate the role of IVIM in patients with DCCC.

Methods: The study group comprised 28 DCCC patients, 16 of them with clinical signs of DCM and 12 asymptomatic subjects. A group of 18 healthy controls without signs of DCCC was also included. All study participants underwent MRI of the cervical spine comprising IVIM sequence using IRIS ZOOM technique (Philips, Netherlands) with 8 different b values (0-800 s/mm^2). The spinal cord was segmented semiautomatically, motion correction of different b images was performed and IVIM parameters (D, D* and f) were calculated. Furthermore, spinal cord cross-sectional area (CSA) and compression ratio (CR) were measured on axial T_2-weighted images. Finally, IVIM parameters were established for the whole spinal cord volume (C2-7) and for the level of maximal compression (MCL) in patients and a reference level (C4/5) in controls and these values were compared between the study groups using t-test.

Results: We found significant differences in mean f and D values, when the whole spinal cord volume was compared between all patients and healthy controls ($p<0.0001$), all three IVIM parameters differed significantly also between patients and controls when measured at MCL (C4/5 in controls) ($p<0.05$). In patients with symptoms of DCM, CSA was significantly lower and CR higher at MCL compared to asymptomatic patients, but no significant differences were observed in case of IVIM parameters.

Discussion & Conclusion: Our preliminarily data indicate that DCCC has significant impact on IVIM parameters measured within the spinal cord. However, in our comparatively small sample, we were not able to prove significant changes of these parameters in relation to clinical manifestation of DCM. Despite that, we believe that IVIM is a promising technique, which deserves further investigation on larger groups of patients with DCCC.

5-P2

POTENTIAL PREDICTIVE FACTORS OF SPONTANEUOS REGRESSION OF EXTRUDED DISC HERNIATION ON MR IMAGING

Svjetlana Jefić[1], Daliborka Marić[2], Dalibor Vranješ[3], Biljana Kecman[2]
[1]Polyclinic "Dr Al-Tawil", Radiology Department, Sarajevo, Bosnia and Herzegovina, Banja Luka, Bosnia and Herzegovina. [2]University Clinical Centre of the Republic of Srpska, Department of Radiology, Banja Luka, Bosnia and Herzegovina, Banja Luka, Bosnia and Herzegovina. [3]University Clinical Centre of the Republic of Srpska, Ear, Throat and Nose Department, Banja Luka, Bosnia and Herzegovina, Banja Luka, Bosnia and Herzegovina

Introduction: The phenomenon of spontaneuos regression of herniated disc material has already been described in literature but still not widely recognized by medical professionals who are involved in management of patients with back pain. Due to its ability to regress spontaneously, the massive herniated disc should be surgically treated only in cases of progressive motor deficite and cauda equina syndrome. Neuroradiologists are in position to suggest potential predictive factors in favor of spontaneous regression of herniated disc as the most preferable outcome of this disorder and therefore impact the therapeutic approach to it.

Background: Reasons for spontaneous regression of herniated disc can be: 1) dehydration and shrinkage, 2) retraction, 3) inflammation and neovascularization. In our opinion, all of these theories are complementary and most probably applicable to different types of herniation so that mechanism of dehydration and shrinkage as well as retraction can

provide reparation of protrusions where the regenerative capacity of anulus fibrosus is still effective, while in extruded herniations inflammation and neovascularization are the most probable underlying mechanisms. The rim enhancement of the extruded disk on MR imaging is considered a sign of neovascularization and thus the potential predictive factor of spontaneuos regression. Higher T2-weighted (T2W) signal of extrusion, compared to the parent disc, that correlates with presence of liquid within the extruded disc material can suggest not only the process of degradation and resorption but also the duration of the condition.

Method: We present three instructive cases of patients with extruded discs, treated conservatively, with complete recovery and full disappearance of the extruded disk material on the control MR exam.

Case 1: 40y, F: large left-sided L5-S1 disc extrusion with cranial migration and increased T2W signal of the distal part of extruded material.

Case 2: 55y, F: large left-sided L5-S1 disc extrusion with cranial migration and markedly higher T2W signal of the extruded material compared to the parent disc.

Case 3: 35y, M: large right-sided L4/L5 disc extrusion with cranial migration and also high T2W signal of the whole extruded material.

Results: All three patients had good outcomes without surgery.

Conclusion: The radiological report of extruded disc that usually carries dramatic information about size and compression degree of corresponding nerve roots also needs to have the impression about aspects of potential spontaneous regression of extruded material which, in adequate clinical settings, can prevent unnecessary surgery.

Keywords: disc herniation, sponatenous regression, MR imaging, radiological report

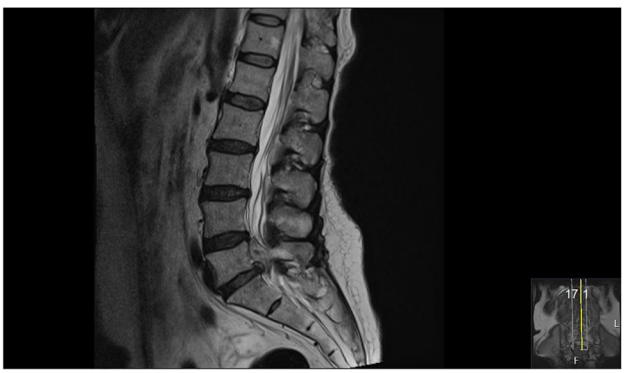

INFLAMATORY

5-P3

POST-VACCINATION HEMORRHAGIC LONGITUDINALLY EXTENSIVE TRANSVERSE MYELITIS – 2 CLINICAL CASES

José Sá Silva[1], João Tarrio[1], Eduarda Pinto[1], António Costa[1], José Pedro Rocha[1], Cristina Ferreira[1], João Pedro Filipe[1]
[1]Centro Hospitalar Universitário do Porto, Porto, Portugal

Introduction: Acute hemorrhagic longitudinally extensive transverse myelitis (LETM) is a severe rare presentation of transverse myelitis. Although often associated with autoimmune diseases, para-infectious and post-vaccination are also possible etiologies.

Case 1: 55-year-old women with unremarkable past medical history presented to the emergency department with a week-long progressive trunk and inferior limb dysesthesia, first left and then bilateral, which developed into gait disturbance. Neurological examination revealed hypoesthesia with sensory level at T8 and mild asymmetric paraparesis, as well as impaired proprioception and brisk deep tendon reflexes in the lower limbs. Spine MR revealed multi-segment central cord lesions from T3 to T8, with a focal hemorrhagic lesion, and no enhancement.
She was treated with a methylprednisolone cycle followed by Immunoglobulin therapy, but kept deteriorating, evolving into paraplegia and anesthesia with sensory level at T4. Follow-up MR showed cephalic and caudal progression (T1 to T9) and a new focal hemorrhage. She was then started on prednisolone and rituximab and the symptoms stabilized. She didn't recover any function.
All infectious, immune and vascular etiologies tested were negative. She had a presumed upper respiratory infection three days before the symptoms started, and a first dose of COVID-19 vaccination a month before.

Case 2: 55-year-old women, with treated bladder cancer 12 years prior, but otherwise healthy. She was brought to the hospital because of an acute severe lumbago which progressed to paraplegia and lower limb anesthesia in about one hour. Neurological examination confirmed the deficits, as well as loss of bladder and deep tendon reflexes. MR showed a conus medullaris lesion involving only the gray matter, with restricted diffusion, but no specific vascular territory affected. She was started on a methylprednisolone cycle. The patient still got worse, with anesthesia progressing to the trunk, with sensory level at T10. Follow-up MR showed cephalic progression of the lesion to T4, now affecting gray and with matter, with multiple hemorrhagic foci,

medullary expansion and patchy contrast enhancement. She was started on plasmapheresis and did another methylprednisolone cycle, after which she stabilized. She didn't recover from the deficits.

All etiologies sought were negative. She had a second dose of COVID-19 vaccination two months before.

Conclusion: Although these two cases have only a temporal relation with COVID-19 vaccination, which is not enough to prove a causative effect, post-vaccination hemorrhagic LETM has been described with other vaccines and this relation should be equated in the diagnostic work-up of these patients.

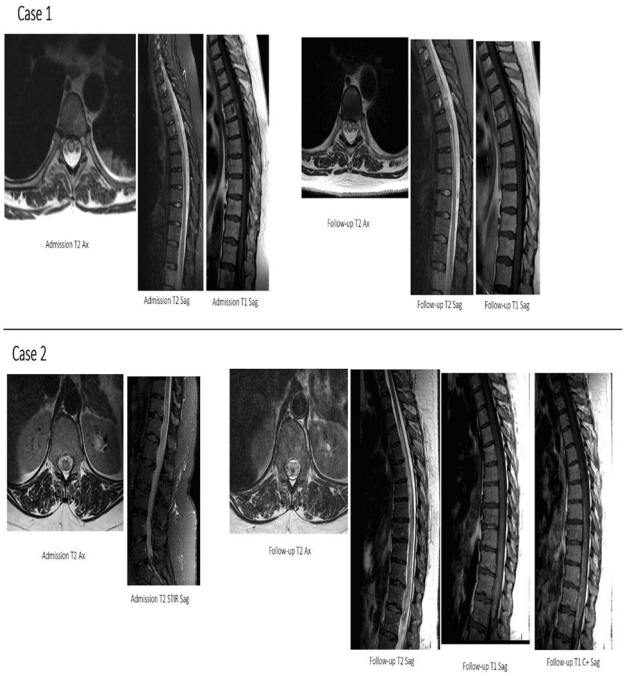

TRAUMA

5-P4
LUMBAR MOREL-LAVALLÉE LESION IN A MOTORCYCLE CRASH

Miguel Rocha[1], Frederic Ramalho[1], Joana Costa[1], Ana Batista[2], João Costa[1], Fernando Macedo[1], João Lucas[1], Rui Cerqueira[1], Patricia Cunha[1], Fernando Lima[1]
[1]Hospital Senhora da Oliveira, Guimarães, Portugal. [2]Centro Hospitalar Médio Tejo, Abrantes, Portugal

Introduction: The Morel-Lavallée lesion (MLL) is a closed degloving injury caused by traumatic separation of the skin and subcutaneous tissues from the solid underlying fascia. The emergency department should be aware of this syndrome since its early diagnosis allows a conservative management. On the contrary, a delayed diagnosis often leads to surgical exploration. Additionally, improper or untimely diagnosis and management can result in undesirable consequences such as infection, pseudocyst formation, and cosmetic deformity.

Case presentation: A 25-year-old male entered the emergency department after a fall from a motorcycle. The patient suffered from back pain and the physical examination showed local pain and fluctuation at lower lumbar region. A CT scan demonstrated a fluid collection of 19.5 × 5.3 cm in dimensions, between L1 and S3 in extension, associated with a L4 and L5 AO type A0 injury. The patient was diagnosed with a lumbar MLL and admitted to the Orthopedic service. Needle aspiration guided by ultrasound was performed and a vacuum drain was left for 3 days, due to the size of the lesion and significant risk of infection. Clinically, the injured area did not show any characteristic signs of inflammation and a decreased soft-tissue swelling was evident. The patient was discharged with prophylactic antibiotics and instructions to apply compression banding, activity cessation and ice. Follow-up appointments were scheduled for close monitoring.

Results: One week after discharge, the patient was relieved of his pain and the collection was stabilized, although with mild fluctuance on the center of the lower back region. After 4 weeks the swelling was improving and at 8 weeks follow up the collection completely disappeared.

Discussion: The Morel-Lavallée lesion is a rare condition. Studies show that the variation of the anatomical structure of the adipose tissue determines the most commonly involved regions. Various treatment options have been described including conservative management, percutaneous drainage, incision and debridement. When diagnosis and treatment are not achieved in the early phase, surrounding granulation tissue may eventually organize into a pseudo-capsule, preventing reabsorption of the content of the lesion and leading to a chronic fluid collection.

Conclusion: The literature on the topic is limited and lumbar MLL has been rarely reported, but awareness of this injury is important to avoid serious complications. Emergency physicians should recall this clinical entity especially when facing a high-energy trauma, where clinical examination is of the utmost relevance.

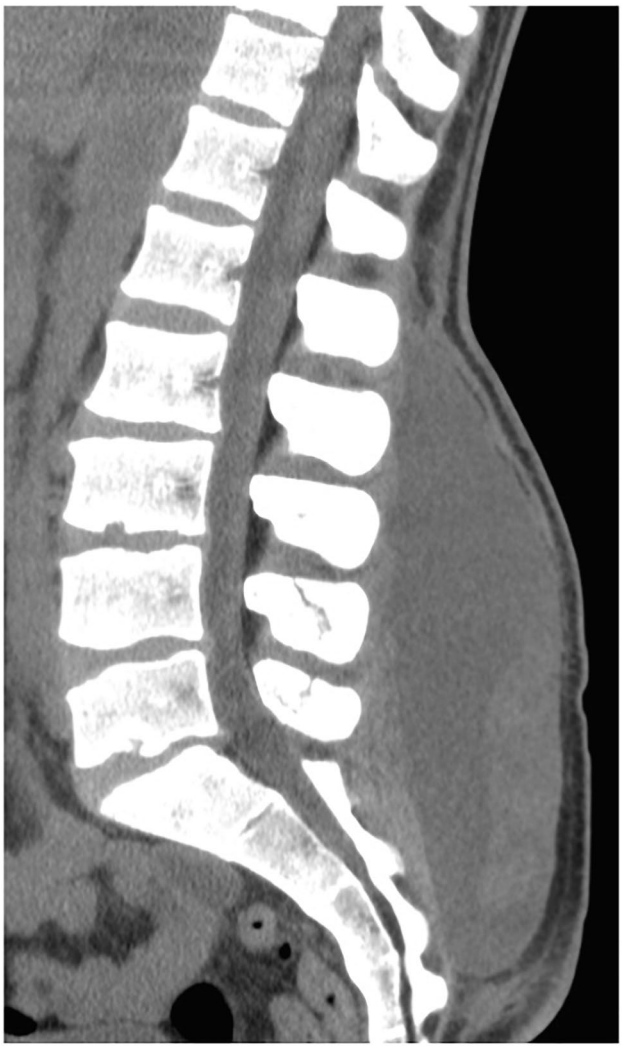

TUMOR

5-P5
LYTIC LESION OF THE SPINE: MYXOID/ROUND CELL LIPOSARCOMA: (UN)USUAL SITE OF NEOPLASTIC SPREAD

Filipa Castelao[1], Diogo Marques[1], Francisca Batista[1], Sergio Costa[1], Cristina Marques[1], Ana Cristina Rios[1]
[1]Hospital Garcia de Orta, Almada, Portugal

Introduction: Liposarcomas are rare malignant tumors of the soft tissue which exhibit adipocytic differentiation. Myxoid/round cell lipossarcoma is the second most common subtype of liposarcoma accounting for about 30% to 35% of all liposarcomas. It is believed that these two entities are intimately related and represent a spectrum of the disease. Myxoid liposarcomas can transgress into round cell liposarcoma which is a more aggressive neoplasm with much greater potential for metastasizing. Unlike most sarcomas, myxoid/round cell lipossarcoma is well known to have an unusual proclivity for extrapulmonary metastasis. Some reports show a tendency to bone dissemination, particularly the spine. However, it is not clear if bone metastisis represent the usual pattern of spread of myxoid/round cell liposarcoma and the true frequency of this phenomenon.

Methods: In addition to the presentation of a clinical case, a MEDLINE research was performed for metastatic patterns of myxoid/round cell lipossarcoma.

Results and Discussion: We report on the case of a 49-year-old-female who presented progressive difficulty with ambulation for five days. Physical examination demonstrated motor strength of 4 in 5 on both inferior limbs, hyperreflexia and severe proprioception deficit in the lower extremities. Spine CT and MRI scan were done and revealed diffuse infiltration of the vertebrae and paraspinal lesions with central canal extension at D9, D10, D11, D12 and L3. The MRI also revealed a mass involving the left kidney, which turned out to be the primary tumor. Decompressive surgery with partial resection was performed and the tissue of the paraspinal lesions revealed round cell lipossarcoma. The patient was treated with adjuvante chemotherapy and radiotherapy. While on treatment, she developed soft tissue, pulmonar, lymph nodes and cerebral metastasis. She died one year after the diagnosis.

Conclusion: The purpose of this report is through the demonstration of a clinical case, whose first presentation was spinal cord compression, to reinforce the hypothesis that the spine is a preferential site of metastasis in myxoid/round cell lipossarcoma.
Furthermore, to emphasize the importance of performing spine imaging in myxoid/round cell lipossarcoma patients.

Keywords: lytic lesions, metastic spread, Myxoid/round cell lipossarcoma

5-P6
INTRADURAL EXTRAMEDULLARY TUMOURS

Sofia Bettencourt[1], Pedro S. Brandão[1], Gonçalo Lobo[1], Mariana Baptista[1], Carla Conceição[1]
[1]Neuroradiology Department, Centro Hospitalar de Lisboa Central, Lisbon, Portugal

Introduction: Spinal tumours are rare, being responsible for 5-10% of all CNS tumours. They can be divided according to their topographic location as arising extradurally, intradural-extramedullary or intramedullary.
Intradural extramedullary tumours are responsible for 70-80% of all spinal tumours, with schwannoma and meningioma being the most frequent ones. However, other

noteworthy, less common neoplasms must be considered when evaluating this compartment.
The most frequent complaint of patients with intradural extramedullary tumours is axial back pain, which may be nonspecific. Radicular pain can also affect these patients, particularly those with nerve sheath tumours. If there is spinal cord compression myelopathy or cauda equina syndrome can occur. Usually, these are slow-growing tumours, and there can be a delay of several months before a radiological diagnosis is established.

Method: We retrospectively collected multiple cases of intradural extramedullary spinal tumours and provide a pictorial review depicting the key clinical and imaging findings that can help narrow the differential diagnosis.

Result: In our series, we describe seven different cases of intradural extramedullary spinal tumours, including a poorly differentiated carcinoma metastasis, one hemangioblastoma, one spinal ependymoma, one lipoma, a disseminated glioneuronal tumour with spinal drop metastasis, and also a schwannoma and a meningioma.

Conclusion: Imaging, particularly MRI is a cornerstone in the diagnosis of intradural extramedullary tumours, evaluating its morphologic and signal characteristics, enhancement pattern and tumour extension. Since prompt treatment is essential for preventing the progression of neurological deficits and allowing symptomatic relief, the knowledge of the clinical background and the distinct imaging characteristics of the neoplasms that may affect this region can help narrow the differential diagnosis.

Keywords: spine, spinal tumours, MR imaging, intradural extramedullary tumour, poorly differentiated carcinoma metastasis, hemangioblastoma, spinal ependymoma, lipoma, disseminated glioneuronal tumour with spinal drop metastasis, schwannoma, meningioma

5-P7

SPINAL TUMORS AND TUMOR-LIKE MASSES: REPORT OF A SERIES CASES WITH CHALLENGES IN THE INTERPRETATION OF IMAGING FINDINGS

Daliborka Maric[1,2], Svjetlana Jefic[3], Biljana Kecman[1], Dalibor Mikic[2], Sasa Vujnovic[4]
[1]University Clinical Centre of the Republic of Srpska, Department of Radiology, Banja Luka, Bosnia and Herzegovina. [2]Special Hospital S-tetik, Banja Luka, Bosnia and Herzegovina. [3][2] Polyclinica "Al-Tawil", Radiology Department, Sarajevo, Bosnia and Herzegovina. [4]University Clinical Centre of the Republic of Srpska, Banja Luka, Bosnia and Herzegovina

Introduction: Masses of the spinal canal are classified by their anatomic location. They may involve the extradural, intradural–extramedullary, or intramedullary space. Localizing a mass to a specific compartment is often helpful in narrowing the differential diagnosis. Many masses affect multiple compartments, the most common pattern being extradural tumors with intradural involvement.

Methods: We present a pictorial review of the various lesions of the spine, as well as rare tumors with challenges in the interpretation of imaging findings. Spinal tumor types by aggressiveness: there are several types of masses that can be found in the spine: Some are malignant tumors, which means they can spread to other areas of the body. Some are benign tumors, which means they are not aggressive and don't spread, but it doesn't mean they are harmless. Some may look like tumors but are actually cysts, plaques or similar masses. The bony spinal column is the most common site for bone metastasis. The most common primary spine tumor (originated in the bony spine) is vertebral hemangiomas.

Results: Only 10% of spinal tumors show abnormalities on plain radiographs such as widening of the neural foramina, vertebral body scalloping, or calcifications. CT may be useful for the more precise evaluation of calcifications and osteolytic lesions. CT with intravenous contrast can provide an effective alternative: opacification of the extradural venous plexus can aid anatomic orientation and improve the delineation of masses. MRI is the imaging modality of choice, as its multiple planes and contrasts allow for the precise anatomic localization of a mass. It may also be helpful to add a diffusion sequence. Neoplastic fractures often show restricted diffusion whereas traumatic and osteoporotic fractures do not.

Conclusion: Syringohydromyelia and cystic lesions are frequently associated with intramedullary tumors. Nontumoral cysts tend to be located at the poles of the tumors and do not enhance on contrast-enhanced MR images, whereas cysts within the substance of the tumor are considered tumoral cysts and typically demonstrate peripheral enhancement. Although primary spinal epidural lymphoma and spinal extraskeletal Ewing's sarcoma is a rare entity it should be considered in the differential diagnosis of the spinal epidural tumors.

Keywords: Spinal tumors, Imaging, Location, Primary spinal epidural lymphoma,

VASCULAR

5-P8
CASE REPORT OF SPINAL CAVERNOUS MALFORMATION ASSOCIATED WITH PERIMEDULLARY VENOUS ANOMALY

Eduarda Pinto[1], Vasco Abreu[1], João Tarrio[1], Catarina Pinto[1]
[1]Centro Hospitalar Universitário do Porto, Porto, Portugal

Introduction: Spinal cavernous malformations are vascular malformations pathologically identical to intracranial ones, but rarer than those. They can be associated with venous anomalies, which may be superficial or intramedullary. We report a case of a probable spinal cord cavernous malformation associated with prominent perimedullary flow voids, with unremarkable digital subtraction angiography (DSA).

Case presentation: A 59-year-old woman with a probable cavernous malformation of the spinal cord at T10 level, performed a follow-up MRI of the thoracic and lumbar spine in which was noted prominent perimedullary flow voids. Additionally, the patient had a subcutaneous and paravertebral slow flow vascular malformation. To determine the nature of the perimedullary flow voids, DSA was performed, which was unremarkable, with no signs of arteriovenous shunt. Contrast-enhanced MRI of the spine was then performed and showed perimedullary enhancing vessels in the thecal sac corresponding to veins. It was assumed that it was a cryptic venous anomaly. Clinically the patient had a slight deficit in the segmental motor strength of the lower limbs that had been progressively worsening but with autonomous gait and some errors in deep sensation. She preferred no to be submitted to a surgical procedure.

Conclusion: Spine cryptic venous anomalies associated with cavernous malformations are considered analogous of intracranial development venous anomalies. In this case report we intend to raise awareness to this rare entity and to the distinction between superficial and intramedullary ones, particularly in case of surgery because the latter is known to cause a higher risk of surgical complications. Some authors suggest that flat-panel catheter angiotomography is useful is this distinction.

VARIOUS

5-P9
OPTIMIZED MRI PROTOCOL IN HIRAYAMA'S DISEASE: CASE REPORT AND LITERATURE REVIEW

Cristine Zelaquett S R Luz[1], Christiane P Guimarães[1], Taciana Andrade[1]
[1]Hospital da Restauração, Recife, Brazil

Introduction: Hirayama disease (HD) is a cervical myelopathy, self-limited, motor neuron disease. In the present study we report the clinical, electromyography and MRI features of one patient, with a review of the literature. We sinalize an optimized MRI protocol for patients with suspected or diagnosed HD in order to make an early diagnosis and a standardized follow up.

Methods: We present the case of a 16-year-old girl who had the classic radiologic and clinical presentations of Hirayama disease. The patient underwent standard electromyography (EMG) and cervical spine MRI conducted with a 1.5 Tesla MRI scanner in neutral and flexion positions.

Results: The patient with 2 years duration of weakness and wasting of the left- side hand and forearm, progride to involvement bilateral and asymmetric. On MR, the following diagnostic features were find: loss of the normal cervical lordosis, localized cervical cord atrophy(C4-C7), presence of cord flattening, intramedullary signal hyperintensity on T2 weighted, anterior shifting of the posterior wall of the cervical dural sac and presence of flow voids in the posterior epidural space during flexion, with expanded enhancing posterior epidural space.

Discussion: Predominantly affecting male adolescents, it is characterized by progressive muscular weakness and atrophy of distal upper limbs, followed by spontaneous arrest within several years. Most case reports in the literature are from Asian countries. HD differs from classical types of motor neuron diseases because of its self-limited nature and the pathological findings of chronic microcirculatory changes in the anterior horns of the lower cervical cord. MRI is the best diagnostic tool in the diagnosis of HD (protocol suggested: Nonflexion sagittal T1 and T2-weighted, nonflexion axial gradient-echo T2- weighted, flexion sagittal T2-weighted, contrast-enhanced flexion and non sagittal T1-weighted). A dynamic MRI should definitely be done in every suspected case. Contrast-enhanced espinal MRI may be done to demonstrate findings better but is not essential.

Conclusion: Hirayama disease should be suspected in patients presenting with unilateral or asymmetrical bilateral lower motor weakness of hands and forearms. MRI is very important to confirm the clinical suspect of HD and a standardized MRI protocol using both neutral and flexing position is needed, in order to diagnose and follow up affected patients. A good understanding of Hirayama disease is essential because early recognition and management can effectively halt the progressive deterioration.

Keywords: Hirayama disease; hand weakness; magnetic resonance imaging.

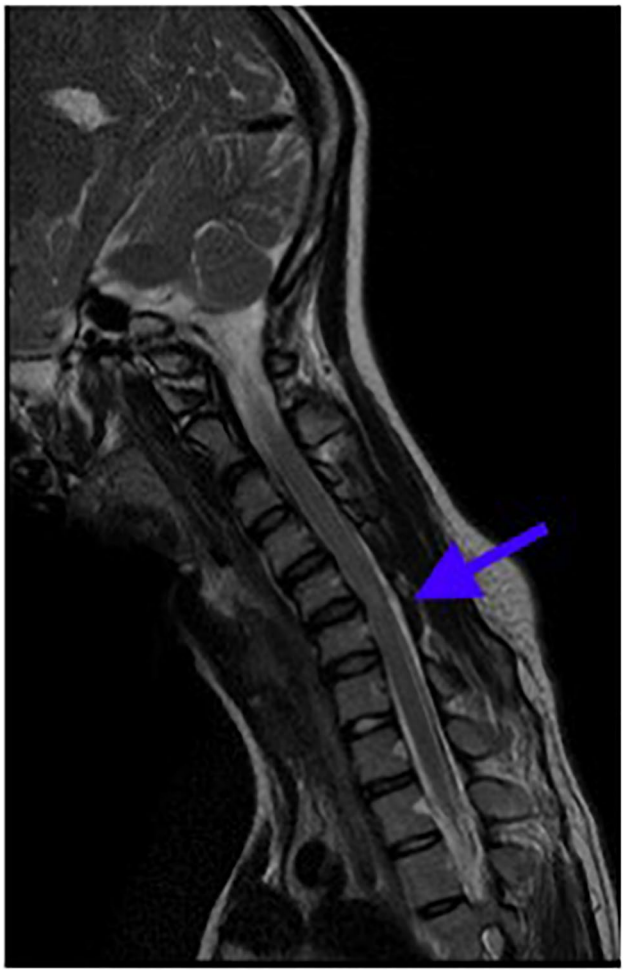

AUTHORS INDEX